Density Functional Theory Studies on Hydrogen Storage in Molecular Anions of Different Sizes and Shapes

Thesis Submitted to AcSIR for the Award of the Degree of
DOCTOR OF PHILOSOPHY
in Chemical Sciences

By

Della Therese Davis

Registration No: 10CC13A39004

Under the Guidance of

Dr. C. H. Suresh

Chemical Sciences and Technology Division
CSIR-National Institute for Interdisciplinary Science and Technology
Thiruvananthapuram-695019, Kerala, India

May 2018

DECLARATION

I hereby declare that the Ph. D. thesis entitled "**Density Functional Theory Studies on Hydrogen Storage in Molecular Anions of Different Sizes and Shapes**" is an original work carried out by me at Chemical Sciences and Technology Division(CSTD), CSIR-National Institute for Interdisciplinary Science and Technology (CSIR-NIIST), Thiruvananthapuram, under the supervision of Dr. C. H. Suresh, Principal Scientist, CSTD, CSIR-NIIST, and it has not been submitted elsewhere for any other degree, diploma or title.

CSIR-NIIST

29/05/2018 **Della Therese Davis**

Council of Scientific & Industrial Research
National Institute for Interdisciplinary Science and Technology
Thiruvananthapuram-695019, Kerala, India

Dr. C. H. Suresh
Principal Scientist
Chemical Sciences & Technology Division
Tel: +91- 4712515472
E-mail: sureshch@gmail.com
sureshch@niist.res.in

29th May 2018

CERTIFICATE

This is to certify that the work incorporated in this Ph. D. thesis entitled "**Density Functional Theory Studies on Hydrogen Storage in Molecular Anions of Different Sizes and Shapes**" submitted by Ms. Della Therese Davis to Academy of Scientific and Innovative Research (AcSIR) in fulfillment of the requirements for the award of the Degree of Doctor of Philosophy, embodies original research work done under my supervision. I further certify that this work has not been submitted to any other University or Institution in part or full for the award of any degree or diploma. Research material obtained from other sources has been duly acknowledged in the thesis. Any text, illustration, table, *etc*. used in the thesis from other sources, have been duly cited and acknowledged.

Della Therese Davis
(Student)

Dr. C. H. Suresh
(Thesis Supervisor)

Acknowledgments

It is hard to put into meaningful words my deep feeling of gratitude for all the people who directly or indirectly have contributed to this achievement. I take this opportunity to express my appreciation to all those who made this Ph. D thesis possible.

I would like to express my sincere gratitude to my advisor, Dr. C. H. Suresh for his continuous support, advice, and motivation throughout my Ph. D work. His immense knowledge and guidance helped me in all the time of research and writing of this thesis.

I record my heartfelt thanks to Dr. A. Ajayaghosh, Director, CSIR-NIIST, and former directors, Dr. Suresh Das and Dr. Gangan Pratap for the academic support and providing me the necessary facilities for carrying out my research work in this institution.

I am grateful to Dr. R. Luxmi Varma, Head, Chemical Sciences and Technology Division and AcSIR coordinator for her timely advice and support for the conduct of academic procedures. I also extend my sincere thanks to former HODs Dr. D. Ramaiah and Dr. K. R. Gopidas and former AcSIR coordinator Dr. Mangalam S. Nair for all their support and guidelines.

I sincerely thank my Doctoral Advisory Committee members Dr. K. K. Maiti, Dr. S. Ananthakumar, Dr. Saju Pillai for their insightful comments and encouragement throughout my AcSIR coursework and Ph. D programme.

I wish to thank former members of our research group - Dr. Sandhya, Dr. Neetha, Dr. Prabha, and Dr. Remya K. for their support, encouragement and fruitful discussions. A very special thanks to present members of our group - Dr. Renjith, Rakhi, Remya P. R., Anjali, Remya G. S., Bijina, Divya, and Anila for their warm friendship and creating a good environment in our lab. I appreciate the support from all of you especially for spending the time to correct this manuscript and giving me valuable suggestions.

I profoundly express my thanks to all friends at CSIR-NIIST for friendship and support. Thanks for all the enjoyable moments that we had together.

I would also like to thank the administrative and technical staff members of CSIR-NIIST for the cooperation and help in their respective roles.

I would like to acknowledge Council of Scientific and Industrial Research (CSIR), for providing me financial support.

I gratefully acknowledge the high-performance computational facilities at CSIR-NCL, Pune, and CSIR-CMMACS, Bangalore.

I express my deep sense of gratitude to all my beloved teachers in the past for teaching me the fundamentals of chemistry and their inspiration.

I owe my deepest gratitude to my family for their love, care, and concern. Thanks for all their sacrifices and support. I would not have been able to reach this goal without them.

Above all, I praise God, the Almighty for giving me strength, knowledge, and opportunity to undertake this research study and granting me the ability to proceed successfully. Without thy blessings, this accomplishment would not have been possible.

Della Therese Davis

CONTENTS

Chapter 2

Dihydrogen Binding Affinity of Anions

Part A: Dihydrogen Binding Affinity of Bare Anions

Part B: Dihydrogen Binding Affinity of Polyatomic Anions

Chapter 3

Dihydrogen Binding Affinity of One-Dimensional Anionic Carbon Chains and Sumanene: An Organic π-Bowl

Part A: Dihydrogen Binding Affinity of One-Dimensional Anionic Carbon Chains

Part B: Dihydrogen Binding Affinity of Sumanene: An Organic π-Bowl

Chapter 4

Anion Encapsulated Fullerenes as Large Anions and Dihydrogen Binding Affinity of Endohedral Fullerenes

Part A: Anion Encapsulated Fullerenes as Large Anions

List of Figures

List of Tables

List of Abbreviations

AB : Ammonia Borane

AMBER : Assisted Model Building with Energy Refinement

AO : Atomic Orbitals

BCP : Bond Critical Point

BO : Born Oppenheimer

BSSE : Basis Set Superposition Error

CBS : Complete Basis Set

CC : Coupled Cluster

CCP : Cage Critical Point

CG : Contracted Gaussian

CGTO : Contracted Gaussian-Type Orbitals

CHARMM : Chemistry at Harvard Macromolecular Mechanics

CI : Configuration Interaction

CNDO : Complete Neglect of Differential Overlap

COF : Covalent-Organic Framework

CP : Critical Point

DFT : Density Functional Theory

DOE : Department of Energy

DZ : Double-Zeta

E_{int} : Interaction Energy

$E_{int/H2}$: Interaction Energy per H_2

FCTO : Fuel Cell Technologies Office

G09 : Gaussian 09

GGA : Generalized Gradient Approximation

GROMACS : Groningen Machine for Chemical Simulations

GROMOS : Groningen Molecular Simulation

GTO : Gaussian-Type Orbitals

HF : Hartree-Fock

INDO : Intermediate Neglect of Differential Overlap

LDA	: Local Density Approximation
LSDA	: Local Spin Density Approximation
MCSCF	: Multi-Configurational Self-Consistent Field
MD	: Molecular Dynamics
MESP	: Molecular Electrostatic Potential
MIA	: Multiplicative Integral Approximation
MM	: Molecular Mechanics
MOF	: Metal-Organic Framework
MP	: Moller-Plesset Perturbation
NBO	: Natural Bond Order
NDDO	: Neglect of Diatomic Differential Overlap
ONIOM	: Our Own N-Layered Integrated Molecular Orbital and Molecular Mechanics
PGTO	: Primitive Gaussian-type Orbital
PPP	: Pariser-Parr-Pople
QM	: Quantum Mechanics
QTAIM	: Quantum Theory of Atoms in Molecules
QZ	: Quadruple-Zeta
RCP	: Ring Critical Point
RHF	: Restricted Hartree-Fock
SCF	: Self Consistent Field
STOs	: Slater-Type Orbitals
Su	: Sumanene
SWCNT	: Single-Walled Carbon Nanotube
TZ	: Triple-Zeta
ZDO	: Zero Differential Overlap

PREFACE

Hydrogen, being eco-friendly, renewable, and abundant is considered as a striking fuel for the modern era. Its low energy density by volume withholds the development of adept storage systems and therefore restricts the use of hydrogen as a fuel for mobile applications. Hydrogen storage techniques can be classified as mechanical storage, chemical storage, and physisorption methods. The nature, strength, and mechanism of the fundamental interaction of H_2 with the hydrogen storage material play a decisive role in determining the ability of a material to store hydrogen. Theoretical investigations are of great significance for the reliable prediction and understanding of such interactions. The main focus of the thesis entitled "**Density Functional Theory Studies on Hydrogen Storage in Molecular Anions of Different Sizes and Shapes"** is to comprehend the binding nature of H_2 with various anionic systems and to predict efficient H_2 storing systems using computational methods. The thesis is divided into four chapters.

The first part of Chapter 1 gives an overview of various hydrogen storage materials. Theoretical studies on different classes of hydrogen storage materials are briefly discussed. Computational chemistry is an exciting and fast-emerging field that has become crucial for most advances made in chemistry these days. A brief account of computational methodologies employed in the thesis is presented in the second part of Chapter 1.

Chapter 2 is divided into two parts. Part A discusses the studies on dihydrogen binding affinity of anions such as F^-, Cl^-, Br^-, OH^-, NH_2^-, NO_2^-, CN^-, and ClO^- using CCSD(T)//CCSD *ab initio* and M06L density functional theory (DFT) techniques. The H_2 coordination number of these anions varies from 12 – 20 which corresponds to the good interaction energy (E_{int}) and interaction energy per H_2 (E_{int/H_2}). The highest coordinated dihydrogen complexes of these anions show substantially good values of E_{int/H_2} in the range 4.2 - 2.0 kcal/mol. A high weight percent of H_2 (40 – 56 wt%) is noted for these anion-H_2 complexes. These findings are well supported by the quantum theory of atoms in molecules (QTAIM) and molecular electrostatic potential (MESP) analyses. The study clearly shows that bare anions have significant affinity to bind with a large

number of hydrogen molecules. Part B of Chapter 2 discusses the dependence of the size of polyatomic anionic systems on their dihydrogen uptake. The dihydrogen binding ability of polyatomic oxohalo anions ClO–, ClO_2^-, ClO_3^-, ClO_4^-, BrO^-, BrO_2^-, BrO_3^-, and BrO_4^- are studied at M06L and CCSD(T)//CCSD methods. An uptake of 17 – 24 H_2 molecules in the first coordination shell is noted for these polyatomic anions with significant interaction energies. This study shows that the polyatomic anions with smaller size and less number of atoms are more efficient in H_2 binding systems. The anion...H_2 noncovalent interactions and H...H dihydrogen interactions within the complex are studied in QTAIM analysis. The MESP is used to estimate the change in negative potential at the interacting nuclei of the anion. The electron density and change in potential at the nuclei are correlated with the interaction energy of the complex.

Part A of Chapter 3 describes the noteworthy ability of one-dimensional anionic and dianionic carbon chains to bind with a large number of H_2 molecules compared to their neutral counterparts. The structure and energetics of H_2 complexes of anionic carbon chains such as HC_2^-, HC_4^- and HC_6^- and dianions such as C_2^{2-}, C_4^{2-}, and C_6^{2-} which have been analyzed using M06L and CCSD(T) methods. The H_2 coordination number of the anions/dianions is in the range 20 - 32 which corresponds to 45.3 to 62.8 wt% of H_2 in the complex. The nature of C…H and H…H noncovalent bonding interactions are established by QTAIM analysis and delocalization of the excess electron in the complex by MESP analysis. The H_2 binding affinity of sumanene and its anionic forms are discussed in Part B of Chapter 3. Anionic and dianionic systems showed much higher interaction energy compared to the neutral sumanene. In reality, anions cannot exist without a counter cation. To account for this, the H_2 binding ability of the ion-pair complexes of monoanionic, dianionic and trianionic sumanenes with K^+ as counter cation have been investigated and found that these systems also have a striking H_2 binding ability. The charge delocalization and the extent of electron transfer in the complexes have been investigated using critical features of MESP. Sumanene...H_2 noncovalent interactions and secondary dihydrogen interactions within the complex are established by locating bond critical points (bcp) in QTAIM analysis. The structured network of these interactions can be accounted for the stability of the complex.

Sumanene systems with Li^+ and Na^+ as counter cations instead of K^+ have also been studied. These systems possess a remarkable ability to bind H_2 which can be utilized for developing novel hydrogen storage systems.

Part A of Chapter 4 discusses the properties of anion encapsulated endohedral fullerenes. The structure and properties of anions such as F^-, Cl^-, Br^-, OH^-, NH_2^-, NO_2^-, CN^-, and ClO^- encapsulated in C_{60} fullerene have been investigated, and these anionic molecules are proposed as large anions. Also, a few other larger fullerene systems have also been analyzed. The molecular orbital, MESP, and various spectroscopic analyses show that in these anion encapsulated cages, the negative charge on the anion is delocalized and partially felt on the surface of the cage. The H_2 storage capacity of anion encapsulated endohedral fullerenes along with cation encapsulated fullerenes as their counterparts are discussed in Part B of Chapter 4. These non coordinating cation-anion systems show substantial H_2 binding affinity with $\sim$ 9wt % of gravimetric density. The theoretical studies presented in the thesis shed light on the development of novel hydrogen storage materials for improved storage capacity.

It may be mentioned that each chapter of the thesis is presented as an independent unit and therefore the structural formulae, schemes and figures are numbered chapter wise.

Chapter 1

Introduction

Part A- Hydrogen Storage

&

Part B - Computational Chemistry

Part A: Hydrogen Storage

1.1 An Overview of Hydrogen Storage

Hydrogen is considered as a clean, abundant, renewable, and efficient energy carrier of choice for the twenty-first century. Moreover, the decline of non-renewable fossil fuels, as well as its impact on global warming has made hydrogen as an alternate energy source.[1, 2] Researchers have been trying to substitute fossil-fuel sources with hydrogen for automotive purposes and other applications. The benefits of switching from petroleum to hydrogen include energy security, reduced pollution issues, *etc.* Hydrogen is striking fuel as it can be burned or combined with oxygen in a fuel cell releasing energy and water as a byproduct without generating any greenhouse gases or other pollutants. Also, hydrogen can be produced from abundant sources such as water, thus reducing dependence on fossil fuels. Several scientific and technological barriers have to be solved before the implementation of a hydrogen economy on a large scale.

Hydrogen storage is a key enabling technology for the improvement of hydrogen as a fuel for transportation, portable and stationary power and other applications.[3, 4] The use of hydrogen as a fuel for everyday life is limited due to difficulties in developing compact, dependable and cost-effective hydrogen storage techniques.[5-9] Hydrogen gas has high energy density by weight, but energy density by volume is very low, about ten times lower than that of conventional fuels at ambient conditions[10, 11] and therefore its storage becomes very challenging for any practical applications.[12] Energy density refers to the amount of usable energy that can be derived from the fuel system. Hydrogen storage implies the reduction of the enormous volume of H_2 gas with the ultimate goal of packing H_2 as close as possible.[13] Another decisive factor for a hydrogen storage system is the reversibility of uptake and release of H_2.[14]

Governmental institutions and other funding bodies have set some goals for developing hydrogen storage technology which set limits to cost, the density of the storage system, refilling time, and cycle lifetime. The gravimetric and volumetric

densities of H_2 are given prior attention. In 2004, the U. S. Department of Energy (DOE) introduced a few objectives regarding the storage densities stimulating the research in this field. Nevertheless, none of the existing technologies meet all these demands put forward by DOE. The targets based on light-duty vehicles were revised in 2009 and set to 4.5 wt% and 5.4 MJ kg^{-1} (target for 2010), 5.5 wt% and 6.48 MJ kg^{-1} (target for 2015), and 7.5 wt% and 9 MJ kg^{-1} (ultimate target).[15] Researchers have been actively working on approaches to pack a large quantity of hydrogen in low-weight and low-volume systems. In recent years, considerable progress has been made in the search for suitable materials for hydrogen storage. The Fuel Cell Technologies Office (FCTO) works on developing onboard automotive hydrogen storage systems that have the potential to meet DOE targets and requirements of cost, safety, and performance criteria.

Hydrogen storage techniques can be broadly classified into physical storage, chemical storage, and physisorption methods which will be discussed in detail in the following sections. At present, materials-based research on metal hydride, chemical hydrogen storage, and sorbent materials is carried out with much importance.[16] The improvement in volumetric and gravimetric capacities, hydrogen adsorption/desorption kinetics, reaction thermodynamics, and cycle life are the key factors for metal hydride materials research.[17] Research on chemical hydrogen storage materials focuses on improving transient performance, reducing the release of volatile impurities, improving volumetric and gravimetric capacity, and developing proficient regeneration methods for the spent storage material. The enhancement of storage ability by optimizing the material's pore size, increasing pore volume and surface area, increasing effective adsorption temperature through the increase of dihydrogen binding energies are of prior importance in the case of sorbent materials.

1.1.1 Physical Storage

Physical methods include storing hydrogen in its pure form either as a compressed gas or as a cryogenic liquid and cryoadsorption on high surface area materials.[11, 18, 19] In compressed hydrogen storage method, hydrogen gas is stored in high-pressure tanks with pressure varying between 200 and 350 bar.[20] This pressure range is volumetrically and gravimetrically insufficient for automotive purposes. The

development of systems with at least 700 bar capacity is underway.[21] By storing hydrogen in liquid form can attain greater densities than the compressed gas. Liquid hydrogen, often used as a concentrated form of hydrogen storage requires cryogenic storage (~ 20 K). The problem is with the practical application as liquefying H_2 is energy intensive and require specialized infrastructure.[7, 22] The storage tank needs to be well insulated for maintaining cryogenic temperature. Cryoadsorption involves the adsorption of H_2 on high surface area materials at low temperatures (~ 80 K).[18] No chemical bonds are formed between the host molecules and H_2 in this case. None of the presently known adsorbents has as storage capacity which would satisfy the target values at ambient temperature and pressure. The physical storage is not practically viable as these techniques require high pressure and low temperature.

1.1.2 Chemical Storage

In chemical storage approach, atomic hydrogen is trapped *via* strong chemisorption process with the storage material and generated through a chemical reaction.[23, 24] Metal hydrides, complex hydrides, ammonia borane, metal alloys, *etc*. come under this category.[13, 25-29] Storing hydrogen in solids at low pressure is much encouraged from a safety point of view and is advantageous over conventional storage methods.[30] Also, storage in solids provides design flexibility of the fuel containers as compared to high-pressure gas cylinders in conventional storage. In addition to this, the waste heat generated from the fuel cells can be utilized for the evolution of hydrogen from the stored solids.

Several hydrides of alkali metals, alkaline metals, transition metals, rare earth metals have been studied for H_2 storing ability over the years.[7, 13, 31] Hydrogen atoms are chemically bonded to the metal in a metal hydride. H_2 is released either by increasing the temperature or decreasing the pressure. Due to their high storage hydrogen capacity, lightweight metal hydrides have attracted much attention. For instance, about 7 wt% H_2 can be stored in simple hydrides such as MgH_2. But these materials do not satisfy the kinetic and thermodynamic requirements for hydrogen uptake and release.[24] Generally, at a temperature and pressure suitable for onboard hydrogen storage, only ~ 2 wt% of H_2 can be stored and released. Thus metal hydrides

in their pure form are not viable as H_2 storage materials for practical applications. Enduring research on modifying these hydride systems is in progress on till date. Johnson *et al*. suggested chemically activated MgH_2 by adding small amounts of $LiBH_4$ as a superior H_2 storage material.[32]

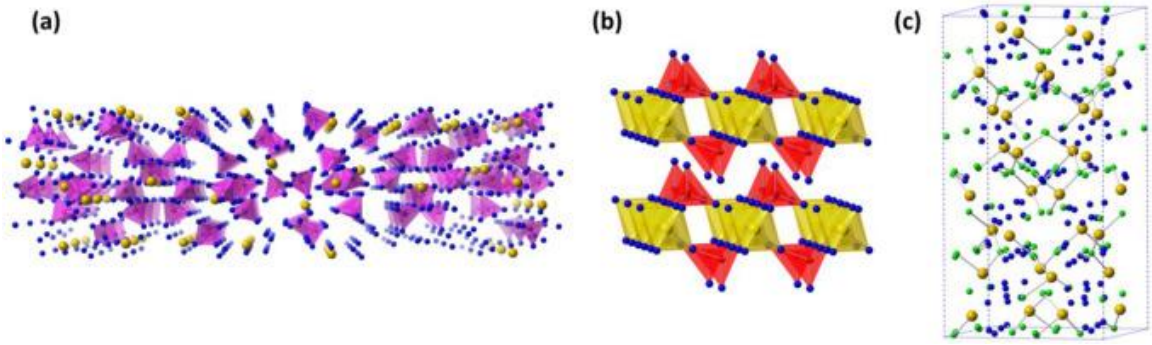

Figure 1.1 Crystal structure of (a) $Mg(BH_4)_2$ with B: purple, Mg: yellow and H:blue; (b) $Mg(AlH_4)_2$ with Al: red, Mg: yellow and H:blue; and (c) $Mg(NH_2)_2$ with N: green, Mg: yellow and H:blue.[33]

Complex hydrides in which hydrogen atoms are covalently bonded to a central atom in an anion complex stabilized by a cation show a better H_2 storage ability than simple hydrides.[24, 25, 31] Alanates, borohydrides and amides are the three classes of complex hydrides. $NaAlH_4$ catalyzed with 2% Ti is one of the well studied, and complex hydride system which could store and release 3.7 wt% H_2 reversibly under mild conditions.[34] Although it offers slow kinetics, the reversibility in the complex hydride marked an advancement in solid-state hydrogen storage. Reversible hydrogen cycling in Ti-catalyzed sodium alanate over 100 cycles with ~ 4 wt% H_2 at 160 °C was revealed by Srinivasan *et al*.[35] The storage capacity of $NaAlH_4$ can be enhanced to 5 wt% by using Ti nanoparticles as doping agents.[36] Using graphite combined with Ti lowers the dehydrogenation temperature by 15 °C compared to $TiNaAlH_4$.[37] In addition to $NaAlH_4$, there are many other alanates such as Na_3AlH_6, $KAlH_4$, K_3AlH_6, K_2LiAlH_6 and K_2NaAlH_6, $LiAlH_4$, Li_3AlH_6, $Mg(AlH_4)_2$, $Ca(AlH_4)_2$, $Ti(AlH_4)_4$, *etc*. Alkali borohydrides have a large decomposition enthalpy and need high temperatures for H_2 release.[25] $LiBH_4$ decomposes to give LiH and B with the release of 13.5 wt% hydrogen at 438°C.[38] Alkaline earth and transition metal borohydrides such as ($Mg(BH_4)_2$,[39] $Ca(BH_4)_2$,[40] $Zr(BH_4)_4$,[41] $Zn(BH_4)_2$[41], *etc.* have been verified for good storage capacities at reasonable

decomposition temperatures. But the problem persists with the reversibility of the system as in the case of some alanates. Amide/imide system reversibly stores hydrogen under moderate reaction temperatures.[42] Chen *et al.* reported that 10.4 wt% hydrogen could be reversibly stored in Li-N-H system.[43] This system offers slow reaction kinetics and requires high temperature for dehydrogenation. Ichikawa *et al.* proved that the addition of $TiCl_3$ improves the reaction kinetics.[44] A mixture of Li_3N and Mg_3N_2 has shown to improve the storage properties with 9 wt% hydrogen.[45] In a recent review by Sun *et al.* Mg based hydrides and complex hydrides have been investigated for their H_2 storage ability.[33] The synthetic strategies and interaction of H_2 with these materials have been discussed in detail. The complex hydride systems with Mg show favourable thermodynamics for H_2 storage. $Mg(BH_4)_2$, $Mg(AlH_4)_2$ and $Mg(NH_2)_2$ show 14.9 , 9.3, and 7.3 wt% gravimetric capacity. The crystal structures of these systems are shown in Figure 1.

Ammonia Borane (AB), H_3NBH_3 has become a captivating candidate for hydrogen storage applications owing to high gravimetric hydrogen density (19.6 wt%), and significant enthalpy (–21 kJ/mol H_2).[46-49] H_2 is released from AB either by thermolysis or by hydrolysis. Developing an energy-efficient chemical process for regeneration of H_3NBH_3 from dehydrogenated B–N–H_x system is a key step for storage application. The increase in hydrogen desorption kinetics by dispersing ammonia borane in nanometer-sized pores of silica relative to the bulk form of ammonia borane has been reported by Gutowska *et al*.[50] The possibility of reversible generation of AB through modified reverse reaction pathways have been demonstrated by Hausdorf *et al*.[51] The regeneration of AB by direct reaction with N_2H_4 and liquid NH_3 has been demonstrated by Sutton *et al.*[52] According to them, the reaction product consisted of 8% hydrazineborane and 92% AB. Nanoconfinement of AB in metal-organic framework has been found to be effective for enhancing the hydrogen release kinetics and preventing the formation of ammonia (Figure1.2).[53] Recent studies show that metal nanoparticle catalysts can be used for hydrogen evolution from AB.[54, 55]

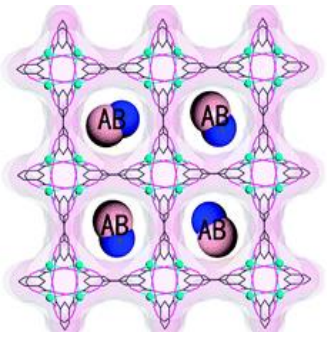

Figure 1.2 3D structure image views of the (001) faces of AB/JUC-32-Y.[53]

1.1.3 Physisorption

Carbon nanostructures, metal–organic frameworks (MOFs), covalent organic frameworks (COFs), and other microporous solids have been proposed as potential materials for H_2 storage *via* physisorption in which van der Waals forces play the major role.[56, 57] Hydrogen gas is adsorbed in molecular form with interaction energy lying in the range 0.24 – 2.4 kcal/mol H_2.[42] Physisorption usually takes place at lower temperature with fast kinetics. Carbon nanostructures with large surface area to volume ratio are extensively investigated for hydrogen storage properties.[58] Hydrogen adsorption in carbon nanotubes has been studied using temperature programmed desorption by Dillon *et al.*[59] A wide variety of carbon nanomaterials in pure form as well as metal decorated moieties have been studied for hydrogen storage ability.[60] The H_2 uptake capacity of these materials ranges from 0.1 wt% to 10 wt% with variation in adsorption temperature and pressure as well as nature metal incorporated in the system.[60-64]

MOFs synthesized by a self-assembly process are crystalline solids with three dimensional framework enclosing uniform pores which are interconnected to form an ordered network of channels have been an interesting candidate for H_2 storage.[42, 65] MOFs contain organic ligands connected to metal ions or small metal containing clusters.[66] The design strategies for enhancing hydrogen adsorption include customizing pore size, preparation of catenating network, impregnating large pores with guest molecules for additional adsorption, *etc.*[67] To date, a large number of MOFs have been synthesized and analyzed for hydrogen adsorption properties. Zn based

MOF-5 with a cubic three-dimensional extended porous structure could adsorb H_2 up to 17.2 H_2 molecules per formula unit (4.5 wt%) at 78 K and 1.0 wt% at room temperature and pressure of 20 bar.[68] H_2 uptake of excess 7.1 wt% at 77 K and 40 bar with total capacities of 10 wt% at 77 K and 100 bar, and 11.5 wt% at 77 K and 170 bar was noted when MOF-5 was prepared under N_2 atmosphere.[69] MOF-505 made up of $Cu_2(CO_2)_4$ units joined by biphenyltetracarboxylic acid linker groups (Figure 1.3) reported by Chen *et al.* could store 2.5 wt% of hydrogen.[70] Farha *et al.* reported the synthesis of NU-100, a MOF with the ultrahigh surface area and high H_2 absorption ability.[71] Furukawa *et al.* developed different MOFs with $Zn_4O(CO_2)_6$ units joined by organic linkers (MOF-180, MOF-200, MOF-205, MOF-210) for adsorption of various gases. Out of these MOFs, MOF-210 showed highest total H_2 storage capacity of 176 mg/g at 77 K and 80 bar.[72] Li *et al.* reported the remarkably enhanced capacity and speed of hydrogen storage in Pd nanocrystals covered with copper based MOF.[73]

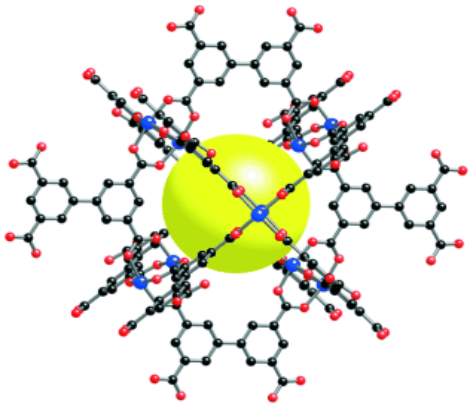

Figure 1.3 The single-crystal X-ray structure of MOF-505 showing Cu blue, C black, O red, and the yellow sphere represents the largest sphere that would occupy the cavity without contacting the interior van der Waals surface.[70]

Other metal ions such as Mn(II), Cr(III), and lanthanides(III), and diverse types of ligands such as carboxylates, imidazolates, triazolates, tetrazolates, *etc.* have been employed for the synthesizing various MOFs.[65] Another class of covalent porous crystalline polymers materials called COFs with elaborate integration of organic building blocks into an ordered structure also used for hydrogen storage.[74, 75] Under same conditions, COFs with larger surface areas possess higher hydrogen uptake

capacities. Among similar 2D COFs with different alkyl chain lengths, COF-18Å having BET surface area of 1263 m^2g^{-1} shows the highest hydrogen uptake of 1.55 wt% at 1 bar, 77 K.[76] Due to the higher surface areas and lower densities, 3D COFs show better hydrogen storage capacity. Of the different COFs, COF-102 shows the largest hydrogen storage capacity of 7.24 wt% at saturation (~35 bar, 77 K).[77, 78] Zheng *et al.* reported that incorporation of undulated macrocyclic cyclotricatechylene enhances the hydrogen storage capacity of 2D COFs.[79] Even though several design strategies and modifications have been made, MOFs and COFs as a hydrogen storage material encounter many practical problems.

Hydrogen can also be encapsulated inside guest molecules such as clathrates and can be released by varying pressure and temperature.[80, 81] A clathrate is a cage compound with a lattice of one type molecule trapping the second type of molecule. Dyadin *et al.* reported hydrogen clathrate hydrates in 1999 which prompted extensive research on other hydrogen clathrates as potential materials for hydrogen storage.[82] Lee *et al.* reported that hydrogen storage capacities in THF-containing binary-clathrate hydrates can be increased to 4 wt% at modest pressures by tuning their composition. The tuning mechanism allows the hydrogen guests to enter both the larger and the smaller cages, while retaining low-pressure stability.[83] Hu and Ruckenstein reported that inclusion of THF as a second guest allows the storage of significant amount of hydrogen with the clathrate stabilized at pressures of only 5 MPa at 279.6 K.[84] Multiple H_2 occupancies of cages of clathrate hydrate by reacting H_2 gas with N_2 hydrate at a temperature of 243 K and a pressure of 15 MPa.[85] H_2 storage using clathrates needs extensive research for practical applications especially to stabilize the clathrates under reasonable operating conditions.

Another class of microporous aluminosilicate networks called zeolites had received interest as possible hydrogen storage candidates.[86] Zeolites have cavities of the molecular sieves of different pore architecture and are known for their high thermal stability, low cost and adjustable composition.[87] H_2 molecules are forced to move into these cavities by applying high pressure at elevated temperatures. When cooled to room temperature, H_2 gets trapped inside the cavity and is released by raising the temperature of the system. Li and Yang studied the H_2 storage capacity of low silica type

X zeolites. They have shown that the hydrogen uptake was enhanced by a factor of 2.6 by building carbon bridges to facilitate hydrogen spillover.[88] Palomino *et al.* have shown that magnesium-containing porous materials are good candidates in the search for suitable adsorbents for reversible hydrogen storage.[89] Dong *et al*. investigated the H_2 storage properties of several zeolites at 77 K and pressures in the range 0–1.6 MPa.[90] The noted H_2 storage capacities were up to 2.07 wt% on zeolite Na-LEV, 1.75 wt% on zeolite H-OFF, 1.64 wt% on zeolite Na-MAZ and 1.02 wt% on zeolite Li-ABW. Almasoudi and Mokaya reported that activated carbon nanocast prepared from zeolitic imidazolate framework with enhanced micropore surface area and micropore volume show high hydrogen storage density in the range 13.0–15.5 μmol H_2 m^{-2}, which is much higher than the majority of high surface area activated carbons.[91] Even though there are several significant reports on H_2 storage in zeolites, from the capacity point of view zeolites are not yet the right candidates to be used for automotive purposes.

1.1.4 Fundamental Interactions of H_2 with Storage Material

The nature, strength, and mechanism of fundamental interaction of H_2 with the storage material play an important role in determining storage ability of the material.[92] If the interaction is very strong, extreme conditions are required to release H_2, or an irreversible condition may occur due to the chemical interaction of H_2 with the storage material. On the other hand, if the interaction of H_2 with the storage material is very weak, it can result in a lower rate of H_2 sorption at reasonable temperatures. For attaining DOE targets, interaction energy (E_{int}) of 5 – 10 kcal/mol is desirable. Hence, to accomplish improved hydrogen storage materials, a meticulous knowledge about the interaction mechanism of H_2 with storage material is required. Computational studies are of great implication for understanding such interactions and making reliable predictions.

The interaction of dihydrogen with the storage material can be broadly classified into four classes, *viz*. electrostatic, van der Waals, orbital and non-classical σ-bonding interactions.[93-95] These interactions play a key role in designing new materials for storing hydrogen. In general, the H_2 adsorption capacity of materials due to van der Waals interactions is very poor whereas the electrostatic interactions due to charged

centers provide high adsorption capacity.[96-98] The orbital and σ-interactions are mainly found in metal-dihydrogen complexes.[93, 99] Such complexes are stabilized by synergistic bonding interaction, *i.e.,* a forward donation of electron density from H-H σ bond (HOMO) to low lying vacant d orbital of the metal and back donation of electron density from the metal orbital to the vacant σ*orbital of H_2 leading to the H-H bond activation.[92, 93, 100] The side-on contact of H_2 molecule with the metal cation results in a T-shaped complex (Figure 1.4).[101]

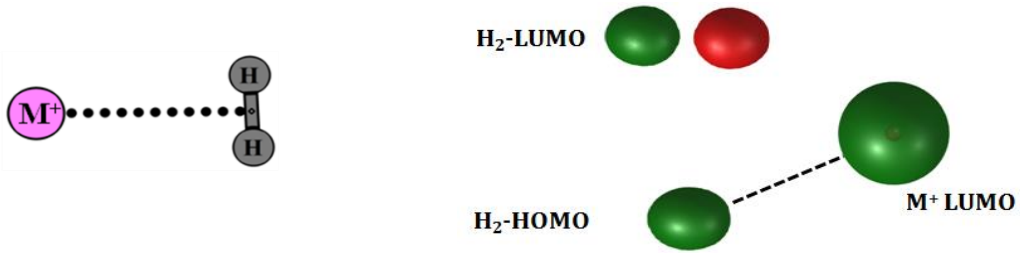

Figure 1.4 (a) Geometry of $M^+...H_2$ complex (b) Schematic representation of orbital interaction of H_2 with Li^+ cation.

In the case of anions, the LUMO of the H_2 molecule accepts electrons from the anion inducing a dipole on H_2 and results in a charge-induced dipole interaction and the resultant complex show end-on coordination (Figure 1.5). [102-105] The E_{int} of $M^+...H_2$ is in the range 5 – 40 kcal/mol for various alkali, alkaline, and transition metals whereas for $X^-...H_2$ systems the E_{int} is found to be in the range 2 – 8 kcal/mol.

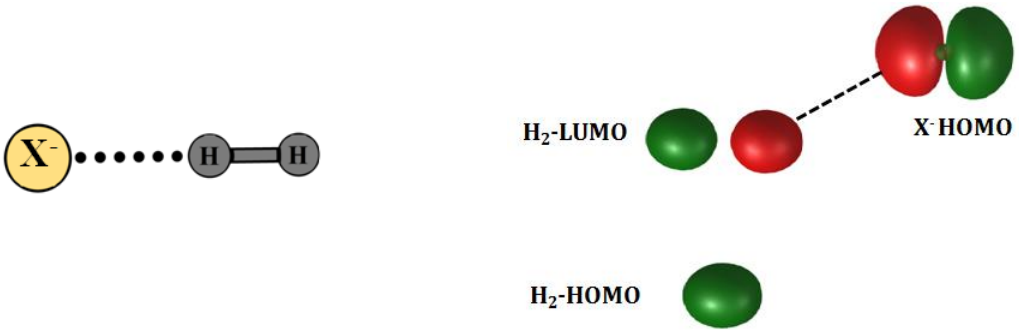

Figure 1.5 (a) Geometry of $X^-...H_2$ complex (b) Schematic representation of the orbital interaction of H_2 with F^- anion.

Studies focusing on the interaction of H_2 with anions are rather limited compared to that of cations. These studies include H_2 complexes of halides, cyanide, sulphate, *etc.* which will be further discussed in detail in Chapter 2 of this thesis.

Metal-H_2 interactions have been studied for the last five decades. In 1970, Clampitt and Jeffries produced $Li^+(H_2)_n$ clusters by the treatment of a solid H_2 source with a Li^+ ion beam.[106] Since then the H_2 complexes of cations have been investigated widely using both experimental and theoretical methods. Some of the relevant theoretical works include the studies focusing on structure and energetics of $M^+...H_2$ complexes of Li^+,[107, 108] Na^+,[109] K^+,[109] B^+,[110] Al^+,[111] Sc^+,[112] Ti^+,[113] V^+,[114] Cr^+,[115] Fe^+,[116] Co^+,[117] Ni^+,[118] Cu^+,[119] Zn^+ [120] *etc*. In a recent review by Dryza and Bieske, the infrared spectroscopic studies on $M^+...H_2/D_2$ complexes of alkali metals, alkaline earth metals, and transition metals have been discussed.[103] The fundamental information on the $M^+...H_2/D_2$ is obtained by resolving the rotational structure. The influence of size and electronic structure of the cation on the nature of the H_2 bonding is conferred in this review. In a theoretical work by Lochan and Head-Gordon, the H_2 binding interactions of cations such as Li^+, Na^+, Mg^{2+}, and Al^{3+} are discussed.[92] According to their reports, interaction energy varies over a wide range of ~ 3 - 55 kcal/mol and the $M^{n+}...H_2$ interaction distance decreases in the order $Na^+ > Li^+ > Mg^{2+} > Al^{3+}$. Studies on $M^+(H_2)_n$ complexes of alkali metal cations unveil that the complexes from n = 1 - 6 adopt T-, linear, triagonal planar, tetrahedral, triagonal bipyramidal and octahedral arrangement of H_2 around the cation, respectively.[92, 102, 107, 108] Apart from metals, metal complexes such as MgF_2, MgS, AlF_3, BeO, and BeS have been theoretically investigated for their H_2 binding capacity with the E_{int} varying from 1.2 to 17.3 kcal/mol.[121-123] Among these systems BeS and BeO showed stronger interaction with H_2. Davy *et al.* reported that like Li^+ ion, LiH^+ and LiH form H_2 complexes with E_{int} 6.0 and 2.5 kcal/mol, respectively.[108] The large charge/size ratio of the Li^+ ion results in the formation of complexes with multiple H_2 molecules. These spectroscopic and theoretical studies on the interaction of bare cations give much insight into the intermolecular forces underlying hydrogen storage in various materials containing metal cations.

1.1.5 Theoretical Studies on Hydrogen Storage

The search for new materials for hydrogen storage materials with acceptable properties can be realized by the synergy between theory and experiment.[124] Computational simulations can help in understanding the properties of storage materials and modifications for improving the storage capacity. Several hierarchical computational methods have been used for evaluating the binding strength, nature, and mechanism of H_2 with storage material.[95] *Ab initio* and density functional theory (DFT) calculations are mainly used to investigate binding energies of H_2 with the storage material. Grand canonical Monte-Carlo (GCMC) simulations are done to predict the H_2 uptake and molecular dynamics (MD) simulations to study H_2 diffusion in the storage system.[125, 126] Computational studies on hydrogen storage gained much attention during the last two decades owing to the efficiency and predictive power of computational affords[127]. These studies are briefly discussed in the following sections.

1.1.5.1 *Ab initio* and DFT Studies on H_2 Binding

Hamel and Côté studied the adsorption of H_2 on benzene with different methods such as WS77, CCSD(T), MP2, LDA, and PBE.[128] The geometry in which H_2 is perpendicular to the plane of the benzene ring emerged as the most favorable adsorption geometry in all first-principle calculations. Hüber *et al.* studied the interaction of H_2 with the aromatic systems such as benzene, naphthalene, anthracene, coronene, *etc.* at the MP2/TZVPP level of theory.[129] The E_{int} reported for benzene and naphthalene are 0.9 and 1.0 kcal/mol, respectively showing that as the size of aromatic system increases, the interaction energy increases. Using DFT and MP2 methods, Sagara *et al.* compared the H_2 binding energies of metal oxide part and organic linker part of MOF-5, and showed that the zinc oxide cluster (1.6 kcal/mol) has a higher H_2 binding energy than the organic linker part (1.2 kcal/mol).[130] In their calculations, Dunning basis sets aug-cc-pVTZ, and aug-cc-pVQZ were used, and the results were extrapolated to the basis set limit for higher accuracy. Theoretical studies using MP2 calculations by the same group has reported that the larger linkers have higher E_{int} and enhanced surface area available for H_2 binding in MOFs.[131] Also, the addition of $-CH_3$ or $-NH_2$ groups to the linker enhances the E_{int} by 33%. Buda and Dunietz have investigated chemically modified models of organic

linkers in MOF calculations for improving the uptake properties at the MP2 level of theory.[132] By employing MP2, CCSD(T), and PW91 levels of theory Negri and Saendig studied binding properties of H_2 to polar aromatic molecules which are model systems for the metal-oxide corner of MOFs showing promising H_2 storage ability.[133] The interaction of H_2 with IRMOF-1 family was explored by Klontzas *et al.* at PBE and MP2 levels of theory.[134] According to their study, the E_{int} of H_2 with the inorganic part of IRMOF-1 is in the range 0.13 - 0.74 kcal/mol, which can be recognized as dipole-induced dipole forces. Han *et al.* reported The improvement of MOF by increasing the aromatic content of the organic linkers and by replacing Zn with Mg was reported by Han et al. in a theoretical study at RI-MP2/TZVPP level.[135] Their studies showed that Mg-MOF-C30 could achieve 8.08 wt% storage at 77 K and 0.33 wt% at 300 K.

Sagara and Ganz calculated the E_{int} of H_2 with various Be and B doped carbon nanostructures at MP2/TZVPP level.[136] The E_{int} 4.2 and 2.9 kcal/mol observed for $C_{11}H_8Be$ and $C_{16}Be_2H_8$, respectively indicated that these systems are noteworthy for storage applications. The qualitative assessment of the role of the fundamental non-bonding interactions between H_2 and MOFs at MP2/cc-pvTZ level have been reported by Kuc *et al*.[137] Prakash *et al.* reported the H_2 storage capacity of alkali metal ion (Li^+, Na^+, and K^+) decorated boric acid based bowl, sheet and ball structures have been investigated at B3LYP/6-31+G** level.[138] The maximum gravimetric density of 8.8 wt% was observed for bowl-shaped Na^+ complexes and these systems have been suggested for storage applications. Srinivasu *et al.* explored the H_2 storage ability of bimetallic clusters such as Be_3M_2, Mg_3M_2 and Al_4M_2 (M = Li, Na, and K) using *ab initio* and DFT methods. Be_3M_2 and Al_4M_2 classes showed H_2 uptake in the range 9.4 – 22.6 wt % whereas the Mg_3M_2 compounds exhibited poor H_2 uptake.[139] Using DFT studies Sun *et al.* reported that $Li_{12}C_{60}$ could store 60 H_2 molecuels with substantial interaction energy. These systems could store 9 wt% of H_2 and could be proposed as a potential solid state storege material (Figure 1.6).[140] Pan *et al.* reported the potential H_2 storage ability of lithium decorated star-like clusters and super-alkali systems at M06/6-311+G(d,p) and the M052X/6-311+G(d) levels of DFT.[141] Kumar *et al.* reported the DFT studies using M05-2X, wB97xD, and M06 methods on improving the hydrogen storage capacity of MOF by chemical functionalization.[142] Using DFT methods, Rahali *et al.* predicted that Pb(II)

based MOF could be a good candidate for H_2 storage by physisorption with E_{int} varying between 3.2 and 2.5 kcal/mol.[143]

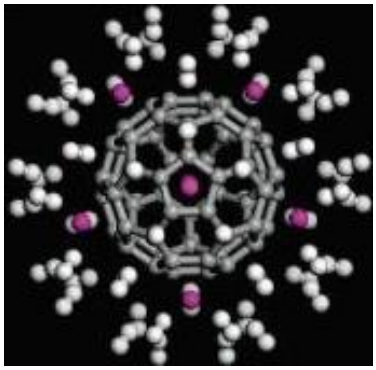

Figure 1.6 Adsorption of H_2 on $Li_{12}C_{60}$.[140]

Yildirim and Ciraci reported a first-principles study on dissociative adsorption of H_2 on Ti decorated single-walled carbon nanotube (SWCNT) binds up to four hydrogen molecules. A gravimetric capacity of 8 wt% H_2 was is observed on these SWCNT with high Ti coverage (Figure 1.7).[144] Shalabi *et al.* reported DFT study on Ti functionalized carbon nanocones and carbon nanocone sheets as potential H_2 storage materials at wb97xd/6-31g(d,p) level of theory.[145] The thermodynamic properties of these systems meet the DOE targets with 9.3 – 11.0 wt% of gravimetric capacity. Gopalsamy and Subramanian studied the H_2 storage capacity of alkali (Li^+, Na^+, and K^+) and alkaline earth metal ion (Mg^{2+} and Ca^{2+}) doped cubane, cyclohexane and adamantane at M05-2X/6-31+G** level of theory.[146] The number of H_2 adsorbed depends on the ionic radii and charge of the metal ions. Among all the complexes studied, Mg^{2+} ion doped systems showed higher binding energy per H_2 in the range 8.1 - 9.3 kcal/mol with gravimetric density 4.8 – 7.3 wt%. Using PBE method Tang *et al.* proposed that by doping $C_{48}B_{12}$ fullerene with transition metals such as Fe, Co, Ni could enhance the H_2 storage ability.[147] These metal decorated systems could bind with 48 – 60 H_2 molecules with 6.8 – 8.7 wt% of gravimetric capacity. The interaction energy per H_2 ($E_{int/H2}$) of these complexes are in the range 7.3 – 11.5 kcal/mol.

Konda *et al.* reported 6.2 – 6.5 wt% H_2 uptake of transition metal atom (Sc, Ti, and V) decorated closoborate (B_6H_6) using MP2, M06, and B3LYP methods with 6-311++G** basis set.[148] Er *et al.* studied the functionalization of boron heterofullerenes with Ca atoms

for high density H_2 storage using DFT methods and found that the binding energies are in the range needed for onboard hydrogen storage, yielding 7.1 wt% H_2.[149]

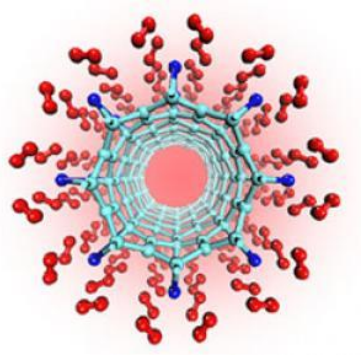

Figure 1.7 Dissociative adsorbtion of H_2 on Ti decorated SWCNT.[144]

Computational studies at PBE/6-31G(d,p) level by Kalamse *et al.* revealed that Ti functionalized naphthalene complexes have stronger interaction with hydrogen molecules than Li functionalized complexes.[150] $C_{10}H_8Ti_4$ and $C_6B_4H_8Ti_4$ could adsorb 16 and 14 H_2 respectively with high gravimetric uptake capacity. *Ab initio* study on hydrogen interaction with calcium decorated silicon carbide nanotube by Gueriba *et al.* proposed Ca/SiCNT as the good H_2 storage material.[151] This system could hold 7 H_2 for one calcium decoration with E_{int} 5.1 kcal/mol E_{int} for the first interacting H_2.The E_{int/H_2} decreases with increase in a number of adsorbed H_2. Guo and Wang investigated the structures and hydrogen storage capacities of $B_6Ti_3^+$ using PBE/6-311G(d,p) and found that the most stable cluster ($B_6Ti_3^+01$) could maximally adsorb 10 H_2 which corresponds to 8.82 wt% gravimetric capacity.[152] Tavhare *et al.* reported the hydrogen adsorption properties of Be and Sc doped pentalene at MP2/6-311++G** level.[153] The Be complexes showed an H_2 uptake capacity less than DOE targets whereas Sc complexes showed a notable uptake in the range 7.8 - 8.8 wt%. All these theoretical works establish that *ab initio* and DFT theories are very useful in predicting the thermodynamic properties of the storage systems.

1.1.5.2 GCMC Simulations on H_2 Uptake Capacity

Sagara *et al.* studied the H_2 uptake in MOF-5 by GCMC simulation and showed that in comparison to an experimental result, a simulated H_2 loading curve up to 1 bar at 78 K was overestimated by 25%.[154] Yang and Zhong simulated the H_2 adsorption isotherms

for a set of MOFs (IRMOF-1, -8, and -18) using GCMC simulations.[155] Garberoglio *et al.* calculated H_2 adsorption isotherms of different MOFs such as MOF-2, -3, IRMOF-1, -6, -8, and -14 using GCMC simulations.[156] Frost *et al.* studied the effects of heat of adsorption on H_2 uptake, surface area, and free volume in MOFs and found that hydrogen uptake correlates with heat of adsorption, surface area, and free volume at low (0.1 bar), intermediate (30 bar), and high pressure (100 bar).[157] Using GCMC simulations Jung *et al.* showed that the H_2 adsorption capacity of interpenetrating MOFs could be higher than that of the non-interpenetrating ones because the small pores generated by catenation can play a role in dense confinement of H_2 molecules.[158] Ryan *et al.* also reported the role of catenation in improving the H_2 uptake at cryogenic temperatures and low pressures.[159] The synthesis and GCMC simulations on MOF UiO-66 by Zhao *et al.* showed an H_2 uptake of 3.35 wt% at 77 K and 1.8 MPa.[160] Meng *et al.* proposed Li-doped IRMOF-9 could achieve H_2 storage of 4.91 wt% at ambient conditions.[161] Using *ab inito* and GCMC simulation methods Volkova *et al.* modeled Li-containing MOFs with 6.6 wt% of H_2 at 300 K and 100 bar.[162] GCMC simulation study by Gopalsamy *et al.* showed that IRMOF-1 with rhombus shaped carbon flakes as linkers have an enhanced H_2 binding affinity.[163]

Garberoglio simulated H_2 adsorption isotherms of 3D COFs such as COF-102, -103, -105, and -108 and found that COF-105 showed a maximum uptake of ~ 10.5 wt% at 77 K.[164] In a similar work, Klontzas *et al*. predicted that the gravimetric uptake for COF-108 reaches a value of 21 wt% at 77 K and 100 bar and 4.5 wt% at room temperature and 100 bar.[165] Garberoglio and Vallauri simulated the H_2 uptake in 2D COFs such as COF-6, COF-8, and COF-10.[166] According to their findings, gas diffusion in 2D COFs is one order of magnitude more rapid than in MOFs or zeolites. Using a multiscale theoretical method by combining the first-principles calculation and GCMC simulation, Lan *et al.* investigated the H_2 adsorption capacities of Li-doped COF-202 and found that this system could be a promising candidate for H_2 storage with 4.39 wt% of gravimetric capacity.[167] Papadimitriou *et al.* studied the H_2 storage capacity of clathrate hydrates using GCMC simulations.[168] Their studies recommended that hydrates without promoters could store more H_2 than promoter-stabilized hydrates. Li *et al.* proposed that H_2 binding energy of COF can be enhanced by a factor of four by substituting the bridge rings with various metal-containing rings.[169] Assfour *et al.* reported *ab initio* and

GCMC studies on H_2 storage on zeolite imidazolate framework and found that ZIF-20 could store ~ 5 wt% of H_2 at moderate and high pressures(> 10 bar).[170] Using DFT and GCMC, Guo *et al.* designed Li-doped fullerene-intercalated phthalocyanine covalent organic frameworks for H_2 storage.[171] Similarly, DFT and GCMC combined studies by Xia and Liu proposed Li-doped COF-320 as a potential storage material.[172]

Blanco *et al.* studied the micropore volume, pore size distribution, and differential isosteric enthalpy of adsorption for H_2 and CH_4 storage in activated carbon monoliths.[173] With the aid of GCMC simulations Burress *et al.* showed that graphene oxide could be easily turned into a potentially useful H_2 storage material.[174] GCMC simulations by Cho *et al.* showed that the H_2 storage capacity of 10 at% Si-doped single-walled carbon nanotube (Si-CNT10) could reach a maximum of 2.5 wt%, which is almost twice the storage capacity of undoped SWCNTs.[175] Studies on energetics, mechanical and sorption properties of packings constructed out of (6,0) and (5,5) carbon nanotubes by Assfour *et al*. proposed that these materials are good candidates for H_2 storage.[176] Lu *et al.* suggested that doping porous graphene with metals could enhance the H_2 storage capacity. Their GCMC simulations showed that Li- and Ca-decorated 2B-PG possess 6.4 and 6.8 wt% of gravimetric capacities respectively at at 298 K and 100 bar.[177] Using GCMC simulations Firlej *et al.* modeled truncated carbon slit pores with increased H_2 gravimetric storage capacity.[178] Colón *et al.* assessed the H_2 storage capacity of Mg functionalized porous crystalline materials using GCMC and quantum mechanical approaches and have shown that the introduction of an optimum amount of magnesium alkoxide could be a promising strategy to improve hydrogen uptake and delivery near ambient temperature.[179] Mahdizadeh and Goharshadi reported a combined quantum mechanics and GCMC study on H_2 storage on silicon, carbon, and silicon carbide nanotubes and the results suggested carbon nanotubes as better storage materials.[180] Tylianakis *et al.* designed novel nanoporous architectures of carbon nanotubes called super diamond with tunable pore size and surface area.[181] These materials possess gravimetric H_2 storage capacity of > 20 wt% at 77 K and 8 wt% at room temperature. A multi-scale approach combining first-principles calculations and GCMC simulations reported by Zhu *et al.* proposed Li-doped g-C_3N_4 porous sheet with 4.50 wt% gravimetric capacity at 298 K and 100 bar, as potential H_2 storage

material.[182] Ozturk *et al.* performed GCMC simulations to investigate the H_2 adsorption on sandwiched graphene-fullerene composite and the effect of Li doping on adsorption.[183] Li-doped systems showed a gravimetric capacity of 5 wt% whereas undoped systems showed 3.83 wt% at 77 K and 1 bar. GCMC approach is a powerful tool for studying gas storage in various systems. The results obtained using GCMC simulations show good concordance with experimental data.

1.1.5.3 MD Simulations on H_2 Diffusion

Yang and Zhong reported the MD simulation on the diffusion of H_2 molecules in MOFs such as IRMOF-1, -8, and -18. Their calculation on self-diffusivity of H_2 as a function of pressure at 77 K showed that the diffusion of H_2 in IRMOF-18 is much lower than diffusion in the other two MOFs.[184] Skoulidas and Sholl calculated the self-diffusivity and transport diffusivity of H_2 adsorbed in the IRMOF-1 as a function of pressure at room temperature.[185] The self-diffusivity of H_2 in IRMOF-1 decreases with increase in pressure whereas the transport diffusivity increases monotonically. In their studies on different type of MOFs, Liu *et al.* reported that at room temperature, H_2 diffusivity is reduced by a factor of 2 to 3.[186] Salles *et al.* studied the self-diffusivity of H_2 in MIL-47(V) and MIL-53(Cr) MOFs and found that the hydrogen diffusivity at low pressure is about two times that of zeolites.[187] Garberoglio and Vallauri studied the H_2 diffusion in COFs such as COF-6, -8, and -10.[166] According to their calculations H_2 diffusion in COFs is much faster compared to MOFs.

Bhattacharya *et al.* reported an *ab initio* MD simulation for transition metal decorated defected graphene structure and showed that the system could store 5.1 wt% of H_2 at room temperature.[188] MD simulations by Jalili *et al.* showed that Pd-decorated SWCNT bundles had enhanced H_2 adsorption/desorption capacity than bare ones.[189] Wu *et al.* studied the adsorption of H_2 on a 3D-pillared graphene structure and the effect of pressure, temperature, and geometric structure of pillared graphene on hydrogen storage capacity using MD simulations.[190] As per their results, a low temperature, a high pressure, and a large gap between graphene sheets could result in maximum storage capacity. With the aid of MD simulations, Liu *et al.* demonstrated that hydrogen storage and release could be made easier by bending carbon nanotubes at

room temperature.[191] Hu *et al.* predicted 2D-Ti_2C and 2D-Sc_2C as a reversible and high-capacity hydrogen storage material.[192, 193] *Ab initio* MD simulations confirmed that 2D-Ti_2C and 2D-Sc_2C could store 3.4 and 3.6 wt% H_2 by Kubas-type interactions that can be adsorbed and released reversibly at ambient conditions. Jiang *et al.* reported MD simulations on novel 3D carbon systems called pillared bilayer graphene bubble structure.[194] These systems showed a gravimetric H_2 capacity of 21.3 wt%. Using MD calculations, Faginas-Lago *et al.* demonstrated that SWCNTs with larger diameter possess high H_2 storage capacity.[195] This could be attributed to the high surface area offered by large diameter of the tube. In all these studies, MD simulations provide the kinetic properties of the systems which are very important for designing storage materials.

Part B: Computational Chemistry

1.2 An Overview of Computational Chemistry

Computational chemistry is a branch of theoretical chemistry in which computer-assisted simulations of molecules and molecular behavior are done using mathematical calculations based on the fundamental laws. Quantum mechanics based on Schrödinger equation and classical mechanics based on Newton's equation of motion are the two basic theories in computational chemistry. *Ab initio* quantum chemical methods, density functional theory (DFT) methods, semiempirical methods, molecular mechanics (MM), molecular dynamics (MD), and hybrid quantum mechanics/molecular mechanics (QM/MM) methods are important computational methods. Any system in quantum mechanics is represented by a wavefunction. The wavefunction is obtained by solving Schrödinger wave equation, and any property of the system is obtained by applying suitable operators on the wavefunction. To solve the wavefunction for any system other than hydrogen atom, different approximations are used. Semiempirical methods are derived from experimental data and use approximations and empirical parameters.[196-198] Calculations using these methods involve less computational cost and apply to large molecular systems. *Ab initio* which means "from first principles" based on Schrödinger equation uses several constants such as speed of light, mass, and charge of electrons, Plank's constant, *etc*. These methods are very accurate, but the high computational demand restricts the applicability to smaller systems. In DFT, the total energy of a system is represented as a functional of electron density. DFT methods maintain a good balance between accuracy and computational cost and apply to atoms, molecules, clusters, solids, quantum and classical fluids, *etc*. The Newtonian force field is used in MM where atoms are considered as balls and bonds as spring (ball and spring model).[199-202] Molecular mechanics deals with vibrational and conformational motions of large molecules such as molecular systems ranging in size and complexity from small to large biomolecules. In MD simulations atoms and molecules are allowed to interact for a fixed period of time and the physical movements of these particles are calculated using Newton's equations of motion for a system of interacting particles. MM force

fields or interatomic potentials are used for calculating forces between the particles and their potential energies.

In computational chemistry, various models, functions, and approximations are used for understanding the concepts of molecular bonding, solving chemical problems such as predicting the reaction feasibility and reaction mechanism pathways.[203, 204] The available computational chemistry methods range from very precise ones viable for small systems to very approximate methods for larger systems. Nowadays, the handling of molecules ranging from the small to large biological systems with better accuracy at the lower cost of time has been realized due to the rapid development of the computational facilities. Thus computational chemistry has become exciting and fast-emerging field that has become crucial for most advances made in chemistry these days.

1.2.1 *Ab initio* Quantum Chemical Methods

The electronic structure of matter is described using time-independent non-relativistic Schrödinger equation[205], which in its simplest form is

$$H\Psi = E\Psi \qquad \text{(Eq. 1.1)}$$

where H is the Hamiltonian operator, Ψ is the N-body wave function and E is the energy eigenvalue of the system. The Hamiltonian operator for a system of N electrons and M nuclei consists of electronic and nuclear kinetic energy operators and the potential energy operators corresponding to nuclear-electron and electron-electron, and nuclear-nuclear interactions and may be written in the atomic unit as:

$$H = -\sum_{i=1}^{N}\frac{1}{2}\nabla_{i}^{2} - \sum_{A=1}^{M}\frac{1}{2M_A}\nabla_{A}^{2} - \sum_{i=1}^{N}\sum_{A=1}^{M}\frac{Z_A}{r_{iA}} + \sum_{i=1}^{N}\sum_{j>i}^{N}\frac{1}{r_{ij}} + \sum_{A=1}^{M}\sum_{B>1}^{M}\frac{Z_A Z_B}{R_{AB}} \qquad \text{(Eq. 1.2)}$$

where M_A is the ratio of the mass of the nucleus A to the mass of an electron, Z_A is the atomic number of nucleus A, r_{ij} is the distance between the i^{th} and j^{th} electrons and R_{AB} is the distance between A^{th} and B^{th} nuclei.

Several approximations are made to solve the Schrödinger equation for molecular systems, the most common and reasonable one being the Born Oppenheimer (BO) approximation.[206] Nuclei are much heavier than electrons and they move very

slowly. The nuclear and electronic motions can be separated as both of these take place at different time scales. According to BO approximation, a moving electron feels relatively static nuclei, and thus the nuclear kinetic energy term in Eq. 1.2 becomes zero, and the repulsion term between the nuclei becomes a constant. The electronic Hamiltonian can be written as:

$$H_{\text{elec}} = -\sum_{i=1}^{N}\frac{1}{2}\nabla_i^2 - \sum_{i=1}^{N}\sum_{A=1}^{M}\frac{Z_A}{r_{iA}} + \sum_{i=1}^{N}\sum_{j>i}^{N}\frac{1}{r_{ij}} \qquad \text{(Eq. 1.3)}$$

The corresponding Schrödinger equation becomes:

$$H_{\text{elec}}\Phi_{\text{elec}}\left(\{\mathbf{r}_i\};\{\mathbf{R}_A\}\right) = E_{\text{elec}}\Phi_{\text{elec}}\left(\{\mathbf{r}_i\};\{\mathbf{R}_A\}\right) \qquad \text{(Eq. 1.4)}$$

where, $\{\mathbf{r_i}\}$ represents the position of electrons and $\{\mathbf{R_A}\}$ the positions of nuclei. The solution to Eq. 1.4 gives the electronic wave function represented as a product of electronic and nuclear counterparts:

$$\Psi\left(\{\mathbf{r}_i\};\{\mathbf{R}_A\}\right) = \Phi_{\text{elec}}\left(\{\mathbf{r}_i\};\{\mathbf{R}_A\}\right)\Phi_{\text{nuc}}\left(\{\mathbf{R}_A\}\right) \qquad \text{(Eq. 1.5)}$$

The electronic wavefunction which describes the motion of electrons depends unambiguously on the electronic coordinates and parametrically on nuclear coordinates. Thus the separation of electronic and nuclear Hamiltonians, as well as their corresponding wavefunctions is achieved using BO approximation. Any experimental observable can be calculated as the expectation value of appropriate operator, once the wave function Ψ is known from the Schrödinger equation. Approximations are required to get qualitatively correct solutions to the many-body Schrödinger equation as an exact solution is not so easy.

1.2.1.1 Hartree-Fock Theory

Hartree–Fock (HF) method is the most imperative type of *ab initio* calculation that uses BO approximation to solve Schrödinger wave equation for obtaining an approximate solution.[207-209] In HF approximation, the total electronic energy of an N electronic system is calculated, by assuming that the electrons are non-interacting and the total Hamiltonian can be expressed as a sum of one electron Hamiltonians as given by Eq. 1.6

where *H* is total Hamiltonian of a many-electron system, and *h* is single electron Hamiltonian:

$$H = \sum_{i=1}^{N} h(i) \qquad \text{(Eq. 1.6)}$$

The wavefunction of the system is obtained as a simple product of single electron spin-orbital wavefunctions as given by Eq. 1.7, χ'_{i} represents one electron wavefunctions with spatial and spin coordinates $\mathbf{x}_{\mathrm{i}}$.

$$\Psi^{\mathrm{HP}}(\mathbf{x}_1, \mathbf{x}_2, ..., \mathbf{x}_N) = \chi_i(\mathbf{x}_1)\chi_j(\mathbf{x}_2).....\chi_k(\mathbf{x}_N) \qquad \text{(Eq. 1.7)}$$

This N electron wavefunction referred to as Hartree product is an independent electron wavefunction, *i.e.*, the probability of finding one electron at a position is independent of the position of other electrons. But in reality, the electronic motion is correlated as they experience coulombic repulsion due to the same charge. The Ψ^{HP} is an eigenfunction of the total Hamiltonian *H,* and the sum of the energies of each spin-orbitals, eigenvalue *E* is given by Eq. 1.8.

$$E = \varepsilon_i + \varepsilon_j + ... + \varepsilon_k \qquad \text{(Eq. 1.8)}$$

The N electron wavefunction must be antisymmetric concerning the interchange of both spatial and spin coordinates of any two electrons. The Hartree product does not obey this antisymmetry principle. The N electron wavefunction, when written as an anti-symmetrized product of spin orbitals in the form of Slater determinant, solves the problem.

$$\Psi(\mathbf{x_1}, \mathbf{x_2}, ..., \mathbf{x_N}) = \frac{1}{\sqrt{\mathrm{N!}}} \begin{vmatrix} \chi_{\mathrm{i}}(\mathbf{x_1}) & \chi_{\mathrm{j}}(\mathbf{x_1}) ..... & \chi_{\mathrm{N}}(\mathbf{x_1}) \\ \chi_{\mathrm{i}}(\mathbf{x_2}) & \chi_{\mathrm{j}}(\mathbf{x_2}) ..... & \chi_{\mathrm{N}}(\mathbf{x_2}) \\ ... & ... & ... \\ \chi_{\mathrm{i}}(\mathbf{x_N}) & \chi_{\mathrm{j}}(\mathbf{x_N}) ..... & \chi_{\mathrm{N}}(\mathbf{x_N}) \end{vmatrix} \qquad \text{(Eq. 1.9)}$$

where $\frac{1}{\sqrt{\mathrm{N!}}}$ is a normalization factor. Also, the electrons are all indistinguishable, and the motion of electrons with parallel spins is correlated when the many-electron wave

function is represented in Slater determinant form.[207, 209] The normalized Slater determinant can also be represented in a shorter notation as given in Eq. 1.0.

$$\Psi(\mathbf{x_1},\mathbf{x_2}.....\mathbf{x_N}) = \left| \chi_i \chi_j .....\chi_N \right\rangle \qquad \text{(Eq. 1.10)}$$

The variational method is one approach to find approximations to the lowest energy eigenstate or ground state. According to the variational principle, the wavefunction that gives the lowest possible energy is calculated as:

$$E_0 = \left\langle \Psi_0 \middle| H \middle| \Psi_0 \right\rangle \qquad \text{(Eq. 1.11)}$$

The energy can be minimized by choice of appropriate spin orbitals χ_i. By minimizing the energy, an eigenvalue equation called Hartree-Fock equation can be derived, which is given as:

$$f(i)\chi(\mathbf{x}_i) = \varepsilon\chi(\mathbf{x}_i) \qquad \text{(Eq. 1.12)}$$

where *f(i)* is an effective one-electron operator, called the Fock operator, of the form:

$$f(i) = -\frac{1}{2}\nabla_i^2 - \sum_{A=1}^{M}\frac{Z_A}{r_{iA}} + V^{HF}(i) \qquad \text{(Eq. 1.13)}$$

The term $V^{HF}(i)$ is called the Hartree–Fock potential which is the average potential experienced by the i^{th} electron due to the remaining electrons. Thus in HF approximation, the complicated many-electron problem is replaced by a one-electron problem, as the electron repulsion is treated in an average way. The Fock operator depends on its eigenfunction as the potential $V^{HF}(i)$ depends on the spin orbitals of the remaining electrons.

The HF potential for the electron (1) is defined as:

$$V^{HF}(1) = \sum_{j}^{N}\left(J_j(1) - K_j(1)\right) \qquad \text{(Eq. 1.14)}$$

where the Coulomb operator J_j accounts for the Coulombic repulsion between the electrons and the exchange operator K_j represents the quantum correlation due to Pauli exclusion principle.

$$J_j(1) = \int d\mathbf{x_2} \left|\chi_j(2)\right|^2 \frac{1}{r_{12}} \qquad \text{(Eq. 1.15)}$$

$$K_j(1)\chi_i(1) = \left[\int d\mathbf{x_2}\chi_j(2)\frac{1}{r_{12}}\chi_i(2)\right]\chi_j(1) \qquad \text{(Eq. 1.16)}$$

Roothaan and Hall derived the HF equations for closed shell systems.[210, 211] The HF equation in (Eq. 1.12) may be rewritten by substituting (Eq. 1.17), where the spin-orbital is expressed as the linear combination of basis functions (Φ_μ).

$$\Psi_i = \sum_{\mu=1}^{K} C_{\mu i}\phi_\mu \qquad \text{i = 1, 2,....., K} \qquad \text{(Eq. 1.17)}$$

where $C_{\mu i}$ are the coefficients of Φ_μ, and K is the total number of basis functions.

The Roothan-Hall equation for closed shell systems, otherwise called as restricted Hartree-Fock theory (RHF) can be written in a single matrix form as:

$$\mathbf{FC=SC}\varepsilon \qquad \text{(Eq. 1.18)}$$

where the Fock matrix **F** is the matrix representation of the Fock operator in (Eq. 1.13) in the basis function Φ_μ, **S** is the overlap matrix, and ε are orbital energies. Diagonalization of the Fock matrix yields the unknown molecular orbital coefficients to find out the eigenvalues from Roothaan Hall equation (Eq. 1.18).

An iterative procedure known as the Self Consistent Field (SCF) method is used to solve the HF equation. In this method, $V^{HF}(i)$ is calculated from an initial guess of trial spin-orbitals, and then the eigenvalue equation (Eq. 1.12) is solved for a new set of spin orbitals. A new field is calculated using this new set of spin orbitals and this procedure is repeated until the convergence criterion is satisfied. By solving Eq. 1.12 a set of orthonormal spin-orbitals, $\{\chi_K\}$ are obtained with a corresponding set of energies, $\{\varepsilon_K\}$. The N spin orbitals with the lowest energies are called the occupied orbitals, and the

remaining orbitals are known as virtual or unoccupied orbitals. Though an infinite number of virtual orbitals is possible, the HF equation is usually solved by providing a finite set of K spatial basis functions $\{\phi_\mu(r)|\ \mu = 1, 2, ..., K\}$, corresponding to which, 2K set of spin orbitals are generated. Out of these orbitals, N will be occupied, and 2K-N will be virtual orbitals. With the increase in the size of the basis set used, the energy expectation value of $E_0 = \langle\Psi_0|H|\Psi_0\rangle$ decreases until the HF limit is attained. A finite value of K usually yields an energy value above this limit.

1.2.1.2 Post Hartree-Fock Methods

HF method does not consider electron correlation which limits the accuracy of the method. Post Hartree-Fock methods are a set of electron correlation methods which go further than SCF to add electron correlation more precisely. These methods include configuration interaction (CI),[212] coupled cluster theory (CC),[213] Moller-Plesset perturbation theory[214, 215] (MPn, where n is the order of correlation), multi-configurational self-consistent field (MCSCF),[216] *etc.* More flexible wave functions are used in most of these methods which are obtained using excitations of electrons from occupied to virtual orbitals. The energy contribution resulting from the correlated motion defined as the difference between the exact energy and the energy obtained by the HF method, given by:

$$E_{corr} = \varepsilon_0 - E_0 \qquad \text{(Eq. 1.9)}$$

where ε_0 denotes the exact eigenvalue of H_{elec} and E_0 the "best" HF energy obtained by the basis set extrapolated to completeness.[217]

1.2.1.2.1 Configuration Interaction Method

Configuration interaction (CI) is the simplest method for incorporating electron correlation effect into an *ab initio* molecular orbital calculation. In CI method, a multiple determinant wavefunction with determinants corresponding to excitation of electrons from occupied to unoccupied orbitals along with the ground state HF wavefunction is used. The general form of CI wavefunction can be written as:

$$\left|\Phi_0\right\rangle = c_0\left|\Psi_0\right\rangle + \sum_{ar} c_a^r\left|\Psi_a^r\right\rangle + \sum_{\substack{a<b \\ r<s}} c_{ab}^{rs}\left|\Psi_{ab}^{rs}\right\rangle + \sum_{\substack{a<b<c \\ r<s<t}} c_{abc}^{rst}\left|\Psi_{abc}^{rst}\right\rangle + \ldots. \qquad \text{(Eq. 1.20)}$$

The first term in Eq. (1.20) denotes the Slater determinant corresponding to the HF wave function and all other terms constitute singly, doubly, triply, ..., n-tuply excited determinants with appropriate expansion coefficients. The indices a, b, c, *etc.* represent the occupied orbitals and r, s, t, *etc*. represent the virtual orbitals involved in the electron excitations. The energy of the system is then minimized for determining the coefficients by linear variation approach. The CI methods are categorized based on the number of excitations used to construct each determinant.[218, 219] In configuration interaction single-excitation (CIS) calculation, only one electron is moved from each determinant. The CIS calculation gives an approximation to the excited states of a molecule without changing the ground state energy. Single and double excited CI method (CISD) gives ground-state energy corrected for correlation. Triple-excitation (CISDT) and quadruple-excitation (CISDTQ) calculations are done only on the requirement of highly precise results. CI methods are very accurate, but computationally very costly (N^8 times complexity or worse). A full CI calculation corresponds to a configuration interaction with all possible excitations. Even though a full CI calculation gives exact quantum mechanical results, it is rarely done due to highly demanding computational facility.[220, 221]

1.2.1.2.2 Coupled Cluster Theory

Coupled cluster (CC) method is regarded as one of the most accurate electron correlation methods for describing ground-state electronic structures of molecule. This method employs the basic HF molecular orbital method and constructs multi-electron wave functions using the exponential cluster operator to account for electron correlation. [222-224] Even though the method for choosing the wavefunction is different from CI method, the total wavefunction is a linear combination of several determinants similar in both the methods. The CC method assumes the full CI wave function:

$$\Psi_{CC} = e^{T}\Psi_{HF} \qquad \text{(Eq. 1.21)}$$

where Ψ_{HF} is a Slater determinant constructed from HF molecular orbitals and e^T is given by Eq. 1.22.

$$e^T = 1 + T + \frac{1}{2}T^2 + \frac{1}{6}T^3 + \ldots = \sum_{k=0}^{\infty} \frac{1}{k!}T^k \qquad \text{(Eq. 1.22)}$$

Here, T is called cluster operator which acts on Ψ_{HF} to produce a linear combination of excited slater determinants and can be given as:

$$T = T_1 + T_2 + T_3 + \ldots + T_n \qquad \text{(Eq. 1.23)}$$

where n represents the total number of electrons, and various T_i operators generate all possible determinants having i^{th} excitation from the reference.

$$T_2 = \sum_{i<j}^{occ.} \sum_{a<b}^{vir.} t_{ij}^{ab} \Psi_{ij}^{ab} \qquad \text{(Eq. 1.24)}$$

The amplitude values t are determined by the constraint that (Eq. 1.21) should be satisfied. Considering the double excitation $T = T_2$, the Taylor expansion of the exponential function in (Eq. 1.21) gives:

$$\Psi_{CCD} = \left(1 + T_2 + \frac{1}{2!}T_2^2 + \frac{1}{3!}T_2^3 + \ldots\right)\Psi_{HF} \qquad \text{(Eq. 1.25)}$$

where CCD implies coupled cluster with only the double excitation operator. The configuration double excitation method is defined by the first to terms in parenthesis, $(1 + T_2)$ and the rest of the terms correspond to the product of excitation operators. The approximate solution $|\Psi_{cc}\rangle$ is obtained by solving the unknown coefficients t_{ij}^{ab} .The singles and doubles coefficients and two electron MO integrals determine the coupled cluster correlation energy. Coupled cluster methods are classified based on the highest number of excitations allowed in the definition of T. The various orders of CC expansion are CCSD, CCSDT, *etc*. where S, D, and T represents single, double and triple excitations. If the excitations are included successively, the energy provided by a coupled cluster

method will be variational. Thus, CCSD calculations give variational energy, whereas CCD calculations do not. When many excitation terms are included in the expansion, CC methods become computationally very expensive compared to HF calculations.[220, 221] Formally, CCSD, CCSDT, CCSD(T) computationally scales as N^6, N^8, and N^7, respectively where N is the total number of basis functions.

1.2.1.2.3 Møller-Plesset Perturbation Theory

These methods proposed by Møller and Plesset undertake problem of electron correlation based on Rayleigh-Schrödinger perturbation theory. These calculations are not variational, and the difference between the exact Hamiltonian and the Fock operator is considered as a perturbation.[214, 215] A Møller-Plesset calculation of order n is denoted as MPn. Using a second-order perturbation method (MP2), a minimal amount of correlation is added; MP3 and MP4 methods being commonly used methods. The precision of the MP4 method is almost comparable to that of CISD calculation. Owing to high computational cost MP5 and higher order methods are not commonly used; the complexity being N^{10} or even higher. In Møller and Plesset method the 'true' Hamiltonian operator H is expressed as:

$$H = H_0 + \lambda U \qquad \text{(Eq. 1.26)}$$

where H_0 represents 'zeroth order' Hamiltonian, U is the perturbation and λ is a dimensionless parameter that varies between 0 and 1. When λ = 0, then $H = H_0$ and when λ = 1, then H equals its true value. The eigenfunctions of the 'true' Hamiltonian operator and zeroth-order Hamiltonian are Ψ_i and $\Psi_i^{(0)}$, respectively with energies E_i and $E_i^{(0)}$ as the corresponding energies. Thus $\Psi_0^{(0)}$ represents the ground-state wave function with energy $E_0^{(0)}$. The eigenfunctions Ψ_i and eigenvalues E_i of H are expressed in powers of λ as:

$$\Psi_i = \Psi_i^{(0)} + \lambda \Psi_i^{(1)} + \lambda^2 \Psi_i^{(2)} \ldots = \sum_{n=0} \lambda^n \Psi_i^{(n)} \qquad \text{(Eq. 1.27)}$$

$$E_i = E_i^{(0)} + \lambda E_i^{(1)} + \lambda^2 E_i^{(2)} + \ldots = \sum_{n=0} \lambda^n E_i^{(n)} \qquad \text{(Eq. 1.28)}$$

The terms $E_i^{(1)}$, $E_i^{(2)}$, *etc*. are the first-order, second-order correction to the energy, and so on. These energies are calculated from the eigenfunctions as follows:

$$E_i^{(0)} = \int \Psi_i^{(0)} \, H_0 \, \Psi_i^{(0)} \, d\tau \qquad \text{(Eq. 1.29)}$$

$$E_i^{(1)} = \int \Psi_i^{(0)} \, U \, \Psi_i^{(0)} \, d\tau \qquad \text{(Eq. 1.30)}$$

$$E_i^{(2)} = \int \Psi_i^{(0)} \, U \, \Psi_i^{(1)} \, d\tau \qquad \text{(Eq. 1.31)}$$

$$E_i^{(3)} = \int \Psi_i^{(0)} \, U \, \Psi_i^{(2)} \, d\tau \qquad \text{(Eq. 1.32)}$$

It is indispensable to resolve the wave functions to a given order in order to find out the corrections to the energy. The unperturbed Hamiltonian H_0 is the sum of the one-electron Fock operator for the N electrons and the zeroth-order energy E_0 is the sum of orbital energies for the occupied molecular orbitals.[215]

$$H_0 = \sum_{i=1}^{N} f_i = \sum_{i=1}^{N} \left(H^{core} + \sum_{j=1}^{N} (J_i + K_i) \right) \qquad \text{(Eq. 1.33)}$$

$$E_0^{(0)} = \sum_{i=1}^{occupied} \varepsilon_i \qquad \text{(Eq. 1.34)}$$

The perturbation, U is recognized as the difference between the 'real' Hamiltonian, H and the zeroth-order Hamiltonian, H_0. The true Hamiltonian is equal to the sum of the nuclear attraction terms and electron repulsion terms and represented as:

$$H = \sum_{i=1}^{N} (H^{core}) + \sum_{i=1}^{N} \sum_{j=i+1}^{N} \frac{1}{r_{ij}} \qquad \text{(Eq. 1.35)}$$

From Eqs. 1.33 and 1.35, the perturbation U is given by:

$$U = \sum_{i=1}^{N} \sum_{j=i+1}^{N} \frac{1}{r_{ij}} - \sum_{j=1}^{N} (J_j + K_j) \qquad \text{(Eq. 1.36)}$$

The first-order energy $E_0^{(1)}$ is given by:

$$E_0^{(1)} = -\frac{1}{2}\sum_{i=1}^{N}\sum_{j=1}^{N}\frac{1}{r_{ij}}[(ii \mid jj) - (ij \mid ij)] \qquad \text{(Eq. 1.37)}$$

The HF energy is the sum of zeroth-order and first-order energies and is given by

$$E_0^{(0)} + E_0^{(1)} = \sum_{i=1}^{N}\varepsilon_i - \frac{1}{2}\sum_{i=1}^{N}\sum_{j=1}^{N}[(ii \mid jj) - (ij \mid ij)] \qquad \text{(Eq. 1.38)}$$

To obtain an improvement on the HF energy it is necessary to use Møller-Plesset theory which involves perturbation to second order, known as MP2 theory. The higher order wave function $\Psi_0^{(1)}$ is represented as linear combinations of solutions to the zeroth-order Hamiltonian:

$$\Psi_0^{(1)} = \sum_j c_j^{(1)}\Psi_j^{(0)} \qquad \text{(Eq. 1.39)}$$

The term $\Psi_j^{(0)}$ in Eq. 1.39 includes single, double *etc*. excitations attained by the promotion of electrons into virtual orbitals which are obtained from a HF calculation. The second order energy is given by:

$$E_0^{(2)} = \sum_{i}^{\text{occupied}}\sum_{j>i}\sum_{a}^{\text{virtual}}\sum_{b>a}\frac{\iint d\tau_1 d\tau_2 \chi_i(1)\chi_j(2)\left(\frac{1}{r_{12}}\right)[\chi_a(1)\chi_b(2) - \chi_b(1)\chi_a(2)]}{\varepsilon_a + \varepsilon_b - \varepsilon_i - \varepsilon_j} \qquad \text{(Eq. 1.40)}$$

These integrals will be non-zero only for double excitations, According to the Brillouin theorem,[225] the integrals in Eq. 1.40 are non-zero only for double excitations. Third- and fourth-order Møller-Plesset calculations with higher orders such as MP3 and MP4 are also available. Even though computationally costly, MP2 methods are the most accepted ones that incorporate electron correlation in molecular quantum mechanical calculations.[226, 227] Also, MP2 theory is size-independent which makes it advantageous over CI method. As MP2 theory is not variational, at times the obtained energy may be lower than the true value.

1.2.1.3 Basis Set

Basis sets are defined as any set of non-orthogonal one-particle functions used to build molecular orbitals which are expanded as a linear combination with coefficients to be determined. These basis functions are usually centered on atoms. A minimal basis set takes into account only the most fundamental aspects of a molecule. Minimal basis sets being less accurate, extended basis sets are used these days for computational calculations. J. C. Slater developed a set of basis functions which decay exponentially with the distance from the nuclei.[228, 229] These basis functions are called Slater-type orbitals (STO) and are mathematically expressed as:

$$\Phi_{abc}^{STO}(x,y,z) = Nx^a y^b z^c e^{-\zeta r} \qquad \text{(Eq. 1.41)}$$

where N is the Normalization constant, a, b, c are components of angular momentum (L = a +b + c), and ζ is the orbital exponent which determine the expansion of the orbital, x, y, z are the cartesian coordinates and r is the radius in angstrom. As some of the integrals are difficult to calculate particularly when the atomic orbitals are centered on different nuclei, STOs are not mostly used in molecular orbital calculations. S. F. Boys introduced another type of orbitals known as Gaussian-type orbitals (GTOs) having the exponential dependence $e^{-\zeta r^2}$.[217, 230, 231] GTOs are mathematically expressed as:

$$\Phi_{abc}^{GTO}(x,y,z) = Nx^a y^b z^c e^{-\zeta r^2} \qquad \text{(Eq. 1.42)}$$

This function is usually known as primitive Gaussian-type orbital (PGTO). According to Gaussian product theorem, the product of two primitive Gaussians gives rise to another Gaussian function centered at the weighted midpoint of the two functions. This makes the GTOs more advantageous over STOs.[232, 233] But the limitation of using GTOs is that these functions are less accurate compared to STOs. To surmount this limitation, linear combinations of primitive gaussians known as contracted Gaussian-type orbitals (CGTOs) are used. The CGTO functions can mimic STOs and are expressed as:

$$\Phi_{abc}^{CGTO}(x,y,z) = N\sum_{i}^{n} c_i\, x^a y^b z^c e^{-\zeta_i r^2} \qquad \text{(Eq. 1.43)}$$

where n gives the number of Gaussians to mimic the STO and c_i corresponds to their coefficients.[234-236] The simplest type of contracted gaussians (CGs) is the STO-nG basis sets which attempt to approximate Slater-type orbitals (STOs) by n primitive Gaussians.[237, 238] The STO-nG basis sets are rather inadequate as they include only one CG per atomic orbital. For improving the calculations, two or more functions can be used to describe each type of orbital. Double-zeta (DZ), triple-zeta (TZ) and quadruple-zeta(QZ) basis sets are examples of such kind which use more than one basis functions.[239]

Thom Dunning pointed out that basis sets optimized at the HF level might not be ideal for correlated computations and developed "correlation consistent" basis sets which are optimized using correlated CISD wavefunctions.[240, 241] The notation cc-pVXZ means a Dunning correlation-consistent, polarized valence, X-zeta basis; X=D, T, Q, *etc*. For instance, cc-pVDZ, cc-pVTZ for C atom consists of 3s2p1d and 4s3p2d1f, respectively. A prefix "aug" implies the addition of one set of diffuse functions for every angular momentum present in the basis; aug-cc-pVDZ for C atom has diffuse s ,p, and d.

Split valence basis sets were introduced by Pople and coworkers in which the valence orbitals are represented by multiple zeta and the core orbitals by a single basis function.[242] The basis sets such as 3-21G, 4-21G, 6-311G, *etc*. are examples of split-valence basis sets. In 3-21G basis set, the core electrons are represented as the sum of three gaussian functions and the valence orbitals are represented by two basis functions of which one is a sum of two primitive gaussians and the second is one gaussian function. Moreover, the addition of polarization or diffuse functions improves the basis sets. By taking into consideration of the distortions in electron density of atoms in a molecule, functions of higher angular momentum than the occupied atomic orbitals are added to the basis sets. These functions represented as * or ** [(d) or (d, p)] following G in the notation of the basis sets are called polarization functions. The (d, p) polarization function employs an extra set of d-orbitals on heavy atoms and p-orbitals on hydrogens. Diffuse basis sets are useful for describing anions, molecules with lone pairs, excited states, and transition states.[243] The diffuse functions are denoted by + or ++ signs. For example, 6-31+G basis set adds s and p diffuse functions to non hydrogen atoms and 6-311++G adds diffuse functions to both non-hydrogen and hydrogen atoms.

The obtained solutions are only within the confined space of the basis set used. Increasing the number of CGs improves the quality of basis sets and using an infinite number of functions lead to a complete basis set. Any molecular orbital can be represented by a complete basis set (CBS), but using infinite functions are not practical for calculations. The CBS can be estimated by a methodical increase in the number of basis functions and extrapolating to an infinite-size basis set limit.[244] Dunning basis sets (cc-pVDZ, cc-pVTZ, ccpVQZ, *etc*.) are intended to converge smoothly towards the CBS limit by extrapolation.

The basis sets employed for the calculations in the thesis are (a) Pople's split-valence basis sets 6-31G(d,p) and 6-311++G(d,p) with d polarization functions for non-hydrogen atoms and p polarization function for hydrogen atom in addition to diffuse functions for non-hydrogen and hydrogen atom[243, 245] (b) Dunning's basis functions aug-cc-pvdz, aug-cc-pvtz, and aug-cc-pvqz[241] and (c) extrapolation to CBS limit.[244]

1.2.1.4 Basis Set Superposition Error

When two atoms of interacting molecules approach each other to form a new species, their basis functions overlap, and each fragment borrows the basis functions from the nearby components. This results in improvement of basis set leading to an artificial decrease in intermolecular distances and associated strengthening of intermolecular interactions in weakly bound clusters referred to as basis set superposition error (BSSE). The calculations using finite basis sets are susceptible to BSSE error. The basis functions on each molecule endow with a better description of the electronic structure around the other molecule thus improving the interaction energy. The counterpoise correction method introduced by Boys and Bernardi is one of the widely used methods to eliminate BSSE.[246] In this method, the entire basis set is included in all calculations. The binding energy (ΔE) of a dimer can be expressed as:

$$\Delta E = E(AB)_{ab} - [E(A)_a + E(B)_b] \qquad \text{(Eq. 1.44)}$$

where $E(AB)_{ab}$, $E(A)_a$ and $E(B)_b$ are the energies of AB, monomer A, and monomer B, respectively. The subscripts in the equation denote the corresponding basis sets for AB, A, and B. The energy of the individual species A is calculated in the presence of 'ghost' orbitals

of B, without the nuclei or electrons of B in counterpoise method. Using the 'ghost' orbitals of A, a similar calculation is done for the monomer B. The BSSE is given by:

$$\Delta E_{BSSE} = E(\tilde{A})_{ab} + E(\tilde{B})_{ab} - E(\tilde{A})_{a} - E(\tilde{B}_{b}) \qquad \text{(Eq. 1.45)}$$

where $E(\tilde{A})_{ab}$ and $E(\tilde{B})_{ab}$ are the energies of monomer A and B respectively, in the structure they adopt in the dimer (AB) with the full basis set of the dimer available. $E(\tilde{A})_{a}$ and $E(\tilde{B})_{b}$ are the energies of A and B, respectively, in the structure they adopt in the dimer with only their basis functions. The BSSE correction to the binding energy is taken as the difference between ΔE and ΔE_{BSSE} (ΔE - ΔE_{BSSE}).

1.2.2 Molecular Mechanics

Molecular mechanics (MM) method was developed out of a need to model molecules that are too big to be handled by quantum mechanics. Considering atoms as spheres and bonds as springs, mathematics of spring deformation is used to explain stretching, bending, and twisting of bonds.[200, 247] The interactions of non-bonded atoms through van der Waals attraction, electrostatic attraction/repulsion, steric repulsion, *etc*. are simply described by ball and spring model. Instead of using wavefunction in calculations, force fields are used in MM calculations. The set of equations along with the parameters required to describe the behavior of different kinds of atoms and bonds is called a force field. The parameters are obtained either from *ab initio* calculations or experimental data. The fundamental idea of molecular mechanics is that the constants obtained are transferrable to other molecules. A simple MM energy equation is given by:

$$E = E_{\text{str}} + E_{\text{bend}} + E_{\text{tor}} + E_{\text{vdw}} + E_{\text{elec}} \qquad \text{(Eq. 1.46)}$$

Thus the energy expression consists of the sum of simple classical equations expressing bond stretching, bending, torsion, van der Waals, electrostatic interaction, *etc*. All force fields possess at least one valence term that describes molecular motions such as angle bending, bond stretching or torsional motion. The effect of the motion of a molecule on another molecule is described by a cross term. The complexity of force

field depends on the number and complexity of each term involved. In MM methods, the bond stretching and bending are usually expressed by harmonic oscillator equations based on Hook's law. At times, Morse potential is used to explain bond stretching. The torsion energy is mainly used to correct the remaining energy terms rather than to represent a physical process. This energy term represents the amount of energy that must be added to or subtracted from the sum of stretching, bending and non-bonded interaction energy terms to make the total energy agree with experiment or rigorous quantum mechanical calculation for a model dihedral angle. The electrostatic term involving the energy of attraction or repulsion between charged centers is calculated using Coulomb's law. Lennard-Jones potential is often used to describe intermolecular forces such as van der Waals forces and hydrogen bonds. Partial atomic charges are obtained for small molecules using an *ab initio* or semiempirical quantum technique such as MOPAC or AMPAC. For macromolecules, programs assign charges using rules or templates, and in some force-fields, the torsional potential is calibrated to a particular charge calculation method. The solvation effects are usually calculated using dielectric constants. AMBER (Assisted model building with energy refinement),[248] CHARMM (Chemistry at Harward molecular mechanics),[249, 250] GROMOS (Groningen molecular simulation),[220] *etc.* are the commonly used force fields in MM software packages.

The energy values obtained in MM method have no significance as absolute quantities; only the difference in energy between two or more conformations makes sense. Thus MM is used to calculate the energy associated with a given conformation of a molecule and these energies are not comparable with *ab initio* or semiempirical methods. The accomplishment of MM force field method depends on the energy expression, the database used for parameterization, and the familiarity of the user with the advantages and disadvantages of each method. Several force fields accounting for coupling between bending and stretching in adjacent bonds, bond deformations, *etc*. have been developed over the years.

1.2.3 Molecular Dynamics

Molecular dynamics (MD) is concerned with molecular motion inherent to all chemical processes. The mechanism by which chemical processes occur, *i.e.,* the sequence or rate of events as molecules transform between their various possible states is explained by kinetics.[251-253] The driving force for chemical processes is described by thermodynamics by dictating the energetic relationships between different chemical states. Local vibrations and conformational transitions are typically studied using MD simulations. The intramolecular degrees of freedom are altered in a step-wise manner, analogous to energy minimization. The steps in energy minimization are directed at establishing a down-hill direction to a minimum whereas, in MD, each step corresponds to changes in atomic position over time (velocity) which is governed by the forces that the atoms of the system exert on each other as described by Newton's equation. The force on an atom is calculated from the change in energy between two positions recognized as the derivative of the energy concerning the change in the atom's position. MM or QM methods are used to calculate the energy of the system. An appropriate force field for the problem under consideration is selected, and an algorithm is used for numerical integration of the equations of motion. GROMOS is force field used for bulk systems and Verlet algorithm, is a typical algorithm which requires minimum computational resources.[254] Other than the amount of time that can be practically covered, MD has no defined point of termination. The accuracy of the simulations depends on the choice of the time step. In general, a time step of one order lesser of magnitude than the period of the shortest motion is used. For large conformational transitions in proteins, the picosecond order of magnitude limit for time step is often not long enough to follow the state transformations. The extent of accuracy of the methods used is determined by comparing with experimental values. MD calculations are performed using AMBER, CHARMM, HyperChem, GROMACS (Groningen Machine for Chemical Simulations) and Gaussian programs.

1.2.4 Semiempirical Methods

Semi-empirical quantum mechanical methods signify a middle road between molecular mechanics and *ab initio* methods.[197, 198] These methods are based on Schrödinger

equation and are logically regarded as simplifications of the *ab initio* method since parameterizations and approximations from experimental data are used to provide input into mathematical models.[255] Even though semiempirical methods are much faster compared to *ab initio* methods, the results may not be very accurate. These methods do not use all the information available for a system for calculations. Typically, only valence electrons are considered in the calculation. The core is treated by reducing the nuclear charge or by adding special core functions. The empirical parameters obtained either experimentally or from *ab initio* calculations are included as a correction factor.

Hückel theory, one of the primitive and simplest semiempirical method considers only the valence π electrons of a planar conjugated hydrocarbons whereas the extended Hückel method models all valence orbitals and it is used for all elements across the periodic table.[256] The extended Hückel method is often used for and band structure calculations and inorganic modeling. The Pariser-Parr-Pople (PPP) method is another distinction of the Hückel method which is used when electronic effects are negligible.[257] Usually, a minimal STO basis set is used in semiempirical methods with several approximations. Zero Differential Overlap (ZDO), Complete Neglect of Differential Overlap (CNDO), Intermediate Neglect of Differential Overlap (INDO), Neglect of Diatomic Differential Overlap (NDDO), *etc.* are examples of approximations made. The properties such as geometry, energy, dipole moments, heats of reaction, NMR chemical shifts, solvation effects, solid state properties, ionization potentials, *etc*. are obtained by semiempirical methods. The parameters used in semiempirical methods are fitted to reproduce a given set of experimental data in the gas phase for small molecules, and the worth of a semiempirical computation is dependent on the way these parameters have been built in.

1.2.5 Hybrid QM/MM Methods

Hybrid methods allow the combination of two or more computational techniques in one calculation and make it possible to investigate the chemistry of very large systems with high precision is achieved by hybrid methods in which the combination of two or more computational techniques is used in one calculation.[258] Hybrid quantum

mechanics/molecular mechanics (QM/MM) methods introduced by Warshel and Levitt in 1976 have become a popular tool for investigating chemical reactions in condensed phases. [259] The Nobel Prize in Chemistry in 2013 was awarded to Warshel, Levitt, and Karplus for "the development of multi-scale models for complex chemical systems".[260, 261] Combining the strengths of the QM (accuracy) and MM (speed) approaches, hybrid QM/MM methods are used in the study of chemical processes in solution and proteins. The region of the system in which the chemical process such as bond formation or bond breaking occurs is treated at a suitable level of quantum chemical theory and the rest with molecular mechanics force field. The chemical reactivity in large systems like enzymes can be studied using this approach.[262, 263] The QM/MM simulations provide not only the experimentally accessible quantities such as structural intermediates, fluorescence lifetimes, quantum yields and spectra, *etc.* but also information on reaction mechanisms and the influence of individual amino acid residues which are difficult to measure using experimental techniques.

ONIOM (our own n-layer integrated molecular orbital molecular mechanics) method developed by Morokuma and co-workers is one of the most successful and admired hybrid QM/MM methods to treat complex molecular systems. [149, 264] In this hybrid method different *ab initio* or semi-empirical methods are applied to different parts of the molecular system and combined to generate trustworthy geometry and energy at a reduced computational cost. An important characteristic of ONIOM method is a simple linear extrapolation procedure. This permits the method to be extended to two-layer ONIOM (QM1: QM2), three-layer ONIOM (QM1: QM2: MM), and, in principle, any n-layer n-level-of-theory methods. ONIOM computational approach is used for biological macromolecules, homogeneous and heterogeneous catalysis, nanomaterials, *etc.*

1.2.6 Density Functional Theory

The basics of density functional theory (DFT) are rooted in the Thomas-Fermi model of the electronic structure. The extensive application of DFT in computational calculations was realized after the works of Hohenberg, Kohn, and Sham in 1960s. Contrary to HF theory based on wavefunctions, DFT is based on electron density. DFT is made on the

principle that the energy of an electronic system can be defined regarding its electron probability density, $\rho(\mathbf{r})$ which depends on three spatial coordinates (or four, if the spin is included) regardless the number of electrons in the system. Thus the complexity of 3N variables in wavefunction method is reduced to 3 in DFT methods. DFT maintains a good balance between accuracy and computational cost and applies to larger systems with hundreds or even thousands of atoms. According to DFT formalism, the electronic energy, E is regarded as a functional of the electron density, $E[\rho(\mathbf{r})]$. This implies that the given function $\rho(\mathbf{r})$ corresponds to single energy, *i.e.*, a one-to-one correspondence exists between the electron density and energy of a system. $\rho(\mathbf{r})$ is defined as the number of electrons in the unit volume around a point $\mathbf{r}$ in space. The integration of electron density over all space gives the total number of electrons, N.

$$\mathrm{N} = \int \rho(\mathbf{r})\mathrm{d}\mathbf{r} \qquad \text{(Eq. 1.47)}$$

1.2.6.1 Thomas-Fermi Model

Thomas and Fermi introduced the concept of expressing the energy of a system as a function of the total electron density in the late 1920s.[265-267] In Thomas-Fermi model, the kinetic energy of the electrons is derived from the quantum statistical theory based on the uniform electron gas and the electron-nucleus and electron-electron interactions are treated classically. The kinetic energy of the electron gas, $T_{TF}[\rho(\mathbf{r})]$ is expressed as:

$$T_{TF}[\rho(\boldsymbol{r})] = \frac{3}{10}(3\pi^2)^{2/3}\int \rho(\mathbf{r})^{5/3}\,\mathrm{d}\mathbf{r} \qquad \text{(Eq. 1.48)}$$

The approximation that the kinetic energy of the electrons depends exclusively on the electron density is made from Eq. 1.48 The total energy in terms of electron density is obtained by adding electron-nucleus and electron-electron interactions.

$$E[\rho(\boldsymbol{r})] = \frac{3}{10}(3\pi^2)^{2/3}\int \mathrm{d}\boldsymbol{r}\ \rho^{5/3}(\boldsymbol{r}) - Z\int \frac{\rho(\boldsymbol{r})}{\boldsymbol{r}}\mathrm{d}\boldsymbol{r} + \frac{1}{2}\iint \frac{\rho(\boldsymbol{r}_1)\rho(\boldsymbol{r}_2)}{|\boldsymbol{r}_1 - \boldsymbol{r}_2|}\mathrm{d}\boldsymbol{r}_1\,\mathrm{d}\boldsymbol{r}_2 \qquad \text{(Eq. 1.49)}$$

In Eq. 1.49 the second term represents electron-nucleus interaction, and the third term represents the electron-electron interactions. Thomas-Fermi theory is considered as

the forerunner of DFT formalism, but the accuracy of this theory is not adequate to treat chemical systems.

1.2.6.2 Hohenberg-Kohn Theorems

Hohenberg and Kohn formulated two theorems which recognized DFT as a precise quantum chemical methodology.[268] The theorems state that (i) the external potential (V_{ext}), and hence the total energy (E) is a functional of electron density $\rho(\mathbf{r})$ and (ii) the ground state energy can be obtained variationally: the density that minimizes the total energy is the exact ground state density. A straightforward consequence of this theorem is that the ground-state energy of a system and its properties are uniquely defined by its electron density, *i.e.* $E[\rho(\mathbf{r})]$.

The energy functional can be written as the sum of two terms:

$$E[\rho(\mathbf{r})] = \int V_{ext}(\mathbf{r})\rho(\mathbf{r})d\mathbf{r} + F[\rho(\mathbf{r})] \qquad \text{(Eq. 1.50)}$$

The first term in Eq. 1.51 arises from the interaction of the electrons with an external potential $V_{ext}(\mathbf{r})$ typically due to the Coulomb interaction with the nuclei. The sum of the kinetic energy of the electrons and the contribution from the inter-electronic interactions is given by the second term $F[\rho(\mathbf{r})]$. The minimum value in the energy corresponds to the exact ground-state electron density, permitting a variational approach to be used. The DFT equivalent of Schrödinger equation can be written as:

$$\left(\frac{\delta E[\rho(\mathbf{r})]}{\delta\rho(\mathbf{r})}\right)_{V_{ext}} = \mu \qquad \text{(Eq. 1.51)}$$

where the Lagrangian multiplier μ is known as electronic chemical potential.

1.2.6.3 Kohn-Sham Equations

The practical applications for solving Hohenberg-Kohn theorem for a set of interacting electrons and computing the ground-state density of a system was put forward by Kohn and Sham.[269] According to them, $E[\rho(\mathbf{r})]$ should be approximated as the sum of three terms:

$$E[\rho(\mathbf{r})] = E_{\mathrm{KE}}[\rho(\mathbf{r})] + E_{\mathrm{H}}[\rho(\mathbf{r})] + E_{\mathrm{XC}}[\rho(\mathbf{r})] \quad \text{(Eq. 1.52)}$$

where $E_{\mathrm{KE}}[\rho(\mathbf{r})]$ represents the kinetic energy of non-interacting electrons, $E_{\mathrm{H}}[\rho(\mathbf{r})]$ the Hartree electrostatic energy of the electrons, and $E_{\mathrm{XC}}[\rho(\mathbf{r})]$ corresponds contributions of exchange and correlation to energy. The $E_{\mathrm{KE}}[\rho(\mathbf{r})]$ is defined as the kinetic energy of a system of non-interacting electrons with the same density $\rho(\mathbf{r})$ as the real system:

$$E_{\mathrm{KE}}[\rho(\mathbf{r})] = \sum_{i=1}^{N} \int \Psi_{\mathrm{i}}(\mathbf{r}) \left(-\frac{\nabla^2}{2} \right) \Psi_{\mathrm{i}}(\mathbf{r}) \mathrm{d}\mathbf{r} \quad \text{(Eq. 1.53)}$$

The Hartree electrostatic energy, $E_{\mathrm{H}}[\rho(\mathbf{r})]$ is given by:

$$E_{\mathrm{H}}[\rho(\mathbf{r})] = \frac{1}{2} \iint \frac{\rho(\mathbf{r}_1)\rho(\mathbf{r}_2)}{|\mathbf{r}_1 - \mathbf{r}_2|} \mathrm{d}\mathbf{r}_1 \mathrm{d}\mathbf{r}_2 \quad \text{(Eq. 1.54)}$$

The full expression for the energy of an N-electron system within the Kohn-Sham scheme can be written as:

$$E[\rho(\mathbf{r})] = \sum_{i=1}^{N} \int \Psi_{\mathrm{i}}(\mathbf{r}) \left(-\frac{\nabla^2}{2} \right) \Psi_{\mathrm{i}}(\mathbf{r}) \mathrm{d}\mathbf{r} + \frac{1}{2} \iint \frac{\rho(\mathbf{r}_1)\rho(\mathbf{r}_2)}{|\mathbf{r}_1 - \mathbf{r}_2|} \mathrm{d}\mathbf{r}_1 \mathrm{d}\mathbf{r}_2 + E_{\mathrm{XC}}[\rho(\mathbf{r})] - \sum_{A=1}^{M} \int \frac{Z_A}{r - R_A} \rho(\mathbf{r}) \mathrm{d}\mathbf{r}$$

(Eq. 1.55)

Thus from Eq. 1.55, the exchange-correlation energy functional is defined as the difference between the exact and non-interacting kinetic energies along with the contribution due to exchange and correlation. According to Kohn and Sham, the electron density of an N electron system can be written as the sum of the square moduli of N one-electron orbitals:

$$\rho(\mathbf{r}) = \sum_{i=1}^{N} |\Psi_{\mathrm{i}}(\mathbf{r})|^2 \quad \text{(Eq. 1.56)}$$

By using Eq. 1.56 for electron density and applying the appropriate variational condition, the one-electron Kohn-Sham equation takes the form:

$$\left\{-\frac{\nabla_1^2}{2}-\left(\sum_{A=1}^{M}\frac{Z_A}{r_{1A}}\right)+\frac{\rho(\mathbf{r_2})}{r_{12}}\mathrm{d}\mathbf{r}_2+V_{\mathrm{XC}}[\mathbf{r_1}]\right\}\Psi_{\mathrm{i}}(\mathbf{r}_1)=\varepsilon_{\mathrm{i}}\Psi_{\mathrm{i}}(\mathbf{r}_1) \qquad \text{(Eq. 1.57)}$$

where V_{XC} is the exchange-correlation functional and ε_i are the orbital energies. V_{XC} is given by:

$$V_{\mathrm{XC}}[\mathbf{r}]=\frac{\delta E_{\mathrm{XC}}[\rho(\mathbf{r})]}{\delta\rho(\mathbf{r})} \qquad \text{(Eq. 1.58)}$$

The exchange-correlation potential expresses the effects of the Pauli principle and the Coulomb potential beyond a pure electrostatic interaction of the electrons. The exchange-correlation energy, E_{XC} is generally divided into two terms, an exchange term E_X (associated with the interaction of electrons of the same spin) and a correlation term E_C (associated with the interaction of electrons of opposite spin). The corresponding functionals are exchange functional and correlation functional, respectively.

$$E_{\mathrm{XC}}[\rho(\mathbf{r})]=E_{\mathrm{X}}[\rho(\mathbf{r})]+E_{\mathrm{C}}[\rho(\mathbf{r})] \qquad \text{(Eq. 1.59)}$$

A self-consistent approach is followed to solve the Kohn-Sham equations. An initial guess of the density is supplied into Eq. 1.59 from which a set of orbitals are derived, which leads to an improved value of density. This value is used in the second iteration and so on until convergence is attained.

1.2.6.4 Exchange-Correlation Functionals

Kohn-Sham DFT is formally accurate, and it describes the ground state properties. But it does not lead to the exact form of exchange-correlation functional V_{XC}. Several approximations such as (i) Local density approximation (LDA) (ii) Generalized gradient approximation (GGA) (iii) meta-GGA and, (iv) Hybrid functionals have been designed by modifying the exchange-correlation potential for the practical applications of DFT.

In LDA, the simplest of all approximations, the exchange-correlation energy at any point in space is defined as a function of the electron density at that point and can be given by the electron density of a homogeneous electron gas of the same density. Within the LDA approach, the exchange function is given by:

$$E_{\mathrm{X}}^{\mathrm{LDA}}[\rho(\mathbf{r})] = -\frac{3}{4}\left(\frac{3}{\pi}\right)^{1/3}\int \rho^{4/3}(\mathbf{r})\mathrm{dr} \qquad \text{(Eq. 1.60)}$$

LDA is regarded as the basis for all approximate exchange-correlation functionals. In a more general application of LDA called local spin density approximation (LSDA), spin densities are introduced into the functional. This solves various conceptual problems associated with the LDA. The exchange functional in LSDA approach is given by:

$$E_{\mathrm{X}}^{\mathrm{LSDA}}[\rho(\mathbf{r})] = -2^{1/3}\left(-\frac{3}{4}\left(\frac{3}{\pi}\right)^{1/3}\right)\int\left(\rho_{\alpha}^{4/3}(\mathbf{r}) + \rho_{\beta}^{4/3}(\mathbf{r})\right)\mathrm{dr} \qquad \text{(Eq. 1.61)}$$

where α and β represent spin up and down, respectively.

The correlation energy, E_{C} per particle is difficult to obtain separately from the exchange energy in LDA.[270] By incorporating Monte Carlo results, several formulations for this functional have been developed by Vosko, Wilk and Nusair known as Vosko-Wilk-Nusair or VWN functional.[270]

The assumption in generalized gradient approximation methods (GGAs) is that the exchange-correlation energies depend not only on the density but also on the gradient of the density, $\nabla(\rho)$.

$$E_{\mathrm{XC}}\left[\rho_{\alpha}(\boldsymbol{r}), \rho_{\beta}(\boldsymbol{r})\right] \equiv \int \varepsilon_{\mathrm{XC}}(\rho_{\alpha}(\boldsymbol{r}), \rho_{\beta}(\boldsymbol{r}), \vec{\nabla}\rho_{\alpha}(\boldsymbol{r}), \vec{\nabla}\rho_{\beta}(\boldsymbol{r}))\,\mathrm{d}^3\mathbf{r} \qquad \text{(Eq. 1.62)}$$

The GGA functionals are made by adding a correction term to the LDA functionals. The GGA methods are base on two mainlines; one is the numerical fitting procedures proposed by Becke and the second one is a more rational-based one advocated by Perdew. Becke88 (B), Perdew-Wang (PW), modified Perdew-Wang (mPW), Becke86 (B86), Perdew86 (P), Perdew-Burke-Ernzerhof (PBE) and modified Perdew-Burke-Ernzerhof (mPBE) are examples of exchange functionals based on this principle. Several formulations have been developed for correlation functional which includes Becke88 (B88),[271] Perdew 86,[272] Perdew-Wang 91 (PW91)[273] and Lee-Yang-Parr (LYP). Meta-GGA functionals depend explicitly on higher order density gradients which involve

derivatives of the occupied Kohn-Sham orbitals. These functionals show considerable improvement over GGA methods.

In hybrid density functional (H-GGA) methods a combination of exchange-correlation of a conventional GGA method with a percentage of HF exchange is used. The percentage of HF exchange is precisely built-in semiempirically from experimental atomization energies, ionization potentials, proton affinities, total atomic energies, *etc.* for a representative set of small molecules. Hybrid-meta GGA (HM-GGA) methods represent a new class of density functionals, based on a similar concept of M-GGAs. Instead of standard GGAs, these methods start from M-GGA. HM-GGA methods depend on HF exchange, electron density, the gradient of electron density and the kinetic energy density. B3LYP, B3P86, B3PW91, B97-1, MPWB1K, and X3LYP are examples of H-GGA methods and B1B95, BB1K, MPW1B95 and TPSS1KCIS are examples for HM-GGA methods.

The concept of Jacob's ladder (the famous allusion from the book of Genesis) for a hierarchy of DFT approximations was put forward by Perdew and Schmidt. The Jacob's ladder of density functionals is placed in the ground of the Hartree world and ends in the heaven of chemical accuracy. It contains five different rungs comprising the five generations of density functionals, *viz.* LDA, GGA, M-GGA, H-GGA and HM-HGA, and finally the fully nonlocal description. Each rung has particular strength and weakness adding something more to the design elements of the lower rungs. Recently, Janesko added a new rung on Jacob's ladder called "rung 3.5" which is considered as an intermediate between the local and hybrid functionals.

1.2.6.5 Minnesota Functionals

Minnesota functionals are a new suite of exchange-correlation functionals based on the meta-GGA approximation developed by Truhlar and coworkers at Minnesota University.[274-278] These functionals used in traditional quantum chemistry and solid-state physics calculations are all based on complicated functional forms parameterized on high-quality benchmark databases. The Minnesota functional family includes one meta-GGA (M06-L), two meta-NGAs (M11-L and MN12-L), seven global-hybrid meta-GGAs (M05, M05-2X, M06-2X, M08-HX, and M08-SO), one range-separated hybrid meta-

GGA (M11) and one screened exchange hybrid meta-NGA (MN12-SX). Among all these, the M06 family is the most admired one. It is composed of four functionals that have similar functional forms for the DFT part, with each having parameters optimized with a different percentage of HF exchange. These functionals are (i) M06-L,[275] a local functional (no HF exchange) (ii) M06,[279] a global-hybrid meta-GGA with 27% of HF exchange, (iii) M06-2X, a global hybrid meta-GGA with 54% HF exchange, and (iv) M06-HF, a global-hybrid meta-GGA with 100% HF exchange. M06-L is intended to be fast and is applicable for inorganic and organometallic systems. M06 is the most versatile of the 06 functionals because of its large applicability. M06-2X, is used for top-level across-the-board performances in all areas of chemistry including thermochemistry and reaction kinetics, but excluding multi-reference systems such as those containing transition metals and M06-HF is suitable for calculation of spectroscopic properties of charge-transfer transitions, where elimination of self-interaction error is of prime importance.[280]

1.2.6.6 Dispersion Corrections

To define long-range van der Waals type interaction in molecules, dispersion corrections are added to the KS-DFT functionals.[281-283] The total energy of the system using dispersion correction is represented as:

$$E_{DFT-D} = E_{KS-DFT} + E_{disp} \qquad \text{Eq. 1.63)}$$

where $E_{KS\text{-}DFT}$ is the self-consistent Kohn-Sham energy obtained from the chosen density functional, and the dispersion energy is given by:

$$E_{disp} = -S_6 \sum_{i=1}^{N_{at}-1} \sum_{j=i+1}^{N_{at}} \frac{C_6^{ij}}{R_{ij}^6} f_{dmp}(R_{ij}) \qquad \text{(Eq. 1.64)}$$

where N_{at} is the number of atoms in the system, S_6 is a global scaling factor that depends merely on the dispersion function used, C_6^{ij} is the dispersion coefficient for atom pair ij, R_{ij} is the interatomic distance, and f_{dmp} is the damping function which must be used to avoid near-singularities for small interatomic distance.

All the calculations discussed in this thesis (geometry optimization, vibration analysis, and single point calculations) have been done using Gaussian 09 (G09) suite of programs.[284]

1.2.7 Molecular Electrostatic Potential

According to the Coulomb's law in electrostatics, the force of attraction between two point charges is directly proportional to the product of the magnitudes of charges and inversely proportional to the square of the distance between them.

$$F = \frac{q_1 q_2 \hat{\mathbf{r}}}{4\pi\varepsilon_0 r^2} \qquad \text{(Eq. 1.65)}$$

where q_1 and q_2 are signed magnitudes of charges, the scalar r is the distance between the charges, $\hat{\mathbf{r}}$ is a unit vector joining the position vectors of q_1 and q_2, and $4\pi\varepsilon_0$ is the proportionality constant. The electric field, E produced by a fixed point charge q at a site **r** is given as:

$$E = \frac{\mathrm{qr}}{4\pi\varepsilon_0|\mathrm{r}|^3} \qquad \text{(Eq. 1.66)}$$

The electrostatic potential, V at a point r_0 in the field produced by a point charge q_0 can be written as:

$$V = \frac{q_0}{4\pi\varepsilon_0 \mathrm{r}} \qquad \text{(Eq. 1.67)}$$

Any allocation of electric charge creates potential in the surrounding space. Molecular electrostatic potential (MESP),[285-289] $V(\mathbf{r})$ is defined as the work done in bringing a unit test non-interacting positive charge from infinity to a reference point with the molecule and is given by the equation:

$$V(\mathbf{r}) = \sum_{A}^{N} \frac{Z_A}{|\mathbf{r} - \mathbf{R}_A|} - \int \frac{\rho(\mathbf{r}')\mathrm{d}^3\mathrm{r}'}{|\mathbf{r} - \mathbf{r}'|} \qquad \text{(Eq. 1.68)}$$

where Z_A is the charge on the nucleus located at a distance $\mathbf{R}_A$, $\rho(\mathbf{r}')$ is the electron density and $\mathbf{r}'$ is a dummy integration variable. In Eq. 1.68, first term describes the bare

nuclear potential while the second term accounts for the potential due to electron distribution. Both terms are positive and the subtraction operation leads to three different situations. The MSEP value vanishes when the first and second terms are equal. When the first term dominates, the MESP is positive and a higher second term leads to negative MESP value. This explains the positive MESP at the nuclear proximity and negative MESP at lone pair sites, π-bonds *etc.* where negative charge is concentrated. The extra electron in the anion leads to rich negative MESP features. MESP at the nucleus (V_n) is obtained by dropping out the nuclear contribution due to Z_A and is given by:

$$V_{0,A} = \sum_{B \neq A} \frac{Z_B}{\left| \mathbf{R}_B - \mathbf{R}_A \right|} - \int \frac{\rho(\mathbf{r}')d^3\mathbf{r}'}{\left| \mathbf{r} - \mathbf{r}' \right|} \qquad \text{(Eq. 1.69)}$$

Equipotential surface is defined as a collection of points in space having identical electrostatic potential values. The MESP features of a molecule are envisaged by viewing such equipotential surfaces. The electronic distribution of molecules is analyzed using critical points (CPs) the points at which the partial derivatives of MESP vanish. A CP is represented as ordered pair (R, S) where the rank R is the number of non-zero eigenvalues of the Hessian matrix rank and the signature S is the algebraic sum of the signs of these eigenvalues. CPs with at least one zero eigenvalue are called as degenerate and those with three non zero eigenvalues are called non-degenerate ones. Thus, there exist four types of non-degenerate critical points with rank 3 namely (3, -3), (3, -1), (3, +1) and (3, +3). The electron rich sites are characterized by (3, +3) critical points, often referred to as MESP minimum, V_{min}. The CPs (3, –1) and (3,+1) correspond to saddle points and (3, –3) is a local maximum. Figure 1.8 shows the MESP contour plot of hexafluorobenzene on 0.003 au isodensity surface with the electron rich and electron deficient regions in blue red, respectively.

MESP is a three-dimensional (3D) scalar field and real physical property which can be determined experimentally by X-ray diffraction techniques. MESP is a one-electron property, and its topological features are valuable implement for analyzing the structure, reactivity, Hammet free energy relationships, aromaticity, molecular recognition, intermolecular interactions, hydration patterns, *etc.* The semi-quantitative

rationalizations on more complex problems such as protein-ligand interactions, drug binding sites, Bronsted acidity, *etc*. are also done using MESP analysis.[288-290]

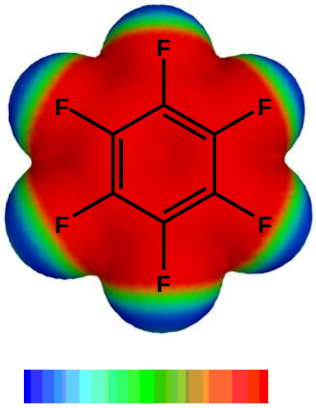

Figure 1.8 MESP contour plot of hexafluorobenzene on 0.003 au isodensity surface.

In this thesis, MESP is used as an implement for analyzing noncovalent interactions. The electronic parameters derived from MESP are used to correlate the stability of dihydrogen complexes and their charge delocalization. MESP analysis has been done using G09 program suite.[284]

1.2.8 Quantum Theory of Atoms in Molecules

Quantum theory of atoms in molecules (QTAIM) introduced by R. W. F. Bader describes molecular features such as bonds, atoms, and structure using the topology of electron density, $\rho(\mathbf{r})$.[291-293] The spatial distribution of electronic charge in the field of the nuclei and its flow in the presence of external field are derived from the $\rho(\mathbf{r})$. According to this theory, the topological distribution of electronic charge in the field of nuclei and its flow in the presence of external field derived from $\rho(\mathbf{r})$, a scalar quantity provides physical information about the molecule. The electron density reaches a maximum at the nuclear positions, and each atom is portrayed by its boundaries dependent on the balance of forces of the system under consideration. The point on the electron density surface at which the first derivative of density vanishes is called critical point (CP) and is given by:

$$\nabla\rho(\mathbf{r}) = \boldsymbol{i}\frac{d\rho}{dx} + \boldsymbol{j}\frac{d\rho}{dy} + \boldsymbol{k}\frac{d\rho}{dz} \longrightarrow \begin{cases} = 0 \text{ (at critical points } (\mathbf{r}_c) \text{ and at } \infty) \\ \neq 0 \text{ (at all other points)} \end{cases}$$

(Eq. 1.70)

The gradient of electron density, $\nabla\rho(\mathbf{r})$ at a point in space points in the direction in which $\rho(\mathbf{r})$ undergoes the maximum rate of increase, and its magnitude is equal to the rate of increase in that direction. Thus $\nabla\rho(\mathbf{r})$ is a vector quantity. A critical point may correspond to maximum, minimum or a saddle point. The second derivative of $\rho(\mathbf{r})$, $\nabla\nabla\rho(\mathbf{r})$ is considered for distinguishing a local minimum, a local maximum or a saddle point. The 'Hessian matrix' at a critical point is formed from the nine possible second derivatives of electron density and the Laplacian $\nabla^2\rho(\mathbf{r})$ is expressed as the sum of the eigenvalues of the Hessian matrix (Eq. 1.71).

$$\nabla^2\rho(\mathbf{r}) = \nabla.\nabla\rho(\mathbf{r}) = \frac{\partial^2\rho(\mathbf{r})}{\partial x^2} + \frac{\partial^2\rho(\mathbf{r})}{\partial y^2} + \frac{\partial^2\rho(\mathbf{r})}{\partial z^2} \qquad \text{(Eq.1.71)}$$

A critical point (CP) is labeled as an ordered pair (ω,σ), where ω is the rank and σ the signature. The rank (ω) is the number of non-zero curvatures of $\rho(\mathbf{r})$ at the critical point, and the signature (σ) is the algebraic sum of the signs of curvature. For energetically stable nuclear configurations ω is equal to 3, and there are four types of CPs with rank 3.

i. (3,-3) critical point known as nuclear critical point (NCP) with three negative curvatures where $\rho(\mathbf{r})$ is a local maximum.
ii. (3,-1) critical point known as bond critical point (BCP) with two negative curvatures where $\rho(\mathbf{r})$ is a maximum in the plane defined by these two eigenvectors and minimum along the third axis, which is perpendicular to this plane.
iii. (3,+1) critical point known as ring critical point (RCP) with two positive curvatures where $\rho(\mathbf{r})$ is a minimum along the plane defined by the

corresponding eigenvectors and maximum along the third axis, which is perpendicular to this plane.

iv. (3,+3) critical point known as cage critical point (CCP) with three positive curvatures where $\rho(\mathbf{r})$ is a local minimum.

Figure 1.9 depicts the QTAIM molecular graph of cubane showing bond paths, BCPs (red spheres), RCPs (blue spheres), and CCPs (green spheres).

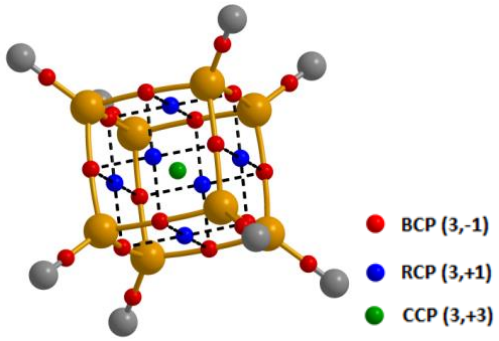

Figure 1.9 QTAIM molecular graph of cubane showing bond paths, BCPs, RCPs, and CCPs.

The analysis of electron density at a BCP, ρ_{bcp} is used for the characterization of interatomic bonding interaction, bond orders, the extent of charge accumulation in inter atomic surface, *etc*. Also, the strength of intermolecular interactions such as hydrogen bonds is measured from ρ_{bcp} values. The sign of Laplacian of electron density at BCP $\nabla^2\rho_{bcp}$ is used to determine the nature of the bond. $\nabla^2\rho_{bcp}$ is negative for shared interactions such as covalent and polarized bonds due as electron density is concentrated in the atom-atom region. Laplacian is positive for interactions like van der Waals, ionic and hydrogen bonds where there is depletion of electron charge in the atom-atom region. In this thesis, AIMAll program developed by Keith *et al.*[294] has been used for the topological analysis of electron density of dihydrogen complexes.

1.3 Conclusions

Hydrogen storage is a key facilitating technology for the development of hydrogen as a fuel for automotive purposes. Hydrogen has the highest energy per mass of any fuel; conversely, it has a low density at ambient temperature resulting in a low energy per

unit volume. This necessitates the development of advanced methods for storing hydrogen. The first part of Chapter 1 gives an overview of various hydrogen storage methods such as mechanical storage, chemical storage, and physisorption methods. An account of experimental and theoretical studies on hydrogen storage is discussed. The nature and strength of the interaction of H_2 with various storage materials have been highlighted in the discussion. These interactions play a crucial role in determining the hydrogen storage capacity of a system. Theoretical investigations are of great significance for the reliable prediction and understanding of such interactions.

Computational chemistry methods have become vital for understanding various chemical phenomena and are used to predict the molecular structure and reactivity with the aid of basic laws and equations that govern the subatomic world. The second part of Chapter 1 discusses the theoretical background of the computational chemistry methods such as density functional theory, *ab initio* methods, semiempirical methods, molecular mechanics, molecular dynamics and hybrid QM/MM methods. The basic principles and applications of molecular electrostatic potential, and quantum theory of atoms in molecules are also summarized in this chapter.

1.4 References

1. G. D. Berry, A. D. Pasternak, G. D. Rambach, J. R. Smith and R. N. Schock, *Energy*, **1996**, *21*, 289-303.
2. B. Johnston, M. C. Mayo and A. Khare, *Technovation*, **2005**, *25*, 569-585.
3. M. A. Rosen and S. Koohi-Fayegh, *Energ. Ecol. Environ.*, **2016**, *1*, 10-29.
4. A. M. Abdalla, S. Hossain, O. B. Nisfindy, A. T. Azad, M. Dawood and A. K. Azad, *Energy Convers. Manag.*, **2018**, *165*, 602-627.
5. R. Coontz and B. Hanson, *Science*, **2004**, *305*, 957.
6. L. Schlapbach, *MRS Bull.* , **2002**, *27*, 675-679.
7. L. Schlapbach and A. Zuttel, *Nature*, **2001**, *414*, 353-358.
8. P. Chen and M. Zhu, *Mater. Today*, **2008**, *11*, 36-43.
9. G. Principi, F. Agresti, A. Maddalena and S. L. Russo, *Energy*, **2009**, *34*, 2087–2091.

10. L. M. Das, *Int. J. Hydrog. Energy*, **1996**, *9*, 789–800.
11. D. J. Durbin and C. Malardier-Jugroot, *Int. J. Hydrog. Energy*, **2013**, *34*, 14595–14617.
12. R. Zacharia and S.-u. Rather, *J. Nanomat.*, **2015**, *2015*, 1-8.
13. A. Züttel, *Mater. Today*, **2003**, *6*, 24-33.
14. K. T. Møller, D. Sheppard, D. B. Ravnsbæk, C. E. Buckley, E. Akiba, H.-W. Li and T. R. Jensen, *Energies*, **2017**, *10*, 1645.
15. M. Kunowsky, J. P. Marco-Lózar and A. Linares-Solano, *J. Renew. Energy*, **2013**, *2013*, 1-16.
16. McWhorter S, Read C, Ordaz G and S. N, *Curr. Opin. Solid State Mater.*, **2011**, *15*, 29-38.
17. Y. Liu, Y. Yang, M. Gao and H. Pan, *Chem. Rec.*, **2016**, *16*, 189-204.
18. U. Eberle, M. Felderhoff and F. Schueth, *Angew. Chem. Int. Ed.*, **2009**, *48*, 6608-6630.
19. H. Barthelemy, M. Weber and F. Barbier, *Int. J. Hydrog. Energy*, **2017**, *42*, 7254-7262.
20. A. F. Dalebrook, W. Gan, M. Grasemann, S. Moret and G. Laurenczy, *Chem. Commun.*, **2013**, *49*, 8735-8751.
21. M. Felderhoff, C. Weidenthaler, R. von Helmolt and U. Eberle, *Phys. Chem. Chem. Phys.*, **2007**, *9*, 2643-2653.
22. A. C. Dillon and M. J. Heben, *Appl. Phys. A*, **2001**, *72*, 133-142.
23. S. Niaz, T. Manzoor and A. H. Pandith, *Renew. Sust. Energ. Rev.*, **2015**, *50*, 457-469.
24. J. Graetz, *Chem. Soc. Rev.*, **2009**, *38*, 73-82.
25. S. Orimo, Y. Nakamori, J. Eliseo, A. Zuttel and C. Jensen, *Chem. Rev.*, **2007**, *107*, 4111-4132.
26. B. Sakintuna, F. Lamari-Darkrim and M. Hirscher, *Int. J. Hydrog. Energy*, **2007**, *32*, 1121–1140.
27. A. Zaluska, L. Zaluski and J. O. Ström-Olsen, *J. Alloys Compd.*, **2000**, *298*, 125-134.
28. K. J. Gross, G. J. Thomas and C. M. Jensen, *J. Alloys Compd.*, **2002**, *330–332*, 683-690.

29. T. Kohno, H. Yoshida, F. Kawashima, T. Inaba, I. Sakai, M. Yamamoto and M. Kanda, *J. Alloys Compd.*, **2000**, *311*, L5-L7.
30. T. Motyka, *Hydrogen Storage: The Key Challenge Facing a Hydrogen Economy*, Citeseer, **2004**.
31. N. Rusman and M. Dahari, *Int. J. Hydrog. Energy*, **2016**, *41*, 12108-12126.
32. S. R. Johnson, P. A. Anderson, P. P. Edwards, I. Gameson, J. W. Prendergast, M. Al-Mamouri, D. Book, I. R. Harris, J. D. Speight and A. Walton, *Chem. Commun.*, **2005**, 2823-2825.
33. Y. Sun, C. Shen, Q. Lai, W. Liu, D.-W. Wang and A.-Z. Kondo-Francois, *Energy Storage Mater.*, **2018**, *10*, 168-198.
34. B. Bogdanović and M. Schwickardi, *J. Alloys Compd.*, **1997**, *253*, 1-9.
35. S. S. Srinivasan, H. W. Brinks, B. C. Hauback, D. Sun and C. M. Jensen, *J. Alloys Compd.*, **2004**, *377*, 283-289.
36. B. Bogdanović, M. Felderhoff, S. Kaskel, A. Pommerin, K. Schlichte and F. SCHüTH, *Adv. Mater.*, **2003**, *15*, 1012-1015.
37. J. Wang, A. D. Ebner, T. Prozorov, R. Zidan and J. A. Ritter, *J. Alloys Compd.*, **2005**, *395*, 252-262.
38. C. Li, P. Peng, D. Zhou and L. Wan, *Int. J. Hydrog. Energy*, **2011**, *36*, 14512-14526.
39. T. Matsunaga, F. Buchter, K. Miwa, S. Towata, S. Orimo and A. Züttel, *Renew.Energ.*, **2008**, *33*, 193-196.
40. E. Rönnebro and E. H. Majzoub, *J. Phys. Chem.*, **2007**, *111*, 12045-12047.
41. Y. Nakamori, H. Li, K. Miwa, S.-i. Towata and S.-i. Orimo, *Mater. Trans.*, **2006**, *47*, 1898-1901.
42. D. Pukazhselvan, V. Kumar and S. Singh, *Nano Energy*, **2012**, *1*, 566-589.
43. P. Chen, Z. Xiong, J. Luo, J. Lin and K. L. Tan, *Nature*, **2002**, *420*, 302-304.
44. T. Ichikawa, N. Hanada, S. Isobe, H. Leng and H. Fujii, *J. Phys. Chem. B*, **2004**, *108*, 7887-7892.
45. S. Orimo, Y. Nakamori, G. Kitahara, K. Miwa, N. Ohba, T. Noritake and S. Towata, *Appl. Phys. A*, **2004**, *79*, 1765-1767.
46. B. Peng and J. Chen, *Energy Environ. Sci*, **2008**, *1*, 479-483.
47. F. H. Stephens, V. Pons and R. T. Baker, *Dalton Trans.*, **2007**, 2613-2626.

48. R. Lan, J. T. Irvine and S. Tao, *Int. J. Hydrog. Energy*, **2012**, *37*, 1482-1494.
49. U. B. Demirci, *Int. J. Hydrog. Energy*, **2017**, *42*, 9978-10013.
50. A. Gutowska, L. Li, Y. Shin, C. M. Wang, X. S. Li, J. C. Linehan, R. S. Smith, B. D. Kay, B. Schmid and W. Shaw, *Angew. Chem. Int. Ed.*, **2005**, *44*, 3578-3582.
51. S. Hausdorf, F. Baitalow, G. Wolf and F. O. Mertens, *Int. J. Hydrog. Energy*, **2008**, *33*, 608-614.
52. A. D. Sutton, A. K. Burrell, D. A. Dixon, E. B. Garner, J. C. Gordon, T. Nakagawa, K. C. Ott, J. P. Robinson and M. Vasiliu, *Science*, **2011**, *331*, 1426-1429.
53. Z. Li, G. Zhu, G. Lu, S. Qiu and X. Yao, *J. Am. Chem. Soc.*, **2010**, *132*, 1490-1491.
54. Q. Yao, Z.-H. Lu, W. Huang, X. Chen and J. Zhu, *J. Mater. Chem. A*, **2016**, *4*, 8579-8583.
55. W.-W. Zhan, Q.-L. Zhu and Q. Xu, *ACS Catal.*, **2016**, *6*, 6892-6905.
56. H. Reardon, J. M. Hanlon, R. W. Hughes, A. Godula-Jopek, T. K. Mandal and D. H. Gregory, *Energy Environ. Sci*, **2012**, *5*, 5951–5979.
57. M. Dincâ, A. F. Yu and J. R. Long, *J. Am. Chem. Soc.*, **2006**, *128*, 8904–8913.
58. S. Iijima, *Nature*, **1991**, *354*, 56-58.
59. A. C. Dillon, K. Jones, T. Bekkedahl, C. Kiang, D. Bethune and M. Heben, *Nature*, **1997**, *386*, 377-379.
60. C. Liu and H.-M. Cheng, *J. Phys. D: Appl. Phys.*, **2005**, *38*, R231.
61. M. De la Casa-Lillo, F. Lamari-Darkrim, D. Cazorla-Amoros and A. Linares-Solano, *J. Phys. Chem. B*, **2002**, *106*, 10930-10934.
62. A. Züttel, P. Sudan, P. Mauron, T. Kiyobayashi, C. Emmenegger and L. Schlapbach, *Int. J. Hydrog. Energy*, **2002**, *27*, 203-212.
63. C. Liu, Y. Chen, C.-Z. Wu, S.-T. Xu and H.-M. Cheng, *Carbon*, **2010**, *48*, 452-455.
64. Y. Yürüm, A. Taralp and T. N. Veziroglu, *Int. J. Hydrog. Energy*, **2009**, *34*, 3784-3798.
65. M. P. Suh, H. J. Park, T. K. Prasad and D. W. Lim, *Chem. Rev.*, **2012**, *112*, 782-835.
66. J. L. Rowsell and O. M. Yaghi, *Microporous Mesoporous Mater.*, **2004**, *73*, 3-14.
67. J. L. Rowsell and O. M. Yaghi, *Angew. Chem. Int. Ed.*, **2005**, *44*, 4670-4679.
68. N. L. Rosi, J. Eckert, M. Eddaoudi, D. T. Vodak, J. Kim, M. O'keeffe and O. M. Yaghi, *Science*, **2003**, *300*, 1127-1129.

69. S. S. Kaye, A. Dailly, O. M. Yaghi and J. R. Long, *J. Am. Chem. Soc.*, **2007**, *129*, 14176-14177.

70. B. Chen, N. W. Ockwig, A. R. Millward, D. S. Contreras and O. M. Yaghi, *Angew. Chem.*, **2005**, *117*, 4823-4827.

71. O. K. Farha, A. Ö. Yazaydın, I. Eryazici, C. D. Malliakas, B. G. Hauser, M. G. Kanatzidis, S. T. Nguyen, R. Q. Snurr and J. T. Hupp, *Nat. Chem.*, **2010**, *2*, 944-948.

72. H. Furukawa, N. Ko, Y. B. Go, N. Aratani, S. B. Choi, E. Choi, A. Ö. Yazaydin, R. Q. Snurr, M. O'Keeffe and J. Kim, *Science*, **2010**, *329*, 424-428.

73. G. Li, H. Kobayashi, J. M. Taylor, R. Ikeda, Y. Kubota, K. Kato, M. Takata, T. Yamamoto, S. Toh and S. Matsumura, *Nat. Mater.*, **2014**, *13*, 802.

74. X. Feng, X. Ding and D. Jiang, *Chem. Soc. Rev.*, **2012**, *41*, 6010-6022.

75. S.-Y. Ding and W. Wang, *Chem. Soc. Rev.*, **2013**, *42*, 548-568.

76. R. W. Tilford, S. J. Mugavero, P. J. Pellechia and J. J. Lavigne, *Adv. Mater.*, **2008**, *20*, 2741-2746.

77. H. Furukawa and O. M. Yaghi, *J. Am. Chem. Soc.*, **2009**, *131*, 8875-8883.

78. T. Ben, C. Pei, D. Zhang, J. Xu, F. Deng, X. Jing and S. Qiu, *Energy Environ. Sci.*, **2011**, *4*, 3991-3999.

79. J.-T. Yu, Z. Chen, J. Sun, Z.-T. Huang and Q.-Y. Zheng, *J. Mater. Chem.*, **2012**, *22*, 5369-5373.

80. W. L. Mao, H.-k. Mao, A. F. Goncharov, V. V. Struzhkin, Q. Guo, J. Hu, J. Shu, R. J. Hemley, M. Somayazulu and Y. Zhao, *Science*, **2002**, *297*, 2247-2249.

81. H. P. Veluswamy, R. Kumar and P. Linga, *Appl. Energy*, **2014**, *122*, 112-132.

82. Y. A. Dyadin, E. G. Larionov, A. Y. Manakov, F. V. Zhurko, E. Y. Aladko, T. V. Mikina and V. Y. Komarov, *Mendeleev Commun.*, **1999**, *9*, 209-210.

83. H. Lee, J.-w. Lee, D. Y. Kim, J. Park, Y.-T. Seo, H. Zeng, I. L. Moudrakovski, C. I. Ratcliffe and J. A. Ripmeester, *Nature*, **2005**, *434*, 743-746.

84. Y. H. Hu and E. Ruckenstein, *Angew. Chem. Int. Ed.*, **2006**, *45*, 2011-2013.

85. H. Lu, J. Wang, C. Liu, C. I. Ratcliffe, U. Becker, R. Kumar and J. Ripmeester, *J. Am. Chem. Soc.*, **2012**, *134*, 9160-9162.

86. H. Langmi, A. Walton, M. Al-Mamouri, S. Johnson, D. Book, J. Speight, P. Edwards, I. Gameson, P. Anderson and I. Harris, *J. Alloys Compd.*, **2003**, *356*, 710-715.

87. H. Langmi, D. Book, A. Walton, S. Johnson, M. Al-Mamouri, J. Speight, P. Edwards, I. Harris and P. Anderson, *J. Alloys Compd.*, **2005**, *404*, 637-642.
88. Y. Li and R. T. Yang, *J. Phys. Chem. B*, **2006**, *110*, 17175-17181.
89. G. T. Palomino, M. L. Carayol and C. O. Areán, *J. Mater. Chem.*, **2006**, *16*, 2884-2885.
90. J. Dong, X. Wang, H. Xu, Q. Zhao and J. Li, *Int. J. Hydrog. Energy*, **2007**, *32*, 4998-5004.
91. A. Almasoudi and R. Mokaya, *J. Mater. Chem.*, **2012**, *22*, 146-152.
92. R. C. Lochan and M. Head-Gordon, *Phys. Chem. Chem. Phys.*, **2006**, *8*, 1357-1370.
93. G. J. Kubas, *Metal Dihydrogen and S-Bond Complexes: Structure, Theory, and Reactivity* Kluwer Academic/Plenum Publishers, New York, **2001**.
94. R. Z. Khaliullin, E. A. Cobar, R. C. Lochan, A. T. Bell and M. Head-Gordon, *J. Phys. Chem. A*, **2007** *111*, 8753-8765.
95. N. Park, K. Choi, J. Hwang, D. W. Kim, D. O. Kim and J. Ihm, *Proc. Natl. Acad. Sci.*, **2012**, *109*, 19893-19899.
96. L. Zhou, *Renew. Sust. Energ. Rev*, **2005**, *9*, 395- 408.
97. A. Zuttel, *Naturwissenschaften*, **2004**, *91*, 157-172.
98. M. Fichtner, *Adv. Eng. Mater*, **2005**, *7*, 443-455.
99. A. W. Ehlers, S. Dapprich, S. F. Vyboishchikov and G. Frenking, *Organometallics*, **1996**, *15*, 105–117.
100. G. J. Kubas, R. R. Ryan, B. I. Swanson, P. J. Vergamini and H. J.Wasserman, *J. Am. Chem. Soc.*, **1984**, *106*, 451–452.
101. V. Dryza, B. L. J. Poadw and E. J. Bieske, *Phys. Chem. Chem. Phys.*, **2012**, *14*, 14954-14965.
102. M. Barbatti, G. Jalbert and M. A. C. Nascimento, *J. Chem. Phys.*, **2001**, *114*, 2213–2218.
103. V. Dryza and E. J. Bieske, *Int. Rev. Phys. Chem.*, **2013**, *32*, 559-587.
104. D. A. Wild, P. S. Weiser, Z. M. Loh and E. J. Bieske, *J. Phys. Chem. A*, **2002**, *106*, 906–910.
105. D. A. Wild, R. L. Wilson, Z. M. Loh and E. J. Bieske, *Chem. Phys. Lett.*, **2004**, *393*, 517-520.

106. R. Clampitt and D. K. Jefferies, *Nature*, **1970**, *226*, 141-142
107. J. Easterfield and J. W. Linnett, *Nature*, **1970**, *226*, 142 -143.
108. R. Davy, E. Skoumbourdis and T. Kompanchenko, *Mol. Phys.*, **1999**, *97*, 1263-1271.
109. J. E. Bushnell, P. R. Kemper and M. T. Bowers, *J. Phys. Chem.*, **1994**, *98*, 2044-2049.
110. P. R. Kemper, J. E. Bushnell, P. Weis and M. T. Bowers, *J. Am. Chem. Soc.*, **1998**, *120*, 7577-7584.
111. P. R. Kemper, J. Bushnell, M. T. Bowers and G. I. Gellene, *J. Phys. Chem.*, **1998**, *102*, 8590–8597.
112. J. E. Bushnell, P. R. Kemper, P. Matre and M. T. Bowers, *J. Am. Chem. Soc.*, **1994**, *116*, 9710-9718.
113. J. E. Bushnell, P. Matre, P. R. Kemper and M. T. Bowers, *J. Chem. Phys.* , **1997**, *106*, 10153-10167.
114. J. E. Bushnell, P. R. Kemper and M. T. Bowers, *J. Phys. Chem.* , **1993**, *97*, 11628–11634.
115. C. W. Bauschlicher Jr, H. Partridge and S. R. Langhoff, *J. Phys. Chem.*, **1992**, *96*, 2475-2479.
116. J. E. Bushnell, P. R. Kemper and M. T. Bowers, *J. Phys. Chem.*, **1995**, *99*, 15602–15607.
117. P. R. Kemper, J. Bushnell, G. V. Helden and M. T. Bowers, *J. Phys. Chem.*, **1993**, *97*, 52–58.
118. P. R. Kemper, P. Weis and M. T. Bowers, *Chem. Phys. Letters*, **1998**, *293*, 503-510.
119. P. R. Kemper, P. Weis, M. T. Bowers and P. Matre, *J. Am. Chem. Soc.*, **1998**, *120*, 13494–13502.
120. P. Weis, P. R. Kemper and M. T. Bowers, *J. Phys. Chem. A* **1997**, *101*, 2809–2816.
121. C. A. Nicolaides and E. D. Simandiras, *Chem. Phys. Lett.*, **1992**, *196*, 213-219.
122. D.-Y. Hwang and A. M. Mebel, *J. Am. Chem. Soc.*, **2000**, *122*, 11406-11410.
123. D.-Y. Hwang and A. M. Mebel, *Chem. Phys. Lett.*, **2000**, *321*, 95-100.
124. P. Jena, *J. Phys. Chem. Lett.* , **2011**, *2*, 206-211.

125. S. S. Han, J. L. Mendoza-Cortés and W. A. Goddard Iii, *Chem. Soc. Rev.*, **2009**, *38*, 1460-1476.
126. Q. Yang, D. Liu, C. Zhong and J.-R. Li, *Chem. Rev.*, **2013**, *113*, 8261-8323.
127. J. Yang, A. Sudik, C. Wolverton and D. J. Siegel, *Chem. Soc. Rev.*, **2010**, *39*, 656-675.
128. S. Hamel and M. Côté, *J. Chem. Phys.*, **2004**, *121*, 12618-12625.
129. O. Hübner, A. Glöss, M. Fichtner and W. Klopper, *J. Phys. Chem. A*, **2004**, *108*, 3019-3023.
130. T. Sagara, J. Klassen and E. Ganz, *J. Chem. Phys.*, **2004**, *121*, 12543-12547.
131. T. Sagara, J. Klassen, J. Ortony and E. Ganz, *J. Chem. Phys.*, **2005**, *123*, 014701.
132. C. Buda and B. D. Dunietz, *J. Phys. Chem. B*, **2006**, *110*, 10479-10484.
133. F. Negri and N. Saendig, *Theor. Chem. Acc.* , **2007**, *118*, 149-163.
134. E. Klontzas, A. Mavrandonakis, G. Froudakis, Y. Carissan and W. Klopper, *J. Phys. Chem. C*, **2007**, *111*, 13635-13640.
135. S. S. Han, W. Q. Deng and W. A. Goddard, *Angew. Chem.*, **2007**, *119*, 6405-6408.
136. T. Sagara and E. Ganz, *J. Phys. Chem. C*, **2008**, *112*, 3515-3518.
137. A. Kuc, T. Heine, G. Seifert and H. A. Duarte, *Chem. Euro. J.*, **2008**, *14*, 6597-6600.
138. M. Prakash, M. Elango and V. Subramanian, *Int. J. Hydrog. Energy*, **2011**, *36*, 3922-3931.
139. K. Srinivasu, S. K. Ghosh, R. Das, S. Giri and P. K. Chattaraj, *RSC Adv.*, **2012**, *2*, 2914-2922.
140. Q. Sun, P. Jena, Q. Wang and M. Marquez, *J. Am. Chem. Soc.*, **2006**, *128*, 9741-9745.
141. S. Pan, G. Merino and P. K. Chattaraj, *Phys. Chem. Chem. Phys.*, **2012**, *14*, 10345-10350.
142. R. M. Kumar, J. V. Sundar and V. Subramanian, *Int. J. Hydrog. Energy*, **2012**, *37*, 16070-16077.
143. S. Rahali, M. Seydou, Y. Belhocine, F. Maurel and B. Tangour, *Int. J. Hydrog. Energy*, **2016**, *41*, 2711-2719.
144. T. Yildirim and S. Ciraci, *Phys. Rev. Lett.*, **2005**, *94*, 175501.
145. A. S. Shalabi, K. A. Soliman and H. O. Taha, *Phys. Chem. Chem. Phys.*, **2014**, *16*, 19333-19339.
146. K. Gopalsamy and V. Subramanian, *Int. J. Hydrog. Energy*, **2014**, *39*, 2549-2559.

147. C. Tang, S. Chen, W. Zhu, A. Zhang, K. Zhang and H. Zou, *Int. J. Hydrog. Energy*, **2014**, *39*, 12741-12748.
148. R. Konda, V. Kalamse, A. Deshmukh and A. Chaudhari, *RSC Adv.*, **2015**, *5*, 99207-99216.
149. L. W. Chung, W. M. C. Sameera, R. Ramozzi, A. J. Page, M. Hatanaka, G. P. Petrova, T. V. Harris, X. Li, Z. Ke, F. Liu, H.-B. Li, L. Ding and K. Morokuma, *Chem. Rev.*, **2015**, *115*, 5678-5796.
150. V. Kalamse, R. Krishna, E. Titus and A. Chaudhari, *Int. J. Hydrog. Energy*, **2016**, *41*, 11723-11729.
151. J. S. Gueriba, A. A. B. Padama, M. David, N. Arboleda Jr and H. Kasai, *Int. J. Hydrog. Energy*, **2017**, *42*, 11452-11460.
152. C. Guo and C. Wang, *Int. J. Hydrog. Energy*, **2018**, *43*, 1658-1666.
153. P. Tavhare, E. Titus and A. Chaudhari, *Int. J. Hydrog. Energy*, **2018**, 1-9.
154. T. Sagara, J. Klassen and E. Ganz, *J. Chem. Phys.*, **2004**, *121*, 12543-12547.
155. Q. Yang and C. Zhong, *J. Phys. Chem. B*, **2005**, *109*, 11862-11864.
156. G. Garberoglio, A. I. Skoulidas and J. K. Johnson, *J. Phys. Chem. B*, **2005**, *109*, 13094-13103.
157. H. Frost, T. Düren and R. Q. Snurr, *J. Phys. Chem. B*, **2006**, *110*, 9565-9570.
158. D. H. Jung, D. Kim, T. B. Lee, S. B. Choi, J. H. Yoon, J. Kim, K. Choi and S.-H. Choi, *J. Phys. Chem. B*, **2006**, *110*, 22987-22990.
159. P. Ryan, L. J. Broadbelt and R. Q. Snurr, *Chem. Commun.*, **2008**, 4132-4134.
160. Q. Zhao, W. Yuan, J. Liang and J. Li, *Int. J. Hydrog. Energy*, **2013**, *38*, 13104-13109.
161. Z. Meng, R. Lu, D. Rao, E. Kan, C. Xiao and K. Deng, *Int. J. Hydrog. Energy*, **2013**, *38*, 9811-9818.
162. E. I. Volkova, A. V. Vakhrushev and M. Suyetin, *Int. J. Hydrog. Energy*, **2014**, *39*, 8347-8350.
163. K. Gopalsamy and V. Subramanian, *New J. Chem.*, **2018**, *42*, 4240-4250.
164. G. Garberoglio, *Langmuir*, **2007**, *23*, 12154-12158.
165. E. Klontzas, E. Tylianakis and G. E. Froudakis, *J. Phys. Chem. C*, **2008**, *112*, 9095-9098.

166. G. Garberoglio and R. Vallauri, *Microporous Mesoporous Mater.*, **2008**, *116*, 540-547.
167. J. Lan, D. Cao and W. Wang, *J. Phys. Chem. C*, **2010**, *114*, 3108-3114.
168. N. Papadimitriou, I. Tsimpanogiannis and A. Stubos, *Colloids Surf. A Physicochem. Eng. Asp.* , **2010**, *357*, 67-73.
169. F. Li, J. Zhao, B. Johansson and L. Sun, *Int. J. Hydrog. Energy*, **2010**, *35*, 266-271.
170. B. Assfour, S. Leoni, S. Yurchenko and G. Seifert, *Int. J. Hydrog. Energy*, **2011**, *36*, 6005-6013.
171. J.-H. Guo, H. Zhang and Y. Miyamoto, *Phys. Chem. Chem. Phys.*, **2013**, *15*, 8199-8207.
172. L. Xia and Q. Liu, *J. Solid State Chem.* , **2016**, *244*, 1-5.
173. A. G. Blanco, J. A. de Oliveira, R. López, J. Moreno-Piraján, L. Giraldo, G. Zgrablich and K. Sapag, *Colloids Surf. A Physicochem. Eng. Asp.* , **2010**, *357*, 74-83.
174. J. W. Burress, S. Gadipelli, J. Ford, J. M. Simmons, W. Zhou and T. Yildirim, *Angew. Chem. Int. Ed.*, **2010**, *49*, 8902-8904.
175. J. H. Cho, S. J. Yang, K. Lee and C. R. Park, *Int. J. Hydrog. Energy*, **2011**, *36*, 12286-12295.
176. B. Assfour, S. Leoni, G. Seifert and I. A. Baburin, *Adv. Mater.*, **2011**, *23*, 1237-1241.
177. R. Lu, D. Rao, Z. Lu, J. Qian, F. Li, H. Wu, Y. Wang, C. Xiao, K. Deng and E. Kan, *J. Phys. Chem. C*, **2012**, *116*, 21291-21296.
178. L. Firlej, B. Kuchta, A. Lazarewicz and P. Pfeifer, *Carbon*, **2013**, *53*, 208-215.
179. Y. J. Colón, D. Fairen-Jimenez, C. E. Wilmer and R. Q. Snurr, *J. Phys. Chem. C*, **2014**, *118*, 5383-5389.
180. S. J. Mahdizadeh and E. Goharshadi, *Int. J. Hydrog. Energy*, **2014**, *39*, 1719-1731.
181. E. Tylianakis, G. K. Dimitrakakis, F. J. Martin-Martinez, S. Melchor, J. A. Dobado, E. Klontzas and G. E. Froudakis, *Int. J. Hydrog. Energy*, **2014**, *39*, 9825-9829.
182. G. Zhu, K. Lü, Q. Sun, Y. Kawazoe and P. Jena, *Comput. Mater. Sci.* , **2014**, *81*, 275-279.
183. Z. Ozturk, C. Baykasoglu and M. Kirca, *Int. J. Hydrog. Energy*, **2016**, *41*, 6403-6411.
184. Q. Yang and C. Zhong, *J. Phys.Chem. B*, **2005**, *109*, 11862-11864.

185. A. I. Skoulidas and D. S. Sholl, *J. Phys. Chem. B*, **2005**, *109*, 15760-15768.
186. B. Liu, Q. Yang, C. Xue, C. Zhong and B. Smit, *Phys. Chem. Chem. Phys.*, **2008**, *10*, 3244-3249.
187. F. Salles, H. Jobic, G. Maurin, M. Koza, P. Llewellyn, T. Devic, C. Serre and G. Ferey, *Phys. Rev. Lett.* , **2008**, *100*, 245901.
188. A. Bhattacharya, S. Bhattacharya, C. Majumder and G. Das, *J. Phys. Chem. C*, **2010**, *114*, 10297-10301.
189. S. Jalili, A. Jaberi, M. G. Mahjani and M. Jafarian, *Mol. Phys.*, **2012**, *110*, 361-368.
190. C.-D. Wu, T.-H. Fang and J.-Y. Lo, *Int. J. Hydrog. Energy*, **2012**, *37*, 14211-14216.
191. Z. Liu, Q. Xue, C. Ling, Z. Yan and J. Zheng, *Comput. Mater. Sci.*, **2013**, *68*, 121-126.
192. Q. Hu, D. Sun, Q. Wu, H. Wang, L. Wang, B. Liu, A. Zhou and J. He, *J. Phys. Chem. A*, **2013**, *117*, 14253-14260.
193. Q. Hu, H. Wang, Q. Wu, X. Ye, A. Zhou, D. Sun, L. Wang, B. Liu and J. He, *Int. J. Hydrog. Energy*, **2014**, *39*, 10606-10612.
194. H. Jiang, X.-L. Cheng, H. Zhang, Y.-J. Tang and C.-X. Zhao, *Comput. Theor. Chem.*, **2015**, *1068*, 97-103.
195. N. Faginas-Lago, D. Yeni, F. Huarte, Y. Wang, M. Alcamí and F. Martin, *J. Phys. Chem. A*, **2016**, *120*, 6451-6458.
196. J. A. Pople and D. L. Beveridge, *Approximate Molecular Orbital Theory*, McGraw-Hill, New York, **1970**.
197. J. J. Stewart, *Semiempirical Molecular Orbital Methods*, Wiley Online Library, **2007**.
198. M. C. Zerner, *Semiempirical Molecular Orbital Methods*, **2007**.
199. D. B. Boyd and K. B. Lipkowitz, *J. Chem. Educ.*, **1982**, *59*, 269274.
200. J. P. Bowen and N. L. Allinger, *Rev. Comp. Chem.*, **1991**, *2*, 81-97.
201. U. Dinur and A. T. Hagler, *Rev. Comp. Chem.*, **1991**, *2*, 99-164.
202. P. K. Weiner and P. A. Kollman, *J. Comput. Chem.*, **1981**, *2*, 287-303.
203. S. Grimme and P. R. Schreiner, *Angew. Chem. Int. Ed.*, **2018**, *57*, 4170-4176.
204. T. Sperger, I. A. Sanhueza and F. Schoenebeck, *Acc. Chem. Res.*, **2016**, *49*, 1311–1319.
205. E. Schrödinger, *Annalen der physik*, **1926**, *79*, 361-376.

206. M. Born and R. Oppenheimer, *Annalen der Physik*, **1927**, *389*, 457-484.
207. V. Fock, *Z. Phys.*, **1930**, *61*, 126-148.
208. R. R. Hartree, Proc. Cambridge Phil. Soc., **1928**.
209. J. C. Slater, *Phys. Rev.*, **1930**, *35*, 210-211.
210. G. G. Hall, *Proc. Royal Soc. A*, **1951**, *205*, 541-552.
211. C. C. J. Roothaan, *Rev. Mod. Phys.*, **1951**, *23*, 69-89.
212. I. Shavitt, *Mol. Phys.*, **1998**, *94*, 3-17.
213. R. J. Bartlett and M. Musiał, *Rev. Mod. Phys.*, **2007**, *79*, 291-352.
214. D. Cremer, *Wiley Interdiscip. Rev. Comput. Mol. Sci.*, **2011**, *1*, 509-530.
215. C. Møller and M. S. Plesset, *Phys. Rev.*, **1934**, *46*, 618-622.
216. H. Nakano, *J. Chem. Phys.*, **1993**, *99*, 7983-7992.
217. S. F. Boys, *Proc. Royal Soc. A*, **1950**, *200*, 542-554.
218. H. J. Werner and P. J. Knowles, *J. Chem. Phys.*, **1988**, *89*, 5803-5814.
219. P. J. Knowles and H.-J. Werner, *Chem. Phys. Lett.*, **1988**, *145*, 514-522.
220. D. C. Young, *Ab Initio Methods*, **2001**.
221. A. Szabo and N. S. Ostlund, *Modern Quantum Chemistry: Introduction to Advanced Electronic Structure Theory*, Courier Corporation, **2012**.
222. J. Čížek, *Theor. Chim. Acta*, **1991**, *80*, 91-94.
223. J. Čížek and J. Paldus, *Phys. Scr.*, **1980**, *21*, 251-254.
224. J. Čížek, *J. Chem. Phys.*, **1966**, *45*, 4256-4266.
225. L. Brillouin, *Actualities Sci. Ind.*, **1934**, *159*, 37.
226. D. Cremer, *Møller–Plesset Perturbation Theory*, **1998**.
227. D. G. Fedorov and K. Kitaura, *J. Chem. Phys.*, **2004**, *121*, 2483-2490.
228. L. C. Allen and A. M. Karo, *Rev. Mod. Phys.*, **1960**, *32*, 275-285.
229. J. C. Slater, *Phys. Rev.*, **1930**, *36*, 57-64.
230. P. M. W. Gill, in *Advances in Quantum Chemistry*, eds. J. R. Sabin and M. C. Zerner, Academic Press, **1994**, *25*, 141-205.
231. D. Feller and E. R. Davidson, in *Rev. Comp. Chem.*, John Wiley & Sons, Inc., **2007**, 1-43.
232. E. Besalú and R. Carbó-Dorca, *J. Math. Chem.*, **2011**, *49*, 1769-1784.
233. I. Shavitt and M. Karplus, *J. Chem. Phys.*, **1965**, *43*, 398-414.

234. Y. Sakai, H. Tatewaki and S. Huzinaga, *J. Comput. Chem.*, **1981**, *2*, 100-107.
235. R. F. Stewart and W. J. Hehre, *J. Chem. Phys.*, **1970**, *52*, 5243-5247.
236. H. Tatewaki and S. Huzinaga, *J. Chem. Phys.*, **1979**, *71*, 4339-4348.
237. J. B. Collins, P. v. R. Schleyer, J. S. Binkley and J. A. Pople, *J. Chem. Phys.*, **1976**, *64*, 5142-5151.
238. W. J. Hehre, R. F. Stewart and J. A. Pople, *J. Chem. Phys.*, **1969**, *51*, 2657-2664.
239. E. R. Davidson and D. Feller, *Chem. Rev.*, **1986**, *86*, 681-696.
240. A. K. Wilson, D. E. Woon, K. A. Peterson and T. H. Dunning Jr, *J. Chem. Phys.*, **1999**, *110*, 7667-7676.
241. T. H. Dunning Jr, *J. Chem. Phys.*, **1989**, *90*, 1007-1023.
242. R. Ditchfield, W. J. Hehre and J. A. Pople, *J. Chem. Phys.*, **1971**, *54*, 724-728.
243. M. J. Frisch, J. A. Pople and J. S. Binkley, *J. Chem. Phys.*, **1984**, *80*, 3265-3269.
244. G. Petersson and M. A. Al-Laham, *J. Chem. Phys.*, **1991**, *94*, 6081-6090.
245. R. Krishnan, J. S. Binkley, R. Seeger and J. A. Pople, *J. Chem. Phys.*, **1980**, *72*, 650-654.
246. S. F. Boys and F. D. Bernardi, *Molecular Physics*, **1970**, *19*, 553-566.
247. D. B. Boyd and K. B. Lipkowitz, *J. Chem. Educ.* , **1982**, *59*, 269-274.
248. P. K. Weiner and P. A. Kollman, *J. Comput. Chem.*, **1981**, *2*, 287-303.
249. J. Wang, R. M. Wolf, J. W. Caldwell, P. A. Kollman and D. A. Case, *J. Comput. Chem.*, **2004**, *25*, 1157-1174.
250. K. Vanommeslaeghe, E. Hatcher, C. Acharya, S. Kundu, S. Zhong, J. Shim, E. Darian, O. Guvench, P. Lopes and I. Vorobyov, *J. Comput. Chem.*, **2010**, *31*, 671-690.
251. K. Binder, J. Horbach, W. Kob, W. Paul and F. Varnik, *J. Phys. Condens. Matter*, **2004**, *16*, S429.
252. T. Hansson, C. Oostenbrink and W. van Gunsteren, *Curr. Opin. Struct. Biol.*, **2002**, *12*, 190-196.
253. G. Ciccotti, M. Ferrario and C. Schuette, *Entropy*, **2014**, *16*, 233-257.
254. H. Grubmüller, H. Heller, A. Windemuth and K. Schulten, *Mol. Simulat.*, **1991**, *6*, 121-142.
255. W. Thiel, *Wiley Interdiscip. Rev. Comput. Mol. Sci.*, **2014**, *4*, 145-157.
256. R. Hoffmann, *J. Chem. Phys.*, **1963**, *39*, 1397-1412.

257. R. Pariser and R. G. Parr, *J. Chem. Phys.*, **1953**, *21*, 767-776.
258. J. R. Sabin and S. Canuto, *Combining Quantum Mechanics and Molecular Mechanics. Some Recent Progresses in Qm/Mm Methods*, Academic Press, **2010**.
259. A. Warshel and M. Levitt, *J. Mol. Biol.*, **1976**, *103*, 227-249.
260. M. Karplus, *Annu. Rev. Biophys. Biomol. Struct.*, **2006**, *35*, 1-47.
261. M. Levitt, *Nat. Struct. Mol. Biol.*, **2001**, *8*, 392-393.
262. U. C. Singh and P. A. Kollman, *J. Comput. Chem.*, **1986**, *7*, 718-730.
263. J. Gao and M. A. Thompson, *Combined Quantum Mechanical and Molecular Mechanical Methods*, ACS Publications, **1998**.
264. L. W. Chung, H. Hirao, X. Li and K. Morokuma, *Wiley Interdiscip. Rev. Comput. Mol. Sci.*, **2012**, *2*, 327-350.
265. L. H. Thomas, *Proc. Cambridge Phil. Soc.*, **1927**.
266. E. Fermi, *Rend. Acad. Lincei*, **1927**, *6*, 602.
267. E. Fermi, *Z. Phys.*, **1928**, *48*, 73-79.
268. A. D. Becke, *J. Chem. Phys.*, **2014**, *140*, 18A301.
269. W. Kohn and L. J. Sham, *Phys. Rev.*, **1965**, *140*, A1133-A1138.
270. S. H. Vosko, L. Wilk and M. Nusair, *Can. J. Phys.*, **1980**, *58*, 1200-1211.
271. A. D. Becke, *Phys. Rev. A*, **1988**, *38*, 3098-3100.
272. J. P. Perdew, *Phys. Rev. B*, **1986**, *33*, 8822-8824.
273. K. Burke, J. P. Perdew and Y. Wang, in *Electronic Density Functional Theory*, Springer, **1998**, 81-111.
274. R. Peverati and D. G. Truhlar, *Phil. Trans. R. Soc. A*, **2014**, *372*, 20120476.
275. Y. Zhao and D. G. Truhlar, *J. Chem. Phys.*, **2006**, *125*, 194101.
276. Y.-S. Lin, C.-W. Tsai, G.-D. Li and J.-D. Chai, *J. Chem. Phys.*, **2012**, *136*, 154109.
277. Y. Zhao, N. E. Schultz and D. G. Truhlar, *J. Chem. Phys.*, **2005**, *123*, 161103.
278. R. Peverati and D. G. Truhlar, *J. Chem. Theory Comput.*, **2012**, *8*, 2310-2319.
279. Y. Zhao and D. G. Truhlar, *Theor. Chem. Acc.*, **2008**, *120*, 215-241.
280. Y. Zhao and D. G. Truhlar, *Acc. Chem. Res.*, **2008**, *41*, 157-167.
281. E. R. Johnson, I. D. Mackie and G. A. DiLabio, *J. Phys. Org. Chem.*, **2009**, *22*, 1127-1135.

282. S. Grimme, J. Antony, T. Schwabe and C. Muck-Lichtenfeld, *Org. Biomol. Chem.*, **2007**, *5*, 741-758.

283. S. Grimme, *Wiley Interdiscip. Rev. Comput. Mol. Sci.*, **2011**, *1*, 211-228.

284. M. J. Frisch, G. W. Trucks, H. B. Schlegel, G. E. Scuseria, M. A. Robb, J. R. Cheeseman, G. Scalmani, V. Barone, B. Mennucci, G. A. Petersson, H. Nakatsuji, M. Caricato, X. Li, H. P. Hratchian, A. F. Izmaylov, J. Bloino, G. Zheng, J. L. Sonnenberg, M. Hada, M. Ehara, K. Toyota, R. Fukuda, J. Hasegawa, M. Ishida, T. Nakajima, Y. Honda, O. Kitao, H. Nakai, T. Vreven, J. A. Montgomery, J. E. Peralta, F. Ogliaro, M. Bearpark, J. J. Heyd, E. Brothers, K. N. Kudin, V. N. Staroverov, T. Keith, R. Kobayashi, J. Normand, K. Raghavachari, A. Rendell, J. C. Burant, S. S. Iyengar, J. Tomasi, M. Cossi, N. Rega, J. M. Millam, M. Klene, J. E. Knox, J. B. Cross, V. Bakken, C. Adamo, J. Jaramillo, R. Gomperts, R. E. Stratmann, O. Yazyev, A. J. Austin, R. Cammi, C. Pomelli, J. W. Ochterski, R. L. Martin, K. Morokuma, V. G. Zakrzewski, G. A. Voth, P. Salvador, J. J. Dannenberg, S. Dapprich, A. D. Daniels, O. Farkas, J. B. Foresman, J. V. Ortiz, J. Cioslowski and D. J. Fox, Gaussian 09, Revision D.01; Gaussian, Inc., Wallingford CT,**2013**.

285. B. Pullman, Intern. J. Quantum Chem. Quantum Biology Symp., **1990**.

286. E. Scrocco and J. Tomasi, in *Adv. Quantum Chem.*, **1978**, 11, 116.

287. S. R. Gadre and R. N. Shirsat, *Electrostatics of Atoms and Molecules*, Universities Press, Hyderabad, India, **2000**.

288. S. R. Gadre, P. K. Bhadane, S. S. Pundlik and S. S. Pingale, *Molecular Electrostatic Potential: Concepts and Applications*, Elsevier, Amsterdam, **1996**.

289. P. Politzer and D. G. Truhlar, *Chemical Applications of Atomic and Molecular Electrostatic Potentials*, Plenum Press, New York, **1981**.

290. F. J. Luque, M. Orozco, P. K. Bhadane and S. R. Gadre, *J. Chem. Phys.*, **1994**, *100*, 6718-6726.

291. R. F. W. Bader, *Acc. Chem. Res*, **1985**, *18*, 9-15.

292. R. F. W. Bader, *Atoms in Molecules: A Quantum Theory*, Clarendon Press,Oxford, UK, **1990.**

293. R. F. W. Bader, *Atoms in Molecules*, John Wiley & Sons, Ltd, **2002**.

294. T. A. Keith, *AIMAll version 14.04.17,* TK Gristmill Software, Overland Park KS, USA, **2014**.

Chapter 2

Dihydrogen Binding Affinity of Anions

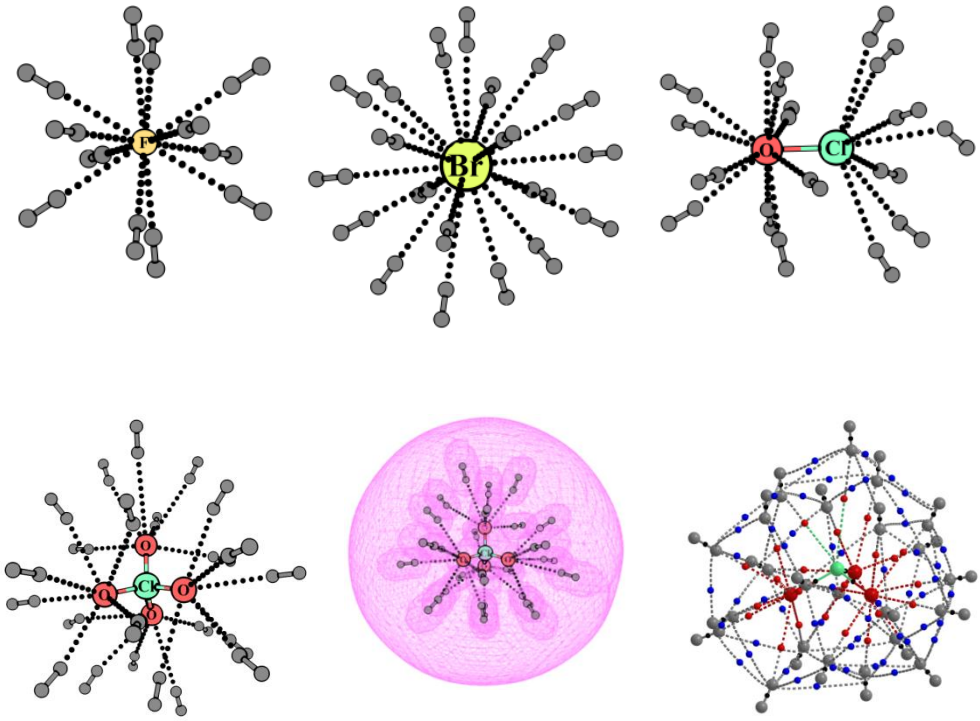

Part A: Dihydrogen Binding Affinity of Bare Anions

2.1 Abstract

The structural features and hydrogen binding affinity of anions F^-, Cl^-, Br^-, OH^-, NH_2^-, NO_2^-, CN^-, and ClO^- have been explored using coupled cluster CCSD(T)/aug-cc-pVTZ//CCSD/6-311++G(d,p) theory and M06L/6-311++G(d,p) level density functional theory along with a two-point extrapolation to complete basis set limit and a benchmark study at CCSD(T) and MP2 levels. The coupled cluster, MP2 and DFT methods yield comparable results and show that anions have very high capacity to store hydrogen as the weight percent of H_2 in the highest H_2-coordinated state of F^-, Cl^-, Br^-, OH^-, NH_2^-, NO_2^-, CN^-, and ClO^- is 56.0, 47.6, 33.5, 64.0, 65.4, 41.2, 55.4, 40.0 wt%, respectively. The CCSD(T)/aug-cc-pVTZ//CCSD/6-311++G(d,p) results are presented for anions coordinated with up to nine or ten H_2 while up to the entire first coordination shell is computed using M06L which revealed H_2 coordination numbers 12, 16, 20, 15, 15, 16, 16, and 17, respectively for F^-, Cl^-, Br^-, OH^-, NH_2^-, NO_2^-, CN^-, and ClO^-. An increase in total interaction energy (E_{int}) and decrease in interaction energy per H_2 ($E_{int/H2}$) with increase in the number of coordinated H_2 is observed. However, the decline in $E_{int/H2}$ is very less and even in the highest coordinated anions, substantially good values for $E_{int/H2}$ is observed, viz. 4.24, 2.59, 2.09, 3.32, 3.07, 2.36, 2.31, and 2.63 kcal/mol, respectively for F^-, Cl^-, Br^-, OH^-, NH_2^-, NO_2^-, CN^-, and ClO^- which are comparable with the values obtained for complexes with lesser H_2 coordination. The stability of the complex is attributed to the formation of large number of non-covalent X^-...H bonds as revealed by the identification of bond critical points in QTAIM analysis. Further, critical features of MESP have been used to correlate the stability of $X^-(H_2)_n$ complexes to the charge delocalization in the complex. These results show that anions have a remarkable ability to bind with a large number of hydrogen molecules and this property can be utilized for the development of novel salt systems for hydrogen storage.

2.2 Introduction

The structure, bonding, and spectral properties of dihydrogen adducts of halide ions have been studied for several years. A high-level *ab initio* study by Nichols *et al.* reported a linear structure for $F^-...H_2$ complex.[1] Boldyrev *et al*. reported the *ab initio* vibration-rotation-tunnelling spectra and dynamics of $F^-...H_2$ and its isotopomers.[2] *Ab initio* calculations on photoelectron spectra of FH_2^- has been reported by Hartke and Werner.[3] Theoretical studies on lower bend-stretch structures $Cl^-...H_2$ and its isotopomers has also been reported.[4] In a series of studies, Bieske and co-workers used experimental infrared spectral and vibration predissociation data along with theoretically derived potential energy and dipole moment data to interpret the mechanism of halide...H_2 complex formation in acid–base proton transfer reactions.[5-13] However, in all these studies the H_2 storage ability of anions has not been conferred.

Later, researchers started studying $X^-...H_2$ interactions focussing on the H_2 storage ability of anions. Nyulasi and Kovács have studied $F^-(H_2)_n$ and $Cl^-(H_2)_n$ (n = 1 – 8) anionic complexes at the MP2/aug-cc-pVTZ and CCSD(T)/aug-cc-pVTZ levels of theory.[14] They have mentioned that the second solvation shell evolves for F^- and Cl^- ions when n = 10 and 15 respectively. However, the structure and energetic of complexes with $n > 8$ have not been reported. The natural bond order (NBO) analysis done by them suggested charge transfer from the halide ion to the $\sigma^*(H_2)$ orbital. Halides are capable of a polarizing nonpolar molecule like H_2 which make them fit for dihydrogen bonding.[15, 16] H_2 forms hydrogen-bonded complexes with anions on account of its permanent quadrupole moment and induced dipole. The strength of $F^-...H_2$ interactions decreased with increase in the number of H_2 whereas that of $Cl^-...H_2$ showed a negligible dependence on the number of H_2. In yet another work carried out by Pichierri the structural and bonding properties of $F^-(H_2)_n$ (n = 1- 6), $Cl^-(H_2)_n$ (n = 1- 6), and $Br^-(H_2)_n$ (n = 1- 7) are described.[17] The calculations were done using MPWB1K/6-31++G(d,p) level of theory and the interaction energy (E_{int}) for $F^-(H_2)$, $Cl^-(H_2)$, and $Br^-(H_2)$ complexes were found to be 7.1, 2.2 and 1.7 kcal/mol, respectively. The bonding features studied by Quantum Theory of Atoms in Molecule (QTAIM) analysis showed the presence of closed–shell interactions and the interaction energy (E_{int}) for $F^-(H_2)$, $Cl^-(H_2)$, and

$Br^-(H_2)$ complexes were found to be 7.1, 2.2 and 1.7 kcal/mol, respectively. *Ab initio* studies on charge separated ammonium fluorides reported by Trewin *et al.* have established naked F^- as good binding sites for H_2 physisorption.[18] The electrostatic analysis of $X^-...H_2$ (X = F, Cl, Br, I) complexes at different levels of theory reported by Vitillo *et al*. suggests that the electrostatic term predominates in the complexation energy of the adduct.[19] In another theoretical work by Lochan and Head−Gordon, the interaction of H_2 with certain anionic ligands such as CN^-, NC^-, F^-, SO_4^{2-}, Cp^-, *etc.* have been discussed at MP2/6−31G** method.[20] According to them, the LUMO of the H_2 accepts electron density from the anion which induces a dipole on H_2 and results in a charge−induced dipole interaction in the complex. The E_{int} of the complexes were in the range 1.9 – 8.1 kcal/mol and the binding affinities followed the order $NC^- < CN^- < Cp^- < SO_4^{2-} < F^-$ for the tested anions.

Theoretical investigations are of great significance in making reliable prediction and understanding of modified materials for the storage of hydrogen. In all the previous studies, the maximum number of H_2 that can be accommodated in the first coordination shell (n_{max}) of the anion has not been explored. Our main focus is to comprehend the binding nature of H_2 with various anions and to predict efficient H_2 storing systems. The present study comprises of the systematic analysis of structure and energetics of H_2 complexes of eight anions which includes F^-, Cl^-, Br^-, OH^-, NH_2^-, NO_2^-, CN^-, and ClO^-. The complete first coordination shells of all the anions with H_2 are revealed which will be useful for comparing the ability of different anions to store dihydrogen. We expect that this study will be beneficial for designing novel hydrogen storage materials.

2.3 Computational Details

In the present work, calculations have been done at coupled cluster CCSD(T)/aug-cc-pVTZ//CCSD/6-311++G(d,p) theory and M06L/6-311++G(d,p) level of density functional theory (DFT). The selection of M06L/6-311++G(d,p) theory is based on the recommendations given in a previous benchmark study that it can reproduce binding energy and geometry of a variety of non-covalent dimers close to the accuracy of CCSD level.[21] The geometries of anion-$(H_2)_n$

complexes are confirmed as energy minimum structures by vibrational frequency calculations. The diffuse functions in the basis set are necessary for the proper description of the anion wave function. The counterpoise method is employed in calculating the BSSE.[22] Further, to validate the accuracy of our results, the E_{int} of smaller complexes has been extrapolated to complete basis set (CBS) limit at MP2, and CCSD(T) levels using aug-cc-pVTZ and aug-cc-pVQZ basis sets by employing Truhlar's method along with BSSE correction.[23, 24]

Topological analysis of electron density at BCP, ρ_{bcp} has been performed by Bader's QTAIM technique.[25] The topographical features of MESP are very useful to correlate the electron dense and electron deficient regions of a molecule to its inherent reactivity and interactive behaviour with other molecules.[26-37] The MESP features of all the anion complexes are investigated at M06L/6-311++G(d,p) level of theory. All optimizations, energy calculations and MESP analysis[32, 38] have been done using Gaussian 09 package[39] and QTAIM analysis using AIMAll package.[40]

2.4 Results and Discussion

2.4.1 Geometry and Energetics Using Coupled Cluster Method

At first the geometry, structural parameters, and energetics of n = 1 – 10 complexes have been discussed based on CCSD(T)/aug-cc-pVTZ//CCSD/6-311++G(d,p) level results. The computational cost of this method limits its usage for larger clusters. The energetics obtained by M06L method shows that the energy values are comparable with the results obtained by CCSD(T) calculations. Hence, for systems with n > 10, the explanations are completely based on M06L method. The energy minimum structures of $F^-(H_2)_n$ complexes (n = 1 to 10) optimized at CCSD/6-311++G(d,p) are represented in Figure 2.1. For all other anions, some representative structures (n = 1, 3, 5, 10) are given in Figure 2.2. In all the complexes, H_2 binds to the anion in an end-on fashion. This is due to the ability of H_2 to accept electron density to its lowest unoccupied molecular orbital (LUMO). Occupancy of the antibonding LUMO activates the H-H bond resulting to

the elongation of that bond in all the anion-$(H_2)_n$ clusters.[41, 42] For instance, the H-H bond lengths of $F^-(H_2)$, $Cl^-(H_2)$, and $Br^-(H_2)$ are 0.776, 0.750, and 0.748 Å respectively which is higher compared to the normal H-H bond length 0.740 Å.

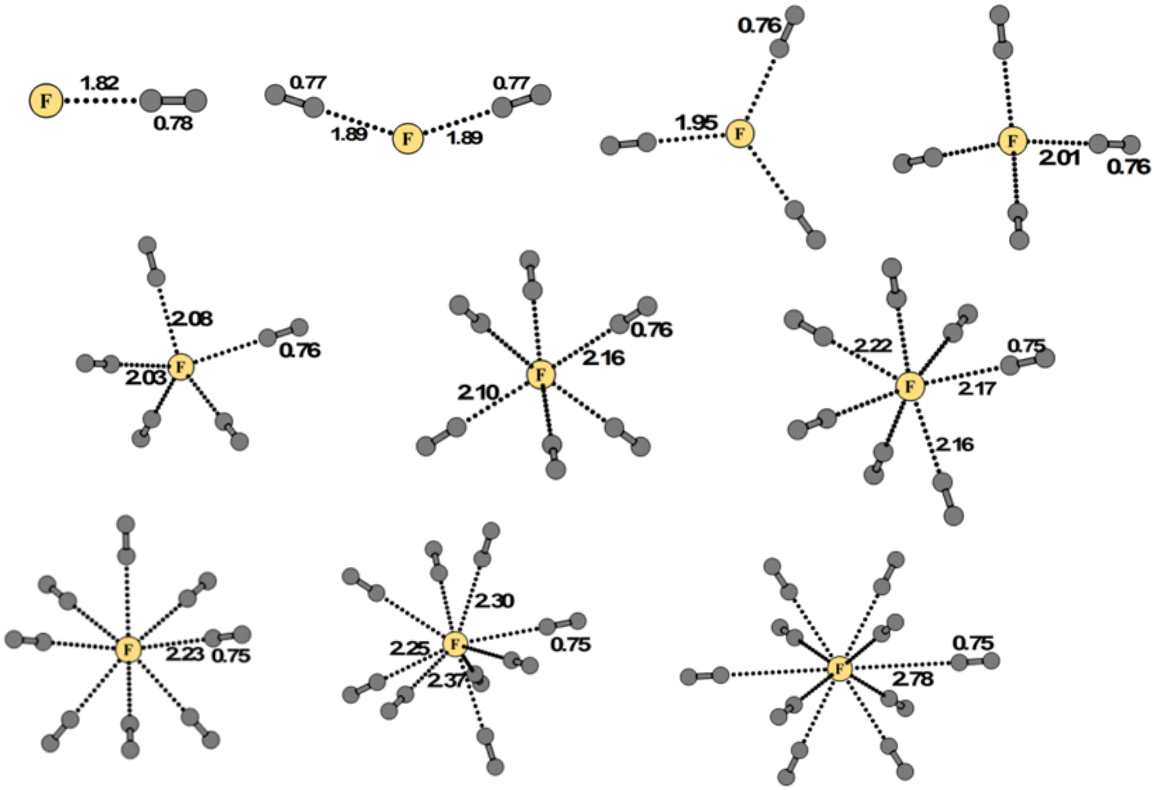

Figure 2.1 Optimized geometries of $F^-(H_2)_n$ (n = 1 – 10) complexes at the CCSD/6-311++G(d,p) level. Bond distances are in Å.

Among the halide anions, $F^-(H_2)_n$ complexes are linear, slightly bent, trigonal planar, tetrahedral, trigonal bipyramidal and octahedral, respectively from n = 1 - 6. These structures are in agreement with the previously reported studies.[14, 17] The complexes with n = 7 - 10 adopt a symmetrical three dimensional arrangement around the anion. The structures of $Cl^-(H_2)_n$ and $Br^-(H_2)_n$ complexes with n = 1 - 3 are planar with H_2 molecules interacting with anion center similar to that of $F^-(H_2)_n$ complexes. The complexes of Cl^- and Br^- with n > 3 show irregular shapes. Moving from F^- to Br^-, the significant increase in ionic radii causes a more diffused electron density distribution in Cl^- and Br^- compared to F^-. Further, the polarization of anion by quadrupole and induced dipole of the

surrounding H_2 molecules become more efficient in the case of bigger Cl^- and Br^- anions than F^- leading to dissimilarity in their H_2 coordination features.[14]

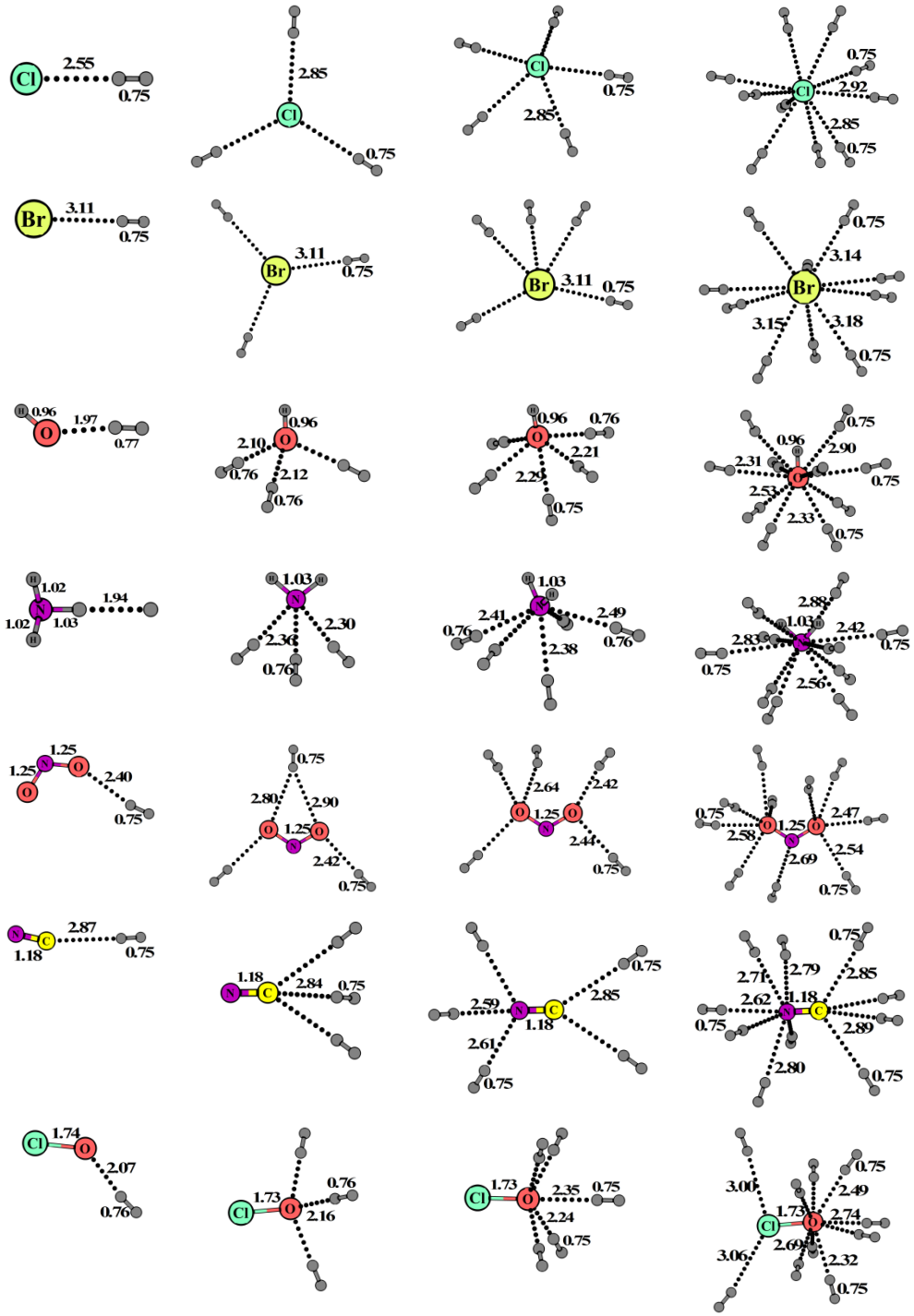

Figure 2.2 Optimized geometries of $X^-(H_2)_n$ complexes at the CCSD/6-311++G(d,p) level. Bond distances are in Å.

Table 2.1 shows the average X^-...H distances of complexes of all anions optimized at CCSD/6-311++G(d,p) level. This distance increases with increase in the size of the anion which is well understood from the distances 1.825, 2.554, and 3.112 Å observed for F^-, Cl^-, and Br^-, respectively for n = 1 complexes. Further, in the case of F^-, the distance increases as n goes from 1 – 10 and reaches to the highest value 2.378 Å for $F^-(H_2)_{10}$ whereas it remains almost a constant for Cl^- and Br^- ions. Fluorine being smaller in size, undergoes rapid expansion of coordination sphere to cope up with the space requirement to accommodate several H_2 molecules.

Table 2.1 Average X^-…H distances (in Å) of various $X^-(H_2)_n$ complexes optimized at the CCSD/6-311++G(d,p) level

	F^-	Cl^-	Br^-	OH^-	NH_2^-	NO_2^-		CN^-		ClO^-	
n	F…H	Cl…H	Br…H	O…H	N…H	O…H	N…H	C…H	N…H	O…H	Cl…H
1	1.825	2.554	3.112	1.967	1.033	2.404	-	2.866	-	2.072	-
2	1.891	2.847	3.135	2.025	2.304	2.406	-	2.842	-	2.103	-
3	1.952	2.847	3.105	2.103	2.319	2.634	-	2.842	-	2.160	-
4	2.011	2.854	3.106	2.171	2.391	2.424	-	2.853	2.584	2.203	-
5	2.067	2.848	3.106	2.226	2.437	2.470	-	2.868	2.609	2.263	-
6	2.125	2.867	3.112	2.275	2.496	2.544	-	2.868	2.702	2.296	-
7	2.176	2.872	3.122	2.330	2.544	2.536	-	2.866	2.735	2.407	-
8	2.228	2.895	3.131	2.381	2.629	2.507	-	2.853	2.725	2.489	-
9	2.284	2.939	3.158	2.448	2.646	2.519	2.680	2.855	2.721	2.596	-
10	2.378	2.899	3.156	2.521	2.707	2.543	2.688	2.859	2.720	2.492	3.029

The arrangement of H_2 molecules around OH^- and NH_2^- is almost symmetric with respect to the OH bond axis in the former and the C_2 axis in the latter. The X^-...H distances for complexes of OH^- and NH_2^- increases gradually on moving from n = 1 to 10 (Table 2.1). In the case of $NH_2^-(H_2)$, N^-...H interaction breaks the H-H bond yielding NH_3. This is evident from the anomalous value of H-H bond distance (1.938 Å) in this complex. This complex has to be described as NH_3...H^- and hence omitted from further analyses hereafter. The H-H bond distance of the

dihydrogen complexes of OH^- and NH_2^- varies between 0.770 - 0.747 Å and 0.762 – 0.748 Å, respectively. Taking into account of the complexes of NO_2^-, CN^- and ClO, it is clear that H_2 molecules bind with both the constituent atoms of the anion. Initially added H_2 molecules bind on atom with more charge density. For instance, in NO_2^-, H_2 molecules preferentially bind with more electronegative oxygen than nitrogen till n = 8. Binding of H_2 to nitrogen occurs only after the saturation of oxygen end (n = 9 and 10). For complexes with n = 3, 6, and 7, one H_2 molecule is seen as connected by both oxygen atoms. The average O...H bond distance is in the range 2.404 - 2.634 Å while the N...H distance is 2.680 Å in n = 9 and ~ 2.688 Å in n = 10. The H-H bond distance shows only a minor variation (0.751 to 0.747 Å) for complexes from n = 1 to 10 and N-O bond lengths remain almost a constant (1.253 - 1.255 Å) in all the complexes.

Table 2.2 E_{int} of anion complexes in kcal/mol calculated at the CCSD(T)/aug-cc-pVTZ//CCSD/6-311++G(d,p) level

n	F^-	Cl^-	Br^-	OH^-	NH_2^-	NO_2^-	CN^-	ClO^-
1	6.68	2.55	2.33	5.61	-	2.49	2.10	4.04
2	12.32	5.00	4.58	10.49	7.80	5.36	4.04	7.97
3	17.21	7.39	6.89	14.62	11.56	7.57	5.97	11.50
4	21.54	9.71	9.11	18.30	14.39	9.95	8.68	14.71
5	25.19	12.03	11.30	21.48	17.016	12.23	10.69	17.44
6	28.53	14.18	13.46	24.57	19.68	14.39	12.33	20.20
7	31.36	16.35	15.61	27.05	21.81	16.41	14.56	22.11
8	33.94	18.39	17.68	29.41	23.44	18.20	16.40	23.65
9	35.93	20.24	19.47	31.26	25.60	20.12	18.18	25.30
10	37.15	22.61	21.62	32.64	26.85	21.82	19.85	26.63

CN^- is well known for its slightly enhanced charge density at carbon center which is well reflected at the initial stages of H_2 binding process. For n = 1 to 3, the binding occurs preferentially to the carbon in an end-on fashion while n = 4 onwards the binding is more inclined towards the nitrogen. The values in Table 2.1 show that C...H interaction distance remains nearly unchanged in all the complexes (2.868 – 2.842 Å) while N...H distance shows a steady increase from

2.584 to 2.720 Å on moving from n = 4 to 10 complexes. Further, only a minor variation in H-H bond distance (0.749 - 0.747 Å) is found and the C-N distance is nearly unchanged. The geometric features of $ClO^-(H_2)_n$, complexes clearly show that the H_2 gets bonded to chlorine only after the coordination capacity of oxygen reaches to the saturation limit. This stage is observed in complex with n = 10. The average O...H distance increases from 2.072 to 2.492 Å (Table 2.1). The Cl-O and H-H bond lengths decrease from 1.742 to 1.733 Å and 0.759 to 0.746 Å respectively on going from n = 1 to 10. The total interaction energy (E_{int}) and the interaction energy per H_2 ($E_{int/H2}$) of the complexes calculated at CCSD(T)/aug-cc-pVTZ level for n = 1 – 10 complexes are given in Table 2.2 and Table 2.3 respectively. For all the complexes, E_{int} shows an increasing linear trend with increase in the number of H_2 whereas $E_{int/H2}$ either shows a decreasing trend or maintains almost a constant value (Figure 2.3).

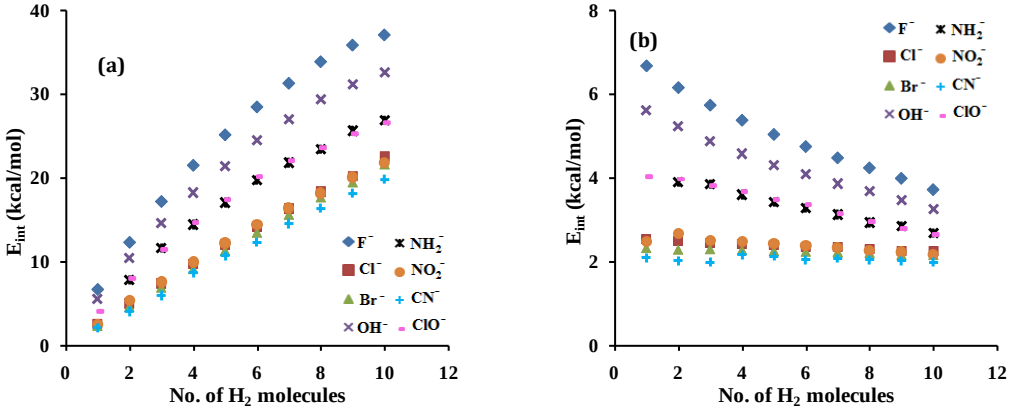

Figure 2.3(a) Variation of E_{int} with number of H_2 molecules of anion complexes (b) Variation of $E_{int/H2}$ with number of H_2 molecules of anion complexes.

The slope of the E_{int} plots of F^-, Cl^-, Br^-, OH^-, NH_2^-, NO_2^-, CN^-, and ClO^- anions are 3.369, 2.207, 2.160, 2.981, 2.350, 2.185, 2.001, and 2.645 respectively, and the corresponding correlation coefficients are 0.983, 0.998, 0.999, 0.986, 0.990, 0.998, 0.998 and 0.988. A high value of the slope indicates the high affinity of the anion to bind with dihydrogen. F^-, the smallest of all the anions has the highest slope and the highest E_{int} for all values of n. The slope observed for OH^- is slightly smaller than F^- and suggests that both the anions possess similar H_2 binding

affinity. For instance, E_{int} of n = 1 complex of F^- and OH^- is 6.68 and 5.61 kcal/mol, respectively and it reaches to 37.15 and 32.64 kcal/mol, respectively for n = 10 complex.

Table 2.3 $E_{int/H2}$ of anion complexes in kcal/mol calculated at the CCSD(T)/aug-cc-pVTZ//CCSD/6-311++G(d,p) level

n	F^-	Cl^-	Br^-	OH^-	NH_2	NO_2^-	CN^-	ClO^-
1	6.68	2.55	2.33	5.61	-	2.49	2.10	4.04
2	6.16	2.50	2.29	5.24	3.90	2.68	2.02	3.98
3	5.74	2.46	2.30	4.87	3.85	2.52	1.99	3.83
4	5.38	2.43	2.28	4.58	3.60	2.49	2.17	3.68
5	5.04	2.41	2.26	4.30	3.43	2.45	2.14	3.49
6	4.75	2.36	2.24	4.09	3.28	2.40	2.05	3.37
7	4.48	2.34	2.23	3.86	3.12	2.34	2.08	3.16
8	4.24	2.30	2.21	3.68	2.93	2.28	2.05	2.96
9	3.99	2.25	2.16	3.47	2.84	2.24	2.02	2.81
10	3.72	2.26	2.16	3.26	2.68	2.18	1.99	2.66

Similarly, NH_2^- and ClO^- exhibit the same style of change in E_{int} and $E_{int/H2}$ with increase in number of H_2 molecules. In fact, E_{int} of $NH_2^-(H_2)_{10}$ (25.60 kcal/mol) is almost identical to that of $ClO^-(H_2)_{10}$ (25.30 kcal/mol). This observation also holds good for the pair CN^- and Br^- as their E_{int} correlation lines nearly coincide with each other. These two anions have the lowest rate of increase in E_{int} with increase in the number of H_2. The E_{int} correlation lines of Cl^- and NO_2^- fall between that of ClO^- and CN^-. The analysis of the E_{int} suggest that the binding affinity of the anions follow the order $F^- \approx OH^- > NH_2^- \approx ClO^- > Cl^- > NO_2^- > Br^- \approx CN^-$. It is noteworthy that even for anions such as CN^- and Br^- with weak binding affinity to H_2, $E_{int/H2}$ maintains a steady value ~ 2 kcal/mol for all values of n leading to significant total interaction energy in higher order complexes. For instance, $CN^-(H_2)_{10}$ shows an E_{int} value of 19.85 kcal/mol. F^- outperforms all the others in binding H_2 and their E_{int} for n = 10 complexes are nearly twice as that of the weakly binding CN^- and Br^- anions.

2.4.2 Geometry and Energetics Using M06L Method

The optimized geometries of $X^-(H_2)_{nmax}$ complexes of all the anions at M06L/6-311++G(d, p) level are represented in Figure 2.4. Overall, the orientation of H_2 around the anion as well as the H-H bond and the X^-...H interaction distance parameters of the geometries obtained with M06L agreed well with the CCSD level geometries (n = 1 to 10). The similarity in the results obtained from the two methods improved with increase in the size of the complexes.

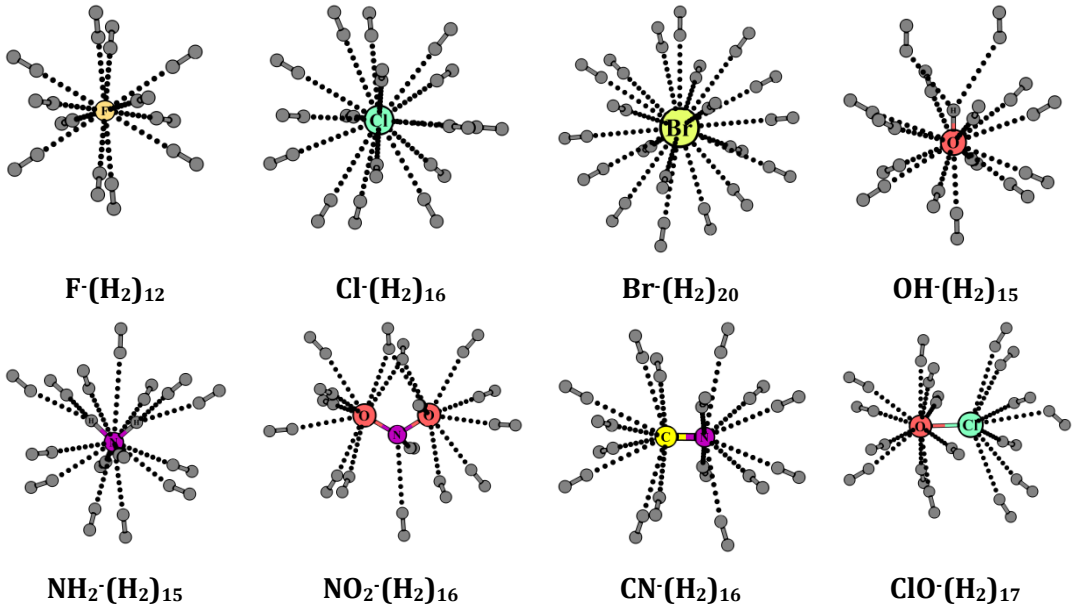

Figure 2.4 Optimized geometries of $X^-(H_2)_{nmax}$ at the M06L/6-311++G(d,p) level.

However, M06L level geometries showed more planar distribution of H_2 around the anion than the CCSD geometries for some random cases such as $F^-(H_2)_4$, $Cl^-(H_2)_4$, $Cl^-(H_2)_5$, $Br^-(H_2)_4$ and $Br^-(H_2)_5$. The BSSE corrected M06L level $E_{int/H2}$ of the complexes of anions with n = 1 to 10 are given in Table 2.4. In general, these values show good agreement with those obtained from CCSD(T)//CCSD level (Table 2.3). The n = 9, 10 complexes of Cl^-, Br^-, NO_2^-, CN^- and ClO^- show a deviation of < 0.65 kcal/mol in the magnitude of $E_{int/H2}$. The M06L binding energy for n = 10 complexes of F^-, OH^- and NH_2^- exhibits a variation of 0.87, 1.0 and 1.02 kcal/mol respectively from the values calculated using CCSD(T) level. The choice

of the DFT method M06L to compute higher order structures is reasonable as it shows accuracy close to CCSD(T)//CCSD results.

Table 2.4 BSSE corrected $E_{int/H2}$ of anion complexes with $n \leq 10$ in kcal/mol at the M06L/6-311++G(d, p) level

n	F^-	Cl	Br^-	OH^-	NH_2^-	NO_2^-	CN^-	ClO^-
1	9.94	2.77	2.19	9.62	-	3.10	2.45	5.43
2	8.17	2.77	2.14	7.98	6.45	2.98	2.41	4.90
3	7.13	2.74	2.09	7.00	5.52	2.86	2.47	4.58
4	6.36	2.74	2.15	6.21	4.86	2.80	2.45	4.32
5	5.88	2.73	2.19	5.67	4.61	2.77	2.31	4.02
6	5.54	2.72	2.20	5.30	4.43	2.69	2.46	3.94
7	5.26	2.79	2.34	4.99	4.20	2.60	2.38	3.75
8	5.06	2.77	2.34	4.77	3.98	2.53	2.39	3.59
9	4.83	2.86	2.42	4.56	3.88	2.53	2.41	3.46
10	4.59	2.84	2.41	4.26	3.70	2.48	2.46	3.27

Table 2.5 BSSE corrected $E_{int/H2}$ of anion complexes with $n > 10$ in kcal/mol at the M06L/6-311++G(d,p) level

n	F^-	Cl^-	Br^-	OH^-	NH_2^-	NO_2^-	CN^-	ClO^-
11	4.31	2.83	2.38	4.18	3.54	2.44	2.42	3.09
12	4.24	2.86	2.36	3.97	3.40	2.45	2.40	2.97
13	-	2.74	2.38	3.62	3.28	2.41	2.39	2.83
14	-	2.74	2.39	3.51	3.17	2.35	2.42	2.74
15	-	2.67	2.38	3.32	3.07	2.39	2.40	2.76
16	-	2.59	2.37	-	-	2.36	2.31	2.73
17	-	-	2.28	-	-	-	-	2.63
18	-	-	2.20	-	-	-	-	-
19	-	-	2.13	-	-	-	-	-
20	-	-	2.09	-	-	-	-	-

This is also supported by a previous benchmark study from our group on DFT methods to compute E_{int} and geometry of a variety of small noncovalent dimers.

Among the 382 density functional used including LDA, GGA, meta-GGA, hybrid, double hybrid, dispersion-corrected and long range-corrected functionals, the M06L method gave the best performance against the high accuracy Ave-CCSD(T)/(Q-T)//CCSD/aug-cc-pVTZ results.[21]

In Table 2.5 the BSSE corrected $E_{int/H2}$ of anion-H_2 complexes with n = 11 to n_{max} at M06L level is depicted. When n_{max} is attained, the subsequently added H_2 molecule interacts with the anion at a significantly longer distance than the rest. For instance, the n_{max} of F^- anion is 12 and the addition of 13th H_2 molecule results in a minimum energy structure with an interaction distance of 4.362 Å for the lastly added H_2 molecule. The n_{max} values obtained for Cl^-, Br^-, OH^-, NH_2^-, NO_2^-, CN^-, and ClO^- are 16, 20, 15, 15, 16, 16, and 17 respectively. The X^-…H bond strength and the magnitude of $E_{int/H2}$ depends on the number of H_2 molecules around the anion center. This is more pronounced in the case of smaller anions such as F^- and OH^-. For instance, for n = 1 complexes of F^- and OH^-, $E_{int/H2}$ is 9.94 and 9.62 kcal/mol respectively and this decreases to 4.59 and 3.32 kcal/mol respectively for $F^-(H_2)_{12}$ and $OH^-(H_2)_{15}$. For larger anions such as Cl^- and Br^-, the $E_{int/H2}$ is almost independent of the number of H_2 molecules. For instance, $E_{int/H2}$ for $Br^-(H_2)_n$ varies in the small range 2.09 to 2.19 kcal/mol for all values of n up to 20. The analysis of $E_{int/H2}$ clearly shows that even for complexes with n > 10, significant bonding interaction between the anion and H_2 exist in all cases.

2.4.3 Benchmark Study on Accuracy of Computational Methods

The CBS limit of $E_{int/H2}$ at CCSD(T) is taken as the benchmark for comparison with the energy values obtained by *ab initio* and DFT methods for complexes with n = 1 – 3. The data used for extrapolation method are given in Table 2.6 and the extrapolation graph of a representative case $F^-(H_2)$ is shown in Figure 2.5. The comparison of $E_{int/H2}$ at various levels is given in Table 2.7. The values obtained at CCSD(T)/aug-cc-pVTZ//CCSD/6-311++G(d,p) are very close to the CCSD(T)/CBS//MP2/aug-cc-pVTZ values. The deviation is ≤ 0.1 kcal/mol in most of the cases with a few exemptions. The n = 1 - 3 complexes of Br^- show a deviation in the range 0.32 - 0.35 kcal/mol and $OH^-(H_2)$, and $NH_2^-(H_2)_2$ show deviations -0.24 and -0.28 kcal/mol, respectively.

Table 2.6 Extrapolation of $E_{int/H2}$ (kcal/mol) to the CBS limit

Anion	*n*	HF			MP2			CCSD(T)		
		T	Q	CBS	T	Q	CBS	T	Q	CBS
F^-	1	4.47	4.51	4.53	5.76	5.94	6.12	6.21	6.41	6.59
	2	4.29	4.31	4.33	5.36	5.51	5.67	5.76	5.93	6.08
	3	4.05	4.07	4.08	4.99	5.12	5.26	5.35	5.49	5.63
Cl^-	1	1.17	1.17	1.17	2.26	2.34	2.44	2.32	2.41	2.51
	2	1.16	1.15	1.15	2.23	2.31	2.40	2.29	2.38	2.47
	3	1.14	1.14	1.14	2.19	2.27	2.36	2.25	2.34	2.42
Br^-	1	0.57	0.57	0.57	1.75	1.85	1.96	1.78	1.89	1.99
	2	0.60	0.60	0.59	1.74	1.84	1.95	1.78	1.87	1.97
	3	0.59	0.58	0.58	1.72	1.81	1.92	1.75	1.85	1.94
OH^-	1	3.85	3.86	3.87	4.84	4.96	5.09	5.22	5.54	5.85
	2	3.64	3.65	3.65	4.47	4.60	4.73	4.85	4.99	5.13
	3	3.39	3.40	3.41	4.15	4.27	4.40	4.52	4.65	4.78
NH_2^-	2	2.48	2.47	2.46	3.79	3.86	3.95	4.02	4.10	4.18
	3	2.20	2.20	2.20	3.30	3.38	3.48	3.56	3.65	3.74
NO_2^-	1	1.49	1.49	1.49	2.13	2.18	2.24	2.24	2.30	2.36
	2	1.45	1.46	1.46	2.32	2.38	2.46	2.43	2.50	2.57
	3	1.42	1.43	1.43	2.21	2.27	2.33	2.32	2.38	2.44
CN^-	1	1.17	1.17	1.16	1.45	1.96	2.54	1.98	2.02	2.06
	2	0.96	0.96	0.96	1.62	1.90	2.21	1.91	1.95	1.99
	3	0.84	0.83	0.83	1.68	1.87	2.10	1.88	1.92	1.97
ClO^-	1	1.65	1.67	1.68	3.80	3.92	4.05	3.82	3.94	4.05
	2	1.67	1.69	1.70	1.20	3.77	3.66	3.69	3.80	3.90
	3	1.64	1.66	1.67	3.52	3.62	3.72	3.54	3.65	3.74

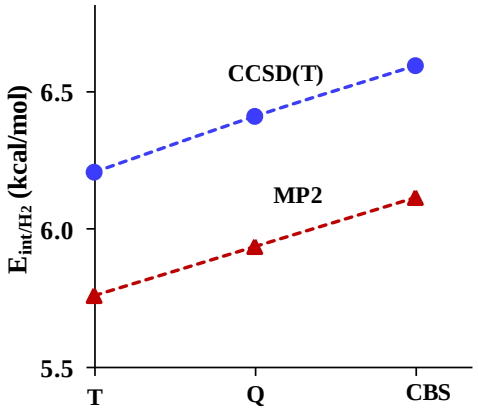

Figure 2.5 Extrapolation of $E_{int/H2}$ of $F^-(H_2)$ to the CBS limit.

This suggests that the accuracy of CCSD(T)/aug-cc-pVTZ//CCSD/6-311++G(d,p) is close to the CBS limit. The $E_{int/H2}$ calculated at CCSD(T)/6-311++G(d,p)//CCSD/6-311++G(d,p) are lower than the CBS limit for complexes of F^-, Br^-, OH^- (n = 1), NO_2^-, CN^-, and ClO^- (n = 1, 3) with discrepancy from -0.1 to -0.9 kcal/mol. All other complexes show a positive deviation in the range 0.1 – 1.3 kcal/mol. Except for complexes of CN^-, $E_{int/H2}$ at MP2/CBS// MP2/aug-cc-pVTZ show a negative deviation from CCSD(T)/CBS//MP2/aug-cc-pVTZ values. The deviations are found to be ≤ 0.1 kcal/mol for larger anions such as Cl^-, Br^- and ClO^- (except n = 2 complex) and for other anions such as the difference falls in the range -0.1 to -0.75 kcal/mol with smaller anions such as F^- and OH^- showing higher variation. The values obtained at MP2/aug-cc-pVTZ level are close to CCSD(T)/6-311++G(d,p)//CCSD/6-311++G(d,p) which showed a deviation of -0.2 to -1.0 kcal/mol from CCSD(T)/CBS//MP2/aug-cc-pVTZ values. The M06L/6-311++G(d,p) values of all the complexes are higher than the CBS limit values. For anions such as Cl^-, CN^- and Br^- deviation of M06L/6-311++G(d,p) values fall in the range 0.15 – 0.5 kcal/mol and complexes of NO_2^- and ClO^- deviates in the range 0.4 – 1.4 kcal/mol from the CBS limit. The complexes of F^-, OH^-, and NH_2^- show a comparatively higher deviation of 1.5 – 3.7 kcal/mol and this divergence decreases with increase in size of the complex. For instance, as n increases from 1 to 3, the variation decreases from 3.3 to 1.5 for complexes of F^- anion. Even though M06L results deviate from the CBS limit for complexes with lower n values of smaller anions, the results obtained for larger anions are comparable with the benchmark value.

Table 2.7 Comparison of $E_{int/H2}$ calculated at various levels for complexes with n = 1 - 3

Method	n	F^-	Cl^-	Br^-	OH^-	NH_2^-	NO_2^-	CN^-	ClO^-
CCSD(T)/CBS//	1	6.59	2.51	1.99	5.85	-	2.36	2.06	4.05
MP2/aug-cc-pVTZ	2	6.08	2.47	1.97	5.13	4.18	2.57	1.99	3.90
	3	5.63	2.42	1.94	4.78	3.74	2.44	1.97	3.74
CCSD(T)/aug-cc-pVTZ//	1	6.68	2.55	2.33	5.61	-	2.49	2.10	4.04
CCSD/6-311++G(d,p)	2	6.16	2.50	2.29	5.24	3.90	2.68	2.02	3.98
	3	5.74	2.46	2.30	4.87	3.85	2.52	1.99	3.83
CCSD(T)/6311++G(d,p)//	1	5.63	3.84	1.71	5.55	-	2.23	1.61	1.61
CCSD/6311++G(d,p)	2	5.34	3.23	1.60	5.28	4.40	2.24	1.60	1.60
	3	5.06	2.89	1.73	4.87	4.08	2.15	1.59	1.59
MP2/CBS// MP2-aug-cc-pVTZ	1	6.12	2.44	1.96	5.09	-	2.24	2.54	2.54
	2	5.67	2.40	1.95	4.73	3.95	2.46	2.21	2.21
	3	5.26	2.36	1.92	4.40	3.48	2.33	2.10	2.10
MP2/aug-cc-pVTZ	1	5.76	2.26	1.75	4.84	-	2.13	1.45	1.45
	2	5.36	2.23	1.74	4.47	3.79	2.32	1.62	1.62
	3	4.99	2.19	1.72	4.15	3.30	2.21	1.68	1.68
M06L/6311++G(d,p)	1	9.94	2.77	2.19	9.62	-	3.10	2.45	2.45
	2	8.17	2.77	2.14	7.98	6.45	2.98	2.41	2.41
	3	7.13	2.74	2.09	7.00	5.52	2.86	2.47	2.47

Also as the variation decreases with increase in the size of the complex, the $E_{int/H2}$ obtained at M06L/6-311++G(d,p) method can be trustworthy for larger complexes. From the benchmark study it can be concluded that among the methods used CCSD(T)/aug-cc-pVTZ//CCSD/6-311++G(d,p) shows the accuracy close to that of CCSD(T)/CBS//MP2/aug-cc-pVTZ limit.

2.4.4 MESP Analysis

The MESP isosurface of a representative case $F^-(H_2)_n$ is depicted in Figure 2.6 for all n values (n = 1 - 13). According to Gadre-Pathak theorem, always a negative-valued isosurface that engulfs the whole complex can be located for any anionic systems.[43] This observation holds true for all the cases studied.

Table 2.8 Average V_{min} (kcal/mol) of $X^-(H_2)_n$ complexes at M06L/6-311++G(d,p) level

n	F^-	Cl^-	Br^-	OH^-	NH_2^-	NO_2^-	CN^-	ClO^-
1	-126.1	-75.4	-69.8	-132.7	-	-77.3	-72.6	-96.6
2	-103.8	-73.3	-68.3	-110.3	-112.1	-71.0	-69.8	-86.2
3	-93.7	-71.3	-66.9	-98.6	-98.1	-70.4	-69.0	-82.0
4	-87.5	-70.2	-66.2	-91.7	-88.8	-69.4	-67.7	-78.5
5	-83.8	-68.8	-65.4	-86.7	-83.7	-68.1	-67.3	-74.9
6	-80.9	-67.7	-64.8	-82.2	-80.1	-66.4	-67.2	-73.0
7	-78.3	-67.3	-64.3	-78.3	-76.6	-65.4	-66.0	-71.0
8	-76.3	-66.9	-64.0	-76.2	-73.9	-64.4	-64.4	-69.5
9	-74.5	-66.0	-63.7	-74.4	-72.1	-64.3	-63.8	-68.6
10	-73.1	-65.2	-62.8	-71.9	-70.5	-63.1	-63.4	-67.1
11	-71.7	-64.5	-62.3	-70.6	-68.6	-62.2	-62.9	-65.7
12	-70.8	-63.8	-61.7	-69.0	-67.3	-61.7	-62.1	-64.1
13	-	-63.2	-61.0	-67.8	-66.0	-60.9	-61.4	-63.3
14	-	-62.8	-60.7	-66.6	-64.7	-60.4	-61.4	-62.1
15	-	-62.0	-60.2	-65.4	-63.9	-59.9	-60.7	-60.7
16	-	-61.5	-59.8	-	-	-59.6	-60.2	-60.4
17	-	-	-59.2	-	-	-	-	-60.0
18	-	-	-58.9	-	-	-	-	-
19	-	-	-58.4	-	-	-	-	-
20	-	-	-57.9	-	-	-	-	-

For every H-H bond directions in the $X^-(H_2)_n$ complex pointing away from the anion center, a negative MESP point with the lowest magnitude can be located. In the topographical notation, every such point describes a (3, +1) saddle point.[32] Thus for an $X^-(H_2)_n$ complex, there exists *n* such points. The MESP value at the saddle point is designated herein as V_{min}. The isosurface plotted with the lowest negative V_{min} engulfs the whole complex. As the number of H_2 molecules increases, the magnitude of V_{min} decreases while the size of the isosurface that engulfs the whole anion increases. This also indicates that X^- behaves like a bigger anion with every H_2 coordinating to it as the electron charge distribution gets

delocalized more in space in the direction of H_2 molecules. The average value of V_{min} for all the complexes are summarized in Table 2.8.

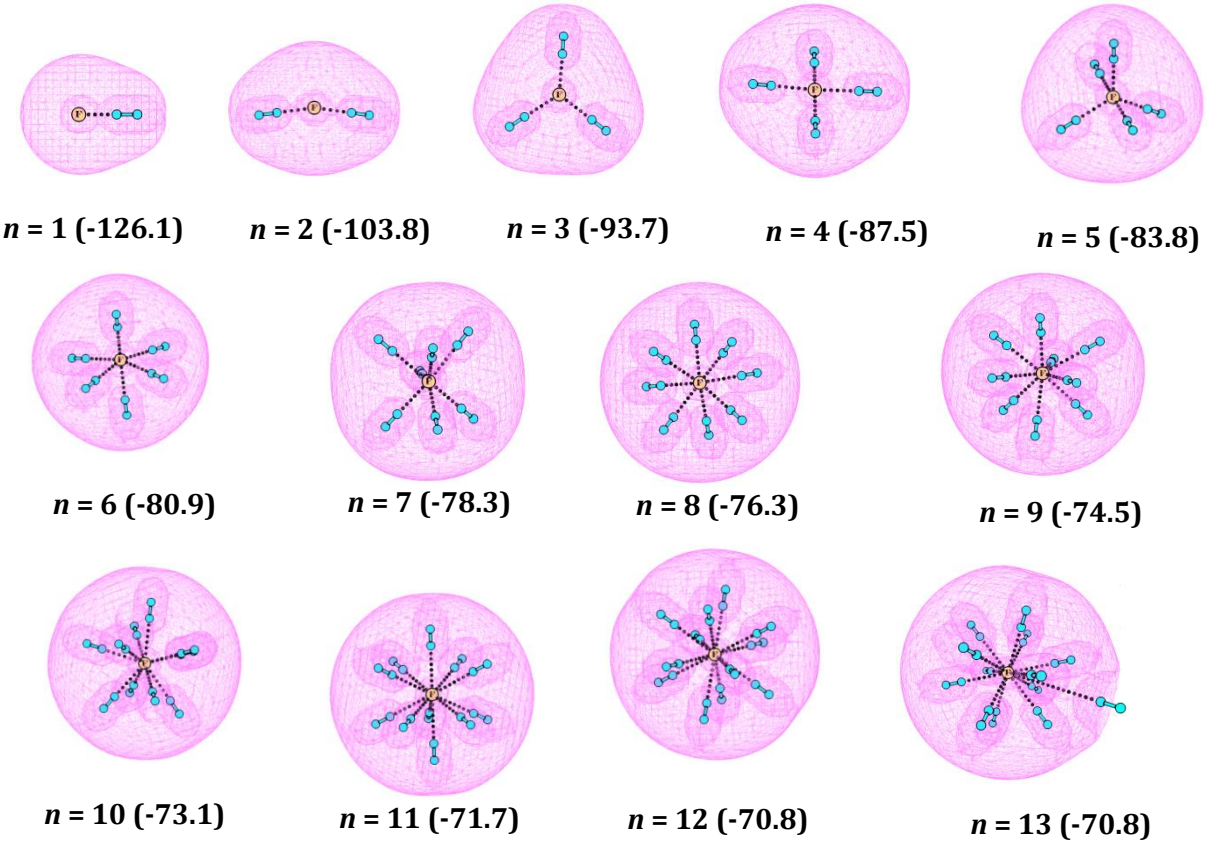

Figure 2.6 MESP of $F^-(H_2)_n$ complexes at M06L/6-311++G(d,p) level (isosurface values in kcal/mol are given in parenthesis for each complex).

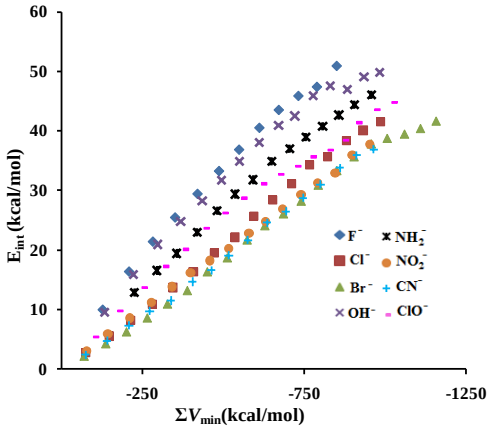

Figure 2.7 Correlation between E_{int} and ΣV_{min} of $X^-(H_2)_n$ complexes at the M06L/6-311++G(d,p) level.

The complexes of F^- and OH^- show higher negative V_{min} value compared to the complexes of other anions. In the case of $F^-(H_2)_n$ complexes, a prominent decrease in magnitude of V_{min} with increase in n from 1 to 4 is observed whereas for higher complexes (n = 5 - 12), only a minor decline is note. MESP isosurface is also useful to understand the coordinatively saturated state of the anion complex. For instance, n_{max} of F^- is 12 and the isosurface that engulfs the whole complex has a value -70.8 kcal/mol. Such an isosurface for $F^-(H_2)_{13}$ can show the clear exclusion of the 13th H_2 from the coordinating region of the anion. This is because the V_{min} value of the 13th H_2 (-47.6 kcal/mol) deviates significantly from the V_{min} value of n = 12 complex by 23.2 kcal/mol. This observation holds good for all the anions studied herein and provides a clear way to identify the saturation level of the first coordination sphere.

The sum of all V_{min} values of a particular complex (ΣV_{min}) correlates linearly to E_{int} (Figure 2.7). As the negative character of ΣV_{min} increases, E_{int} increases. The correlation coefficients for complexes of all the anions are ~ 0.99. H_2 interaction strength of anions can be determined from the correlation data of E_{int} and ΣV_{min}. For a value of ΣV_{min} ~ -1.0 au (627.5 kcal/mol) the E_{int} for F^-, Cl^-, Br^-, OH^-, NH_2^-, NO_2^-, CN^-, and ClO^- are 43.50, 28.41, 24.13, 41.04, 34.94, 24.83, 24.64, 32.72 kcal/mol respectively. For strongly interacting anions such as F^-, OH^- and NH_2^-, ΣV_{min} attains this value when n = 9 whereas for all other anions this value is achieved for n = 10 complex. Thus, based on electrostatic potential the H_2 binding affinity of anions can be arranged in the following order, *viz*. $F^- > OH^- > NH_2^- > ClO^- > Cl^- > NO_2^- \approx CN^- \approx Br^-$.

2.4.5 QTAIM Analysis

The QTAIM analysis showed that anion center is bonded to all the coordinated H_2 molecules as a BCP is observed between the anion and H_2 in all the complexes (n = 1 to n_{max}). To illustrate this point, QTAIM features of anion complexes with n_{max} are depicted in Figure 2.8. The (n_{max+1}) complexes showed no direct interaction between X^- and (n_{max+1})th H_2 molecule suggesting that the first coordination sphere of every anion can accommodate only up to n_{max} number of

H_2 molecules. The $(n_{max+1})^{th}$ H_2 molecule is bonded to nearby H_2 molecules in the first coordination shell of the anion. A representative case of $F^-(H_2)_{13}$ is shown in Figure 2.9. The electron density at BCP (ρ_{bcp}) is widely recognized as a measure to assess the strength of the interaction between bonded atoms. The applicability of this approach is more reliable if the interactions are similar in nature as ρ_{bcp} often shows a strong linear correlation with interaction energy.[44-49]

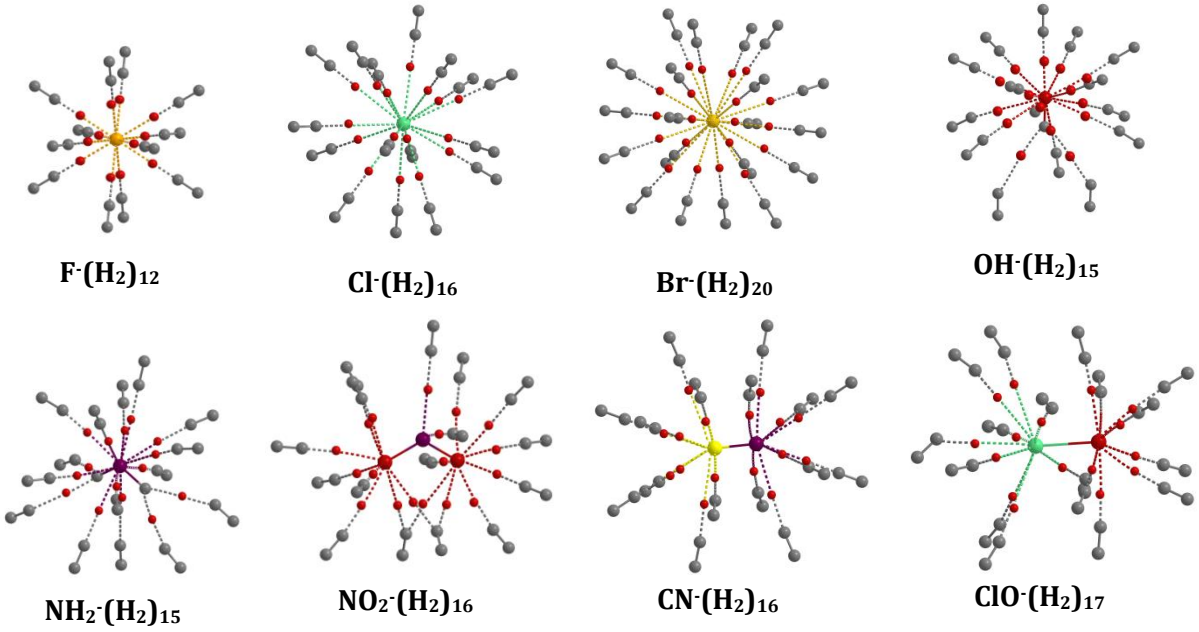

Figure 2.8 QTAIM bond critical points (red dots) and bond paths (dotted lines) of $X^-(H_2)_{nmax}$ complexes. Dihydrogen H...H interactions are neglected in the figure to improve the clarity of the presentation of X^-...H interactions.

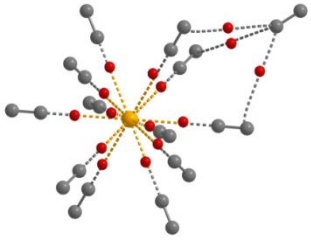

Figure 2.9 QTAIM molecular graph of $F^-(H_2)_{13}$.

Table 2.9 $\Sigma\rho_{bcp}$ (au) of X^-...H bond in complexes at the M06L/6-311++G(d,p) level

n	F^-	Cl^-	Br^-	OH^-	NH_2^-	NO_2^-	CN^-	ClO^-
1	0.0655	0.0134	0.0105	0.0715	-	0.0165	0.0128	0.0373
2	0.0901	0.0261	0.0206	0.0945	0.0886	0.0383	0.0242	0.0615
3	0.1057	0.0374	0.0305	0.1114	0.0955	0.0551	0.0352	0.0788
4	0.1187	0.0487	0.0396	0.1231	0.0978	0.0723	0.0441	0.0956
5	0.1326	0.0587	0.0485	0.1283	0.1039	0.0713	0.0550	0.1034
6	0.1430	0.0673	0.0578	0.1322	0.1097	0.0949	0.0613	0.1119
7	0.1502	0.0774	0.0653	0.1380	0.1149	0.1046	0.0698	0.1129
8	0.1563	0.0890	0.0741	0.1406	0.1181	0.1111	0.0811	0.1156
9	0.1618	0.0960	0.0825	0.1464	0.1228	0.1195	0.0896	0.1208
10	0.1638	0.1060	0.0927	0.1478	0.1247	0.1103	0.0990	0.1284
11	0.1593	0.1168	0.1019	0.1539	0.1330	0.1383	0.1031	0.1378
12	0.1672	0.1264	0.1156	0.1627	0.1380	0.1359	0.1106	0.1453
13	-	0.1294	0.1153	0.1426	0.1406	0.1435	0.1178	0.1502
14	-	0.1327	0.1233	0.1536	0.1458	0.1503	0.1263	0.1550
15	-	0.1341	0.1264	0.1491	0.1501	0.1500	0.1322	0.1637
16	-	0.1346	0.1288	-	-	0.1659	0.1326	0.1687
17	-	-	0.1308	-	-	-	-	0.1702
18	-	-	0.1316	-	-	-	-	-
19	-	-	0.1319	-	-	-	-	-
20	-	-	0.1324	-	-	-	-	-

In the case of $X^-(H_2)_n$ complexes, all the X^-...H interaction can be sorted in the decreasing order by correlating with the ρ_{bcp} for the BCP in the decreasing order. Further, the sum of ρ_{bcp} values, $\Sigma\rho_{bcp}$ (Table 2.9) of all the X^-...H interactions can be considered as a quantity directly correlating with the total interaction energy.[50-53] The ρ_{bcp} values of X^-...H bonds show a gradual decline with respect to increase in n indicating the decrease in bond strength of X^-...H with increase in cluster size. The correlation plot of $\Sigma\rho_{bcp}$ against *n* confirms that the total interaction energy or the thermodynamic stability of the complex is directly related with the total number of interacting H_2 molecules. The stabilizing effect

from H_2 is mostly additive at the initial stages and later on this effect diminishes in higher order complexes (Figure 2.10).

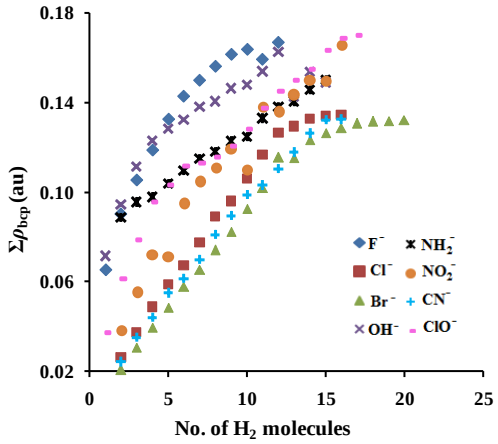

Figure 2.10 Variation of $\Sigma\rho_{bcp}$ values of $X^-(H_2)_n$ complexes with number of H_2 molecules

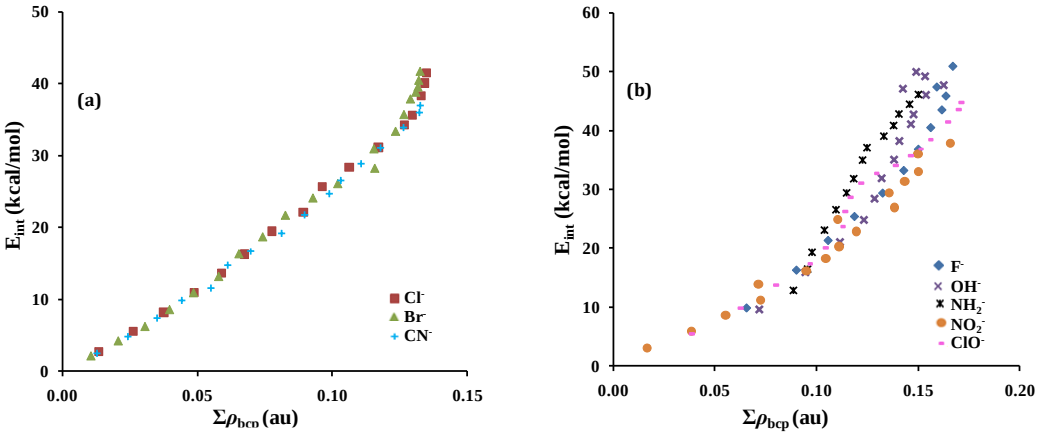

Figure 2.11 Correlation between $E_{int/H2}$ and $\Sigma\rho_{bcp}$ values of $X^-(H_2)_n$ complexes at the M06L/6-311++G(d,p) level.

The plots of E_{int} versus $\Sigma\rho_{bcp}$ shown in Figure 2.11 reveal direct linear correlation between the two for all anions (correlation coefficients in the range 0.951 – 0.993 au). The anions such as Cl^-, Br^- and CN^- (Figure 2.11a) show nearly identical E_{int} trend with respect to $\Sigma\rho_{bcp}$ as the slope (309.2, 313.6, 287.5) and intercept (-3.55, -3.62, -2.88) of their correlation lines show close similarity indicating similar binding affinity of these anions to dihydrogen. For all other anions, *viz*. NH_2^-, OH^-,

F^-, ClO^- and NO_2^-, the ordered pair of (slope, intercept) are (544.3, -33.69), (498.3, -31.09), (388.5, -18.87), (310.3, -9.11), (241.8, -4.17), respectively. NH_2^- has the highest slope and suggests the higher rate of stabilization of the complexes with increase in the number of H_2.

Table 2.10 Average $\nabla^2(\rho_{bcp})$ values (au) of X^-...H bond in complexes optimized at the M06L/6-311++G(d,p) level

n	F^-	Cl^-	Br^-	OH^-	NH_2^-	NO_2^-	CN^-	ClO^-
1	0.1678	0.0378	0.0253	0.1228	-	0.0452	0.0300	0.1063
2	0.1421	0.0367	0.0252	0.1185	0.0821	0.0560	0.0287	0.0929
3	0.1168	0.0354	0.0249	0.1031	0.0709	0.0521	0.0281	0.0793
4	0.0994	0.0343	0.0242	0.0890	0.0607	0.0517	0.0268	0.0721
5	0.0888	0.0330	0.0238	0.0776	0.0527	0.0417	0.0301	0.0659
6	0.0790	0.0315	0.0237	0.0652	0.0471	0.0475	0.0279	0.0582
7	0.0704	0.0311	0.0228	0.0576	0.0422	0.0451	0.0273	0.0484
8	0.0632	0.0314	0.0228	0.0506	0.0375	0.0417	0.0276	0.0427
9	0.0576	0.0300	0.0224	0.0462	0.0356	0.0398	0.0267	0.0392
10	0.0519	0.0299	0.0228	0.0423	0.0336	0.0338	0.0266	0.0375
11	0.0448	0.0300	0.0229	0.0393	0.0312	0.0387	0.0249	0.0367
12	0.0430	0.0298	0.0241	0.0383	0.0295	0.0337	0.0245	0.0354
13	-	0.0279	0.0219	0.0290	0.0274	0.0342	0.0241	0.0337
14	-	0.0263	0.0217	0.0292	0.0262	0.0319	0.0239	0.0321
15	-	0.0244	0.0206	0.0265	0.0250	0.0301	0.0233	0.0321
16	-	0.0227	0.0195	-	-	0.0309	0.0216	0.0308
17	-	-	0.0185	-	-	-	-	0.0294
18	-	-	0.0174	-	-	-	-	-
19	-	-	0.0164	-	-	-	-	-
20	-	-	0.0155	-	-	-	-	-

In other words, the collective strength of interaction provided by a specific number of H_2 is the highest for this anion. For instance, NH_2^-, though weakly interacting to H_2 than F^- as per the $E_{int/H2}$ data, the $\Sigma\rho_{bcp}$ 0.1330 au observed for its $NH_2^-(H_2)_{11}$ complex suggests E_{int} 47.4 kcal/mol while the same amount of $\Sigma\rho_b$

achieved in the case of the case of $F^-(H_2)_5$ corresponds to only 29.4 kcal/mol energy stabilization.

The Laplacian of the charge density given by $\nabla^2(\rho_{bcp})$, is a local property which gives an idea about the nature of the bond.[44, 54] For noncovalent interactions, the accumulation of charge density along the direction of nuclei is very low resulting in low ρ_{bcp} values and positive $\nabla^2(\rho_{bcp})$ values.[44, 55-61] Previously, Popelier has shown that in the case of donor (D)-acceptor (A) type D-H...A hydrogen bonding interactions, $\nabla^2(\rho_{bcp})$ values fall in the range 0.0240 – 0.1390 au. This can be regarded as a typical range of $\nabla^2(\rho_{bcp})$ observed in noncovalent systems. In the present study, the $\nabla^2(\rho_{bcp})$ observed for all the X-...H interactions fall in the range 0.0150 – 0.1680 au. This data strongly indicate the noncovalent nature of X-...H interactions (Table 2.10).

The magnitude of $\nabla^2(\rho_{bcp})$ at BCP is a measure of concentration of electron density in inter atomic space.[62] Electron density is directly related to the strength of the bond and hence the E_{int}. The $\nabla^2(\rho_{bcp})$ values of the complexes show the same trend as that of $E_{int/H2}$. Anions with higher $E_{int/H2}$ show higher values of $\nabla^2(\rho_{bcp})$. For instance, $\nabla^2(\rho_{bcp})$ of n = 1 complexes of F^-, and OH^- are 0.1678 and 0.1228 au respectively. Anions which exhibit lower H_2 binding affinity possess lower values of $\nabla^2(\rho_{bcp})$. In the case CN^- and Br^-, $\nabla^2(\rho_{bcp})$ of n = 1 complexes 0.0300 and 0.0253 au, respectively. Also for all anions as the coordination sphere approaches to saturation, $\nabla^2(\rho_{bcp})$ value decreases. For example, $\nabla^2(\rho_{bcp})$ of $F^-(H_2)_n$ complexes decreases from 0.1678 to 0.0430 au as n varies from 1 to 12. From QTAIM analysis, low ρ_{bcp} values and positive $\nabla^2(\rho_{bcp})$ values suggest that these complexes show weak closed shell interactions.[25]

2.4.6 Quantification of H_2 Affinity of Anions

The calculated weight percent of H_2 that can be stored per total weight of the system (wt%) for all anions are given in Table 2.11. The obtained wt% of all the anions are very high compared to the DOE targets, ~ 6.5 wt% for automotive purposes.[63] Among all the anions, the highest values 65.4 and 64.0 wt% are observed for NH_2^- and OH^- anions, respectively. Even for the heaviest anion Br^-,

due to its capacity to hold 20 H_2 molecules in the first coordination sphere, wt% of H_2 shows a significant value of 33.5. These data clearly indicate that anions possess a remarkable ability to store H_2 in large quantities and this property can be explored for the development of potential H_2 storage systems.

Table 2.11 H_2 affinity of anions

Anion	Atomic weight (amu)	n_{max}	Weight percent of H_2 (wt%)
F^-	18.998	12	56.0
Cl^-	35.450	16	47.6
Br^-	79.904	20	33.5
OH^-	17.007	15	64.0
NH_2^-	16.023	15	65.4
NO_2^-	46.005	16	41.2
CN^-	26.018	16	55.4
ClO^-	51.449	17	40.0

2.5 Conclusions

The H_2 binding affinity of various anions has been systematically analyzed using DFT method and the accuracy of obtained results have been verified using CCSD(T)//CCSD methods. This study reveals that the anions can bind a large number of H_2 molecules in their coordination shell. Apart from the electrostatic attractions between the anion and the H_2, significant charge transfer from the anion to H_2 also occurs. The electron transfer takes place from the anion to LUMO of H_2 leading to H-H bond elongation. This favours end-on coordination of H_2 to the anion. Anions with smaller size are more likely to bind strongly with H_2 (F^-, OH^-, NH_2^-) where as larger anions can hold many H_2 molecules around the charge center (Br^-). It is worth mentioning that for all the anions beyond a certain value of n, $E_{int/H2}$ remains almost a constant which is a positive indication that anions can bind with a significant number of H_2 molecules. The QTAIM and MESP analyses also support the notable capability of anions to bind with several H_2

molecules. The calculated weight percent of H_2 in $X^-(H_2)_{nmax}$ complexes are very high compared to the DOE targets. Though these calculated wt% values are highly promising, practical applications can be limited in salt systems wherein the strong electrostatic interaction of the cation with the anion has to be surmounted by the interaction forces of the H_2 with the anion. The present results suggest that strategy to incorporate suitable anionic centers in hydrogen storage materials could improve their overall hydrogen uptake.

Part B: Dihydrogen Binding Affinity of Polyatomic Anions

2.6 Abstract

The dihydrogen binding ability of polyatomic oxohalo anions ClO^-, ClO_2^-, ClO_3^-, ClO_4^-, BrO^-, BrO_2^-, BrO_3^-, and BrO_4^- has been studied at M06L/6–311++G(d,p) DFT and CCSD(T)/aug-cc-pVTZ//CCSD/aug-cc-pVDZ ab initio theory. The maximum number of dihydrogen adsorbed by the anions (n_{max}) varies from 17 – 24 in the first coordination shell. As the number H_2 adsorbed varies from 1 to n_{max}, the oxochloro and oxobromo anions show a wide range for the interaction energy (E_{int}), viz. 1.5 – 45.4 kcal/mol for the former and 1.4 – 46.0 kcal/mol for the latter. These results indicate that both series of anions show very similar and high affinity to bind with several dihydrogen molecules. Further, an increase in coordination ability and decrease in strength of the dihydrogen interaction is observed with increase in number of oxygen atoms in the polyatomic anion. In contrast to this, the neutral oxohaloacids show negligible interaction with dihydrogen. The anion...H_2 noncovalent interactions along with H...H dihydrogen interactions within the complex are ascertained by locating bond critical points (bcp) in quantum theory of atoms in molecules (QTAIM) analysis. The electron density at bcp summed up for all the anion...H_2 interactions ($\Sigma\rho_{bcp}$) showed a strong linear relationship with E_{int} indicating that the stability of the complex is due to the formation of a large network of noncovalent bonds in the complex. The amount of electron density donated from the anion to the dihydrogen during complex formation is also gauged from the molecular electrostatic potential (MESP) values at the nuclei (V_n) of all the atoms in the anion. Hydrogen uptake led to significant reduction in the negative character of V_n and the total change in V_n from all anion atoms ($\Sigma\Delta V_n$) is found to be directly proportional to E_{int}. The polyatomic anions have a very high affinity towards dihydrogen binding which can be utilized for the development of new storage systems.

2.7 Introduction

Hydrogen is an admirable replacement for non-renewable fossil fuels while its low energy density by volume encumbers the development of efficient storage systems and limits its use as a fuel for automotive purposes.[63-66] In Part A of this chapter we have discussed the ability of molecular anions such as F^-, Cl^-, Br^-, OH^-, NH_2^-, NO_2^-, CN^-, ClO^- to bind with a very large number of H_2 molecules (12 – 20).[67] These studies conducted using coupled cluster CCSD(T)/aug-cc-pVTZ//CCSD/6−311++G(d,p) theory and M06L/6−311++G(d,p) level density functional theory showed that even for the highest number of H_2 coordinated anionic complexes, the observed interaction energy per H_2 ($E_{int/H2}$) was substantial (2.09 – 4.24 kcal/mol) and the weight percent of H_2 was very high (40 – 65 wt%) signifying that these anions could be incorporated for the development of novel hydrogen storage systems. In general, strength of anion−H_2 interactions decreased with increase in size of the anion whereas the number of H_2 accommodated in the coordination sphere of the anion increased with increase in size of the anion. Herein, we undertake a systematic study on the size effect on the H_2 uptake of anions using two sets of anions showing systematic increase in size. The analyses on structure, energetics, electron density and molecular electrostatic potential have been done to establish the effect of size and charge density of the interacting polyatomic anion on dihydrogen storage ability. The selected anions are ClO^-, ClO_2^-, ClO_3^-, ClO_4^-, BrO^-, BrO_2^-, BrO_3^-, and BrO_4^-; their size increases with increase in the number of oxygen atoms.

2.8 Computational Details

In the present work, all calculations have been done using M06L/6−311++G(d,p) level of density functional theory.[68] The anion−H_2 complexes with n = 1 to n_{max} have been optimized and the geometries have been established as the energy minima by analysing vibrational frequency at standard temperature (298.15 K) and pressure (1 atm). The E_{int} is calculated using supermolecule approach by employing the counterpoise method introduced by Boys and Bernardi.[22] For validating the accuracy of the results obtained, $XO_m^-(H_2)_n$ complexes with n = 1 − 5 have been optimized at CCSD/aug-cc-pVDZ and E_{int}

values have been calculated at CCSD(T)/aug-cc-pVTZ level of theory. All optimizations, energy calculations and MESP analysis have been done using Gaussian 09 suite of programs[39] and QTAIM analysis has been done using AIMAll package.[40]

2.9 Results and Discussion

2.9.1 Geometry and Energetics of $XO_m^-(H_2)_n$ Complexes

The oxohalo anion complexes $XO_m^-(H_2)_n$ of all the anions have been systematically optimized from n = 1 to n_{max}. A representative set of optimized geometries of the complexes are given in Figure 2.12. H_2 binds preferably to the oxygen atoms than X. For instance, in the case of complexes of ClO^-, dihydrogen binding takes place only at the oxygen center for complexes with n = 1 – 9. Binding of H_2 to X occurs only after the saturation of oxygen atoms. This observation holds true for all other polyatomic anions except ClO_4^- and BrO_4^- in which the halogen site is not available for H_2 binding due to the tetrahedral arrangement of oxygen atoms around the halogen. The O...H interaction distance of polyatomic anions increases with increase in number of oxygen atoms. These interaction distances are represented in Tables 2.12 and 2.13 in the supporting information. The X...H interaction distances increase with rise in n both for ClO_m^- and BrO_m^- series. Also the O...H interaction distance is found to fall in similar range for both the series. The O...H distances of n = 1 complexes of ClO^-, ClO_2^-, ClO_3^-, and ClO_4^- are 1.849, 2.039, 2.226, and 2.302 Å and those of BrO^-, BrO_2^-, BrO_3^-, and BrO_4^- are 1.861, 2.056, 2.217, and 2.335 Å, respectively. In general, the O...H distances increases with increase in n with a few exceptions. For instance, the O...H distance of $ClO^-(H_2)_{10}$ (2.339 Å) is higher than $ClO^-(H_2)_{11}$(2.301 Å). The ClO_m^- complexes show a shorter X...H distance compared to those of BrO_m^- series. For example, X...H distance in $ClO^-(H_2)_{11}$ and $BrO^-(H_2)_{11}$ is 2.764 and 3.019 Å respectively. The H−H bond is found to be activated in complexes with lower n values which is evident from the increased H−H bond distance (the bond H−H bond distance of H_2 molecule at M06L/6-311++G(d,p) level is 0.744 Å). For instance, the H−H distance of $ClO^-(H_2)_n$ complexes decreases from 0.791 Å to 0.751 Å as n goes from 1 to 17.

Table 2.12 Average X…H distance (Å) of $ClO_m^-(H_2)_n$ complexes at the M06L/6-311++G(d,p) level

	ClO^-		ClO_2^-		ClO_3^-		ClO_4^-	
n	O…H	Cl…H	O…H	Cl…H	O…H	Cl…H	O…H	Cl…H
1	1.849	-	2.039	-	2.226	-	2.302	-
2	1.930	-	2.062	-	2.218	-	2.364	-
3	2.009	-	2.126	-	2.325	-	2.360	-
4	2.054	-	2.113	-	2.331	-	2.393	-
5	2.097	-	2.194	-	2.375	-	2.422	-
6	2.153	-	2.208	-	2.371	-	2.540	-
7	2.232	-	2.226	-	2.374	-	2.453	-
8	2.290	-	2.230	-	2.366	-	2.453	-
9	2.336	-	2.272	-	2.423	-	2.453	-
10	2.339	2.800	2.287	-	2.386	-	2.513	-
11	2.301	2.764	2.313	-	2.413	-	2.484	-
12	2.301	2.783	2.354	-	2.412	-	2.461	-
13	2.345	2.790	2.348	-	2.437	-	2.466	-
14	2.324	2.823	2.395	-	2.442	-	2.477	-
15	2.354	2.790	2.419	-	2.482	-	2.538	-
16	2.399	2.840	2.418	2.887	2.478	-	2.529	-
17	2.417	2.867	2.417	2.915	2.476	-	2.515	-
18	-	-	2.419	2.887	2.477	3.291	2.552	-
19	-	-	2.438	3.012	2.507	3.110	2.489	-
20	-	-	2.552	2.942	2.501	3.322	2.629	-
21	-	-	2.498	3.238	2.548	3.842	2.598	-
22	-	-	2.492	3.206	2.548	3.841	2.644	-
23	-	-	-	-	2.628	3.355	2.628	-
24	-	-	-	-	-	-	-	-

Table 2.13 Average X...H distance (Å) of $BrO_m^-(H_2)_n$ complexes at the M06L/6-311++G(d,p) level

	BrO^-		BrO_2^-		BrO_3^-		BrO_4^-	
n	O...H	Br...H	O...H	Br...H	O...H	Br...H	O...H	Br...H
1	1.861	-	2.056	-	2.217	-	2.335	-
2	1.937	-	2.071	-	2.214	-	2.302	-
3	2.018	-	2.094	-	2.239	-	2.365	-
4	2.078	-	2.136	-	2.296	-	2.412	-
5	2.120	-	2.154	-	2.318	-	2.395	-
6	2.163	-	2.201	-	2.328	-	2.444	-
7	2.263	-	2.246	-	2.355	-	2.447	-
8	2.307	-	2.226	-	2.355	-	2.456	-
9	2.351	-	2.269	-	2.360	-	2.494	-
10	2.422	-	2.281	-	2.393	-	2.455	-
11	2.362	3.019	2.297	-	2.403	-	2.473	-
12	2.359	3.030	2.334	-	2.428	-	2.449	-
13	2.357	3.030	2.364	-	2.439	-	2.503	-
14	2.361	3.055	2.395	-	2.437	-	2.463	-
15	2.372	3.065	2.399	-	2.434	-	2.479	-
16	2.386	3.048	2.374	3.046	2.459	-	2.476	-
17	2.395	3.007	2.379	3.054	2.469	-	2.510	-
18	2.376	3.019	2.424	3.138	2.478	-	2.504	-
19	2.399	3.046	2.438	3.122	2.507	-	2.542	-
20	-	-	2.465	3.161	2.539	-	2.610	-
21	-	-	2.496	3.184	2.534	3.336	2.597	-
22	-	-	2.511	3.319	2.504	3.273	2.549	-
23	-	-	2.455	3.656	2.504	3.998	2.568	-
24	-	-	-	-	2.529	3.980	2.640	-

Table 2.14 Average H-H distance (Å) of $X^-(H_2)_n$ complexes at the M06L/6-311++G(d,p) level

n	ClO^-	ClO_2^-	ClO_3^-	ClO_4^-	BrO^-	BrO_2^-	BrO_3^-	BrO_4^-
1	0.791	0.767	0.754	0.752	0.788	0.767	0.754	0.750
2	0.778	0.765	0.753	0.751	0.777	0.765	0.754	0.751
3	0.771	0.760	0.753	0.750	0.770	0.763	0.753	0.750
4	0.767	0.761	0.753	0.750	0.764	0.760	0.752	0.750
5	0.762	0.757	0.751	0.749	0.761	0.759	0.752	0.750
6	0.760	0.755	0.751	0.749	0.759	0.755	0.752	0.749
7	0.757	0.755	0.751	0.749	0.756	0.755	0.751	0.749
8	0.755	0.755	0.751	0.749	0.755	0.755	0.751	0.749
9	0.754	0.753	0.750	0.749	0.754	0.754	0.751	0.749
10	0.754	0.753	0.751	0.749	0.754	0.753	0.751	0.749
11	0.753	0.753	0.750	0.748	0.753	0.753	0.750	0.749
12	0.753	0.752	0.750	0.749	0.753	0.752	0.750	0.749
13	0.752	0.752	0.750	0.749	0.752	0.752	0.750	0.748
14	0.752	0.751	0.749	0.749	0.752	0.751	0.750	0.749
15	0.752	0.751	0.749	0.748	0.752	0.751	0.750	0.749
16	0.752	0.751	0.749	0.748	0.751	0.751	0.749	0.748
17	0.751	0.751	0.749	0.748	0.751	0.751	0.749	0.748
18	-	0.750	0.749	0.748	0.751	0.751	0.749	0.748
19	-	0.750	0.749	0.748	0.751	0.750	0.749	0.748
20	-	0.750	0.749	0.748	-	0.750	0.749	0.748
21	-	0.750	0.749	0.748	-	0.750	0.749	0.748
22	-	0.749	0.748	0.747	-	0.750	0.749	0.748
23	-	-	0.748	0.748	-	-	0.749	0.748
24	-	-	-	-	-	-	0.749	0.749

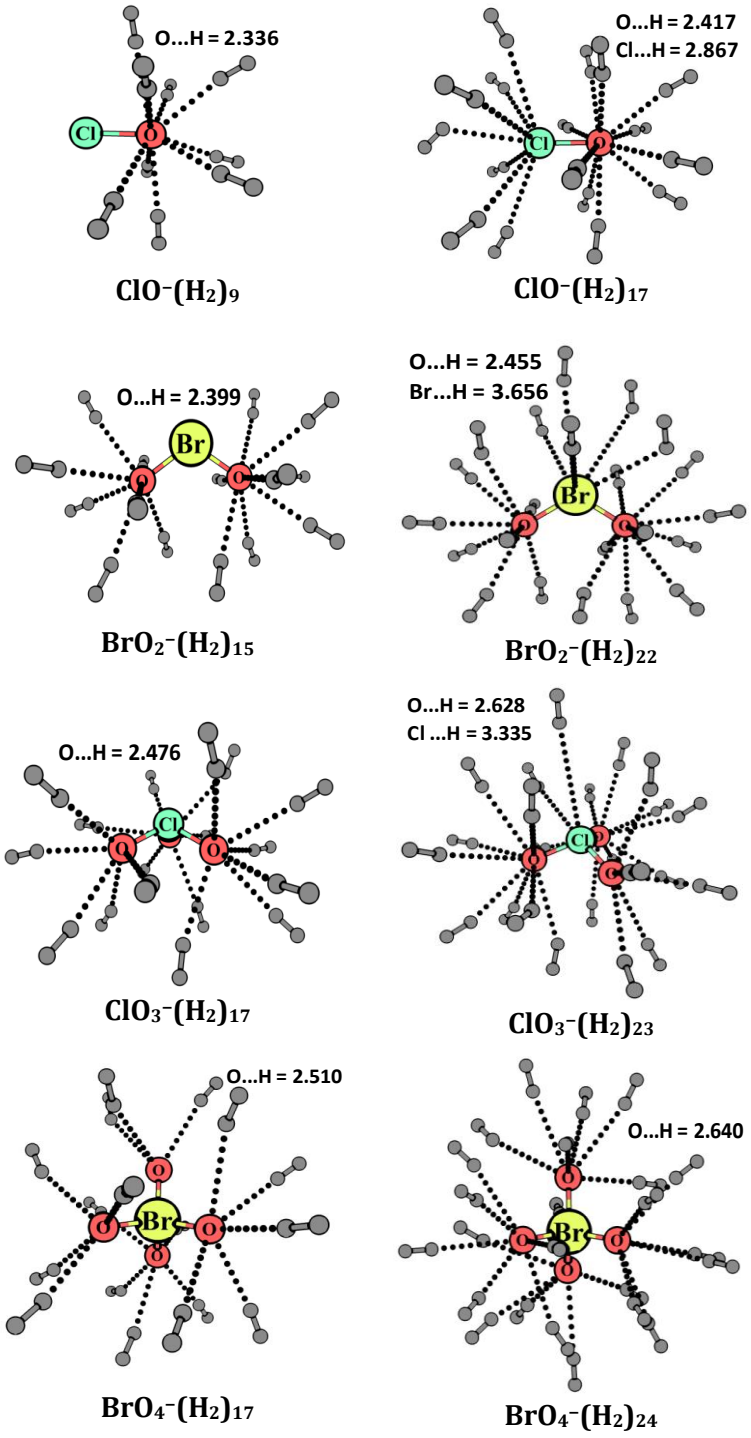

Figure 2.12 Optimized geometries of $XO_m^-(H_2)_n$ complexes at the M06L/6−311++G(d,p) level. Bond distances are in Å.

Similarly, for $BrO^-(H_2)_n$, the H−H distance is in the range 0.788 – 0.751 Å with variation in *n*. The complexes with $n > 10$ show an H−H distance in the range 0.754 – 0.748 Å

(Table 2.14). The n_{max} of polyatomic anions depends on the size of the anion. The BrO_m^- have higher coordination ability than ClO_m^- by 1 – 2 H_2 molecules. The n_{max} value is enhanced with increase in the number of oxygen atoms in the anion. The n_{max} of ClO^- is 17, which increases to 22, 23, 24, respectively for ClO_2^-, ClO_3^-, ClO_4^- anions. Similarly, the n_{max} of BrO^-, BrO_2^-, BrO_3^-, and BrO_4^- anions are 19, 22, 24 and 24 respectively.

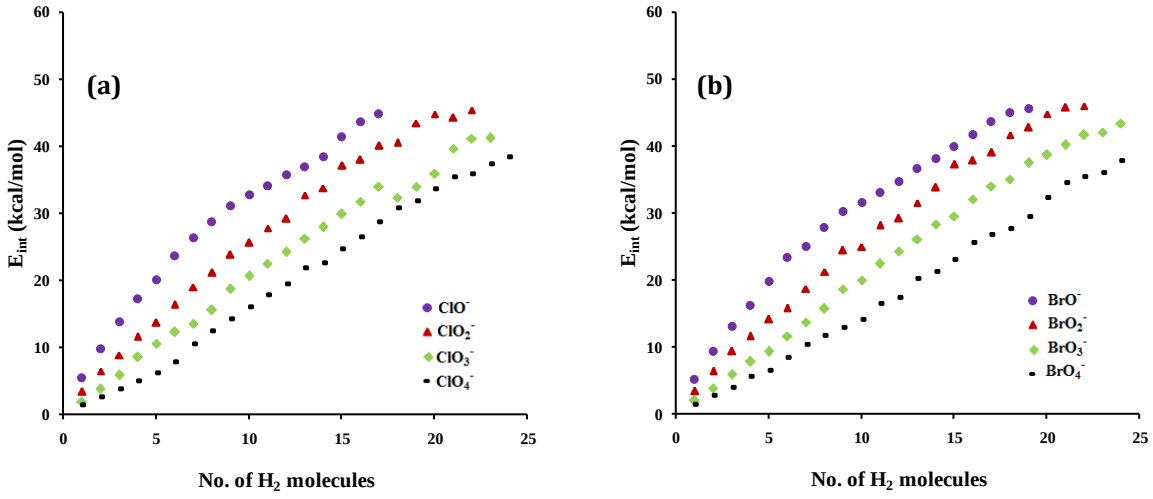

Figure 2.13 Variation of E_{int} with the number of H_2 molecules for (a) $ClO_4^-(H_2)_n$ and (b) $BrO_4^-(H_2)_n$ complexes.

The BSSE corrected E_{int} of a set of selected $ClO_m^-(H_2)_n$ and $BrO_m^-(H_2)_n$ systems are given in Table 2.15. The E_{int} of $XO_m^-(H_2)_n$ increases with increase in n. For complexes of ClO^-, ClO_2^-, ClO_3^-, and ClO_4^-, E_{int} varies from 5.4 – 44.8, 3.4 – 45.4, 1.9 – 41.2, and 1.5 – 38.4 kcal/mol as n goes from 1 to n_{max}. Also for a particular value of n, E_{int} decreases with increase in number of oxygen atoms for both the series. The $E_{int/H2}$ of all the complexes is given in Table 2.16. For complexes of ClO^-, and ClO_2^-, $E_{int/H2}$ decreases from 5.4 to 2.6 kcal/mol and 3.4 to 2.1 kcal/mol respectively. The $E_{int/H2}$ does not vary much with variation of n for ClO_3^- and ClO_4^- anions, falling in the range 1.8 – 2.1 and 1.2 – 1.7 kcal/mol, respectively. These observations also remain true in the case of $BrO_m^-(H_2)_n$ complexes. The E_{int} of any $ClO_m^-(H_2)_n$ complex is comparable with the corresponding $BrO_m^-(H_2)_n$ complex. The correlation graphs (Figure 2.13) show that E_{int} is directly proportional to n for all the series with correlation coefficient R in the range 0.984 – 0.998.

Table 2.15 BSSE corrected E_{int} values (kcal/mol) of $XO_m^-(H_2)_n$ complexes at the M06L/6-311++G(d,p) level

n	ClO^-	ClO_2^-	ClO_3^-	ClO_4^-	BrO^-	BrO_2^-	BrO_3^-	BrO_4^-
1	5.4	3.4	1.9	1.5	5.1	3.4	2.0	1.4
2	9.8	6.5	3.7	2.7	9.3	6.4	3.9	2.7
3	13.7	8.8	5.8	3.8	13.1	9.3	5.9	3.9
4	17.3	11.6	8.5	4.9	16.2	11.6	7.8	5.5
5	20.1	13.7	10.5	6.3	19.8	14.2	9.3	6.5
6	23.7	16.4	12.2	7.8	23.3	15.8	11.5	8.5
7	26.2	19.0	13.5	10.5	25.0	18.7	13.7	10.4
8	28.7	21.1	15.5	12.5	27.8	21.2	15.7	11.6
9	31.1	23.8	18.6	14.2	30.3	24.5	18.6	12.9
10	32.7	25.6	20.6	16.1	31.5	24.9	20.0	14.1
11	34.0	27.8	22.4	17.9	33.1	28.2	22.4	16.5
12	35.7	29.2	24.2	19.5	34.7	29.2	24.3	17.4
13	36.8	32.7	26.2	21.9	36.7	31.5	26.1	20.2
14	38.4	33.8	27.9	22.6	38.1	33.8	28.3	21.2
15	41.4	37.1	29.8	24.7	39.9	37.2	29.5	23.1
16	43.6	38.0	31.7	26.5	41.8	37.9	32.1	25.5
17	44.8	40.1	33.9	28.7	43.7	39.0	34.0	26.8
18	-	40.5	32.3	30.8	44.9	41.6	35.0	27.7
19	-	43.4	34.0	31.9	45.5	42.8	37.5	29.4
20	-	44.8	35.9	33.6	-	44.8	38.6	32.2
21	-	44.3	39.6	35.4	-	45.7	40.1	34.5
22	-	45.4	41.1	35.9	-	46.0	41.6	35.4
23	-	-	41.2	37.3	-	-	42.0	36.1
24	-	-	-	38.4	-	-	43.4	37.8

The slopes and intercepts of ClO_m^- series are very much similar to those of BrO_m^- series. The slope of correlation plots shows a declining trend with increase in the number of oxygen atoms in the anion. As the number of oxygen atoms increases, the size of the anion increases and as a result the charge density per atom of the monoanion

decreases. Thus the H_2 binding ability is lowered in bigger anions, which is reflected in the E_{int} and slope of correlation plots.

Table 2.16 BSSE corrected $E_{int/H2}$ values (kcal/mol) of $XO_m^-(H_2)_n$ complexes at the M06L/6−311++G(d,p) level

n	ClO^-	ClO_2^-	ClO_3^-	ClO_4^-	BrO^-	BrO_2^-	BrO_3^-	BrO_4^-
1	5.4	3.4	1.9	1.5	5.1	3.4	2.0	1.4
2	4.9	3.2	1.9	1.3	4.7	3.2	1.9	1.4
3	4.6	2.9	1.9	1.3	4.4	3.1	2.0	1.3
4	4.3	2.9	2.1	1.2	4.0	2.9	1.9	1.4
5	4.0	2.7	2.1	1.3	4.0	2.8	1.9	1.3
6	3.9	2.7	2.0	1.3	3.9	2.6	1.9	1.4
7	3.7	2.7	1.9	1.5	3.6	2.7	2.0	1.5
8	3.6	2.6	1.9	1.6	3.5	2.7	2.0	1.5
9	3.5	2.6	2.1	1.6	3.4	2.7	2.1	1.4
10	3.3	2.6	2.1	1.6	3.2	2.5	2.0	1.4
11	3.1	2.5	2.0	1.6	3.0	2.6	2.0	1.5
12	3.0	2.4	2.0	1.6	2.9	2.4	2.0	1.4
13	2.8	2.5	2.0	1.7	2.8	2.4	2.0	1.6
14	2.7	2.4	2.0	1.6	2.7	2.4	2.0	1.5
15	2.8	2.5	2.0	1.6	2.7	2.5	2.0	1.5
16	2.7	2.4	2.0	1.7	2.6	2.4	2.0	1.6
17	2.6	2.4	2.0	1.7	2.6	2.3	2.0	1.6
18	–	2.3	1.8	1.7	2.5	2.3	1.9	1.5
19	–	2.3	1.8	1.7	2.4	2.3	2.0	1.5
20	–	2.2	1.8	1.7	–	2.2	1.9	1.6
21	–	2.1	1.9	1.7	–	2.2	1.9	1.6
22	–	2.1	1.9	1.6	–	2.1	1.9	1.6
23	–	–	1.8	1.6	–	–	1.8	1.6
24	–	–	–	1.6	–	–	1.8	1.6

In a previous benchmark study, M06L/6−311++G(d,p) method is rated as one of the most reliable DFT method to reproduce the geometry and interaction energy of CCSD(T) level results for noncovalently bonded small molecular dimers. Herein, $E_{int/H2}$ computed at CCSD(T)/aug-cc-pVTZ//CCSD/aug-cc-pVDZ level for $ClO_m^-(H_2)_n$ and $BrO_m^-(H_2)_n$ complexes (n = 1 – 5; m = 1 - 4), depicted in Table 2.17 show close agreement between the *ab initio* and M06L/6−311++G(d,p) DFT theories. Moreover, structural features of the complexes too agreed very well at both levels of theory. Compared to the anions, the neutral oxohaloacids HClO, $HClO_2$, $HClO_3$, HBrO, $HBrO_2$, $HBrO_3$ show very low H_2 binding affinity in the range 0.37 – 0.45 kcal/mol for the uptake of one H_2 molecule. Their ability to bind with multiple H_2 is negligible. The oxohaloacids of ClO_4^- and BrO_4^- ($HClO_4$ and $HBrO_4$) show E_{int} 1.49 and 1.38 kcal/mol, respectively for binding one H_2 and the $E_{int/H2}$ drops down to 0.65 kcal/mol for former and 0.67 kcal/mol for latter, with the uptake of 3 H_2 molecules. Dihydrogen binding affinity of neutral salt systems have been tested by introducing a cation (Na^+) to anion-H_2 complexes with n = 10. The E_{int} decreases significantly in all the cases; the decline being more pronounced in systems with smaller anions as the anion-cation interaction is much higher in those cases (Table 2.18). These results show that changing a neutral species to anionic form leads to massive improvement in its dihydrogen uptake ability.

Table 2.17 $E_{int/H2}$ values (kcal/mol) of $ClO_m^-(H_2)_n$ and $BrO_m^-(H_2)_n$ complexes at the CCSD(T)/aug−cc−pVTZ level

n	ClO^-	ClO_2^-	ClO_3^-	ClO_4^-	BrO^-	BrO_2^-	BrO_3^-	BrO_4^-
1	4.3	3.1	2.2	1.9	4.3	3.3	2.4	1.9
2	4.1	3.1	2.2	1.9	4.2	3.3	2.4	1.9
3	4.0	2.9	2.2	1.9	4.1	3.2	2.4	1.9
4	3.8	2.9	2.1	1.9	3.9	3.1	2.3	1.9
5	3.6	2.8	2.1	1.8	3.8	3.0	2.3	1.8

The estimated volumes of ClO^-, ClO_2^-, ClO_3^-, and ClO_4^- polyatomic anions using QTAIM analysis at an isodensity surface value of 0.001 au are 402.97, 458.26, 516.56, and

567.46 au The volume (size) increases with increase in the number of oxygen atoms. Similarly in BrO_m^- series, the respective volumes are 455.21, 505.96, 562.67, and 620.04 au as *m* varies from 1 to 4. The E_{int} versus volume correlation plot for dihydrogen complexes of all the polyatomic anions with *n* = 3 is represented in Figure 2.14. The E_{int} decreases with increase in the size of the anion. However, size of the halogen is not reflected in the H_2 binding affinity.

Table 2.18 BSSE corrected E_{int} values (kcal/mol) of $XO_m^-(H_2)_{10}Na^+$ complexes at M06L/6−311++G(d,p) level

Anion	Bare	Na^+ as counter cation
ClO^-	3.3	2.2
ClO_2^-	2.6	1.7
ClO_3^-	2.1	1.5
ClO_4^-	1.6	1.4
BrO^-	3.2	2.2
BrO_2^-	2.5	1.8
BrO_3^-	2.0	1.6
BrO_4^-	1.4	1.2

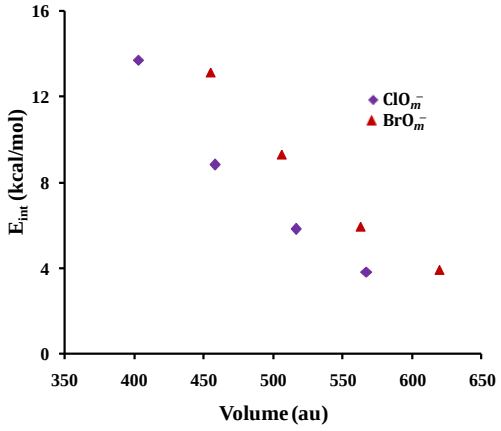

Figure 2.14 Correlation between E_{int} of $XO_m^-(H_2)_3$ and volume of bare anion at the M06L/6-311++G(d,p) level.

2.9.2 MESP Analysis

The MESP isosurface plotted for bare anions shows that the negative charge is concentrated around the oxygen atoms (Figure 2.15). This explains why the initially added H_2 molecules in anion-H_2 complexes bind with the oxygens in all the cases. The anions of ClO_m^- and BrO_m^- series show a decrease in the magnitude of V_{min} values (Table 2.19) with increase in size. All ClO_m^- anions possess a slightly higher negative V_{min} than corresponding BrO_m^- anions. As there is not much difference in the V_{min} values of both the series, the E_{int} and n_{max} also follow similar trends. The potential at the nucleus (V_n) of halogen and one of the oxygen atoms of the polyatomic anion is given in Table 2.19 (the values are denoted in atomic units as the magnitude of V_n is very high compared to V_{min}). The magnitude of V_n at oxygen and halogen decreases with increase in size of the anion for both the series. Also, V_n at oxygen of any ClO_m^- anion is very much comparable with that of corresponding BrO_m^- anion. The E_{int} of $XO_m^-(H_2)_n$ is directly proportional to the magnitude of V_{min} or V_n. As representative examples, the correlation plots of E_{int} with V_{min} and V_n of all the complexes with n = 3 is given in Figure 2.16a and 2.16b, respectively. A MESP isosurface with the lowest negative value that engulfs the whole anion can be always located for an anion/anionic complex. [32, 69] For instance, such a MESP value for $ClO_4^-(H_2)_{24}$ is -47.7 kcal/mol (Figure 2.17). According to Gadre-Pathak theorem,[43] this value is a directional minimum (V_{min}) in MESP and the V_{min} of all the complexes are given in Table 2.20. A decline in the magnitude of V_{min} is noted with increase in n for both series of anionic complexes. Compared to the bare anion, the hydrogen rich anionic complexes show significant change in their V_n values at the halogen and oxygen centers. The total change observed in V_n due to hydrogen uptake ($\Sigma\Delta V_n$) is reported in Table 2.21 for $ClO_m^-(H_2)_n$ and $BrO_m^-(H_2)_n$ complexes. For identical m and n values, $\Sigma\Delta V_n$ corresponding $ClO_m^-(H_2)_n$ are higher than $BrO_m^-(H_2)_n$. For instance, $\Sigma\Delta V_n$ of $ClO^-(H_2)_{10}$ and $BrO^-(H_2)_{10}$ are 84.1 and 76.3 kcal/mol, respectively. The magnitude of $\Sigma\Delta V_n$ is directly proportional to n with both $ClO_m^-(H_2)_n$ and $BrO_m^-(H_2)_n$ showing similar trend in their variation (Figure2.18).

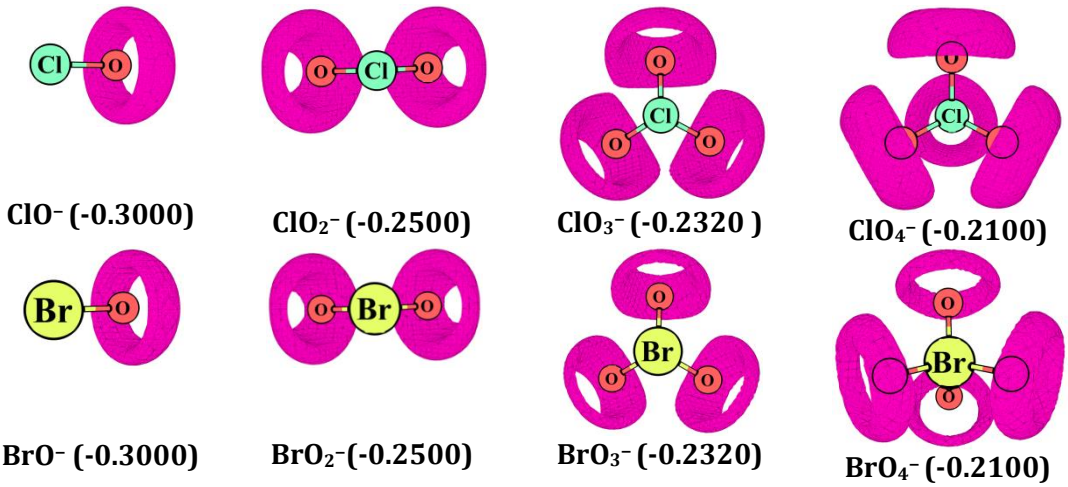

Figure 2.15 MESP features of bare polyatomic anions at the M06L/6−311++G(d,p) level (isosurface values in au are given in parentheses for each anion).

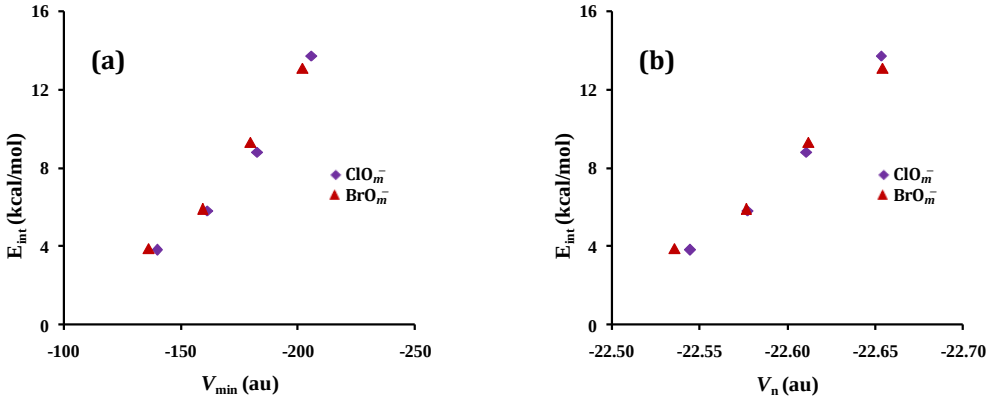

Figure 2.16 Correlation between (a) E_{int} of $XO_m^-(H_2)_3$ and V_{min} and (b) E_{int} of $XO_m^-(H_2)_3$ and V_n at oxygen at the M06L/6−311++G(d,p) level.

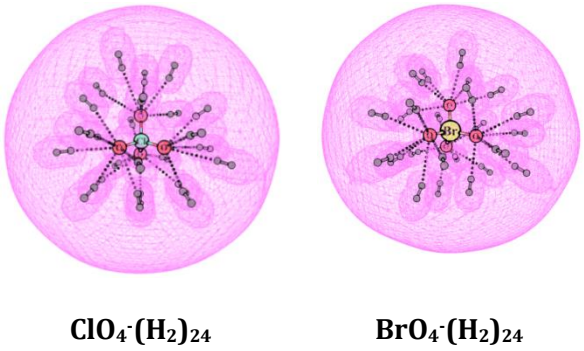

Figure 2.17 MESP of (a) $ClO_4^-(H_2)_{24}$ at −47.7 kcal/mol and (b) $BrO_4^-(H_2)_{24}$ complexes at −47.1 kcal/mol at the M06L/6−311++G(d,p) level.

Table 2.19 MESP features of bare polyatomic anions at the M06L/6−311++G(d,p) level

Anion	V_{min} (kcal/mol)	V_n at halogen (au)	V_n at O (au)
ClO^-	-205.8	-64.6511	-22.6534
ClO_2^-	-182.6	-64.5280	-22.6109
ClO_3^-	-161.3	-64.3816	-22.5774
ClO_4^-	-139.9	-64.2474	-22.5446
BrO^-	-202.0	-176.0707	-22.6543
BrO_2^-	-179.8	-175.9755	-22.6121
BrO_3^-	-159.3	-175.8719	-22.5763
BrO_4^-	-136.4	-175.7839	-22.5358

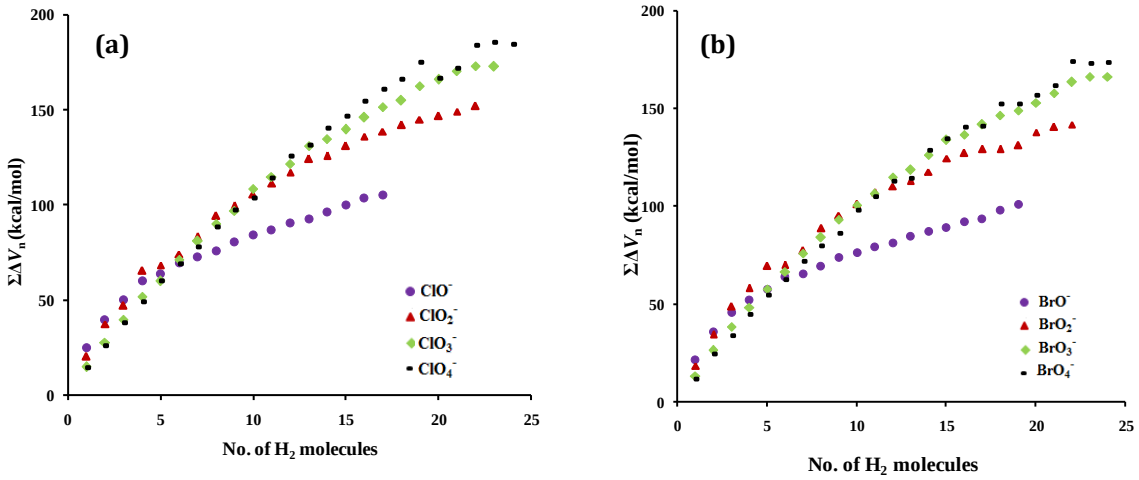

Figure 2.18 Correlation between $\Sigma\Delta V_n$ and number of H_2 molecules of (a) $ClO_4^-(H_2)_n$ and (b) $BrO_4^-(H_2)_n$ complexes at the M06L/6-311++G(d,p) level.

A strong linear correlation is noted between E_{int} and $\Sigma\Delta V_n$ of $ClO_m^-(H_2)_n$ and $BrO_m^-(H_2)_n$ with correlation coefficient R, lying in the range 0.984 – 0.993 (Figure 2.18). The slopes for complexes of ClO^-, ClO_2^-, ClO_3^-, ClO_4^- are 0.516, 0.340, 0.246, and 0.220, respectively. This indicates that the variation of $\Sigma\Delta V_n$ with E_{int} is maximum in the case of ClO^- and this anion can be recommended as the one with maximum affinity towards dihydrogen.

Very similar trend is observed for $BrO_m^-(H_2)_n$ complexes with BrO^- being the anion with the highest affinity towards dihydrogen.

Table 2.20 V_{min} values (kcal/mol) of $XO_m^-(H_2)_n$ complexes at the M06L/6-311++G(d,p) level

n	ClO^-	ClO_2^-	ClO_3^-	ClO_4^-	BrO^-	BrO_2^-	BrO_3^-	BrO_4^-
1	-94.6	-75.6	-66.0	-59.8	-84.0	-74.7	-64.9	-56.2
2	-86.0	-72.5	-62.7	-57.9	-81.1	-71.4	-63.7	-55.7
3	-81.8	-67.3	-67.7	-57.2	-78.6	-69.3	-63.3	-55.4
4	-78.3	-68.0	-66.0	-56.5	-76.1	-68.2	-62.7	-57.0
5	-68.2	-63.1	-61.9	-56.2	-68.9	-66.8	-58.2	-54.3
6	-67.6	-61.5	-57.4	-55.9	-67.8	-61.0	-57.2	-54.6
7	-67.8	-60.7	-57.6	-55.0	-67.8	-61.6	-56.0	-55.0
8	-67.8	-59.9	-56.9	-55.2	-67.7	-60.0	-55.3	-54.2
9	-67.5	-60.1	-57.0	-54.7	-66.2	-59.5	-55.3	-54.4
10	-56.1	-56.9	-56.0	-55.0	-55.4	-58.2	-55.8	-53.0
11	-54.7	-55.1	-54.8	-54.0	-53.1	-54.5	-55.1	-52.1
12	-54.0	-56.2	-54.7	-54.0	-53.0	-52.8	-54.3	-51.8
13	-54.0	-54.3	-54.0	-52.6	-53.0	-52.3	-53.7	-51.8
14	-53.2	-52.9	-53.8	-53.3	-50.8	-51.2	-52.8	-52.1
15	-48.8	-52.2	-52.5	-52.4	-50.6	-53.0	-52.6	-51.2
16	-49.2	-49.9	-52.7	-52.4	-51.0	-48.3	-52.1	-50.5
17	-51.9	-49.3	-52.3	-52.0	-48.9	-43.1	-51.0	-50.5
18	-	-49.0	-44.2	-51.8	-48.4	-43.0	-50.6	-49.6
19	-	-45.7	-45.6	-50.9	-47.6	-43.9	-49.3	-47.5
20	-	-48.1	-44.2	-49.8	-	-45.2	-42.9	-49.1
21	-	-43.4	-42.2	-49.2	-	-37.8	-41.7	-48.6
22	-	-42.4	-42.4	-51.0	-	-41.2	-43.7	-49.6
23	-	-	-42.7	-48.1	-	-	-39.8	-47.7
24	-	-	-	-47.7	-	-	-40.0	-47.1

Table 2.21 $\Sigma\Delta V_n$ values (kcal/mol) of $XO_m^-(H_2)_n$ complexes at the M06L/6-311++G(d,p) level

n	ClO^-	ClO_2^-	ClO_3^-	ClO_4^-	BrO^-	BrO_2^-	BrO_3^-	BrO_4^-
1	24.8	20.5	14.9	14.3	21.8	18.7	13.5	11.9
2	39.7	37.5	27.6	26.1	35.9	34.8	26.4	24.8
3	50.4	47.0	39.8	38.3	46.1	49.0	38.7	34.2
4	60.0	65.4	51.7	49.2	52.5	58.3	48.3	45.0
5	63.9	68.5	60.0	60.0	57.7	69.7	57.7	54.8
6	69.5	74.2	71.2	68.9	64.0	70.2	66.8	62.6
7	72.5	83.4	80.9	77.7	65.5	77.6	76.1	72.2
8	75.9	94.3	90.2	88.2	69.7	89.1	84.2	80.1
9	80.6	99.5	97.0	97.6	73.9	95.7	93.4	86.3
10	84.1	105.6	108.6	103.4	76.3	101.2	100.7	98.3
11	87.1	111.5	114.6	114.1	79.3	107.2	106.5	105.0
12	90.6	117.2	121.5	125.7	81.6	110.4	115.1	113.0
13	92.9	124.4	130.9	131.4	84.8	113.3	118.7	114.5
14	96.3	125.9	134.7	140.5	87.2	117.8	126.4	128.6
15	100.2	131.1	139.7	146.8	89.5	124.7	134.1	134.5
16	103.5	136.1	145.9	154.3	92.4	127.6	136.8	140.7
17	105.1	138.8	151.4	160.7	93.9	129.3	141.9	141.0
18	-	142.3	154.9	166.1	98.3	129.5	146.7	152.3
19	-	145.1	162.5	174.9	101.0	131.4	149.1	152.6
20	-	146.9	165.9	166.7	-	138.1	153.2	157.1
21	-	149.2	170.3	171.7	-	140.8	157.9	162.1
22	-	152.1	172.9	184.1	-	142.1	163.7	174.2
23	-	-	172.7	185.4	-	-	166.3	173.1
24	-	-	-	184.6	-	-	166.3	173.7

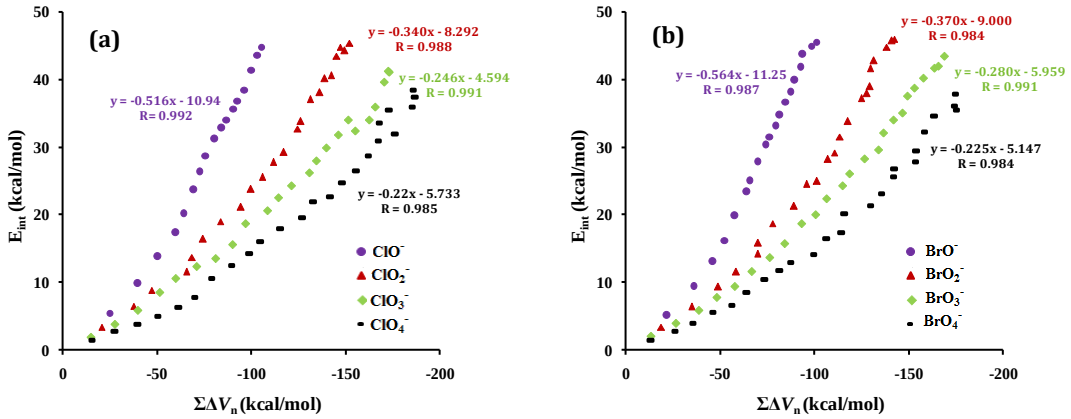

Figure 2.19 Correlation between E_{int} and $\Sigma\Delta V_n$ of (a) $ClO_m^-(H_2)_n$ and (b) $BrO_m^-(H_2)_n$ complexes at the M06L/6−311++G(d,p) level.

2.9.3 QTAIM Analysis

QTAIM analysis shows bond critical points (bcp) for all O...H and X...H interactions. Figure 3 represents the QTAIM features of $ClO_3^-(H_2)_{23}$ and $ClO_4^-(H_2)_{24}$ complexes as typical examples (Figure 2.20). The red dots indicate bcp for O...H or Cl...H interactions while the blue dots indicate bcp for H...H dihydrogen interactions. Since a large number of bcps is present in hydrogen rich complexes, for simplicity, we consider the average value of the electron density at bcp (ρ_{bcp}) for representing the strength of O...H or Cl...H interactions. Table 2.22 depicts ρ_{bcp} for a set of $ClO_m^-(H_2)_n$ and $BrO_m^-(H_2)_n$.

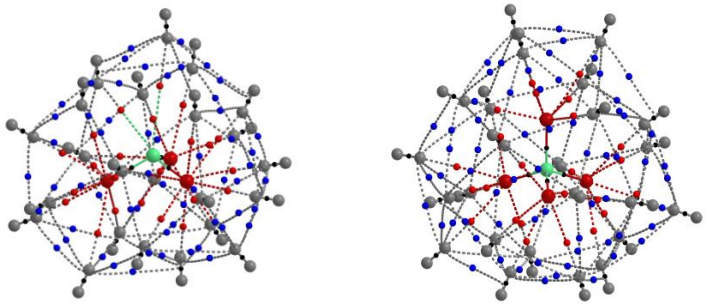

(a) $ClO_3^-(H_2)_{23}$ **(b) $ClO_4^-(H_2)_{24}$**

Figure 2.20 QTAIM features of (a) $ClO_3^-(H_2)_{23}$ and (b) $ClO_4^-(H_2)_{24}$ at the M06L/6−311++G(d,p) level.

The average ρ_{bcp} values of $ClO_m^-(H_2)_n$ and $BrO_m^-(H_2)_n$ are in the range 0.0373 – 0.0072 au and 0.0358 – 0.0074 au respectively. The bond strength is directly proportional to

the size of complex or anion. The E_{int} versus $\Sigma\rho_{bcp}$ correlation plots $ClO_m^-(H_2)_n$ and $BrO_m^-(H_2)_n$ are very much similar with the correlation coefficients lying in the range 0.983 – 0.992 and comparable slope values (Figure 2.21).

Table 2.22 Average ρ_{bcp} values (au) of $XO_m^-(H_2)_n$ complexes at the M06L/6-311++G(d,p) level

n	ClO^-	ClO_2^-	ClO_3^-	ClO_4^-	BrO^-	BrO_2^-	BrO_3^-	BrO_4^-
1	0.0373	0.0241	0.0145	0.0125	0.0358	0.0237	0.0146	0.0109
2	0.0615	0.0454	0.0275	0.0220	0.0600	0.0450	0.0291	0.0240
3	0.0788	0.0579	0.0380	0.0328	0.0767	0.0644	0.0425	0.0330
4	0.0956	0.0817	0.0502	0.0421	0.0888	0.0773	0.0524	0.0416
5	0.1034	0.0856	0.0562	0.0499	0.2331	0.0937	0.0630	0.0630
6	0.1119	0.0940	0.0682	0.0582	0.1100	0.0952	0.0726	0.0580
7	0.1129	0.1077	0.0843	0.0651	0.1074	0.1057	0.0821	0.0673
8	0.1156	0.1223	0.0904	0.0750	0.1127	0.1235	0.0923	0.0758
9	0.1208	0.1283	0.1097	0.0843	0.1182	0.1314	0.1072	0.0804
10	0.1284	0.1388	0.1148	0.0894	0.1236	0.1404	0.1112	0.0940
11	0.1378	0.1465	0.1212	0.1013	0.1295	0.1514	0.1164	0.1005
12	0.1453	0.1470	0.1227	0.1105	0.1364	0.1567	0.1303	0.1104
13	0.1502	0.1623	0.1394	0.1169	0.1436	0.1617	0.1367	0.1104
14	0.1550	0.1626	0.1464	0.1288	0.1485	0.1638	0.1380	0.1317
15	0.1637	0.1742	0.1409	0.1438	0.1596	0.1716	0.1484	0.1371
16	0.1687	0.1747	0.1543	0.1456	0.1644	0.1809	0.1575	0.1408
17	0.1702	0.1871	0.1678	0.1457	0.1714	0.1853	0.1656	0.1415
18	-	0.1887	0.1699	0.1554	0.1716	0.1817	0.1801	0.1544
19	-	0.1895	0.1842	0.1648	0.1693	0.1834	0.1815	0.1528
20	-	0.1848	0.1880	0.1606	-	0.1946	0.1820	0.1642
21	-	0.1884	0.2077	0.1550	-	0.1974	0.2047	0.1721
22	-	0.1902	0.2097	0.1744	-	0.2010	0.1916	0.1802
23	-	-	0.1823	0.1635	-	-	0.1895	0.1806
24	-	-	-	0.1728	-	-	0.1901	0.1785

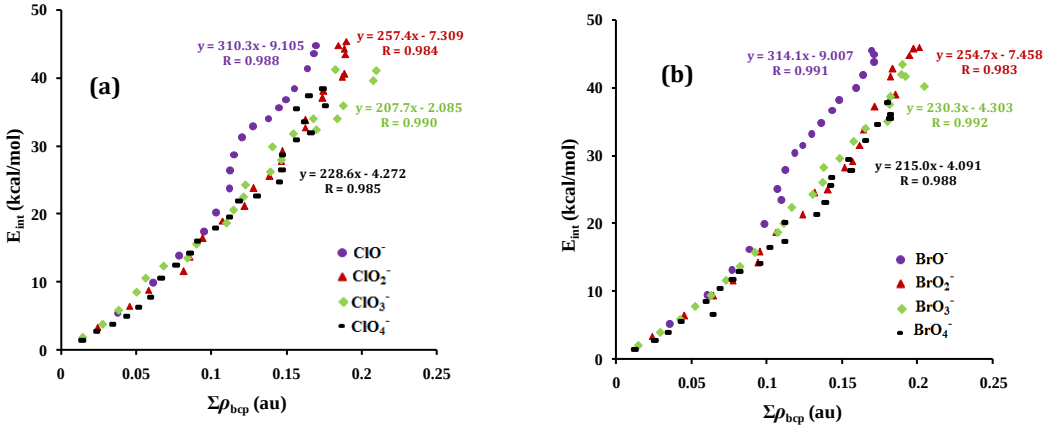

Figure 2.21 Correlation between E_{int} and $\Sigma\rho_{bcp}$ of (a) $ClO_m^-(H_2)_n$ and (b) $BrO_m^-(H_2)_n$ complexes at the M06L/6−311++G(d,p) level.

Table 2.23 ρ_{bcp} range of H…H interactions (au) of $XO_m^-(H_2)_n$ complexes at the M06L/6−311++G(d,p) level

Complex	ρ_{bcp} range
$ClO^-(H_2)_n$	0.0020 – 0.0065
$ClO_2^-(H_2)_n$	0.0011 – 0.0064
$ClO_3^-(H_2)_n$	0.0010 – 0.0054
$ClO_4^-(H_2)_n$	0.0010 – 0.0044
$BrO^-(H_2)_n$	0.0021 – 0.0073
$BrO_2^-(H_2)_n$	0.0012 – 0.0064
$BrO_3^-(H_2)_n$	0.0010 – 0.0054
$BrO_4^-(H_2)_n$	0.0900 – 0.0046

A linear variation of $\Sigma\rho_{bcp}$ with E_{int} is observed in the complexes with lower n values (n < 10) where as for larger complexes the linear trend is slightly deviated. The slopes of the graphs decrease with increase in m in both the series, indicating that the anion−H_2 bond strength is higher in anions with less number of oxygen atoms or smaller anions. The Laplacian of the electron density ($\nabla^2\rho_{bcp}$) is positive lying in the range 0.1063 – 0.0115 au for all $XO_m^-(H_2)_n$. The small ρ_{bcp} and positive $\nabla^2\rho_{bcp}$ support that the anion−H_2 interactions are noncovalent in nature.[70, 71] The H...H secondary interactions are weaker

compared to O...H, Cl…H, and Br…H interactions. These interactions are not found until *n* reaches a value of 10, 7, 3, 5, 9, 7, 3, and 4 respectively for ClO^-, ClO_2^-, ClO_3^-, ClO_4^-, BrO^-, BrO_2^-, BrO_3^-, and BrO_4^- anions. The ρ_{bcp} range of these H…H interactions is given in Table 2.23. The strength of these secondary interactions depends on the number of oxygen atoms and is independent of the halogen present in the anion. The formation of bcp between H atoms indicates that attractive interactions develop between dihydrogen molecules adsorbed to the anion. Otherwise, a repulsive interaction must have resisted the uptake of several dihydrogens by the anion. The complex appears as a system of molecules well connected by a large network of noncovalent interconnections. The increasing number of H...H interactions accounts for almost consistent $E_{int/H2}$ with increase in *n* (only a minor drop is observed especially for smaller anions). The dihydrogen binding ability of polyatomic anions varies from 40.0 – 32.7 and 28.5 – 25.2 wt% for $ClO_m^-(H_2)_{nmax}$ and $BrO_m^-(H_2)_{nmax}$, respectively (Table 2.24). The H_2 uptake capacity is maximum (40.0 wt%) for ClO^- anion.

Table 2.24 H_2 affinity of polyatomic anions

Anion	n_{max}	Weight percent of H_2 (wt%)
ClO^-	17	40.0
ClO_2^-	22	39.7
ClO_3^-	23	35.7
ClO_4^-	24	32.7
BrO^-	19	28.5
BrO_2^-	22	28.4
BrO_3^-	24	27.4
BrO_4^-	24	25.2

2.10 Conclusions

The dependence on H_2 binding affinity on the size and charge density of the anions is studied in the present work by analyzing the dihydrogen complexes of two sets of polyatomic anionic series. Our studies show that the polyatomic anions with smaller size and less number of atoms are more efficient in H_2 binding as the available charge density is more localized in such cases. Among all the anions studied, ClO^- emerged as

the most efficient for dihydrogen binding. This study also emphasizes that the ability of anionic systems for hydrogen uptake is very high compared to their neutral counterparts. All the anions show the ability to simultaneously interact with a large number of H_2 molecules with a steady linear increase in total interaction energy. QTAIM analysis showed that the adsorbed H_2 molecules are not repelled from each other as the neighbouring pairs show stabilizing intermolecular H...H dihydrogen interactions in hydrogen rich complexes. These results suggest that hydrogen uptake ability of materials can be significantly improved by the incorporation of anionic groups. The challenge is designing an efficient salt system for hydrogen storage. In other words, a weakly binding cation-anion combination or a non-coordinating cation along with the counter anion may serve the purpose. In the present study we focused only on the ability of polyatomic anions to bind with hydrogen and studies featuring cation-anion combination is under way.

2.11 References

1. J. A. Nichols, R. A. Kendall, S. J. Cole and J. Simons, *J. Phys. Chem.*, **1991**, *95*, 1074-1076.
2. A. Boldyrev, J. Simons, G. Mil'nikov, V. Benderskii, S. Y. Grebenshchikov and E. Vetoshkin, *J. Chem. Phys.*, **1995**, *102*, 1295-1305.
3. B. Hartke and H.-J. Werner, *Chem. Phys. Lett.*, **1997**, *280*, 430-438.
4. M. H. Alexander, *J. Chem. Phys.*, **2003**, *118*, 9637-9642.
5. E. J. Bieske, *Chem. Soc. Rev*, **2003**, *32*, 231-237.
6. A. A. Buchachenko, T. A. Grinev, J. Kłos, E. J. Bieske, M. M. Szczęśniak and G. Chałasiński, *J. Chem. Phys.*, **2003**, *119*, 12931-12945.
7. D. Wild and E. Bieske, *Int. Rev. Phys. Chem.*, **2003**, *22*, 129-151.
8. D. Wild and E. Bieske, *J. Chem. Phys.*, **2004**, *121*, 12276-12281.
9. D. Wild, P. Weiser, Z. Loh and E. Bieske, *J. Phys. Chem. A*, **2002**, *106*, 906-910.
10. D. A. Wild, Z. M. Loh, R. L. Wilson and E. J. Bieske, *J. Chem. Phys.*, **2002**, *117*, 3256-3262.
11. D. A. Wild, P. S. Weiser and E. J. Bieske, *J. Chem. Phys.*, **2001**, *115*, 6394-6400.

12. D. A. Wild, P. S. Weiser, E. J. Bieske and A. Zehnacker, *J. Chem. Phys.*, **2001**, *115*, 824-832.
13. D. A. Wild, R. L. Wilson, P. S. Weiser and E. J. Bieske, *J. Chem. Phys.*, **2000**, *113*, 10154-10157.
14. B. l. Nyulasi and A. Kovács, *Chem. Phys. Lett.*, **2006**, *426*, 26–29.
15. A. Kovács and Z. Varga, *Coord. Chem. Rev.* , **2006**, *250*, 710-727.
16. S. Scheiner, *Hydrogen Bonding. A Theoretical Perspective*, University Press, Oxford, Oxford, **1997**.
17. F. Pichierri, *Chem. Phys. Lett.*, **2012**, *519*, 83-88.
18. A. Trewin, G. R. Darling and A. I. Cooper, *New J. Chem.*, **2008**, *32*, 17-20.
19. J. G. Vitillo, A. Damin, A. Zecchina and G. Ricchiardi, *J. Chem. Phys.*, **2006**, *124*, 224308
20. R. C. Lochan and M. Head-Gordon, *Phys. Chem. Chem. Phys.*, **2006**, *8*, 1357.
21. K. Remya and C. H. Suresh, *J. Comput. Chem.*, **2013**, *34*, 1341–1353.
22. S. F. Boys and F. Bernardi, *Mol. Phys*, **1970**, *19*, 553-566.
23. D.G.Truhlar, *Chem. Phys. Lett.*, **1998**, *294*, 45-48.
24. S. Scheiner, *Comp. Theor. Chem.*, **2012**, *998*, 9-13.
25. R. F. W. Bader, *Atoms in Molecules: A Quantum Theory*, Clarendon Press, Oxford, **1990**.
26. P. Politzer, R. G. Parr and D. R. Murphy, *J. Chem. Phys.*, **1983**, *79*, 3859-3861.
27. N. K. Ray, L. Samuels and R. G. Parr, *J. Chem. Phys.* , **1979**, *70*, 3680-3684.
28. C. H. Suresh and S. R. Gadre, *J. Am. Chem. Soc.*, **1998**, *120*, 7049–7055.
29. S. P. Gejji, C. H. Suresh, K. Babu and S. R. Gadre, *J. Phys. Chem. A*, **1999**, *103*, 7474–7480.
30. C. H. Suresh and N. Koga, *J. Am. Chem. Soc.* , **2002**, *124*, 1790-1797.
31. J. J. M. Wiener, M. E. Grice, J. S. Murray and P. Politzer, *J. Chem. Phys.* , **1996**, *104*, 5109-5111.
32. S. R. Gadre and R. N. Shirsat, *Electrostatics of Atoms and Molecules*, Universities Press, Hyderabad, **2000**.
33. S. R. Gadre and C. H. Suresh, *J. Org. Chem.* , **1997**, *62*, 2625-2627.

34. J. S. Murray and K. Sen, *Molecular Electrostatic Potentials: Concepts and Applications*, Amsterdam, The Netherlands: Elsevier Science, **1996**.
35. P. Politzer and D. G.Truhlar, *Chemical Applications of Atomic and Molecular Electrostatic Potentials : Reactivity, Structure, Scattering, and Energetics of Organic, Inorganic, and Biological Systems*, Plenum Press New York, **1981**.
36. A. Kumar, S. D. Yeole, S. R. Gadre, R. Lopez, J. F. Rico, G. Ramirez, I. Ema and D. Zorrilla, *J. Comput. Chem.*, **2015**, *36*, 2350-2359.
37. S. R. Gadre, S. A. Kulkarni and I. H. Shrivastava, *J. Chem. Phys.*, **1992**, *96*, 5253-5260.
38. P. Politzer and D. G. Truhlar, *Chemical Applications of Atomic and Molecular Electrostatic Potentials: Reactivity, Structure, Scattering: Energetics of Organic, Inorganic, and Biological Systems*, Springer, New York, **1981**.
39. M. J. Frisch,G. W. Trucks, *et al.* Gaussian 09, Revision D.01; Gaussian, Inc., Wallingford CT, **2013**.
40. T. A. Keith, *AIMAll version 14.04.17*, T. K. Gristmill Software, Overland Park KS, USA, **2014**.
41. R. C. Lochan and M. Head-Gordon, *Phys. Chem. Chem. Phys.*, **2006**, *8*, 1357.
42. D. A. Wild, P. S. Weiser, Z. M. Loh and E. J. Bieske, *J. Phys. Chem. A* **2002**, *106*, 906–910.
43. R. K. Pathak and S. R. Gadre, *J. Chem. Phys.*, **1990**, *93*, 1770-1773.
44. I. S. Bushmarinov, K. A. Lyssenko and M. Y. Antipin, *Russ. Chem. Rev.*, **2009**, *78*, 283- 302.
45. R. Parthasarathi, V. Subramanian and N. Sathyamurthy, *J. Phys. Chem. A*, **2006**, *110*, 3349-3351.
46. N. Mohan and C. H. Suresh, *J. Phys. Chem. A* **2014**, *118* 1697-1705.
47. P. K. Sajith and C. H. Suresh, *J. Organomet. Chem.*, **2011**, *696*, 2086-2092.
48. R. F. W. Bader, *J. Phys. Chem. A*, **1998**, *102* 7314–7323.
49. U. Purushotham, D. Vijay and G. N. Sastry, *J. Comput. Chem.*, **2012**, *33*, 44-59.
50. A. S. Mahadevi, Y. I. Neela and G. N. Sastry, *Phys. Chem. Chem. Phys.*, **2011**, *13*, 15211-15220.
51. K. Remya and C. H. Suresh, *J. Comput. Chem.*, **2014**, *35*, 910–922.

52. K. Remya and C. H. Suresh, *Phys. Chem. Chem. Phys.*, **2015**, *17*, 18380-18392.
53. A. Shahi and E. Arunan, *Phys. Chem. Chem. Phys.*, **2014**, *16*, 22935-22952.
54. R. F. W. Bader and H. Esseén, *J. Chem. Phys.*, **1984**, *80*, 1943–1960.
55. E. Espinosa, I. Alkorta, J. Elguero and E. Molins, *J. Chem. Phys.*, **2002**, *117*, 5529-5542.
56. U. Koch and P. L. A. Popelier, *J. Phys. Chem.*, **1995**, *99*, 9747-9754.
57. P. L. A. Popelier, *J. Phys. Chem. A*, **1998**, *102*, 1873–1878.
58. P. L. A. Popelier and G. Logothetis, *J. Organomet. Chem.*, **1998**, *555*, 101–111.
59. D. Cremer and E. Kraka, *Croat. Chem. Acta*, **1984**, *57*, 1259-1281.
60. M. A. Hussain, A. S. Mahadevi and G. N. Sastry, *Phys. Chem. Chem. Phys.*, **2015**, *17*, 1763-1775.
61. B. G. d. Oliveira, *Phys. Chem. Chem. Phys.*, **2013**, *15*, 37-79.
62. G. V. Baryshnikova, B. F. Minaeva, V. A. Minaevaa, A. T. Podgornayaa and H. Ågrenb, *Russ. J of Gen.Chem.*, **2012**, *82*, 1254–1262.
63. L. Schlapbach and A. Züttel, *Nature*, **2001**, *414*, 353-358.
64. J. Benemann, *Nat. Biotechnol.*, **1996**, *14*, 1101-1103.
65. G. D. Berry, A. D. Pasternak, G. D. Rambach, J. R. Smith and R. N. Schock, *Energy*, **1996**, *21*, 289-303.
66. A. Züttel, *Mater. Today*, **2003**, *6*, 24-33.
67. T. D. Della and C. H. Suresh, *Phys. Chem. Chem. Phys.*, **2016**, *18*, 14588-14602.
68. Y.Zhao and D.G.Truhlar, *J. Chem. Phys.*, **2006**, *125*, 194101-194118.
69. R. K. Pathak and S. R. Gadre, *J. Chem. Phys.*, **1990**, *93*, 1770-1773.
70. R. F. W. Bader and H. Esse´n, *J. Chem. Phys.*, **1984**, *80*, 1943–1960.
71. P. L. A. Popelier, G. Logothetis and *J. Organomet. Chem.*, **1998**, *555*, 101–111.

Chapter 3

Dihydrogen Binding Affinity of One-Dimensional Anionic Carbon Chains and Sumanene: An Organic π-Bowl

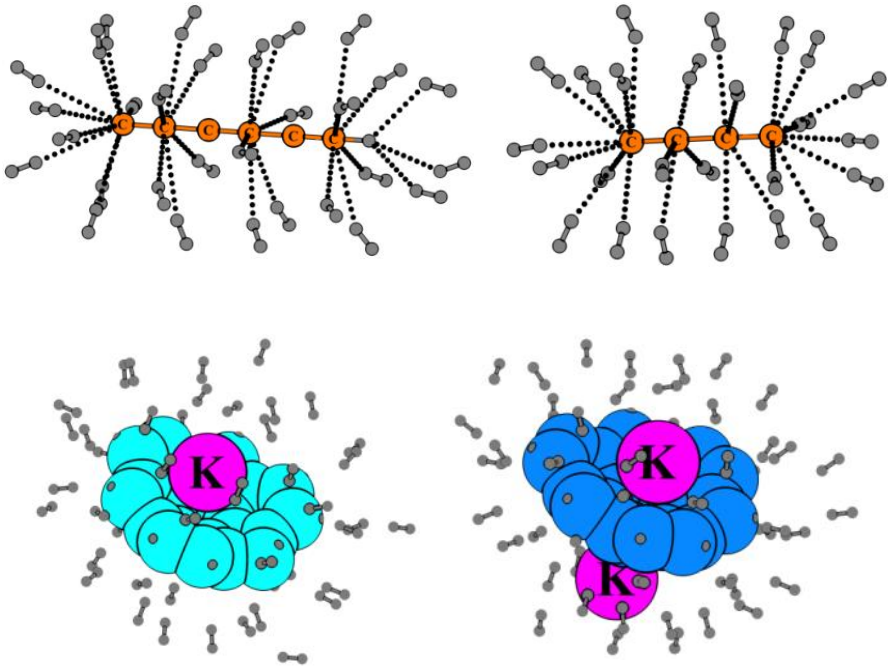

Part A: Dihydrogen Binding Affinity of One-Dimensional Anionic Carbon Chains

3.1 Abstract

Acetylene and polyyne carbon chains show negligible ability to bind even a single dihydrogen molecule. M06L/6-311++G(d,p) DFT and CCSD(T)/aug-cc-pVTZ//CCSD/aug-cc-pVDZ calculations corroborate that these carbon chains in first deprotonated anionic and second deprotonated dianionic forms display massive dihydrogen uptake capability (45.3 to 62.8 wt%). The coordinatively saturated complexes of these anions and dianions with chain lengths up to six carbons hold 20 - 32 H_2 molecules. The interaction energy (E_{int}) of saturated state of monoanions (44.5 – 50.0 kcal/mol) and dianions (79.8 – 87.4 kcal/mol) designates substantial energetic stabilization per H_2 adsorbed. Binding of H_2 to carbon chain is established by the observation of bond critical points in electron density analysis. The noncovalently bonded interconnections of adsorbed H_2 molecules indicated by H_2...H_2 bond critical points, provide additional stability to the complex keeping the system a fully noncovalently allied entity. Further, MESP is done to study the delocalization of the extra electron(s) over the entire complex.

3.2 Introduction

Carbon-based materials such as graphite,[1-3] graphene,[3-7] fullerenes,[3, 8] metal-decorated fullerenes,[9] carbon nanotubes,[3, 10-16] metal-doped carbon nanotubes,[17] metal-decorated carbon nanotubes,[18-21] carbon nanofibres[3, 16, 22, 23], *etc*. have been extensively studied experimentally and theoretically to assess the H_2 storing capacity. The binding nature of H_2 in carbon-based materials arise from van der Waals interactions on the π-electron surface of the sp^2 hybridized carbon.[21] Incorporation of metal improves the efficiency by dissociative adsorption of dihydrogen. Polyynes, the so-called oligomeric cousins of carbynes with general formula $R-(CC)_x-R$ (x >1) having alternate single and triple bonds[24, 25] could be a

fine choice for proficient dihydrogen binding purpose as the cylindrical symmetry of the π-electron allocation endows with more area open for H_2 binding. Since a polyyne is two times more π-electron rich than an sp^2 carbon system, one may speculate that the interactive behavior of the former with H_2 could be stronger than the latter.

In nature, polyynes are found to occur in biological species (plants, fungi, bacteria, marine sponges, corals, *etc.*)[26-29] and astronomical bodies.[30-34] In 1869, Glaser was successful in synthesizing polyyne for the first time by the oxidative dimerization of copper phenylacetylide which yielded diphenylbutadiene.[35] Since then several studies have been reported on the synthesis and characterization of polyynes.[25, 36-39] However, an apparent strategy towards the synthesis of polyynes up to 24 carbons using coupling reactions were developed in 1972 by Walton and coworkers.[40] In another notable study by Chalifoux and Tykwinski, a series of conjugated polyynes capped with various stabilizing end groups up to 44 carbon chain length have been synthesized and characterized.[41] Polyyne syntheses were also realized by liquid-phase laser ablation of diamond[42] and graphite,[43] femtosecond laser irradiation,[44] hydrolysis of calcium carbide in solution,[45] electrochemical preparation [46, 47] *etc*. Polyynes have captivating electronic and optical properties[48] that make them a superlative candidate for the fabrication of molecular wires,[49-51] ultra compact circuits,[52, 53] nonlinear opticals,[25, 54-56] spintronic devices[55, 57], *etc*. In fact, the interaction of a polyyne with H_2 has never been explored experimentally or theoretically, and this work exemplifies that the affinity of a polyyne to H_2 in neutral form is nearly zero. Theoretical studies on Li, Na and Ca terminated polyyne have been reported[58, 59] and proposed 8 - 10 wt% H_2 uptake for them with average binding energy 3.2 - 3.5 kcal/mol per H_2. In such systems, binding of H_2 is mainly governed by the metal center and the influence of the carbon π-system has been very small. Herein, we show that the binding affinity of a polyyne with H_2 undergoes a tremendous increase leading to massive uptake of dihydrogen if the polyyne is deprotonated to an anion or doubly deprotonated to a dianion.

3.3 Computational Details

In the present work, all calculations have been done using M06L/6-311++G(d,p) level of DFT.[60, 61] The structure and energetics of $(HC_m)^-(H_2)_n$ and $(C_m)^{2-}(H_2)_n$ complexes with n = 1 to n_{max} (maximum number of H_2 molecules in the first coordination shell) have been analyzed. All the optimized geometries have been confirmed as the energy minima by vibrational frequency analysis at standard temperature (298.15 K) and pressure (1 atm). The interaction energy, E_{int} has been calculated using the supermolecule approach with counterpoise correction to basis set superposition error (BSSE).[62] To authenticate the accuracy of the results, $E_{int/H2}$ of smaller systems of $(HC_m)^-(H_2)_n$ and $(C_m)^{2-}(H_2)_n$ with n = 1 - 3 have been calculated at CCSD(T)/aug-cc-pVTZ//CCSD/aug-cc-pVDZ level of theory. Additionally, for complexes with n = 4 - 7, $E_{int/H2}$ have been calculated at CCSD(T)/aug-cc-pVTZ//M06L/6-311++G(d,p) level. The electron delocalization in the complex is studied using MESP analysis, and noncovalent interactions are ascertained by locating bond critical points (bcp) in QTAIM analysis. All optimizations, energy calculations and MESP analysis[63, 64] have been done using Gaussian 09 package[65] and QTAIM analysis using AIMAll package.[66]

3.4 Results and Discussion

For $C_2H_2...H_2$ and $C_4H_2...H_2$ complexes, the BSSE corrected interaction energy (E_{int}) at M06L/6-311++G(d,p) level shows that their unbound state is more stable than the bound state by 0.5 and 0.2 kcal/mol, respectively while the $C_6H_2...H_2$ complex exhibits a stabilizing interaction 0.5 kcal/mol. Also in all the three cases, the interaction distance falls in the range 3.6 - 3.4 Å (Figure 3.1). These results indicate that the dihydrogen binding affinity of a one-dimensional neutral carbon chain is trivial. Herein, the CCSD(T)//CCSD results obtained for $C_2H_2...H_2$, $C_4H_2...H_2$ and $C_6H_2...H_2$ showed good concurrence with M06L/6-311++G(d,p) results. The E_{int} at CCSD(T)/aug-cc-pVTZ//CCSD/aug-cc-pVDZ level for these systems are 0.4, 0.4 and 0.5 kcal/mol respectively, signifying negligible

dihydrogen binding affinity of the carbon chains composed of *sp* hybridized carbon centers.

3.4.1 Geometry and Energetics of $(HC_m)^-(H_2)_n$ and $(C_m)^{2-}(H_2)_n$ complexes

The dihydrogen complexes of the deprotonated polyyne, $(HC_m)^-(H_2)_n$ and the doubly deprotonated polyyne $(C_m)^{2-}(H_2)_n$ complexes with m = 2, 4, and 6 have been systematically optimized by increasing one H_2 molecule in the complex in each step until the first coordination shell is saturated. H_2 binds to the carbon chain in an end-on fashion with electron transfer taking from the anion to the LUMO of H_2. The $(HC_m)^-(H_2)_n$ complexes show a well-structured arrangement of H_2 around the anion with initially added H_2 molecules binding preferably to the terminal carbon (C1) as the negative charge is more centered on this carbon.

Table 3.1 Average H-H bond distance (Å) of $(HC_m)^-(H_2)_n$ and $(C_m)^{2-}(H_2)_n$ complexes at the M06L/6-311++G(d,p) level

	$(HC_m)^-(H_2)_n$			$(C_m)^{2-}(H_2)_n$		
n	$(HC_2)^-$	$(HC_4)^-$	$(HC_6)^-$	$(C_2)^{2-}$	$(C_4)^{2-}$	$(C_6)^{2-}$
1	0.767	0.761	0.757	-	0.809	0.777
2	0.763	0.758	0.756	-	0.804	0.776
3	0.761	0.757	0.755	-	0.791	0.771
4	0.759	0.756	0.754	0.817	0.784	0.769
5	0.758	0.755	0.753	0.804	0.779	0.767
6	0.756	0.754	0.753	0.794	0.775	0.765
7	0.756	0.753	0.752	0.788	0.771	0.763
8	0.755	0.753	0.752	0.782	0.769	0.763
9	0.755	0.752	0.751	0.777	0.767	0.761
10	0.754	0.752	0.751	0.774	0.765	0.760
11	0.754	0.752	0.751	0.772	0.764	0.759
12	0.753	0.751	0.751	0.770	0.763	0.759
13	0.753	0.751	0.750	0.769	0.762	0.758
14	0.752	0.751	0.750	0.767	0.761	0.757
15	0.752	0.751	0.750	0.765	0.760	0.757

16	0.752	0.750	0.750	0.764	0.759	0.756
17	0.751	0.750	0.749	0.763	0.759	0.756
18	0.751	0.750	0.749	0.761	0.759	0.755
19	0.751	0.750	0.749	0.760	0.757	0.755
20	0.751	0.750	0.749	0.759	0.757	0.754
21	0.750	0.750	0.749	-	0.756	0.754
22	-	0.750	0.749	-	0.756	0.754
23	-	0.750	0.749	-	0.757	0.754
24	-	0.749	0.749	-	0.755	0.753
25	-	-	0.749	-	0.754	0.753
26	-	-	0.749	-	-	0.753
27	-	-	0.748	-	-	0.752
28	-	-	0.748	-	-	0.752
29	-	-	0.748	-	-	0.752
30	-	-	0.748	-	-	0.752
31	-	-	-	-	-	0.752
32	-	-	-	-	-	0.752

In the case of $(HC_2)^-$ anion, the maximum number of H_2 in the first coordination shell (n_{max}) is 21 (the $n_{max+1}{}^{th}$ H_2 does not coordinate with the anion showing a longer interaction distance from carbon). For n values up to 9, all the H_2 molecules bind with C1 as evident from the C1…H interaction distance. In $(HC_2)^-(H_2)_{15}$, nine H_2 molecules coordinate with C1 and the rest with C2. When both C1 and C2 are coordinatively saturated (n = 16), further added H_2 molecules bind with the terminal hydrogen of the anion. For the fully saturated $(HC_2)^-$ with hydrogen, $n = n_{max} = 21$, a distribution of nine H_2 binding with C1, seven H_2 with C2 and five H_2 with terminal H is observed (Figure 3.2). The H-H distance varies from 0.767 to 0.747 Å for n = 1 to n_{max} and all are longer than the free H-H distance 0.744 Å (Table 3.1). Considering the complexes of $(HC_4)^-(H_2)_n$, C3 is conspicuous by the absence of H_2 coordination (Figure 3.3).

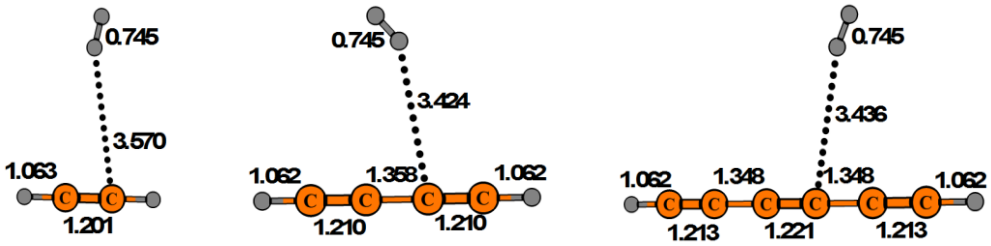

Figure 3.1 Optimized geometries of H_2 complexes of $(C_2)_mH_2$, m = 1 – 3 at the M06L/6-311++G(d,p) level. Bond distances are in Å.

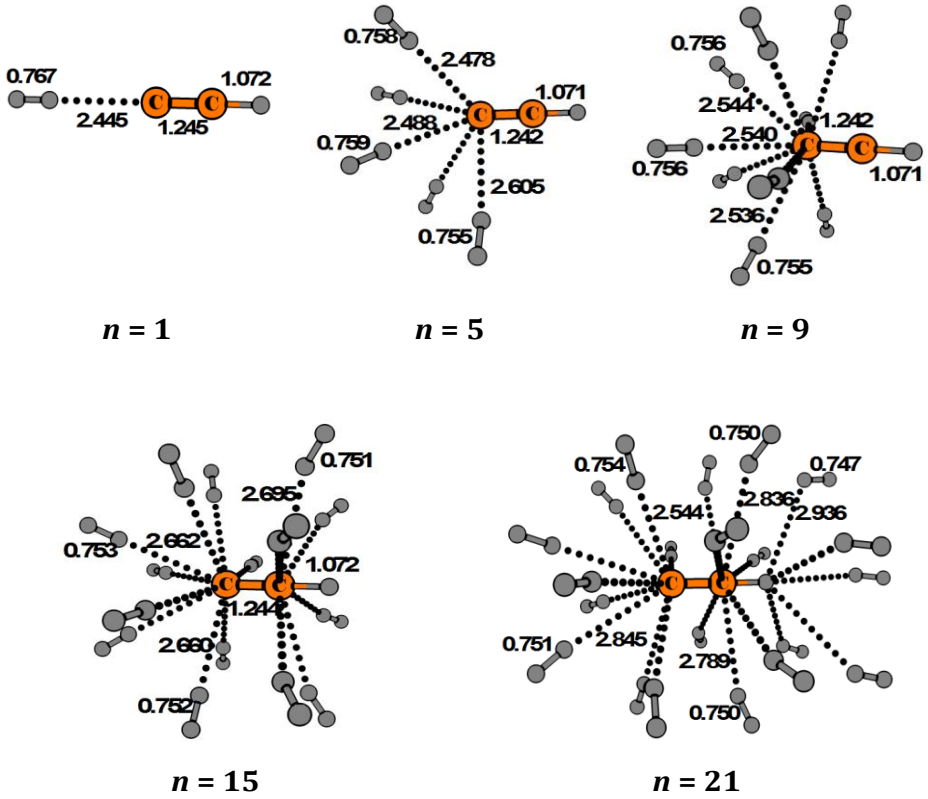

Figure 3.2 Optimized geometries of $(HC_2)^-(H_2)_n$ complexes at the M06L/6-311++G(d,p) level. Bond distances are in Å.

Steric reasons could be invoked to explain the preference of C4 than C3 for H_2 binding because the binding at C3 may lead to steric congestion for the H_2 molecules already bonded with C2. Similarly, for $(HC_6)^-(H_2)_n$ complexes, C3 and C5 are devoid of H_2 coordination (Figure 3.4). The n_{max} of $(HC_4)^-(H_2)_n$ and $(HC_6)^-(H_2)_n$ are 24 and 30 respectively with a minor drop in the average H-H distance. For all anionic complexes, average noncovalent C…H interaction

distance is in the range 2.445 – 2.830 Å which is significantly lower than the C…H distance of neutral carbon chain-H_2 complexes (Table 3.2). The bond distances of the carbon chain remain nearly unchanged in all complexes compared to the free anion. Formation of $(C_2)^{2-}(H_2)$, $(C_2)^{2-}(H_2)_2$ and $(C_2)^{2-}(H_2)_3$ are not observed due to H-H bond breaking resulting in the formation of acetylide anion and hydride anion which tend to move apart due to the Coulombic repulsive forces. Unlike anions, in all other dianionic complexes, dihydrogen binding takes place from both ends due to the symmetric distribution of the negative charge (Figures 3.5 – 3.7).

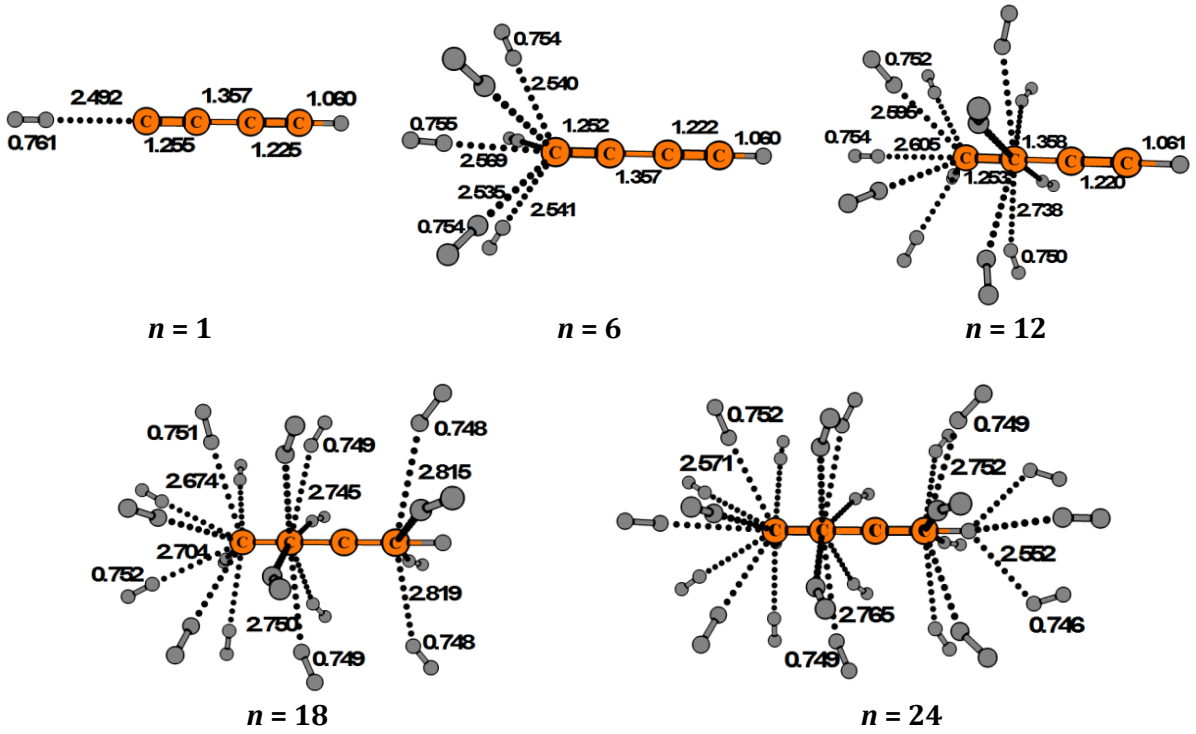

Figure 3.3 Optimized geometries of $(HC_4)^-(H_2)_n$ complexes at the M06L/6-311++G(d,p) level. Bond distances are in Å.

Table 3.2 Average C…H bond distance (Å) of $(HC_m)^-(H_2)_n$ and $(C_m)^{2-}(H_2)_n$ complexes at the M06L/6-311++G(d,p) level

	$(HC_m)^-(H_2)_n$			$(C_m)^{2-}(H_2)_n$		
n	$(HC_2)^-$	$(HC_4)^-$	$(HC_6)^-$	$(C_2)^{2-}$	$(C_4)^{2-}$	$(C_6)^{2-}$
1	2.445	2.492	2.544	-	2.095	2.316
2	2.428	2.499	2.547	-	2.125	2.332

3	2.449	2.510	2.550	-	2.181	2.350
4	2.469	2.524	2.554	2.019	2.219	2.358
5	2.506	2.534	2.562	2.089	2.252	2.369
6	2.534	2.544	2.568	2.153	2.281	2.386
7	2.557	2.589	2.602	2.227	2.323	2.415
8	2.570	2.597	2.626	2.301	2.347	2.420
9	2.599	2.612	2.653	2.318	2.368	2.436
10	2.601	2.628	2.657	2.356	2.395	2.458
11	2.606	2.624	2.697	2.382	2.412	2.465
12	2.655	2.665	2.667	2.399	2.431	2.480
13	2.627	2.691	2.711	2.404	2.446	2.507
14	2.649	2.717	2.725	2.436	2.472	2.521
15	2.651	2.696	2.736	2.455	2.484	2.534
16	2.644	2.711	2.752	2.504	2.509	2.554
17	2.659	2.712	2.768	2.533	2.524	2.564
18	2.622	2.719	2.769	2.539	2.551	2.589
19	2.666	2.726	2.772	2.605	2.557	2.603
20	2.775	2.731	2.774	2.650	2.579	2.614
21	2.755	2.742	2.777	-	2.598	2.607
22	-	2.722	2.778	-	2.620	2.628
23	-	2.701	2.775	-	2.614	2.618
24	-	2.714	2.773	-	2.656	2.648
25	-	-	2.783	-	2.673	2.654
26	-	-	2.784	-	-	2.655
27	-	-	2.829	-	-	2.681
28	-	-	2.807	-	-	2.679
29	-	-	2.799	-	-	2.689
30	-	-	2.784	-	-	2.713
31	-	-	-	-	-	2.730
32	-	-	-	-	-	2.753

The binding of H_2 around the dianions is not well ordered, and more H_2 molecules tend to bind with the end carbons. Further, for complexes with lower

values of *n* H-H bond distance is high compared to the free H_2 indicating a strong interaction between the anion and H_2.

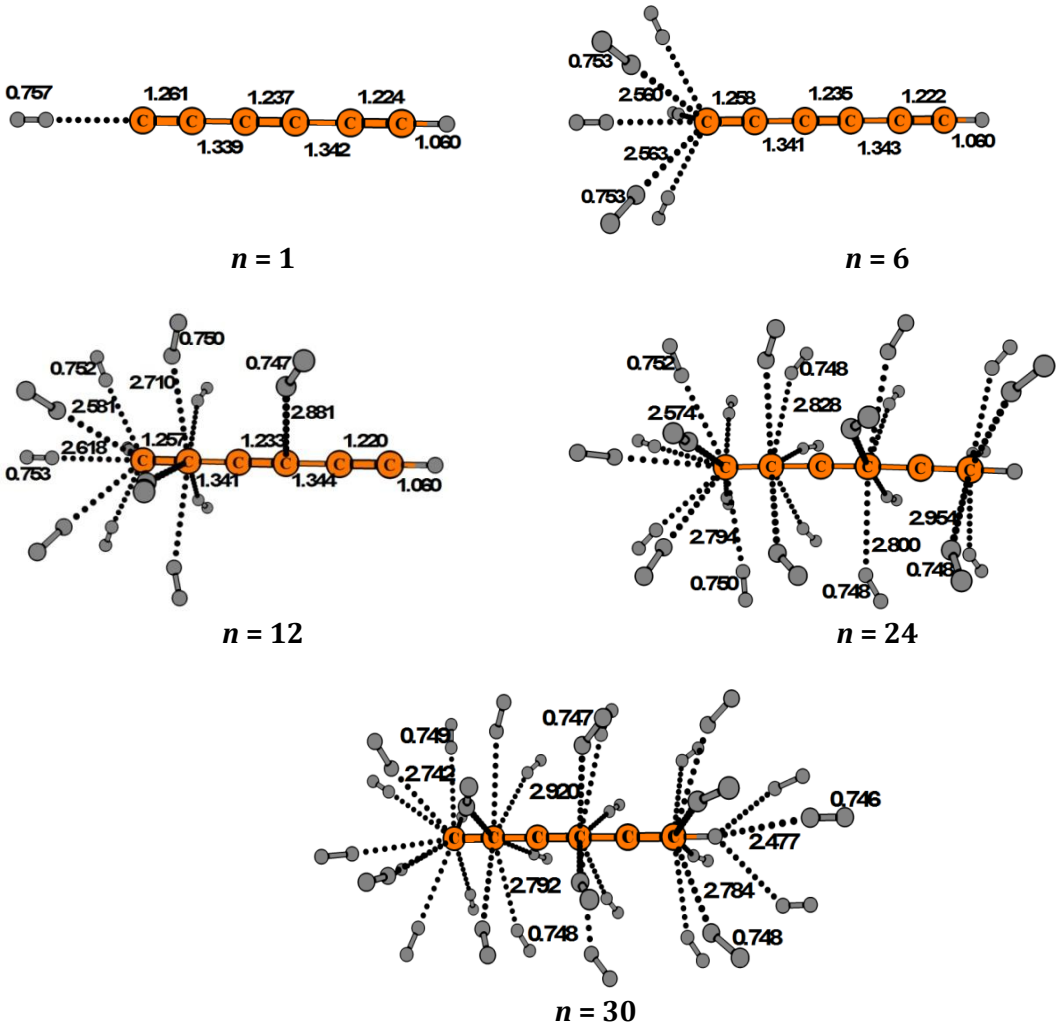

Figure 3.4 Optimized geometries of $(HC_6)^-(H_2)_n$ complexes at the M06L/6-311++G(d,p) level. Bond distances are in Å.

The average H-H bond distance and average C…H distance of all complexes are given in Tables 3.1 and 3.2. The n_{max} of $(C_2)^{2-}$, $(C_4)^{2-}$, and $(C_6)^{2-}$ are 20, 25 and 32, respectively. The E_{int} of a representative set of $(HC_m)^-(H_2)_n$ and $(C_m)^{2-}(H_2)_n$ are given in Table 3.3. In all the cases, E_{int} increases linearly with increase in the number of H_2 molecules (correlation coefficient, R is in the range 0.988 - 0.997, Figure 3.8). The linear trend slightly deviates close to the saturation point $n = n_{max}$. The slopes of the lines corresponding to $(HC_2)^-$, $(HC_4)^-$ and $(HC_6)^-$ are 2.105, 1.827 and 1.651 implying that the rate of increase in E_{int} concerning a number of

H_2 molecules follows the order $(HC_2)^-$ > $(HC_4)^-$ > $(HC_6)^-$. For $(C_2)^{2-}$, $(C_4)^{2-}$, and $(C_6)^{2-}$, the slopes are 3.999, 3.432, 2.702, respectively which suggest that the rate of increase in E_{int} is $(C_2)^{2-}$ > $(C_4)^{2-}$ > $(C_6)^{2-}$; nearly double than that of anions. For a particular value of *n*, a decline in E_{int} is observed with increase in chain length. For instance, E_{int} of $(HC_2)^-(H_2)_{20}$, $(HC_4)^-(H_2)_{20}$, and $(HC_6)^-(H_2)_{20}$ are 43.3, 39.7 and 36.1 kcal/mol, respectively. This can be attributed to the decrease in charge density per interacting carbon centers with an increase in chain length. Further, a decline in $E_{int/H2}$ in the range 3.1 – 1.7 kcal/mol for anions and 5.3 – 2.7 kcal/mol for dianions is seen as *n* increases from 1 to n_{max} (Table 3.4). E_{int} reaches to the maximum 50.0 kcal/mol for $(HC_6)^-(H_2)_{30}$ in the case of anions whereas for dianions the maximum E_{int} 87.4 kcal/mol is observed for $(C_4)^{2-}(H_2)_{25}$.

Table 3.3 BSSE corrected E_{int} (kcal/mol) of $(HC_m)^-(H_2)_n$ and $(C_m)^{2-}(H_2)_n$ complexes at the M06L/6-311++G(d,p) level

	$(HC_m)^-(H_2)_n$			$(C_m)^{2-}(H_2)_n$		
n	$(HC_2)^-$	$(HC_4)^-$	$(HC_6)^-$	$(C_2)^{2-}$	$(C_4)^{2-}$	$(C_6)^{2-}$
1	3.1	2.4	2.0	-	5.3	4.0
2	6.0	4.7	4.0	-	10.6	8.0
3	9.1	7.2	6.2	-	15.3	11.5
4	11.9	9.5	8.1	18.5	19.8	15.0
5	14.5	11.7	9.9	23.2	24.1	18.7
6	17.1	14.2	12.2	27.8	28.5	22.2
7	19.9	16.3	14.0	32.7	32.4	25.5
8	22.5	18.5	16.2	37.6	36.2	28.0
9	25.3	20.4	17.9	41.7	39.8	31.3
10	27.5	23.0	20.1	46.3	43.0	34.3
11	29.9	25.1	22.0	51.1	46.9	36.7
12	32.1	26.9	23.8	56.0	50.2	40.3
13	33.9	28.1	24.5	58.8	53.6	43.0
14	35.6	29.7	26.5	63.9	56.8	45.8
15	37.3	31.0	28.2	68.0	60.4	48.9
16	38.4	33.4	29.4	70.4	63.5	50.6

17	40.1	35.1	31.1	74.2	66.7	54.5
18	41.5	35.8	32.8	76.3	70.3	55.6
19	43.3	37.8	34.4	78.7	73.4	58.5
20	43.3	39.7	36.1	79.8	76.8	60.8
21	44.5	40.5	38.2	-	79.8	63.9
22	-	41.6	39.2	-	82.1	65.9
23	-	43.3	40.8	-	84.1	69.7
24	-	44.8	42.0	-	85.6	71.4
25	-	-	43.4	-	87.4	72.9
26	-	-	44.9	-	-	78.5
27	-	-	46.7	-	-	80.0
28	-	-	47.5	-	-	82.3
29	-	-	48.5	-	-	83.3
30	-	-	50.0	-	-	84.6
31	-	-	-	-	-	85.8
32	-	-	-	-	-	86.3

Table 3.4 BSSE corrected $E_{int/H2}$ (kcal/mol) of $(HC_m)^-(H_2)_n$ and $(C_m)^{2-}(H_2)_n$ complexes at the M06L/6-311++G(d,p) level

	$(HC_m)^-(H_2)_n$			$(C_m)^{2-}(H_2)_n$		
n	$(HC_2)^-$	$(HC_4)^-$	$(HC_6)^-$	$(C_2)^{2-}$	$(C_4)^{2-}$	$(C_6)^{2-}$
1	3.1	2.4	2.0	-	5.3	4.0
2	3.0	2.4	2.0	-	5.3	4.0
3	3.0	2.4	2.1	-	5.1	3.8
4	3.0	2.4	2.0	4.6	5.0	3.7
5	2.9	2.3	2.0	4.6	4.8	3.7
6	2.9	2.4	2.0	4.6	4.7	3.7
7	2.8	2.3	2.0	4.7	4.6	3.6
8	2.8	2.3	2.0	4.7	4.5	3.5
9	2.8	2.3	2.0	4.6	4.4	3.5
10	2.8	2.3	2.0	4.6	4.3	3.4
11	2.7	2.3	2.0	4.6	4.3	3.3
12	2.7	2.2	2.0	4.7	4.2	3.4

13	2.6	2.2	1.9	4.5	4.1	3.3
14	2.5	2.1	1.9	4.6	4.1	3.3
15	2.5	2.1	1.9	4.5	4.0	3.3
16	2.4	2.1	1.8	4.4	4.0	3.2
17	2.4	2.1	1.8	4.4	3.9	3.2
18	2.3	2.0	1.8	4.2	3.9	3.1
19	2.3	2.0	1.8	4.1	3.9	3.1
20	2.2	2.0	1.8	4.0	3.8	3.0
21	2.1	1.9	1.8	-	3.8	3.0
22	-	1.9	1.8	-	3.7	3.0
23	-	1.9	1.8	-	3.7	3.0
24	-	1.9	1.8	-	3.6	3.0
25	-	-	1.7	-	3.5	2.9
26	-	-	1.7	-	-	3.0
27	-	-	1.7	-	-	3.0
28	-	-	1.7	-	-	2.9
29	-	-	1.7	-	-	2.9
30	-	-	1.7	-	-	2.8
31	-	-	-	-	-	2.8
32	-	-	-	-	-	2.7

The free energy change per H_2 (ΔG_{H2}) for $(HC_m)^-(H_2)_n$ and $(C_m)^{2-}(H_2)_n$ complexes are summarized in Table 3.5. For anions and dianions, the range of ΔG_{H2} falls in the range 2.5 – 6.8 and 0.4 – 5.9 kcal/mol, respectively. Compared to dianions, the ΔG_{H2} value for anions is higher in magnitude as anions are characterized with lower $E_{int/H2}$ than dianions. The positive ΔG_{H2} value shows that the reaction is endergonic which can be attributed to the negative entropy factor in the associative reaction (typically 8 – 10 kcal/mol) that easily overtakes the stabilizing interaction energy at standard reaction conditions.

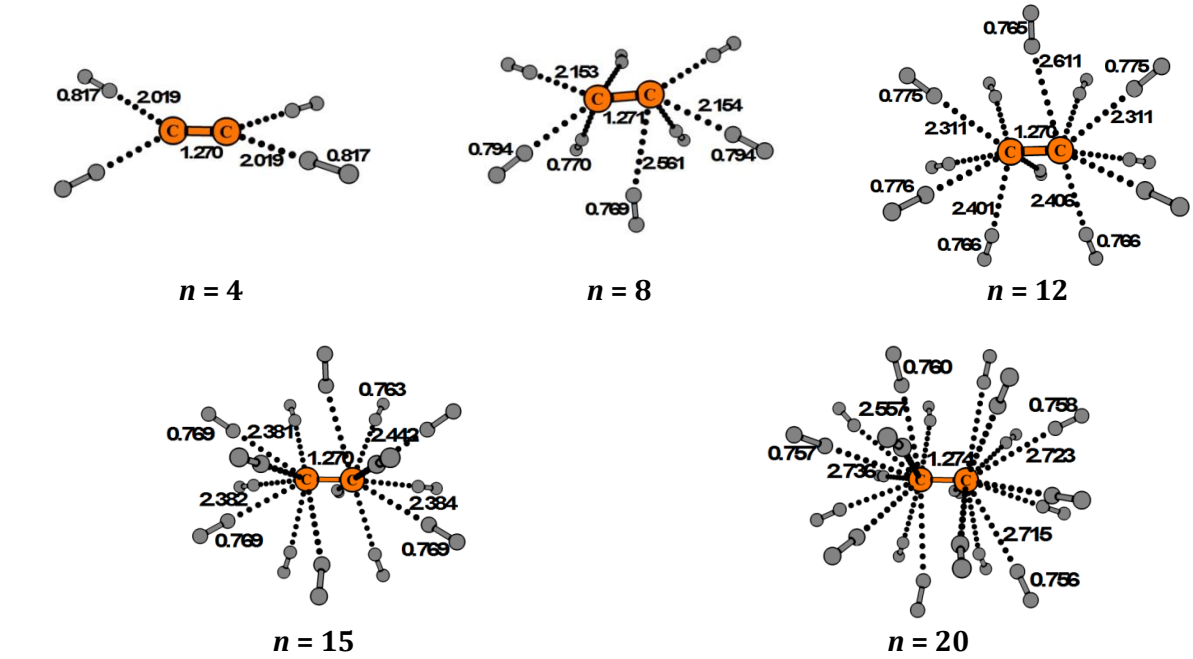

Figure 3.5 Optimized geometries of $(C_2)^{2-}(H_2)_n$ complexes at the M06L/6-311++G(d,p) level. Bond distances are in Å.

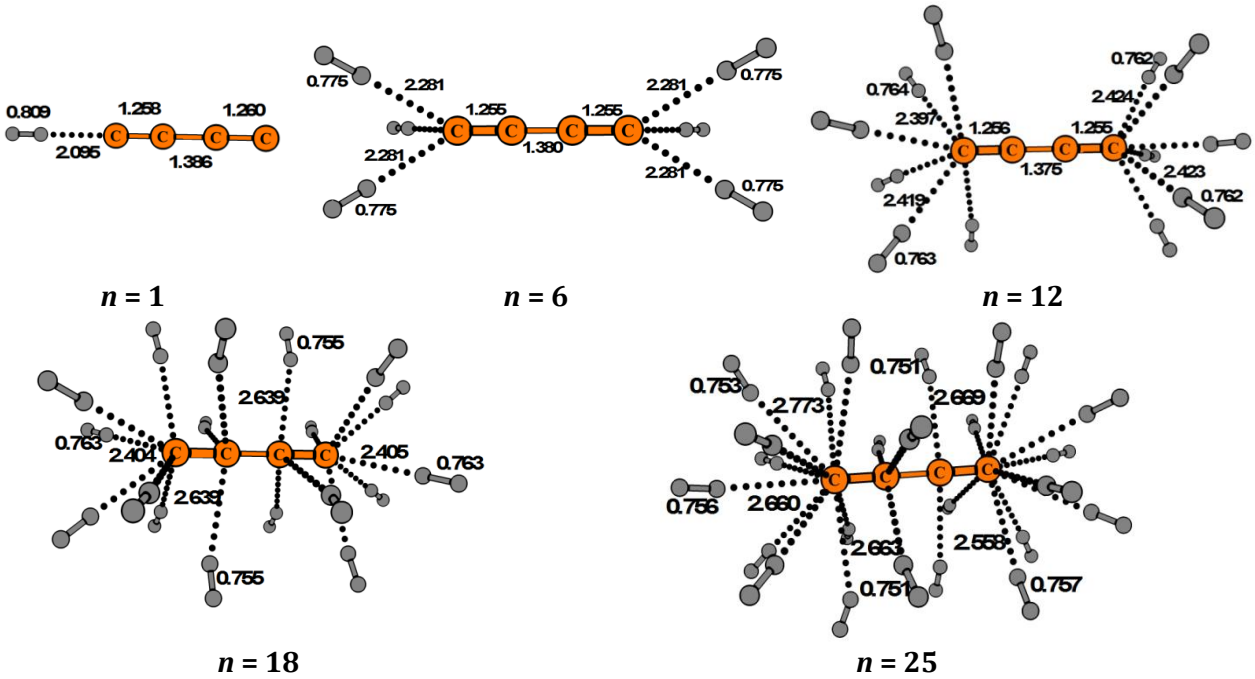

Figure 3.6 Optimized geometries of $(C_4)^{2-}(H_2)_n$ complexes at the M06L/6-311++G(d,p) level. Bond distances are in Å.

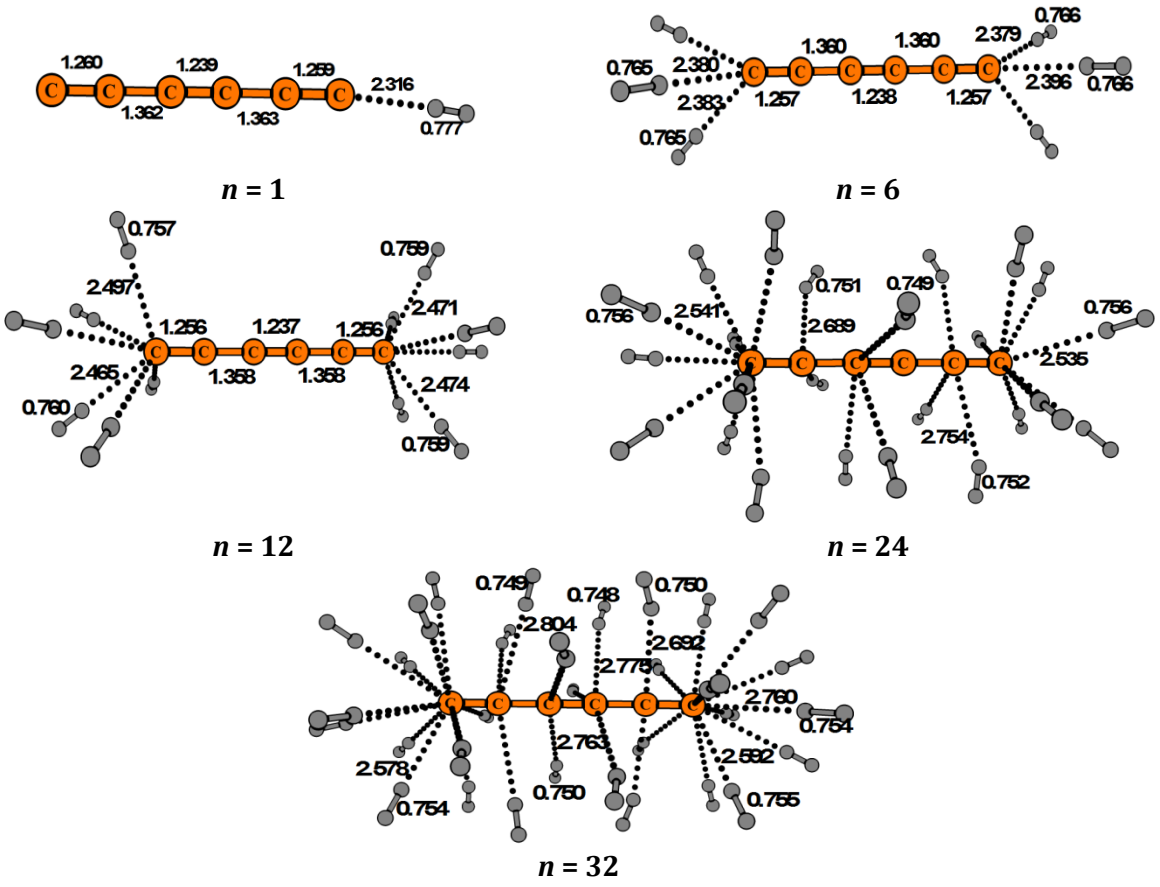

Figure 3.7 Optimized geometries of $(C_6)^{2-}(H_2)_n$ complexes at the M06L/6-311++G(d,p) level. Bond distances are in Å.

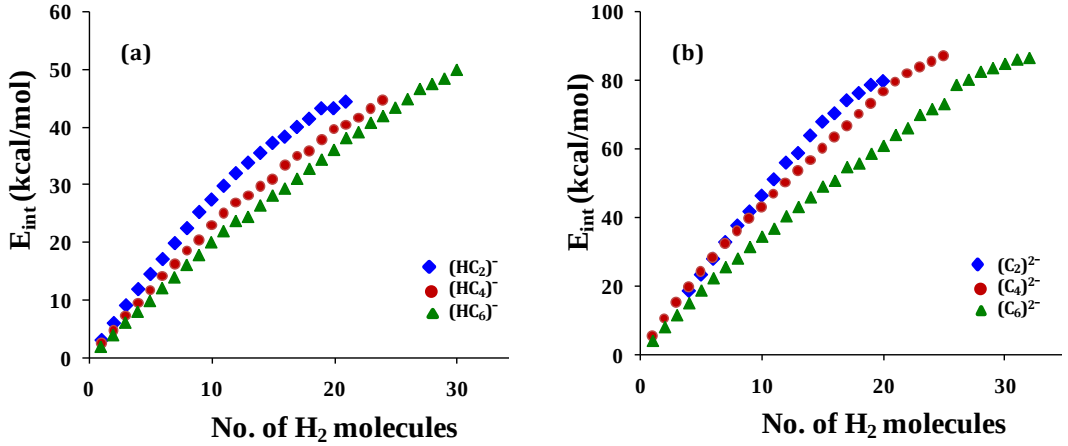

Figure 3.8 Variation of E_{int} with the number of H_2 molecules of (a) $(HC_m)^-(H_2)_n$ complexes (b) $(C_m)^{2-}(H_2)_n$ complexes.

Table 3.5 Free energy change per H_2 (kcal/mol) of $(HC_m)^-(H_2)_n$ and $(C_m)^{2-}(H_2)_n$ complexes at the M06L/6-311++G(d,p) level

	$(HC_m)^-(H_2)_n$			$(C_m)^{2-}(H_2)_n$		
n	$(HC_2)^-$	$(HC_4)^-$	$(HC_6)^-$	$(C_2)^{2-}$	$(C_4)^{2-}$	$(C_6)^{2-}$
1	6.3	5.1	4.9	-	4.9	3.5
2	3.8	2.5	4.6	-	1.4	4.1
3	4.2	3.6	4.9	-	2.1	3.8
4	4.2	3.8	4.3	0.6	2.5	3.8
5	4.8	4.1	4.4	0.4	1.7	3.8
6	5.0	4.3	4.4	1.2	1.9	4.1
7	5.1	5.4	5.6	1.2	3.0	4.5
8	4.1	4.4	5.5	1.4	3.4	4.1
9	5.1	4.5	4.7	1.5	3.5	3.6
10	4.2	4.5	5.9	1.6	3.6	4.7
11	4.5	4.6	6.1	1.8	3.8	4.6
12	5.5	4.6	6.2	1.8	4.0	3.7
13	5.6	4.6	4.8	1.9	4.0	4.9
14	5.8	4.6	6.3	2.6	4.1	3.8
15	4.4	4.7	6.3	2.1	4.2	5.0
16	4.7	4.7	6.5	2.2	4.3	4.9
17	5.9	4.9	6.3	2.5	3.4	5.0
18	4.9	4.8	6.4	2.6	3.5	5.1
19	6.3	4.9	6.5	3.8	3.4	5.2
20	6.5	4.9	6.6	3.9	4.7	5.3
21	6.6	5.0	6.6	-	3.7	5.4
22	-	5.0	6.5	-	3.7	5.3
23	-	5.1	6.7	-	3.8	4.3
24	-	5.0	6.7	-	4.9	5.6
25	-	-	6.7	-	5.2	4.4
26	-	-	6.7	-	-	5.7
27	-	-	6.7	-	-	5.7
28	-	-	6.7	-	-	5.9
29	-	-	6.7	-	-	5.8

30	-	-	6.8	-	-	5.9
31	-	-	-	-	-	4.5
32	-	-	-	-	-	4.7

3.4.2 Benchmark Study

The $E_{int/H2}$ of complexes with n = 1 – 3 at CCSD(T)/aug-pVTZ// CCSD/aug-pVDZ level for anionic and dianionic complexes are given in Table 3.6. For anionic complexes, the deviation fall in the range -0.5 – 0.1 kcal/mol. The CCSD(T) values are found to be lower than the M06L/6-311++G(d,p) level values except for the case of $(HC_6)^-H_2$ complex.

Table 3.6 $E_{int/H2}$ (kcal/mol) of $(HC_m)^-(H_2)_n$ and $(C_m)^{2-}(H_2)_n$ complexes at the CCSD(T)/aug-cc-pVTZ level

	$(HC_m)^-(H_2)_n$			$(C_m)^{2-}(H_2)_n$		
n	$(HC_2)^-$	$(HC_4)^-$	$(HC_6)^-$	$(C_2)^{2-}$	$(C_4)^{2-}$	$(C_6)^{2-}$
1	2.6	2.3	2.1	-	3.8	2.9
2	2.5	2.1	1.9	-	3.7	3.0
3	2.5	2.1	1.9	-	3.7	3.0
4	2.3	4.0	2.0	3.3	1.8	2.7
5	2.3	4.3	1.9	3.4	1.7	2.8
6	2.2	4.4	1.9	3.4	1.7	2.8
7	2.2	4.4	1.9	3.4	1.7	2.7

Dianionic complexes show a higher deviation compared to anionic complexes, falling in the range 0.8 – 1.6 kcal/mol. For $(HC_2)^-(H_2)_n$ and $(HC_6)^-(H_2)_n$ complexes with n = 4 – 7, $E_{int/H2}$ at CCSD(T)/aug-pVTZ//M06L/6-311++G(d,p) level a deviation in the range 0.0 – 0.7 kcal/mol whereas that of $(HC_6)^-(H_2)_n$ complexes deviate from M06L/6-311++G(d,p) level values by -1.6 – 2.1 kcal/mol. Comparatively a higher deviation is observed in the case of dianionic complexes with n = 4 - 7. The deviations of $(C_2)^{2-}(H_2)_n$, $(C_4)^{2-}(H_2)_n$, and $(C_6)^{2-}(H_2)_n$ dianions are in the range 1.2 – 1.3, 2.9 – 3.2, 0.9 – 1.0 kcal/mol respectively.

3.4.3 Stability of Anions and Dianions

The analysis of energetics suggests that C_2^{2-} should be the most efficient for H_2 storage. However, for any practical applications, the stability of the dianion has to be addressed. Compared to monoanion, the presence of two excess electrons in the dianion may lead to unrealistic situations, particularly for short chain lengths. However, with an increase in the carbon chain length, the delocalization of the excess electrons may lead to more realistic situations. To assess the stability of both $(HC_m)^-$ and $(C_m)^{2-}$ polyyne moieties, the first and the second deprotonation energies for m = 2 to 20 have been calculated (Table 3.7).

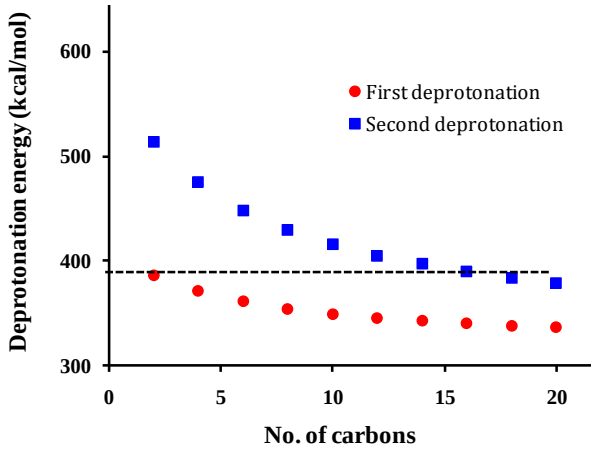

Figure 3.9 Deprotonation energy versus number of carbons.

The first and second deprotonation energies of acetylene are 385.9 and 513.1 kcal/mol, respectively which steadily decreases with increase in carbon chain length and reaches to the lowest 336.0 and 379.1 kcal/mol, respectively for H_2C_{20}. The second deprotonation energy is much higher than the first deprotonation energy in all the cases as the removal of a proton from the anion is electrostatically more energy demanding. It is clear that as the number of carbon atoms increases from 2 to 20, a decline in the second deprotonation energy 134.0 kcal/mol is observed which is much higher than the decrease observed for the first deprotonation energy (49.8 kcal/mol). As a result, the second deprotonation energy of polyyne with m = 16 (389.8 kcal/mol) becomes comparable to the first deprotonation energy of acetylene (385.8 kcal/mol), and for m = 18 and above, the former is even smaller than the latter (Figure 3.9). This means that

deprotonating an anion is possible if sufficient stabilizing energy is generated by delocalizing the extra electrons through a long carbon chain.

Table 3.7 Deprotonation energies (kcal/mol) of polyynes at the M06L/6-311++G(d,p) level

	first deprotonation	second deprotonation
m	energy	energy
2	385.9	513.1
4	370.6	475.2
6	360.9	448.1
8	354.2	429.4
10	349.2	415.7
12	345.4	405.1
14	342.4	396.7
16	339.9	389.8
18	337.8	384.0
20	336.0	379.1

3.4.4 MESP Analysis

The V_{min} values of all complexes are given in Table 3.8, and Figure 3.10 shows demonstrative cases, *viz.* $(HC_6)^-(H_2)_{30}$ and $(C_6)^{2-}(H_2)_{32}$. Dianions and their complexes show more than two-fold enhancement in the magnitude of V_{min} than monoanions and their complexes. In general, the magnitude of V_{min} decreases with increase in chain length as well as *n* values for both monoanions and dianions. This signifies more effective delocalization of the excess electron in the system with an increase in chain length and *n* value. However, when it reaches the saturation of coordination shell there is slight variation in the trend is noted. Previous studies have shown that the electron donation/withdrawal from a molecular system due to noncovalent interactions can be monitored by quantifying the changes in MESP at the interacting nuclei.[67-70] Herein, the electron donation from the carbon chain to hydrogen occurs during the binding process. As a result, MESP at the carbon nucleus (V_n) becomes less negative than the bare anion or dianion. In the case of the anion, MESP of the terminal

hydrogen also becomes less negative. The total change in MESP due to dihydrogen coordination at the nuclei of all the atoms in the carbon chain is computed for both the anions and dianions.

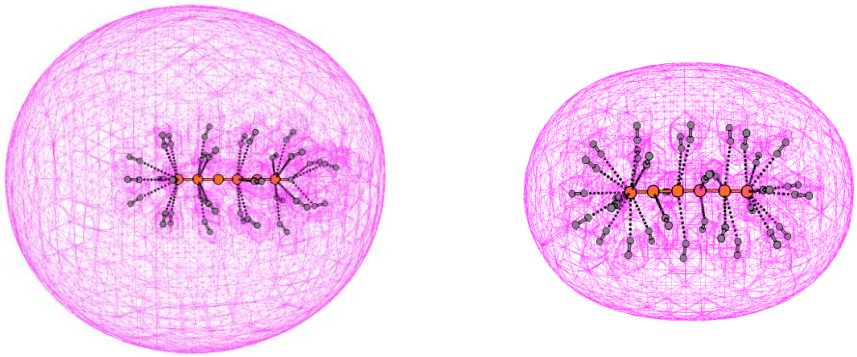

(a) $(HC_6)^-(H_2)_{30}$ **(b) $(C_6)^{2-}(H_2)_{32}$**

Figure 3.10 MESP of (a) $(HC_6)^-(H_2)_{30}$ at -30.3 kcal/mol and (b) $(C_6)^{2-}(H_2)_{32}$ at -88.9kcal/mol at the M06L/6-311++G(d,p) level.

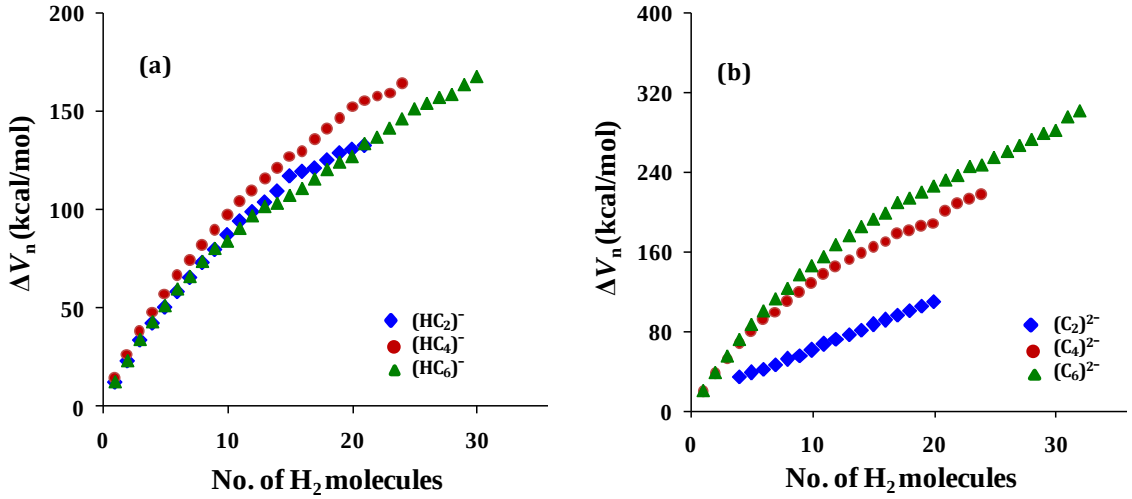

Figure 3.11 Correlation between $\Sigma\Delta V_n$ and number of H_2 molecules of $(HC_m)^-(H_2)_n$ and $(C_m)^{2-}(H_2)_n$ complexes at the M06L/6-311++G(d,p) level.

The difference in MESP at the nuclei of the H_2 bonded system and bare anion/dianion is represented as ΔV_n and the sum of ΔV_n of all atoms constituting the anion/dianion is represented as $\Sigma\Delta V_n$. The $\Sigma\Delta V_n$ values of a few representative $(HC_m)^-(H_2)_n$ and $(C_m)^{2-}(H_2)_n$ complexes are depicted in Table 3.9. The magnitude of $\Sigma\Delta V_n$ increases almost linearly with increase in the number of dihydrogens bonded with the carbon

chain (Figure 3.11). This indicates that the tendency of the anion/dianion to donate electron density to dihydrogen increases with increase in their number.

Table 3.8 V_{min} values (kcal/mol) of $(HC_m)^-(H_2)_n$ and $(C_m)^{2-}(H_2)_n$ complexes at the M06L/6-311++G(d,p) level.

	$(HC_m)^-(H_2)_n$			$(C_m)^{2-}(H_2)_n$		
n	$(HC_2)^-$	$(HC_4)^-$	$(HC_6)^-$	$(C_2)^{2-}$	$(C_4)^{2-}$	$(C_6)^{2-}$
1	-75.0	-50.7	-39.6	-	-140.9	-113.5
2	-73.9	-50.0	-39.2	-	-133.8	-110.1
3	-72.2	-48.6	-38.2	-	-129.9	-109.5
4	-70.8	-48.1	-37.9	-146.7	-127.9	-105.7
5	-67.9	-47.4	-37.6	-146.2	-125.8	-106.1
6	-66.9	-46.6	-36.7	-145.3	-122.6	-100.4
7	-65.5	-46.2	-36.3	-134.6	-113.2	-99.7
8	-64.3	-45.6	-36.2	-133.9	-113.7	-100.2
9	-64.0	-45.2	-36.0	-131.8	-111.5	-100.1
10	-60.5	-44.9	-35.8	-130.5	-111.1	-98.5
11	-59.8	-44.5	-35.1	-129.0	-110.7	-99.2
12	-55.4	-44.4	-35.1	-127.6	-109.4	-98.2
13	-54.7	-44.3	-35.1	-125.0	-109.2	-97.3
14	-54.2	-44.2	-35.0	-123.1	-108.3	-96.5
15	-55.0	-44.6	-35.0	-122.7	-107.4	-96.3
16	-45.8	-44.6	-35.1	-122.2	-107.0	-96.3
17	-44.9	-44.7	-34.6	-121.5	-106.8	-96.0
18	-44.7	-45.0	-34.8	-117.9	-108.3	-96.3
19	-43.7	-44.4	-34.8	-117.2	-107.1	-96.3
20	-40.3	-44.9	-34.8	-116.9	-105.4	-97.2
21	-40.2	-37.1	-34.6	-	-104.8	-95.4
22	-	-36.7	-35.5	-	-104.2	-93.3
23	-	-36.6	-35.7	-	-103.2	-94.6
24	-	-36.4	-36.1	-	-101.0	-93.8
25	-	-	-35.7	-	-100.2	-93.6
26	-	-	-35.7	-	-	-93.6
27	-	-	-36.1	-	-	-93.9

28	-	-	-30.6	-	-	-92.3
29	-	-	-29.2	-	-	-90.6
30	-	-	-30.3	-	-	-90.6
31	-	-	-	-	-	-91.5
32	-	-	-	-	-	-92.1

Further, with an increase in the number of hydrogens, no drastic reduction in the binding energy per hydrogen is observed. This means that the excess electrons in the anion/dianion are delocalized over the entire complex, and they function like an efficient glue for all the hydrogen to bind with the carbon chain. A strong linear correlation between E_{int} and $\Sigma\Delta V_n$ exists for all the $(HC_m)^-(H_2)_n$ and $(C_m)^{2-}(H_2)_n$ complexes which indicate that delocalization effect of the electron density is directly proportional to the total energetic stabilization of the complex (Figure 3.12). Among the anions, HC_2^- shows the highest affinity to dihydrogen while other two anions show similar affinity up to energetic stabilization (E_{int}) ~23.0 kcal/mol and subsequently, the ability of HC_6^- becomes higher than HC_4^- due to its ability to accommodate more hydrogens. For C_2^{2-}, C_4^{2-}, and C_6^{2-} dianaions, the slope of the respective correlation plots, *viz*. -0.823, -0.429, -0.318 indicate that their dihydrogen affinity is in the order $C_2^{2-} >> C_4^{2-} > C_6^{2-}$.

Table 3.9 $\Sigma\Delta V_n$ values (kcal/mol) of $(HC_m)^-(H_2)_n$ and $(C_m)^{2-}(H_2)_n$ complexes at the M06L/6-311++G(d,p) level

	$(HC_m)^-(H_2)_n$			$(C_m)^{2-}(H_2)_n$		
n	$(HC_2)^-$	$(HC_4)^-$	$(HC_6)^-$	$(C_2)^{2-}$	$(C_4)^{2-}$	$(C_6)^{2-}$
1	12.3	14.4	12.7	-	19.3	20.1
2	23.1	26.5	23.4	-	37.4	39.0
3	33.7	38.1	34.2	-	52.6	55.8
4	42.3	48.0	43.2	34.4	66.9	72.2
5	50.4	57.1	51.4	38.2	79.5	87.0
6	58.3	66.6	59.9	41.8	91.2	101.4
7	65.5	74.2	66.2	46.7	99.5	112.8
8	73.1	82.2	73.9	51.6	109.5	123.7
9	79.7	89.8	80.5	55.8	118.6	136.7

10	87.2	97.1	84.2	60.7	127.3	145.9
11	94.2	104.4	90.7	66.8	136.7	154.7
12	98.9	109.7	97.1	72.4	144.1	167.6
13	103.8	115.6	101.8	76.9	152.5	175.9
14	109.4	121.3	103.5	81.1	158.2	185.5
15	117.1	127.0	107.5	86.8	163.7	193.0
16	119.4	129.7	111.0	91.2	170.5	199.5
17	121.1	135.5	115.8	96.5	177.6	209.0
18	125.2	141.2	120.6	101.1	180.5	213.8
19	128.8	146.5	124.4	105.4	185.3	220.3
20	130.6	152.1	127.2	109.7	188.9	225.6
21	132.6	155.3	133.8	-	200.6	232.5
22	-	157.6	137.1	-	207.7	237.4
23	-	159.2	141.7	-	212.7	246.0
24	-	164.2	146.4	-	216.6	246.8
25	-	-	151.5	-	218.8	254.3
26	-	-	154.3	-	-	260.6
27	-	-	157.3	-	-	266.2
28	-	-	158.8	-	-	273.3
29	-	-	163.8	-	-	279.4
30	-	-	167.9	-	-	282.1
31	-	-	-	-	-	295.1
32	-	-	-	-	-	301.3

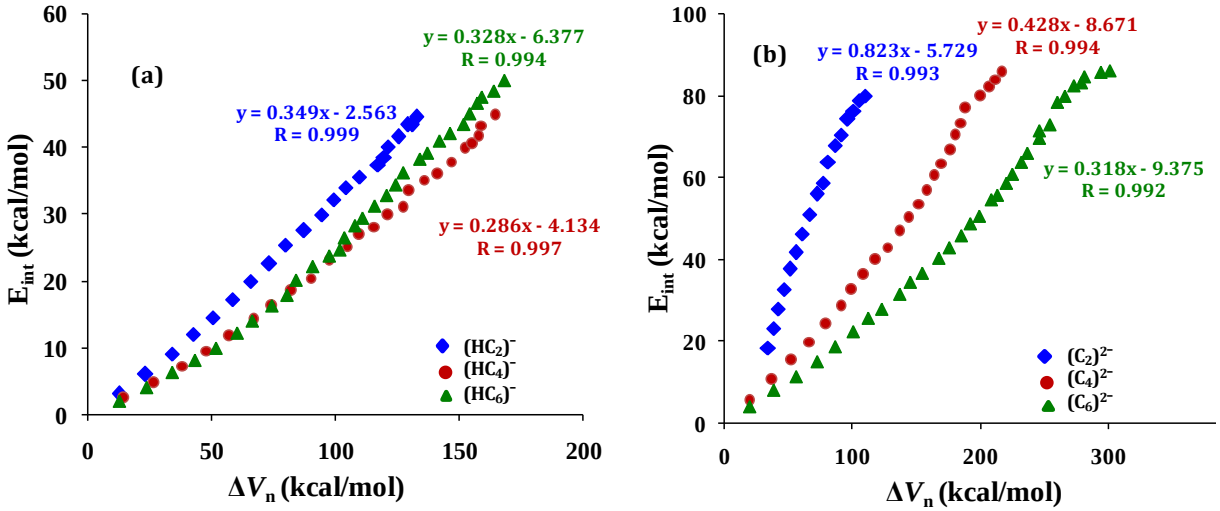

Figure 3.12 Correlation between E_{int} and $\Sigma\Delta V_n$ of $(HC_m)^-(H_2)_n$ and $(C_m)^{2-}(H_2)_n$ complexes at the M06L/6-311++G(d,p) level.

3.4.5 QTAIM Analysis

The dihydrogen binding to the carbon chain can be attributed to the formation of attractive C…H noncovalent interactions. In all the anion and dianion dihydrogen complexes, 'm' a number of C...H bond critical points (BCP) have been observed indicating that all the H_2 participate in noncovalent bonding interaction with the carbon chain. Figure 3.13 depicts the AIM molecular graph of two representative cases, *viz*. $(HC_6)^-(H_2)_{30}$ and $(C_6)^{2-}(H_2)_{32}$. The C...H BCPs are represented using red dots. Apart from these BCPs, the complexes with m values generally higher than 8 in anions and 15 in dianions show BCPs between adjacent adsorbed H_2 molecules (blue dots). This kind of secondary H...H interactions can be considered as a unique feature of the complex and also suggest that the adsorbed H_2 are not repelled from each other. A notable controversy that the existence of BCP alone cannot prove that the atoms are not repelled has been reported by Poater *et al*. They showed that the repelling ortho-hydrogen atoms in biphenyl show a bond path between them.[71] The H...H bonding discussed by Poater *et al*. is intramolecular whereas the present study deals with intermolecular H...H interactions. If repulsive forces were operating, the $E_{int/H2}$ would have decreased significantly with increase in the number of H_2 molecules. Formation of a large number of H...H BCPs does contribute to the overall stability of the complex.

Table 3.10 Average ρ_{bcp} (au) of $(HC_m)^-(H_2)_n$ and $(C_m)^{2-}(H_2)_n$ complexes at the M06L/6-311++G(d,p) level

	$(HC_m)^-(H_2)_n$			$(C_m)^{2-}(H_2)_n$		
n	$(HC_2)^-$	$(HC_4)^-$	$(HC_6)^-$	$(C_2)^{2-}$	$(C_4)^{2-}$	$(C_6)^{2-}$
1	0.0155	0.0130	0.0116	-	0.0290	0.0185
2	0.0144	0.0125	0.0113	-	0.0272	0.0180
3	0.0137	0.0121	0.0110	-	0.0239	0.0169
4	0.0128	0.0115	0.0107	0.0329	0.0219	0.0164
5	0.0118	0.0109	0.0102	0.0284	0.0203	0.0160
6	0.0111	0.0106	0.0101	0.0247	0.0191	0.0155
7	0.0106	0.0101	0.0092	0.0221	0.0174	0.0144
8	0.0102	0.0097	0.0089	0.0195	0.0165	0.0140
9	0.0099	0.0094	0.0088	0.0177	0.0157	0.0136
10	0.0097	0.0091	0.0083	0.0166	0.0148	0.0130
11	0.0098	0.0091	0.0083	0.0161	0.0143	0.0126
12	0.0092	0.0085	0.0079	0.0155	0.0137	0.0116
13	0.0090	0.0083	0.0078	0.0153	0.0133	0.0118
14	0.0086	0.0081	0.0073	0.0146	0.0127	0.0115
15	0.0085	0.0080	0.0069	0.0138	0.0123	0.0112
16	0.0082	0.0075	0.0067	0.0128	0.0119	0.0108
17	0.0077	0.0074	0.0066	0.0122	0.0116	0.0107
18	0.0078	0.0074	0.0065	0.0115	0.0116	0.0102
19	0.0071	0.0073	0.0064	0.0107	0.0109	0.0100
20	0.0069	0.0072	0.0062	0.0099	0.0106	0.0098
21	0.0064	0.0070	0.0063	-	0.0104	0.0097
22	-	0.0069	0.0062	-	0.0101	0.0095
23	-	0.0069	0.0062	-	0.0096	0.0095
24	-	0.0067	0.0062	-	0.0092	0.0090
25	-	-	0.0061	-	-	0.0089
26	-	-	0.0061	-	-	0.0089
27	-	-	0.0060	-	-	0.0086
28	-	-	0.0060	-	-	0.0084
29	-	-	0.0059	-	-	0.0082

30	-	-	0.0059	-	-	0.0079
31	-	-	-	-	-	0.0078
32	-	-	-	-	-	0.0075

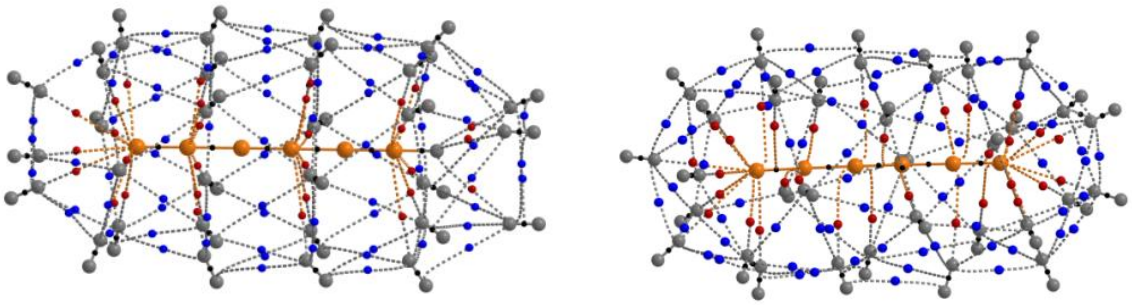

(a) $(HC_6)^-(H_2)_{30}$ **(b) $(C_6)^{2-}(H_2)_{32}$**

Figure 3.13 QTAIM features of (a) $(HC_6)^-(H_2)_{30}$ and (b) $(C_6)^{2-}(H_2)_{32}$ complexes at the M06L/6-311++G(d,p) level.

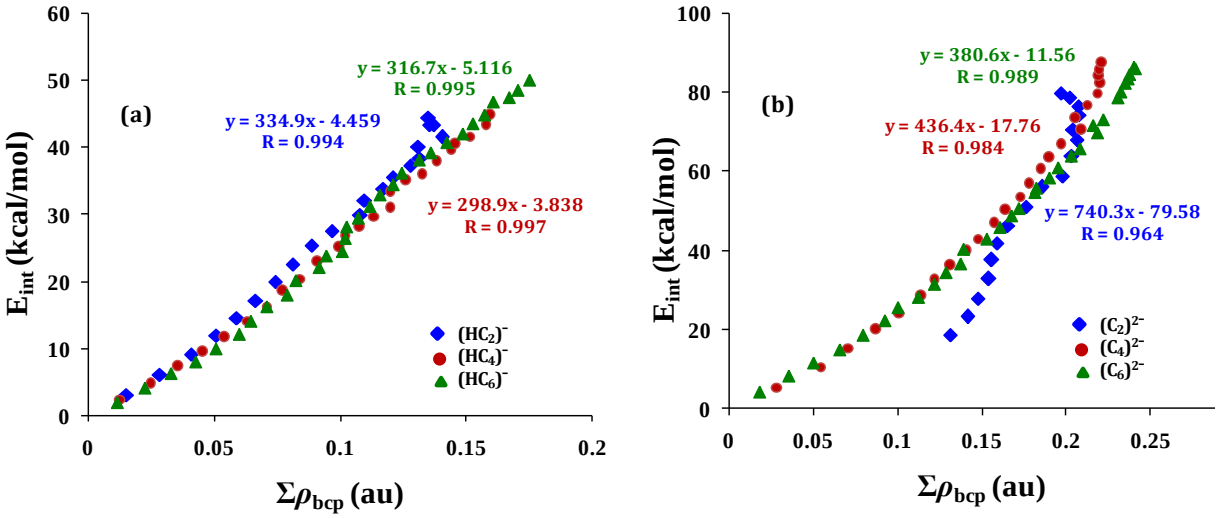

Figure 3.14 Correlation between E_{int} and $\Sigma\rho_{bcp}$ of (a) $(HC_m)^-(H_2)_n$ and (b) $(C_m)^{2-}(H_2)_n$ complexes at the M06L/6-311++G(d,p) level.

The average ρ_{bcp} for such interactions in anionic and dianionic systems are in the range 0.0155 – 0.0059 au and 0.0329 – 0.0075 au respectively (Table 3.10). The Laplacian of the electron density $\nabla^2\rho_{bcp}$ falls in the range 0.0352 – 0.0115 au for anions and 0.0534 – 0.0142 au for dianions. The small ρ_{bcp} and positive $\nabla^2\rho_{bcp}$ indicate the noncovalent nature of the C…H interactions.[72, 73] The ρ_{bcp} decreases with increase in the value of *n* indicating a decrease in bond strength when more

H_2 molecules bind to the anion. The sum of electron density at BCP ($\Sigma\rho_{bcp}$) strongly correlates with E_{int} (Figure 3.14) for both anions and dianions (R = 0.997 – 0.967). For $(HC_2)^-$, $(HC_4)^-$, and $(HC_6)^-$ anions, all the data points fall roughly on the same line. In dianions, $(C_4)^{2-}$ and $(C_6)^{2-}$ show almost similar correlation trend whereas the correlation plot of $(C_2)^{2-}$ deviates to a higher slope. Compared to C…H interactions, ρ_{bcp} of H…H lies in a smaller range 0.0013 – 0.0070 au These H…H dihydrogen interactions connect every H_2 molecules in the system to one or more nearby H_2 molecules leading to the formation of a large network of the noncovalently connected system of hydrogen molecules on a carbon chain. The collective strength of all such interactions accounts for the E_{int}. In other words, significant positive cooperativity effect operates between the adsorbed H_2 molecules, and that facilitates the intake of a large number of H_2 molecules by the anion/dianion carbon chain. This phenomenon also accounts for the minor reduction in $E_{int/H2}$ with an increase in *n* values.

The dihydrogen binding capacity of acetylene is negligible whereas that of $(HC_m)^-$ and $(C_m)^{2-}$ ranges from 45.3 to 62.8 wt% (Table 3.11) indicating the substantial H_2 uptake ability of these systems.

Table 3.11 H_2 affinity of anionic carbon chains

Anion	n_{max}	Weight percent of H_2 (wt%)
HC_2^-	21	62.8
HC_4^-	24	49.7
HC_6^-	30	45.3
C_2^{2-}	20	62.7
C_4^{2-}	25	50.7
C_6^{2-}	32	46.9

3.5 Conclusions

The dihydrogen complexes of anionic and dianionic carbon chains explored in the present study showed that these charged chains have a massive ability to bind with dihydrogen. It is clear that the extra electron in the system drastically

increases the non-covalent binding efficiency of the carbon chain to several fold compared to the neutral species. The extra electron is cylindrically delocalized in the carbon chain and promotes the binding of H_2 from all around the chain. The complex can be well described as a 'noncovalently hydrogen-connected carbon' whereas, in a normal hydrocarbon, atomic hydrogens are covalently connected to carbon centers. Thus, a neutral C_2 chain in acetylene can store only two hydrogen atoms whereas the same in the anion can store up to 21 H_2 molecules in the first coordination shell. This is remarkable indicating that one-dimensional anionic chain composed of sp carbon atoms is highly promising for H_2 storage purpose. Dianions though show more promising non-covalent binding, realistic systems could be envisaged only at long chain lengths which possess synthetic challenges. Even for anionic systems, the challenge is to make them mostly non-coordinating to a properly designed counter cation so that the anion, as well as the cation, can be easily 'solvated in dihydrogen.' If a strong bond is formed, the entire system is neutralized, and the H_2 binding affinity will decrease drastically. This has been proved by considering the H-terminated neutral form of the carbon chains for H_2 binding. The search for such weakly coordinating cationic systems for the practical applications is underway. We feel that the fundamentals explained in this work on 'non-covalently hydrogen-connected carbon' could trigger intense research in pursuit of an ideal material for hydrogen storage.

Part B: Dihydrogen Binding Affinity of Sumanene: An Organic π-Bowl

3.6 Abstract

Density functional theory calculations at M06L/6–311++G(d,p) level show that sumanene (Su), a polycyclic aromatic π-bowl and its anionic forms possess high dihydrogen binding affinity. The dihydrogen rich systems such as $Su(H_2)_{40}$, $Su^{-}(H_2)_{40}$, *and* $Su^{2-}(H_2)_{40}$ *show interaction energy (*E_{int}*) 51.7, 63.0 and 87.6 kcal/mol, respectively. The ion-pair complexes of anionic, dianionic and trianionic sumanenes with* K^+ *also have a significant* H_2 *binding capacity with* E_{int} *61.6 kcal/mol for* $Su^{-}K^{+}(H_2)_{47}$, *77.1 kcal/mol for* $Su^{2-}(K^{+})_2(H_2)_{51}$ *and 132.6 kcal/mol for* $Su^{3-}(K^{+})_3(H_2)_{51}$. *The charge delocalization in the complex increases substantially with increase in the number of* H_2 *adsorbed which parallels with a declining trend in the magnitude of molecular electrostatic potential (MESP) minimum (*V_{min}*) for Su,* Su^{-}, Su^{2-}, $Su^{-}K^{+}$, $Su^{2-}(K^{+})_2$, *and* $Su^{3-}(K^{+})_3$. *Also, using quantum theory of atoms in molecules (QTAIM) analysis, sumanene...*H_2 *noncovalent interactions and secondary dihydrogen interactions within the complex are established by locating bond critical points (bcp). The structured network of noncovalent bonds in the complex accounts for the stability of the complex. Further, by replacing* K^+ *with lighter metals such as* Li^+ *or* Na^+, *66 – 74 % increase in* E_{int} *is observed for anion-*M^+ *and dianion-*$(M^+)_2$ *ion-pairs. Our results prove that sumanene systems possess significant dihydrogen binding affinity which can be employed in developing efficient hydrogen storage systems.*

3.7 Introduction

Carbon-based nanostructures which store hydrogen *via* physisorption have gained attention as storage materials due to their light weight, high surface area with porous structure, adsorption, and desorption at ambient temperature and pressure *etc*.[74-81] Ever since its discovery,[82] fullerene and related compounds have attained much interest in the field of materials chemistry research owing to unique physical and chemical properties.[83-87] The bowl-shaped fullerene

fragments known as bucky bowls are very attractive due to various applications in synthetic organic chemistry as well as electronic device fabrications.[85-89] These π-conjugated organic bowls are unique ligands with two curved binding surfaces (convex and concave) and edge and rim carbon atoms capped by hydrogen atoms possess multisite coordination potential.[90] The advantage of these bucky bowls over fullerene is that they posses concave π-carbon surface readily available for bonding.[91-93] The interactions of these π-bowls with metals,[92, 93] and fullerenes[91] have been recognized.

Sumanene ($C_{21}H_{12,}$ *Su*), a polycyclic aromatic hydrocarbon consisting of three benzene and three cyclopentadiene rings alternatively fused together forming a central six-membered ring is a fine case of such π- bowls.[94] Prior to the synthesis of sumanene, an *ab initio* and pure and hybrid density functional theoretical study have been reported by Priyakumar and Sastry in 2001.[95] They have explained in detail the structure, inversion barrier, suitability of various theoretical procedures, vibrational spectra, population and charge analyses along with the calculation of strain energy using isodesmic equations. The stability, bowl to bowl inversion, NMR parameters, *etc.* of boron substituted isomers of sumanene have also been calculated.[96] Several theoretical studies on this bucky bowl have been reported.[93, 97-101] Molecular mechanics and MNDO studies have been done on sumanene and similar compounds in proposing a synthetic strategy towards fullerene.[102]

Following the successful synthesis of sumanene by Sakurai *et al.,*[103] several groups reported its synthesis and characterization.[88, 104-106] The generation of anionic sumanene, functionalization of benzylic positions of sumanene and asymmetric synthesis of chiral sumanene have been reported.[94, 107-112] The synthesis, characterization and structural features of a variety of heterasumanenes with various hetero atom functionalities have been known to date.[113-123] The enhanced optical and electronic properties of these wide range sumanene derivatives make them attractive promising candidates for the manufacture of electronics and optical materials. [115, 118-123] Facile synthesis of highly strained sumanenes[124] and bi-directional extension π conjugation in

sumanenes have been achieved.[125] The concave-bound cyclopentadienyl-Fe complex of sumanene has been synthesized and the redox properties have been studied by electrochemical methods.[90, 126-128] The double concave encapsulation of a cesium ion by two bowl-shaped sumanenyl anions was studied crystallographically and theoretically by Spisak *et al.* very recently.[129]

Studies recommend that sumanene has viable efficiency to adsorb molecules such as CO, CO_2, NH_3, CH_4, and C_2H_2 comparable to other carbon-based structures such as graphene layers, carbon nanotubes and C_{60} fullerene.[130, 131] The bowl shaped geometry enhances the adsorption of molecules in the concave surface. In a recent theoretical study on complexes of curved aromatic systems and cations, it was established that for cation-π interactions a balanced combination of electrostatic, induction and dispersion contribute to the stability of complexes.[132] The cycloaddition reaction of nitrous oxide on sumanene nanostructure have been theoretically analyzed.[133] Armakovic *et al.* have also been investigated sumanene for its ability to bind H_2 showing that the electron density due to the π-conjugated system enhances the adsorption of H_2 molecules at the six member ring sites.[134] According to this study, when one H_2 is adsorbed the concave surface showed higher binding energy compared to the convex side for the adsorption of one H_2 molecule. The physisorption mechanism of H_2 binding by nitrogen and boron substituted suamanenes was substantiated by fragment analysis.[74] The unsubstituted sumanene exhibited interaction energy of 3.25 kcal/mol whereas nitrogen based systems showed improved adsorption abilities. In contrast, boron based systems showed a decline in the H_2 uptake. Sumanene derivatives with nitrogen and boron substitutions showed 2.24 and 2.32 wt% of H_2 respectively with at least three H_2 molecules binding from the concave face of sumanene. Reisi-Vanani and Mehrdoust reported the interaction of various boron disubstituted sumanene isomers with H_2 using MP2/6-311++G(d,p)//B3LYP/6-31+G(d) level of theory.[135] According to them, the isomers with borons at the rim-rim position exhibited higher affinity towards dihydrogen and those with borons at the hub-hub positions were proven to be the worst of all isomers. Even though there are several reports on H_2 binding of neutral and substituted

sumanene, attempts to find the maximum number of H_2 that can be accommodate in the first coordination shell of this π-bowl and dihydrogen binding ability of anionic sumanene have not been reported to date.

Sumanene can be converted to an anionic π-bowl by the elimination of hydrogens of the five-membered ring as H^+. The synthesis of sumanenyl anions stabilized by K^+ as counter cations have been realized by Spisak *et al.* very recently along with supporting theoretical studies.[136] Anionic systems have been studied for their ability to bind dihydrogen.[137-140] Studies on some anions and polyatomic anions reported from our group suggest that these systems show substantially high interaction energies in the range 37.0 – 50.9 kcal/mol when saturated with dihydrogen. [141, 142] In yet another study, we proposed anionic and dianionc carbon chains as one-dimensional material for dihydrogen binding.[143] Neutral polyyne chains showed a negligible affinity towards H_2 whereas their deprotonated anionic and dianionic forms could bind with 20 – 32 H_2 molecules across the entire chain length with significant energetic stabilization. The E_{int} of the saturated state of the monoanions and dianions were in the range 44.5 – 50.0 and 79.8 – 87.4 kcal/mol, respectively. Extending these studies on dihydrogen binding affinity of simple monoatomic anions, polyatomic anions and one-dimensional carbon chains to systems with higher dimensions, we consider the neutral, anionic and dianionic forms of sumanene. The interaction of these systems with a large number of H_2 molecules have been investigated in a systematic and comprehensive manner in the present work. The H_2 binding ability of anionic and dianionic sumanene in the presence of a counter cations K^+, Na^+ and Li^+ are also studied.

3.8 Computational Details

Su-H_2 complexes with 1 to 20 H_2 molecules have been optimized using M06L/6-311++G(d,p) level as implemented in Gaussian 09 suite of programs.[65] For larger clusters, optimization has been done at M06L/6-31G(d,p) level and single point energy calculations have been done at M06L/6-311++G(d,p) level. The optimized

geometries have been confirmed as the energy minima structures by vibrational frequency analysis. The E_{int} has been calculated using the supermolecule approach and the correction to BSSE has been calculated using counterpoise method introduced by Boys and Bernardi.[62] Further, to substantiate the accuracy of the results, E_{int} of neutral and anionic forms of sumanene-H_2 complexes has been calculated using a benchmark set of DFT/6-311++G(d,p) methods along with Grimme's dispersion correction.[144, 145] The selected DFT methods are M06L-D3, M062X, M062X-D3, wB97XD, B3LYP-D3, B97D, B97-D3, BP86-D3. Further, to gauge the effect of basis set, E_{int} has been calculated at M06L, wB97XD and B97D levels using aug-cc-pVDZ basis set. The complexes optimized using the benchmark methods have been confirmed as energy minima by frequency analysis and E_{int} has been corrected for BSSE. The charge delocalization in sumanene systems, ion–pair complexes and dihydrogen complexes have been studied using MESP topographical analysis.[63, 64] Bader's QTAIM as implemented in AIMAll software has been used to study the noncovalent interactions in sumanene-H_2 complexes.[66, 72]

3.9 Results and Discussion

3.9.1 Geometry and Energetics of Dihydrogen Complexes

Dihydrogen interacts with the concave and convex surfaces of neutral (*Su*), anionic (Su^-), and dianionic (Su^{2-}), sumanene. The side-on interaction of H_2 with the concave surface is the most stable in every case followed by the end-on interaction with the concave surface (Figure 3.15). Both side-on and end-on interaction of H_2 with the convex surface of *Su*, Su^- and Su^{2-} is significantly less stable than the rest (Table 3.12). The highest interaction energy (E_{int}) observed for *Su*(H_2), Su^-(H_2) and Su^{2-}(H_2) are 3.7, 4.2 and 4.4 kcal/mol, respectively. The benchmark study on the side-on concave configurations using twelve different DFT methods (Table 3.13) establishes that the M06L E_{int} values are reliable. The bowl-shaped geometry of *Su* may be invoked to explain the significant difference in E_{int} for the concave and convex surfaces. Previous studies on interaction of

various molecules with *Su* also reported a higher E_{int} for adsorbate on the concave surface.[74, 131, 134] In fact, a 'bowl effect' is evident in sumanene which promotes more number of interactions between adsorbate and the concave surface. To confirm the bowl effect, E_{int} of planar aromatic hydrocarbons such as triphenylene, pyrene, and coronene (Figure 3.16) is calculated, and their respective values 1.3, 1.3 and 1.4 kcal/mol indicates that bowl shape is beneficial for improving the H_2 binding affinity.

Table 3.12 BSSE corrected E_{int} (kcal/mol) of complexes with different orientations of H_2 at the M06L/6−311++G(d,p) level

System	concave		convex	
	side-on	end-on	side-on	end-on
Su(H_2)	3.7	3.3	0.8	0.7
Su^{-}(H_2)	4.2	3.9	1.9	1.6
Su^{2-}(H_2)	4.4	4.3	3.2	2.5

Table 3.13 BSSE corrected E_{int} (kcal/mol) of side-on H_2 complexes at concave surface using different methods

method	*Su*(H_2)	*Su*$^{-}$(H_2)	*Su*$^{2-}$(H_2)
[a]M06L	3.7	4.2	4.4
[a]M06L-D3	3.9	4.3	4.6
[a]M062X	3.7	4.1	4.4
[a]M062X-D3	3.9	4.3	4.9
[a]wB97XD	3.3	3.7	3.8
[a]B3LYP-D3	2.6	3.0	3.3
[a]B97D	2.1	2.6	2.8
[a]B97-D3	2.6	3.0	3.3
[a]BP86-D3	3.3	3.7	4.1
[b]M06L	3.2	3.5	3.7
[b]wB97XD	3.0	3.5	3.5
[b]B97D	2.1	2.6	2.9

[a] basis set = 6−311++G(d,p), [b]basis set = aug-cc-pVDZ

The bowl shape leads to major differences in the electron distribution on the concave and convex surfaces which will be addressed in detail later.

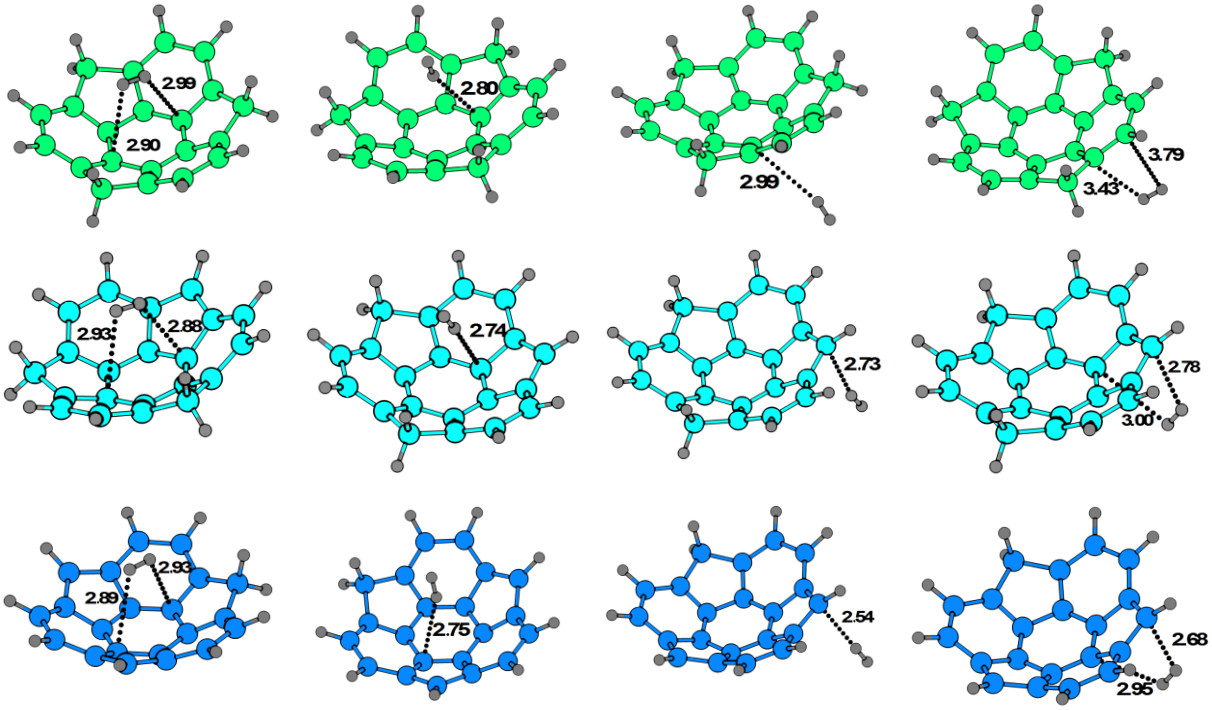

Figure 3.15 Interaction of H_2 with *Su*, *Su*$^-$ and *Su*$^{2-}$ at the M06L/6−311++G(d,p) level (bond distances are in Å and *Su*, *Su*$^-$ and *Su*$^{2-}$ complexes are represented in green, cyan and blue colors, respectively).

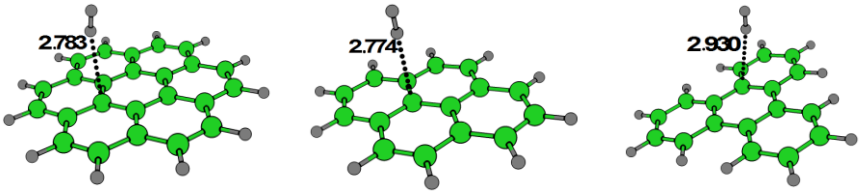

Figure 3.16 Optimized geometries of H_2 complexes of polyaromatic systems at theM06L/6−311++G(d,p) level. Bond distances are in Å.

3.9.2 Interaction of Multiple H_2 with *Su*, *Su*$^-$ and *Su*$^{2-}$

The concave surface of *Su* shows higher dihydrogen binding affinity than the convex surface. Hence, *Su* is populated with increasing number of H_2 from the concave surface followed by the convex surface. Figure 3.17 depicts the optimized geometries of *Su*, *Su*$^-$ and *Su*$^{2-}$ with 20, 30 and 40 H_2 molecules as representative cases. A systematic increase in E_{int} from 3.7 to 51.7 kcal/mol with

$E_{int/H2}$ in the range 3.7 – 1.3 kcal/mol is observed for *Su*...H_2 complexes with *n* varying from 1 to 40 (Table 3.14). For anionic and dianionic systems, E_{int} varies from 4.2 – 63.0 and 4.4 – 87.6 kcal/mol, respectively with increase in *n* from 1 to 40. The $E_{int/H2}$ for Su^- and Su^{2-} systems lies in the range 3.9 – 1.6 and 4.3 – 2.2 kcal/mol, respectively with n varying from 1 to 40 (Table 3.14).

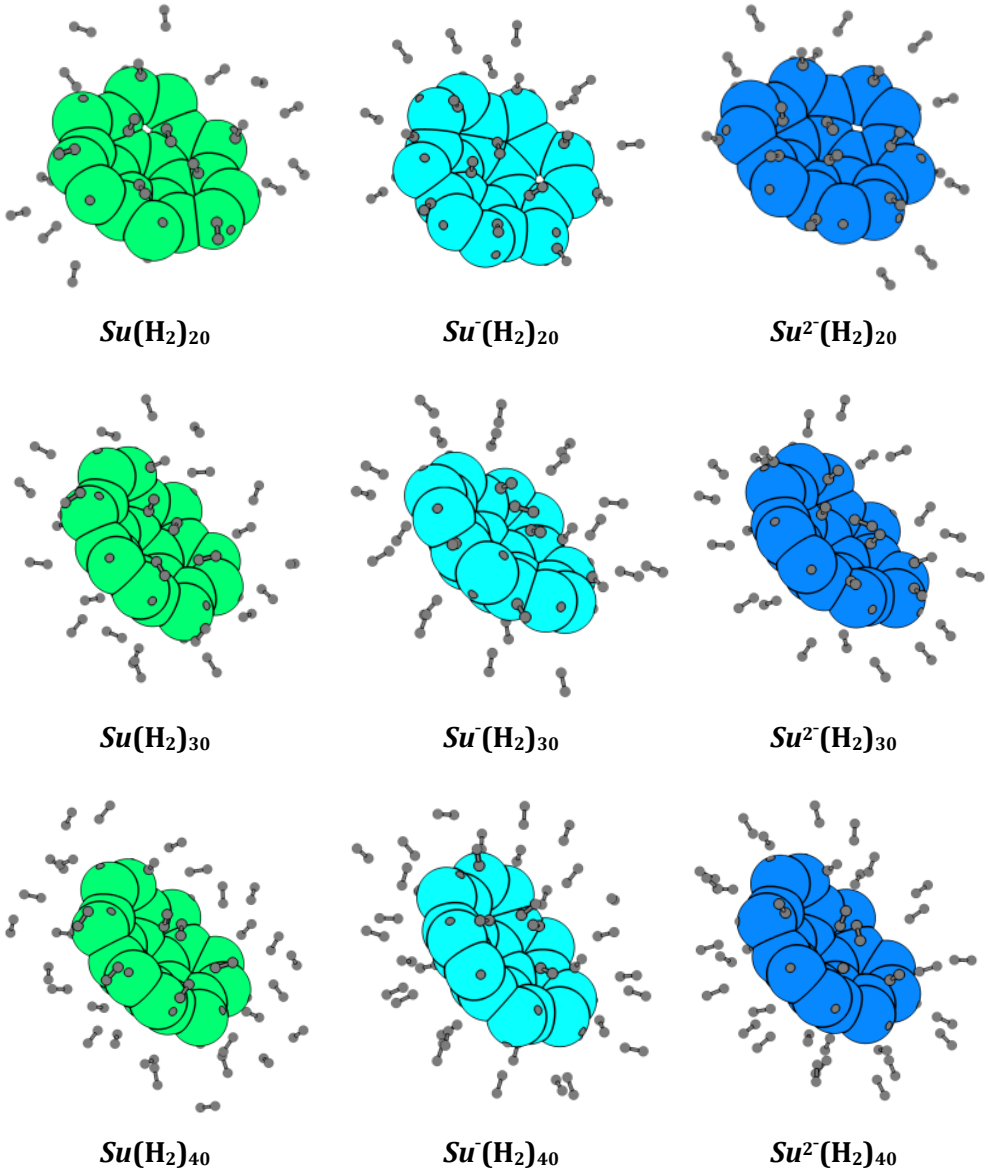

Figure 3.17 Optimized geometries of *Su*, Su^- and Su^{2-} with 20, 30 and 40 H_2 at the M06L/6–311++G(d,p) level.

These results suggest that anionic/dianionic nature of sumanene provides a significant improvement in its ability to bind with a large number of H_2 molecules. Our previous

studies corroborate with a similar observation that anions, in general, show remarkably high affinity to a large number of H_2 than their neutral counterparts.[141-143]

Table 3.14 BSSE corrected E_{int} (kcal/mol) and $E_{int/H2}$ (kcal/mol) of $Su(H_2)_n$, $Su^-(H_2)_n$, and $Su^{2-}(H_2)_n$ complexes at the M06L/6−311++G(d,p) level

n	E_{int}			$E_{int/H2}$		
	$Su(H_2)_n$	$Su^-(H_2)_n$	$Su^{2-}(H_2)_n$	$Su(H_2)_n$	$Su^-(H_2)_n$	$Su^{2-}(H_2)_n$
1	3.3	3.9	4.3	3.3	3.9	4.3
2	4.4	5.5	7.2	2.2	2.8	3.6
3	5.8	7.6	9.4	1.9	2.5	3.1
4	6.9	9.7	11.6	1.7	2.4	2.9
5	8.4	10.5	14.3	1.7	2.1	2.9
6	9.9	12.2	17.2	1.6	2.0	2.9
7	10.8	13.6	19.2	1.5	1.9	2.7
8	11.6	15.2	21.3	1.5	1.9	2.7
9	12.6	16.6	22.7	1.4	1.8	2.5
10	13.5	17.1	24.6	1.4	1.7	2.5
11	14.8	18.5	26.8	1.3	1.7	2.4
12	14.8	19.8	28.7	1.2	1.7	2.4
13	15.9	21.5	30.4	1.2	1.7	2.3
14	16.8	22.4	32.1	1.2	1.6	2.3
15	17.6	23.7	33.4	1.2	1.6	2.2
16	19.2	24.8	34.8	1.2	1.5	2.2
17	20.1	26.0	36.9	1.2	1.5	2.2
18	21.3	27.4	38.9	1.2	1.5	2.2
19	22.7	28.3	40.2	1.2	1.5	2.1
20	23.7	29.6	42.3	1.2	1.5	2.1
30	39.7	48.9	69.3	1.3	1.6	2.3
40	51.7	63.0	87.6	1.3	1.6	2.2

3.9.3 K^+ as Counter Cation for Su^-, Su^{2-}, and Su^{3-} Anions

In reality, anionic systems exist in the presence of counter cations. Anionic sumanenyl systems have been recently synthesized by Spisak *et al.* with K^+ as counter cation.[136] Hence as a more realistic approach, we study the H_2 binding affinity of the ion-pair systems of Su^- and Su^{2-} with K^+. Figure 3.18 represents the optimized geometries of Su^-K^+, $Su^{2-}(K^+)_2$ and $Su^{3-}(K^+)_3$ in two different orientations. Su^-K^+ showing K^+ binding at the concave surface is more stable than that binding at the convex surface. The E_{int} of concave and convex type complexes are 111.5 and 102.9 kcal/mol, respectively. In $Su^{2-}(K^+)_2$, one K^+ ion each at the concave and convex surfaces has E_{int} 296.3 kcal/mol which is 22.1 kcal/mol more stable than the other where two K^+ ions bind from the concave surface. For $Su^{3-}(K^+)_3$ complex, the structure with one K^+ at the concave side and two K^+ at convex side (Figure 3.18e) is found to be more stable than the opposite structure (Figure 3.18f). The most stable Su^-K^+, $Su^{2-}(K^+)_2$ and $Su^{3-}(K^+)_3$ have been studied for their dihydrogen binding ability by saturating with H_2. Figure 3.19 shows the optimized geometries of $Su^-K^+(H_2)_{47}$, $Su^{2-}(K^+)_2(H_2)_{51}$ and $Su^{3-}(K^+)_3(H_2)_{51}$ complexes. Both anionic and cationic portions interact with H_2 leading to total E_{int} 61.6, 77.1 and 132.6 kcal/mol, and $E_{int/H2}$ 1.3, 1.5 and 2.6 kcal/mol, respectively for $Su^-K^+(H_2)_{47}$, $Su^{2-}(K^+)_2(H_2)_{51}$ and $Su^{3-}(K^+)_3(H_2)_{51}$ (Table 3.15). Anionic and dianionic systems exhibit a higher E_{int} than neutral sumanene. The delocalization of extra electron(s) in anionic or dianionic systems can be accounted for this rise in E_{int}. When the metal cation is added to the anionic system, the ion-pair interaction of metal cation and sumanene anion reduces the effective negative charge on the anionic sumanene bowl. Thus a drop in E_{intH2} is noted for anion-M^+ and dianion-$(M^+)_2$ complexes. The trianion complex $Su^{3-}(K^+)_3(H_2)_{51}$ exhibits the highest E_{intH2} 2.6 kcal/mol. When H_2 interacts with electron-rich centers, its LUMO accepts electron density from the occupied orbitals while when it interacts with electron deficient centers, electron donation from HOMO is expected.[137-139, 141-143]

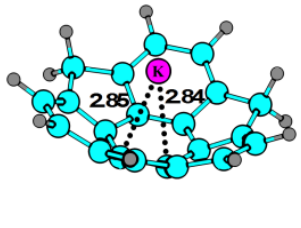

(a) K^+ at [cc]

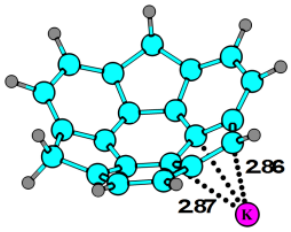

(b) K^+ at [cv]

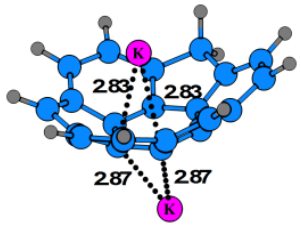

(c) one K^+ each at [cc] and [cv]

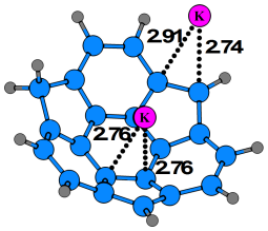

(d) both K^+ at [cc]

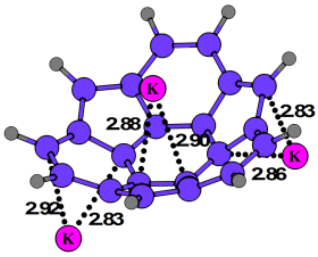

(e) two K^+ at [cv] and one at [cc]

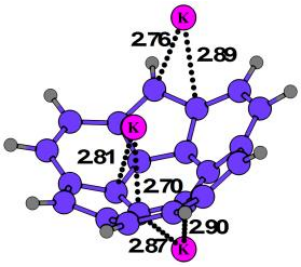

(f) two K^+ at [cc] and one at [cv]

Figure 3.18 Optimized geometries of Su^-K^+, $Su^{2-}(K^+)_2$, and $Su^{3-}(K^+)_3$ at M06L/6−311++G(d,p) level. Bond distances are in Å, [cc] and [cv] indicate concave and convex sides respectively.

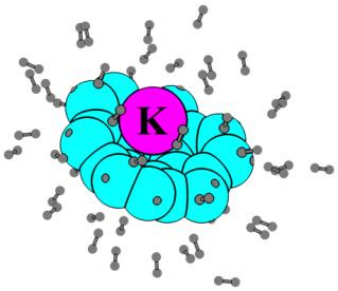

$Su^-K^+(H_2)_{47}$

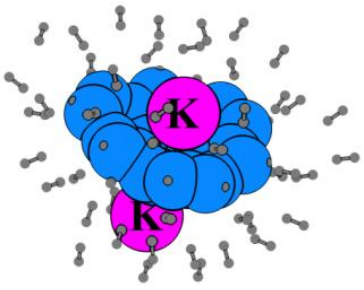

$Su^{2-}(K^+)_2(H_2)_{51}$

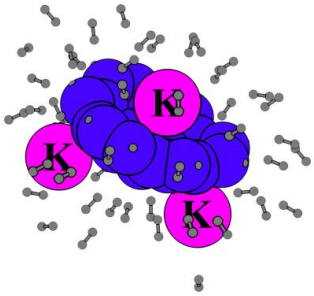

$Su^{3-}(K^+)_3(H_2)_{51}$

Figure 3.19 Optimized geometries of dihydrogen complexes saturated with H_2 at the M06L/6−311++G(d,p) level.

This property of H_2 may be considered as unique and suggests that ion-pair systems have the power to exploit it toward developing novel hydrogen storage systems.

Table 3.15 E_{int} and $E_{int/H2}$ (kcal/mol) of complexes at the M06L/6−311++G(d,p) level

System	E_{int}	$E_{int/H2}$
$Su(H_2)_{43}$	55.7	1.3
$Su^{-}K^{+}(H_2)_{47}$	61.6	1.3
$Su^{2-}(K^{+})_2(H_2)_{51}$	77.1	1.5
$Su^{3-}(K^{+})_3(H_2)_{51}$	132.6	2.6

3.9.4 MESP Analysis

Figure 3.20 represents the MESP of *Su*, Su^{-} and Su^{2-} and their dihydrogen complexes plotted on 0.003 au electron density surface. In the case of *Su*, the negative MESP is concentrated on six-membered rings where the convex surface is more electron dense and shows the deepest MESP value (V_{min}) -16.2 kcal/mol while the concave surface is relatively electron deficient with V_{min} -12.9 kcal/mol.

Table 3.16 V_{min} (kcal/mol) of complexes at the M06L/6−311++G(d,p) level

n	$Su(H_2)_n$	$Su^{-}(H_2)_n$	$Su^{2-}(H_2)_n$
bare	-16.2	-113.5	-189.9
1	-16.0	-112.8	-190.0
5	-15.2	-110.2	-183.8
10	-14.4	-107.4	-178.4
15	-14.3	-105.7	-177.4
20	-13.7	-101.5	-172.0
30	-14.1	-91.9	-161.8
40	-12.8	-88.9	-153.7

For Su^{-} and Su^{2-}, the benzylic positions from which proton is eliminated show the highest negative MESP, -113.5 and -189.9 kcal/mol, respectively and nearly same values are observed on both convex and concave sides. The V_{min} of dihydrogen complexes of *Su*, Su^{-} and Su^{2-} (Table 3.16) data shows that as the number of H_2 molecules increases, the magnitude of V_{min} decreases, indicating the utilization of electron density for dihydrogen binding. From Figure 3.20 it is clear that as H_2 bind to *Su* or its anionic forms, the blue color indicating the electron-rich region diminishes because of charge donation to H_2 molecules.

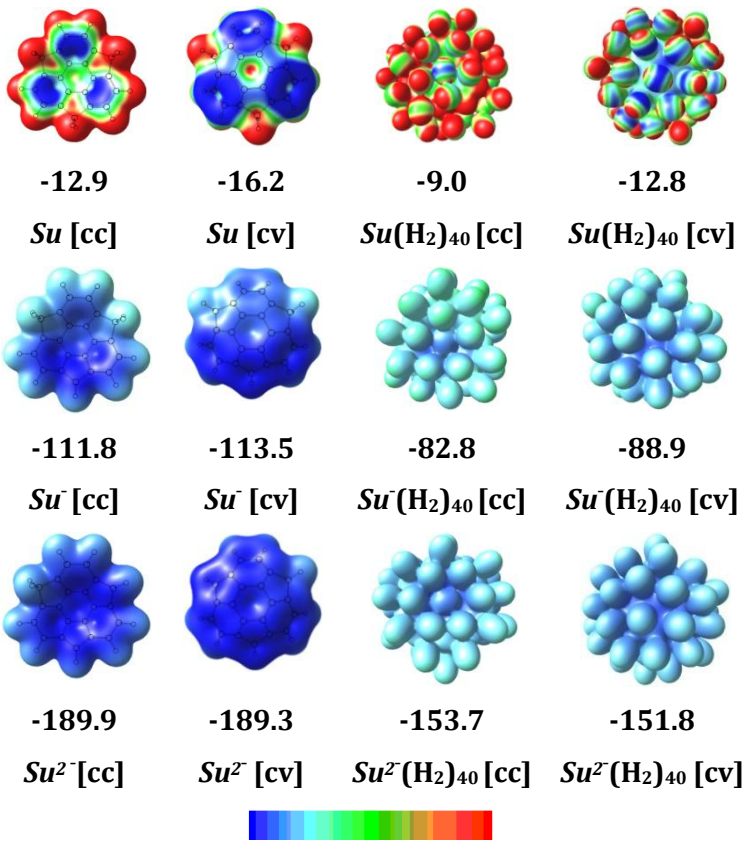

Figure 3.20 MESP of bare *Su*, Su^- and Su^{2-} and complexes with 40 H_2 plotted on 0.003 au electron density surface. The color coding from blue to red indicates MESP values in the range -0.013 to +0.013 au for neutral, -0.160 to +0.160 au for monoanion, and -0.280 to +0.280 au for dianion. V_{min} in kcal/mol is also depicted. [cc] and [cv] indicate concave and convex views, respectively.

Upon binding of 1 to 40 H_2, the V_{min} of *Su* varies from -16.2 to -12.8 kcal/mol. For Su^- and Su^{2-} the variation is from -113.5 to -88.9 and -189.9 to -153.7 kcal/mol, respectively. The MESP of Su^-K^+ (Figure 3.21) shows that the concave side where the cation binds is electron deficient whereas the convex side is highly electron rich (anionic). For $Su^{2-}(K^+)_2$ and $Su^{3-}(K^+)_3$ the presence of K^+ on both convex and concave surfaces gives a more balanced charge distribution than Su^-K^+ (Figure 3.21). The MESP features of $Su^-K^+(H_2)_{47}$ (Figure 3.22) shows a clear distinction between the binding of H_2 on the concave and convex sides as the former is dominated by the charge transfer from H_2 to cation (red region) while the later is

characterized by the charge flow from anion to H_2 (blue region). Similar MESP features can be seen in $Su^{2-}(K^+)_2(H_2)_{51}$ and $Su^{3-}(K^+)_3(H_2)_{51}$ (Figure 3.22) where the anionic effect is mainly arising from the rim region. The V_{min} values of Su^-K^+, $Su^{2-}(K^+)_2$, and $Su^{3-}(K^+)_3$ systems are -34.5, -38.4, and -53.3 kcal/mol, respectively. The magnitude of V_{min} decreases upon H_2 binding for both the systems. The V_{min} for $Su^-K^+(H_2)_{47}$, $Su^{2-}(K^+)_2(H_2)_{51}$, and $Su^{3-}(K^+)_3(H_2)_{51}$ complexes are -25.7, -22.9, and -32.0 kcal/mol, respectively. The MESP analysis suggests strong charge separation in the ion-pair systems of sumanene anion/dianion/trianion and K^+ which promotes the binding of a large number of dihydrogen molecules to the cationic and anionic portions.

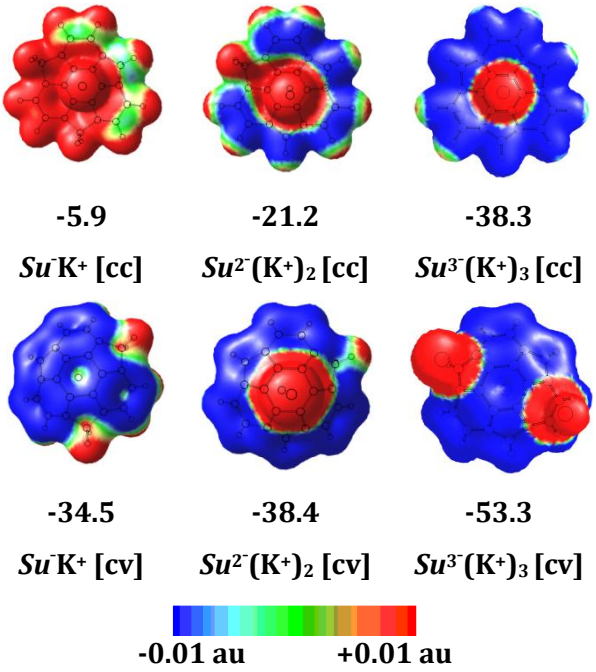

Figure 3.21 MESP of Su^-K^+ $Su^{2-}(K^+)_2$, and $Su^{3-}(K^+)_3$ plotted at an isosurface value of 0.003 au. The color coding from blue to red indicates MESP values in the range -0.01 – 0.01 au. V_{min} in kcal/mol is also depicted. [cc] and [cv] indicate concave and convex views, respectively.

3.9.5 QTAIM Analysis

Analysis of the QTAIM molecular graphs for $Su(H_2)_{43}$, $Su^-K^+(H_2)_{47}$, $Su^{2-}(K^+)_2(H_2)_{51}$ and $Su^{3-}(K^+)_3(H_2)_{51}$ shows a bond critical point (bcp) between every hydrogen molecule and an atom in the sumanene framework or K^+ (Figure 3.23). The Laplacian of electron

density ($\nabla^2\rho_{bcp}$) is positive for all the interactions indicating the formation of C...H_2, H...H_2, and K^+...H_2 type noncovalent bonds. The electron density at these bcps (ρ_{bcp}) is in the range 0.0030 – 0.0073 au for $Su(H_2)_{43}$, 0.0025 – 0.0078 for $Su^-(K^+)(H_2)_{47}$, 0.0027 – 0.0081 au for $Su^{2-}(K^+)_2(H_2)_{51}$, and for $Su^{3-}(K^+)_3(H_2)_{51}$ and among them the ρ_{bcp} for K^+...H_2 interactions fall in the range 0.0025 – 0.0044 au for $Su^-(K^+)(H_2)_{47}$, 0.0038 – 0.0058 au for $Su^{2-}(K^+)_2(H_2)_{51}$, and 0.0025 – 0.0069 au for $Su^{3-}(K^+)_3(H_2)_{51}$.

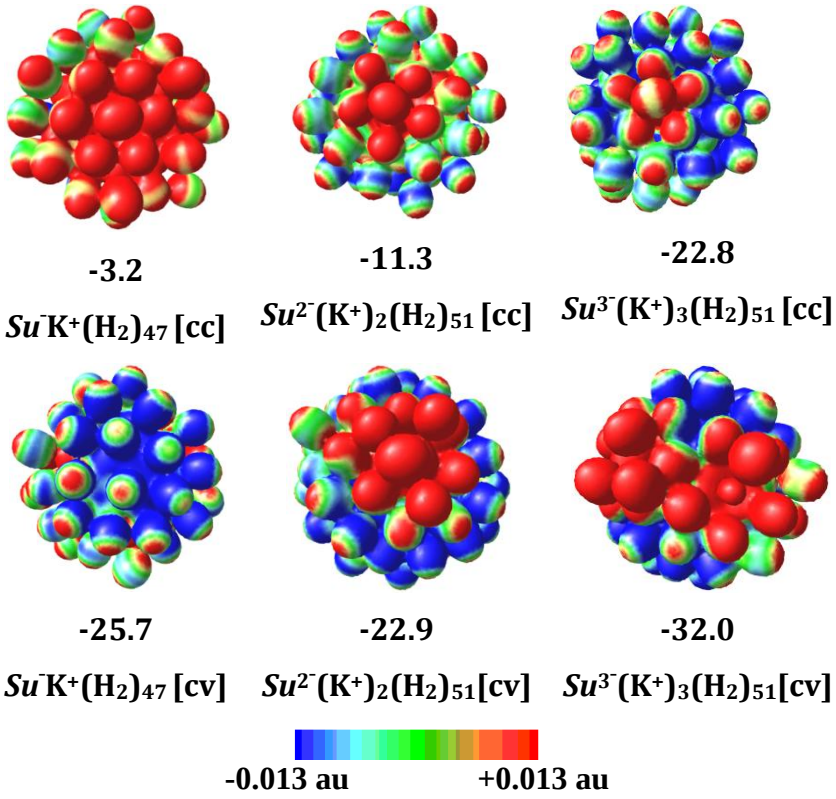

Figure 3.22 MESP of complexes plotted at an isosurface value of 0.003 au. The color coding from blue to red indicates MESP values in the range -0.013 – 0.013 au. V_{min} in kcal/mol is also depicted. [cc] and [cv] indicate concave and convex views, respectively.

There are 6 K^+...H_2 bcps in $Su^-(K^+)(H_2)_{47}$, 11 bcps in $Su^{2-}(K^+)_2(H_2)_{51}$, and 16 bcps in $Su^{3-}(K^+)_3(H_2)_{51}$. Moreover, H_2...H_2 dihydrogen interactions between adjacent H_2 molecules are identified in all the complexes. The ρ_{bcp} values of such interactions fall in the range 0.0008 – 0.0029 au. Presence of these bcps indicates that an attractive interaction develops between the adsorbed dihydrogens which leads to the formation of an extensive network of noncovalently connected molecular entities.

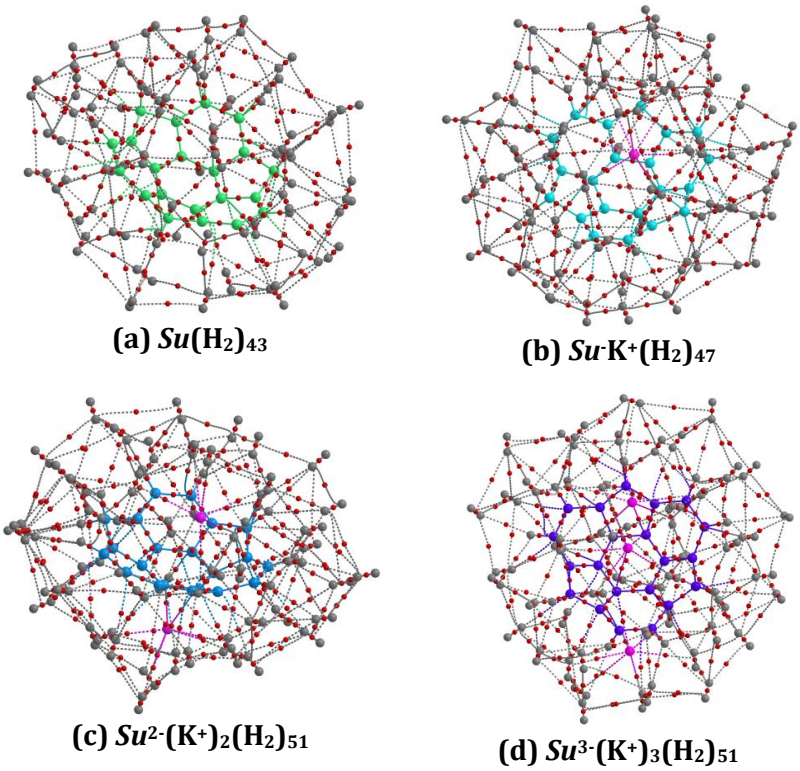

Figure 3.23 QTAIM features of (a) $Su(H_2)_{43}$, (b) $Su^{-}(K^{+})(H_2)_{47}$, (c) $Su^{2-}(K^{+})_2(H_2)_{51}$, and (d) $Su^{3-}(K^{+})_3(H_2)_{51}$ at the M06L/6-311++G(d,p) level.

3.9.6 Systems with Li^{+} and Na^{+} as Counter Cations

The anionic, dianionic and trianionic complexes of *Su* with Li^{+} and Na^{+}, *viz*. $Su^{-}(Li^{+})(H_2)_{47}$, $Su^{-}(Na^{+})(H_2)_{47}$, $Su^{2-}(Li^{+})_2(H_2)_{51}$, $Su^{2-}(Na^{+})_2(H_2)_{51}$ $Su^{3-}(Li^{+})_3(H_2)_{51}$ and $Su^{3-}(Na^{+})_3(H_2)_{51}$ are also optimized for comparing the E_{int} with the corresponding K^{+} complexes. $Su^{-}(Li^{+})(H_2)_{47}$ has E_{int} 108.2 kcal/mol and $E_{int/H2}$ 2.1 kcal/mol whereas $Su^{2-}(Li^{+})_2(H_2)_{51}$ has E_{int} 129.8 kcal/mol and $E_{int/H2}$ 2.5 kcal/mol.

Table 3.17 BSSE corrected E_{int} (kcal/mol) of $Su^{-}M^{+}(H_2)_{47}$, $Su^{2-}(M^{+})_2(H_2)_{51}$ and $Su^{3-}(M^{+})_3(H_2)_{51}$ complexes at the M06L/6−311++G(d,p) level

M =	E_{int}		
	$Su^{-}M^{+}(H_2)_{47}$	$Su^{2-}(M^{+})_2(H_2)_{51}$	$Su^{3-}(M^{+})_3(H_2)_{51}$
Li	108.2	129.8	98.2
Na	107.2	128.3	103.2
K	61.5	77.1	132.6

The E_{int} and $E_{int/H2}$ for Na^+ complexes are much similar to corresponding Li^+ complexes. Compared to K^+ complexes, the Li^+ and Na^+ complexes show 66 – 74 % increase in E_{int}. In contrast to this observation, $Su^{3-}(Li^+)_3(H_2)_{51}$ and $Su^{3-}(Na^+)_3(H_2)_{51}$ complexes show smaller E_{int} values, *viz.* 98.2 and 103.2 kcal/mol, respectively compared to $Su^{3-}(K^+)_3(H_2)_{51}$ (Table 3.17). Being lighter than K^+, Li^+ and Na^+ improve the weight percent of H_2 in the storage material (Table 3.18). A weight percent of H_2 21.4 – 27.1 observed in these complexes is significantly higher than the DOE minimum target recommended for automotive purposes.

Table 3.18 Weight percent (wt%) of H_2 in complexes

M	$Su^-M^+(H_2)_{47}$	$Su^{2-}(M^+)_2(H_2)_{51}$	$Su^{3-}(M^+)_3(H_2)_{51}$
Li	26.0	27.1	26.7
Na	24.9	25.0	23.7
K	23.9	23.2	21.4

3.10 Conclusions

In summary, the H_2 binding ability of neutral sumanene and its anionic forms explored using DFT studies showed that their affinity to H_2 follows the order Su^{2-} > Su^- > *Su*. The bowl-shaped geometry of sumanene enhances a charge separation between the concave and convex surfaces which increases H_2 binding energy compared to planar structures. The delocalized state of π-electrons together with the convex-concave charge separation promotes the interaction of a large number of H_2 molecules with the sumanene framework. These interactions are weak noncovalent in nature as seen in QTAIM studies and classified as C...H_2, H...H_2, M^+...H_2, and H_2...H_2 types. The H_2...H_2 type attractive interactions support the large assembly of H_2 molecules spread across both convex and concave surface of the sumanene framework. MESP studies revealed the delocalized state of sumanene systems as well as the charge separation in ion-pair complexes. The ability of H_2 to bind with the electron rich and electron deficient regions is also unveiled through the MESP analysis. The ion-pair systems of sumanene and alkali metals (K, Na, and Li) provide a more realistic account of the strong hydrogen

storing potential of sumanene. These findings may pave the way for developing sumanene-based ionic systems for hydrogen storage.

3.11 References

1. A. C. Dillon and M. J. Heben, *Appl. Phys. A*, **2001**, *72*, 133-142.
2. S. Orimo, G. Majer, T. Fukunaga, A. Züttel, L. Schlappbach and H. Fujii, *Appl. Phys. Lett.*, **1999**, *75*, 3093-3095.
3. R. Strobel, J. Garche, P. T. Moseley, L. Jorissen and G. Wolf, *J. Power Sources*, **2006**, *159* 781-801.
4. W.-Q. Deng, X. Xu and W. A. Goddard, *Phys. Rev. Lett*, **2004**, *92*, 166103.
5. G. K. Dimitrakakis, E.Tylianakis and G. E. Froudakis, *Nano Lett.*, **2008**, *8*, 3166-3170.
6. S. Patchkovskii, J. S. Tse, S. N. Yurchenko, L. Zhechkov, T. Heine and G.Seifert, *Proc. Natl. Acad. Sci. U.S.A*, **2005**, *102*, 10439-10444.
7. M. Pumera, *Energy Environ. Sci.*, **2014**, *4*, 668-674.
8. O. V. Pupysheva, A. A. Farajian and B. I. Yakobson, *Nano Lett.*, **2008**, *8*, 767-774.
9. T. Yildirim, J. Iniguez and S. Ciraci, *Phys. Rev. B*, **2005**, *72*, 153403.
10. C. Liu, Y. Y. Fan, M. Liu, H. T. Cong, H. M. Cheng and M. Dresselhaus, *Science*, **1999**, *286*, 1127-1129.
11. Y. Ye, C. C. Ahn, C. Whitam, B. Fultz, L. Liu, A. G. Rinzler, D. Colbert, K. A. Smith and R. E. Smalley, *J. Appl. Phys. Lett.*, **1999**, *74*, 2307-2309.
12. A. D. Lueking and R. T. Yang, *AIChE J.*, **2003**, *49*, 1556-1568.
13. H. Lee, Y. S. Kang, S. H. Kim and J. Y. Lee, *Appl. Phys. Lett.*, **2002**, *80*, 577-579.
14. X. Li, H. Zhu, L. Ci, C. Xu, Z. Mao, B. Wei, J. Liang and D. Wu, *Carbon*, **2001**, *39*, 2077-2079.
15. P. Hou, Q. Yang, S. Bai, S. Xu, M. Liu and H. Cheng, *J. Phys. Chem. B*, **2002**, *106*, 963-966.
16. M. Jordá-Beneyto, F. Suárez-García, D. Lozano-Castelló, D. Cazorla-Amorós and A. Linares-Solano, *Carbon*, **2007**, *45*, 293-303.
17. P. Chen, X. Wu, J. Lin and K. L. Tan, *Science*, **1999**, *285*, 91-93.

18. T. Yildirim and S. Ciraci, *Phys. Rev. Lett.*, **2005**, *94*, 175501.
19. R. Zacharia, S.-u. Rather, S. W. Hwang and K. S. Nahm, *Chem. Phys. Lett.*, **2007**, *434*, 286-291.
20. G. Stan and M. W. Cole, *J. Low Temp. Phys.*, **1998**, 539-544.
21. A. C. Dillon, K. M. Jones, T. A. Bekkedahl, C. H. Kiang, D. S. Bethune and M. J. Heben, *Nature*, **1997**, *386*, 377-379.
22. J. M. Blackman, J. W. Patrick, A. Arenillas, W. Shi and C. E. Snape, *Carbon*, **2006**, *44*, 1376-1385.
23. A. Chambers, C. Park, R. T. K. Baker and N. M. Rodriguez, *J. Phys. Chem. B*, **1998**, *102*, 4253–4256.
24. R. Dembinski, T. Bartik, B. Bartik, M. Jaeger and J. Gladysz, *J. Am. Chem. Soc.*, **2000**, *122*, 810-822.
25. S. Eisler, A. D. Slepkov, E. Elliott, T. Luu, R. McDonald, F. A. Hegmann and R. R. Tykwinski, *J. Am. Chem. Soc.*, **2005**, *127*, 2666-2676.
26. R. E. Minto and B. J. Blacklock, *Prog. Lipid Res.*, **2008**, *47*, 233-306.
27. A. L. K. Shi Shun and R. R. Tykwinski, *Angew. Chem. Int. Ed.*, **2006**, *45*, 1034-1057.
28. F. Bohlmann, *Angew. Chem. Int. Ed.*, **1955**, *67*, 389-394.
29. D. J. Faulkner, *Nat. Prod. Rep.*, **2000**, *17*, 7-55.
30. A. El Goresy and G. Donnay, *Science*, **1968**, *161*, 363-364.
31. P. Smith and P. R. Buseck, *Science*, **1982**, *216*, 984-986.
32. R. Hayatsu, R. G. Scott, M. H. Studier, R. S. Lewis and E. Anders, *Science*, **1980**, *209*, 1515-1518.
33. A. G. Whittaker, E. J. Watts, R. S. Lewis and E. Anders, *Science*, **1980**, *209*, 1512-1514.
34. F. Cataldo, *Carbon*, **2004**, *42*, 129-142.
35. W. A. Chalifoux and R. R. Tykwinski, *C. R. Chim*, **2009**, *12*, 341-358.
36. F. Cataldo, L. Ravagnan, E. Cinquanta, I. E. Castelli, N. Manini, G. Onida and P. Milani, *J. Phys. Chem. B*, **2010**, *114*, 14834-14841.
37. T. Gibtner, F. Hampel, J. P. Gisselbrecht and A. Hirsch, *Chem. Eur. J.*, **2002**, *8*, 408-432.
38. S. Szafert and J. A. Gladysz, *Chem. Rev.*, **2003**, *103*, 4175-4206.

39. C. Wang, A. S. Batsanov, K. West and M. R. Bryce, *Org. Lett.*, **2008**, *10*, 3069-3072.
40. R. Eastmond, T. R. Johnson and D. R. M. Walton, *Tetrahedron*, **1972**, *28*, 4601-4616.
41. W. A. Chalifoux and R. R. Tykwinski, *Nat. Chem.*, **2010**, *2*, 967-971.
42. H. Tabata, M. Fujii, S. Hayashi, T. Doi and T. Wakabayashi, *Carbon*, **2006**, *44*, 3168-3176.
43. K. Inoue, R. Matsutani, T. Sanada and K. Kojima, *Carbon*, **2010**, *48*, 4209-4211.
44. Y. Sato, T. Kodama, H. Shiromaru, J. H. Sanderson, T. Fujino, Y. Wada, T. Wakabayashi and Y. Achiba, *Carbon*, **2010**, *48*, 1673-1676.
45. F. Cataldo, *Carbon*, **2005**, *43*, 2792-2800.
46. L. Kavan, *Carbon*, **1998**, *36*, 801-808.
47. F. Cataldo, *Carbon*, **2003**, *41*, 2671-2674.
48. J. A. Januszewski and R. R. Tykwinski, *Chem. Soc. Rev.*, **2014**, *43*, 3184-3203.
49. S. Ballmann, W. Hieringer, D. Secker, Q. L. Zheng, J. A. Gladysz, A. Go¨rling and H. B. Weber, *ChemPhysChem*, **2010**, *11*, 2256-2260.
50. P. Moreno-Garcia, M. Gulcur, D. Z. Manrique, T. Pope, W. Hong, V. Kaliginedi, C. Huang, A. S. Batsanov, M. R. Bryce, C. Lambert and T. Wandlowski, *J. Am. Chem. Soc.*, **2013**, *135*, 12228-12240.
51. O. Cretu, A. R. Botello-Mendez, I. Janowska, C. Pham-Huu, J.-C. Charlier and F. Banhart, *Nano Lett.*, **2013**, *13*, 3487-3493.
52. A. K. Nair, S. W.Cranford and M. J. Buehler, *Europhys. Lett*, **2011**, *95*, 16002.
53. S. W.Cranford, *Nanoscale Res. Lett.* , **2013**, *8*, 490.
54. I. Kminek, J. Klimovic and P. N. Prasad, *Chem. Mater.*, **1993**, *5*, 357-360.
55. M. Liu, V. I. Artyukhov, H. Lee, F. Xu and B. I. Yakobson, *ACS Nano.*, **2013**, *7*, 10075-10082.
56. A. Lucotti, M. Tommasini, D. Fazzi, M. D. Zoppo, W. A. Chalifoux, R. R. Tykwinski and G. Zerbi, *J. Raman Spectrosc.*, **2012**, *43*, 1293-1298.
57. Z. Zanolli, G. Onida and J. C. Charlier, *ACS Nano.*, **2010**, *4*, 5174-5180.
58. C.-S. Liu, H. An, L.-J. Guo, Z. Zeng and X. Ju, *J. Chem. Phys.*, **2011**, *134*, 024522.
59. P. B. Sorokin, H. Lee, L. Y. Antipina, A. K. Singh and B. I. Yakobson, *Nano Lett.*, **2011**, *11*, 2660-2665.

60. Y. Zhao and D. G. Truhlar, *J. Chem. Phys.*, **2006**, *125*, 194101.
61. Y. Zhao and D. G. Truhlar, *Acc. Chem. Res.*, **2008**, *41*, 157-167.
62. S. F. Boys and F. d. Bernardi, *Mol. Phys.*, **1970**, *19*, 553-566.
63. S. R. Gadre and R. N. Shirsat, *Electrostatics of Atoms and Molecules*, Universities Press, Hyderabad, **2000**.
64. P. Politzer and D. G. Truhlar, *Chemical Applications of Atomic and Molecular Electrostatic Potentials: Reactivity, Structure, Scattering: Energetics of Organic, Inorganic, and Biological Systems*, Springer, New York, **1981**.
65. M. J. Frisch, G. W. Trucks, *et al.* Gaussian 09, Revision D.01; Gaussian, Inc., Wallingford CT, **2013**.
66. T. A. Keith, *AIMAll, verion 14.04.17,* T. K. Gristmill Software, Overland Park KS, USA, **2014**.
67. P. Politzer, J. S. Murray and T. Clark, *Phys. Chem. Chem. Phys.*, **2010**, *12*, 7748-7757.
68. G. Naray-Szabo and G. G. Ferenczy, *Chem. Rev.*, **1995**, *95*, 829-847.
69. J. S. Murray and P. Politzer, *J. Mol. Struc.-THEOCHEM*, **1998**, *425*, 107-114.
70. P. Politzer, J. S. Murray and M. C. Concha, *Int. J. Quantum Chem.*, **2002**, *88*, 19-27.
71. J. Poater, M. Solà and F. M. Bickelhaupt, *Chem. Eur. J.*, **2006**, *12*, 2889-2895.
72. R. F. W. Bader and H. Esse´n, *J. Chem. Phys.*, **1984**, *80*, 1943–1960.
73. P. L. A. Popelier, G. Logothetis and *J. Organomet. Chem.*, **1998**, *555*, 101–111.
74. S. Armaković, S. J. Armaković, S. Pelemiš and D. Mirjanić, *Phys. Chem. Chem.Phys.*, **2016**, *18*, 2859-2870.
75. T. Hussain, B. Pathak, M. Ramzan, T. A. Maark and R. Ahuja, *Appl. Phys. Lett.*, **2012**, *100*, 183902.
76. A. Reyhani, S. Z. Mortazavi, S. Mirershadi, A. Z. Moshfegh, P. Parvin and A. N. Golikand, *J. Phys. Chem. C*, **2011**, *115*, 6994-7001.
77. M. Yoon, S. Yang, C. Hicke, E. Wang, D. Geohegan and Z. Zhang, *Phys. Rev. Lett.*, **2008**, *100*, 206806.
78. A. Dillon and M. Heben, *Appl. Phys. A*, **2001**, *72*, 133-142.
79. L. Scanlon, P. Balbuena, Y. Zhang, G. Sandi, C. Back, W. Feld, J. Mack, M. Rottmayer and J. Riepenhoff, *J. Phys. Chem. B*, **2006**, *110*, 7688-7694.

80. Y. Zhang, L. Scanlon, M. Rottmayer and P. Balbuena, *J. Phys. Chem. B*, **2006**, *110*, 22532-22541.
81. C. Cazorla, *Coord. Chem. Rev.*, **2015**, *300*, 142-163.
82. H. W. Kroto, J. R. Heath, S. C. O'Brien, R. F. Curl and R. E. Smalley, *Nature*, **1985**, *318*, 162-163.
83. M. Prato, *J. Mater. Chem.* , **1997**, *7*, 1097-1109.
84. N. Martín, *Chem. Commun.*, **2006**, 2093-2104.
85. H. W. Kroto, M. A. Petrukhina and L. T. Scott, *Fragments of Fullerenes and Carbon Nanotubes: Designed Synthesis, Unusual Reactions, and Coordination Chemistry*, John Wiley & Sons, **2011**.
86. G. Mehta and H. S. P. Rao, *Tetrahedron*, **1998**, *54*, 13325-13370.
87. T. Kawase and H. Kurata, *Chem. Rev.*, **2006**, *106*, 5250-5273.
88. X.-Q. Hou, Y.-T. Sun, L. Liu, S.-T. Wang, R.-L. Geng and X.-F. Shao, *Chin. Chem. Lett.*, **2016**, *27*, 1166-1174.
89. L. Zoppi, A. Ferretti and K. K. Baldridge, *J. Chem. Theory Comput.*, **2013**, *9*, 4797-4804.
90. M. A. Petrukhina, *Angew. Chem. Int. Ed.*, **2008**, *47*, 1550-1552.
91. A. S. Filatov, M. V. Ferguson, S. N. Spisak, B. Li, C. F. Campana and M. A. Petrukhina, *Cryst. Growth Des.*, **2013**, *14*, 756-762.
92. S. N. Spisak, A. V. Zabula, A. S. Filatov, A. Y. Rogachev and M. A. Petrukhina, *Angew. Chem. Int. Ed.*, **2011**, *50*, 8090-8094.
93. D. Vijay, H. Sakurai, V. Subramanian and G. N. Sastry, *Phys. Chem. Chem. Phys.*, **2012**, *14*, 3057-3065.
94. T. Amaya and T. Hirao, *Chem. Commun.*, **2011**, *47*, 10524-10535.
95. U. D. Priyakumar and G. N. Sastry, *J. Phys. Chem. A*, **2001**, *105*, 4488-4494.
96. S. Armaković, S. J. Armaković, J. P. Šetrajčić and L. D. Džambas, *J. Mol. Model.*, **2013**, *19*, 1153-1166.
97. U. D. Priyakumar and G. N. Sastry, *J. Mol. Struc.-THEOCHEM*, **2004**, *674*, 69-75.
98. G. N. Sastry, *J. Mol. Struc.-THEOCHEM*, **2006**, *771*, 141-147.
99. T. Dinadayalane and G. N. Sastry, *Tetrahedron*, **2003**, *59*, 8347-8351.
100. U. D. Priyakumar and G. N. Sastry, *J. Org. Chem.*, **2001**, *66*, 6523-6530.

101. U. D. Priyakumar and G. N. Sastry, *J. Mol. Graph. Model.*, **2001**, *19*, 266-269.
102. G. N. Sastry, *Perkin Trans. 2*, **1993**, 1867-1871.
103. H. Sakurai, T. Daiko and T. Hirao, *Science*, **2003**, *301*, 1878-1878.
104. M. K. Chen, H. J. Hsin, T. C. Wu, B. Y. Kang, Y. W. Lee, M. Y. Kuo and Y. T. Wu, *Chem. Eur. J.*, **2014**, *20*, 598-608.
105. Y.-T. Wu, T.-C. Wu, M.-K. Chen and H.-J. Hsin, *Pure Appl. Chem.*, **2014**, *86*, 539-544.
106. Y.-T. Wu and J. S. Siegel, *Chem. Rev.*, **2006**, *106*, 4843-4867.
107. H. Sakurai, T. Daiko, H. Sakane, T. Amaya and T. Hirao, *J. Am. Chem. Soc.*, **2005**, *127*, 11580-11581.
108. D. Eisenberg, R. Shenhar and M. Rabinovitz, *Anions of Buckybowls*, John Wiley & Sons: Hoboken, **2011**.
109. S. Higashibayashi and H. Sakurai, *Chem. Lett.*, **2011**, *40*, 122128.
110. B. M. Schmidt and D.Lentz, *Chem. Lett.* , **2014**, *43*, 171–177.
111. T. Amaya and T. Hirao, *Chem. Rec.*, **2015**, *15*, 310-321.
112. S. Higashibayashi and H. Sakurai, *J. Am. Chem. Soc.*, **2008**, *130*, 8592-8593.
113. M. Saito, T. Tanikawa, T. Tajima, J. D. Guo and S. Nagase, *Tetrahedron Lett.*, **2010**, *51*, 672-675.
114. M. Saito, S. Furukawa, J. Kobayashi and T. Kawashima, *Chem. Rec.*, **2016**, *16*, 64-72.
115. T. Tanikawa, M. Saito, J. D. Guo and S. Nagase, *Org. Biomol. Chem.*, **2011**, *9*, 1731-1735.
116. Q. Tan, S. Higashibayashi, S. Karanjit and H. Sakurai, *Nat. Commun.* , **2012**, *3*, 891.
117. F. Chen, T. Tanaka and A. Osuka, *Chem. Commun.*, **2017**, *53*, 2705-2708.
118. B. M. Schmidt, B. Topolinski, S. Higashibayashi, T. Kojima, M. Kawano, D. Lentz and H. Sakurai, *Chem. Eur. J.*, **2013**, *19*, 3282-3286.
119. X. Li, Y. Zhu, J. Shao, B. Wang, S. Zhang, Y. Shao, X. Jin, X. Yao, R. Fang and X. Shao, *Angew. Chem. Int. Ed.*, **2014**, *53*, 535-538.
120. S. Wang, X. Li, X. Hou, Y. Sun and X. Shao, *Chem. Commun.*, **2016**, *52*, 14486-14489.

121. T. Tanikawa, M. Saito, J. D. Guo, S. Nagase and M. Minoura, *Eur. J. Org. Chem*, **2012**, *2012*, 7135-7142.
122. S. Furukawa, Y. Suda, J. Kobayashi, T. Kawashima, T. Tada, S. Fujii, M. Kiguchi and M. Saito, *J. Am. Chem. Soc.*, **2017**, 5787-5792.
123. X. Hou, Y. Zhu, Y. Qin, L. Chen, X. Li, H. Zhang, W. Xu, D. Zhu and X. Shao, *Chem. Commun.*, **2017**, 1546-1549.
124. T. Amaya, T. Nakata and T. Hirao, *J. Am. Chem. Soc.*, **2009**, *131*, 10810-10811.
125. T. Amaya, T. Ito, S. Katoh and T. Hirao, *Tetrahedron*, **2015**, *71*, 5906-5909.
126. T. Amaya, H. Sakane and T. Hirao, *Angew. Chem.* , **2007**, *119*, 8528-8531.
127. P. Zanello, S. Fedi, F. F. de Biani, G. Giorgi, T. Amaya, H. Sakane and T. Hirao, *Dalton Trans.*, **2009**, 9192-9197.
128. H. Sakane, T. Amaya, T. Moriuchi and T. Hirao, *Angew. Chem. Int. Ed.*, **2009**, *48*, 1640-1643.
129. S. N. Spisak, Z. Wei, A. Y. Rogachev, T. Amaya, T. Hirao and M. A. Petrukhina, *Angew. Chem.* , **2017**, *129*, 2626-2631.
130. S. Armaković, S. J. Armaković, J. P. Šetrajčić, S. K. Jaćimovski and V. Holodkov, *J. Mol. Model.*, **2014**, *20*, 1-14.
131. M. A. Hussain, D. Vijay and G. N. Sastry, *J. Comput. Chem.*, **2016**, *37*, 366-377.
132. J. A. Carrazana-García, E. M. Cabaleiro-Lago and J. Rodríguez-Otero, *Phys. Chem. Chem. Phys.*, **2017**, *19*, 10543-10553.
133. A. Reisi-Vanani, M. Hamadanian and S. N. Kokhdan, *Comp. Theor. Chem.*, **2016**, *1082*, 49-57.
134. S. Armaković, S. J. Armaković and J. P. Šetrajčić, *Int. J. Hydrog. Energy*, **2013**, *38*, 12190-12198.
135. A. Reisi-Vanani and S. Mehrdoust, *Int. J. Hydrog. Energy*, **2016**, *41*, 15254-15265.
136. S. N. Spisak, Z. Wei, N. J. O'Neil, A. Y. Rogachev, T. Amaya, T. Hirao and M. A. Petrukhina, *J. Am. Chem. Soc.*, **2015**, *137*, 9768-9771.
137. R. C. Lochan and M. Head-Gordon, *Phys. Chem. Chem. Phys.*, **2006**, *8*, 1357-1370.
138. B. Nyulasi and A. Kovács, *Chem. Phys. Lett.*, **2006**, *426*, 26-29.
139. J. G. Vitillo, A. Damin, A. Zecchina and G. Ricchiardi, *J. Chem. Phys.*, **2006**, *124*, 224308.

140. F. Pichierri, *Chem. Phys. Lett.*, **2012**, *519*, 83-88.
141. T. D. Della and C. H. Suresh, *Phys. Chem. Chem. Phys.*, **2016**, *18*, 14588-14602.
142. T. D. Della and C. H. Suresh, *ACS Omega*, **2017**, *2*, 4505-4513.
143. T. D. Della and C. H. Suresh, *Phys. Chem. Chem. Phys.*, **2017**, *19*, 5830-5838.
144. S. Grimme, *J. Comput. Chem.*, **2006**, *27*, 1787-1799.
145. S. Grimme, J. Antony, S. Ehrlich and H. Krieg, *J. Chem. Phys.*, **2010**, *132*, 154104.

Chapter 4

Anion Encapsulated Fullerenes as Large Anions and Dihydrogen Binding Affinity of Endohedral Fullerenes

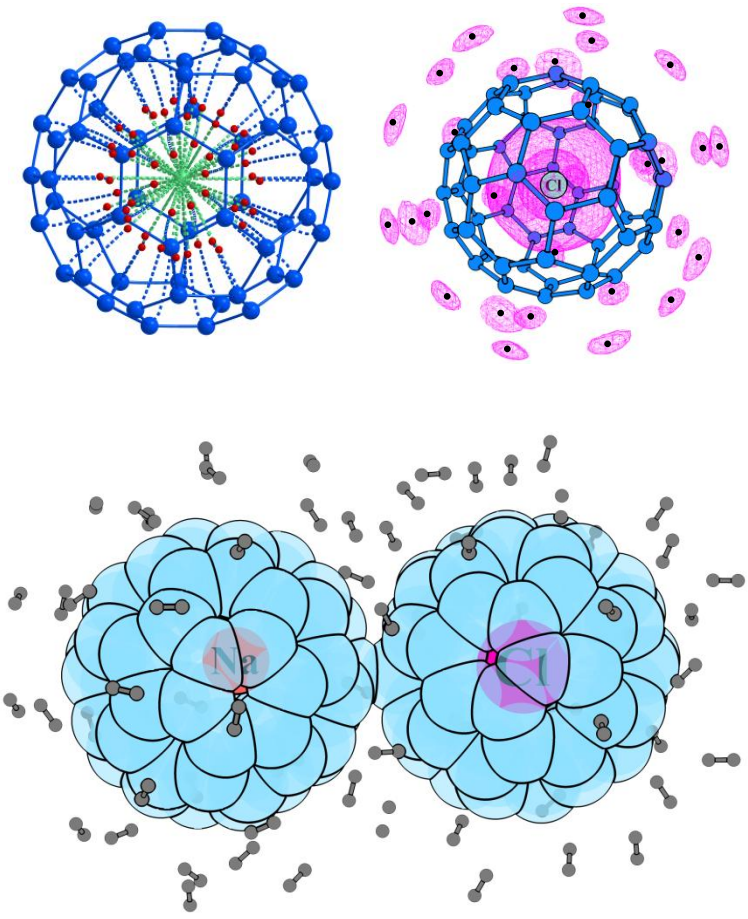

Part A: Anion Encapsulated Fullerenes as Large Anions

4.1 Abstract

The M06L/6–311++G(d,p)//M06L/6–31G(d,p) level density functional theory studies show that endohedral reaction of C_{60} with X^- (X = F, Cl, Br, OH, NH_2, NO_2, CN, and ClO) is exothermic by 37.8 - 65.2 kcal/mol. The study using a benchmark set of DFT methods corrobotrate the highly exothermic nature of the reaction. In all $X^-@C_{60}$, the occupied frontier molecular orbitals (MOs) are located on X^- while the energy levels of MOs centered on C_{60} were very similar to those of C_{60}^- radical anion. Molecular electrostatic potential (MESP) analysis of $X^-@C_{60}$ revealed that the negative character of the MESP minimum (V_{min}) on the carbon cage increases by ~72 fold compared to C_{60}, which is very similar to the enhancement in the negative MESP observed on C_{60}^- radical anion. The encapsulation leads to strong through space charge transfer between anion and fullerene cage, making the cage behave like a very large anion in a closed shell configuration. The anionic nature of the fullerene cages has been verified in the cases of larger systems such as $Cl^-@C_{70}$, $Cl^-@C_{84}$, and $Cl^-@C_{90}$. The binding of a counter cation K^+ with $X^-@C_{60}$ is found to be highly exothermic (~72 kcal/mol) and very similar to the binding of K^+ with C_{60}^- radical anion (72.9 kcal/mol) which suggests that C_{60} in $X^-@C_{60}$ behaves as a closed shell anion. Further, the noncoalent bonding in $X^-@C_{60}$ systems have been assessed by quantum theory of atoms in molecules (QTAIM) analysis.

4.2 Introduction

Endohedral fullerenes have been very much captivating to the scientific world in recent years owing to their chemical, electrochemical and optoelectronic properties.[1-9] These molecules show a wide range of applications in photovoltaic cells for solar energy conversion and storage,[10] MRI scanning as contrast agents, [11, 12] nonlinear optics,[13] *etc*. An exciting area of research has emerged in the field

of organometallic chemistry with the synthesis of fullerene-metal complexes.[8, 14-18] Heath *et al.* were successful in encapsulating lanthanum inside a variety of carbon cages, among which $C_{60}La$ being the most stable one.[19] Since then, several studies on encapsulation of various alkali and alkaline metals[20-26], transition metals[27-29] and lanthanides[25, 30-32] in fullerene has been reported. Other than metals, several neutral species such as H_2O,[33] H_2,[34] N_2,[35] CO,[35] HF[36], nitride, carbide[37-41] *etc.* have been encapsulated in a fullerene cage.

Theoretical studies are of great significance in studying the structure, stability, and chemical reactivity of various endohedral fullerenes.[42-50] The investigation on the extent of electron delocalization in C_{60} has been reported using MESP analysis.[51] Quite a few theoretical studies on endohedral systems with metals,[52-55] metal cations,[56] noble gases,[57] neutral molecules, [58-63] *etc.* have been reported in the literature. However, there are only limited studies on anion encapsulated endohedral systems. The encapsulated species influence the reactivity of the endohedral fullerene. The electronic properties of the endohedral complexes such as the complexation energy, ionization potentials, and the stability concerning internal electron transfer can be determined by the electrostatic potential at the cage center.[64] Restricted Hartree-Fock (RHF) calculations showed that monoanionic species are much stable inside C_{60} cage compared to monocationic species. The stabilization energy of $Na^+@C_{60}$ and $F^-@C_{60}$ are 6.7 and 39.8 kcal/mol, respectively at RHF using 4-31G basis set on the C atoms and DZP basis set on encapsulated species.[65] The encapsulation of cations resulted in a slight increase in the cage radii and when F^- is entrapped in C_{60} a decrease in the cage radii is noted. For $Ne@C_{60}$, destabilization energy of 0.4 kcal/mol was observed.[65] *Ab initio* studies on endohedral complexes of C_{60}, Si_{60}, and Ge_{60} with various monoatomic cations (Li^+, Na^+, K^+, and Rb^+) and anions (F^-, Cl^-, Br^-, and I^-) using the multiplicative integral approximation (MIA) and 3-21G/3-21+G basis sets revealed that stability of the complexes decreased with increase in size of the cation/anion.[66] For instance, $F^-@C_{60}$ and $Cl^-@C_{60}$ showed stabilization energy of 22.5 and 5.3 kcal/mol, respectively. The endohedral electrostatic potential, the ion-induced dipole interaction of the cation/anion

with the polarizable cage, and the electrostatic repulsions between the cation/anion and cage electron clouds are the key factors which determine the stability of the endohedral complexes. Using DFT and BOMD calculations, Ravinder and Subramanian have established the structure and energetics of various anion encapsulated fullerenes.[67] The bonding of fullerene cage with the anion has been demonstrated using atoms in molecule (AIM) analysis. According to their reports, the stability of the endohedral fullerenes depends on the size of both the anion and the fullerene cage. In a recent work by Salehzadeh *et al.* the interaction energy (E_{int}) of fullerenes with halides at MP2/6-311++G** level ranges from 62.5 to 79.2 kcal/mol.[68] Very recently, Cui *et al.* reported DFT studies on encapsulation of anions such as F^-, Cl^-, Br^-, I^-, S^{2-}, and N^{3-} in C_{60} fullerene.[69] Among the halides systems, $Cl^-@C_{60}$ emerged out as the most stable one with stabilization energy of 56.0 kcal/mol at M06-2X/6-31G(d,p) level of theory.

Herein, we propose anion encapsulated endohedral fullerenes as larger anions. Theoretical calculations using DFT methods on the structure and properties of anions such as F^-, Cl^-, Br^-, OH^-, NH_2^-, CN^-, ClO^-, NO_2^- encapsulated in C_{60} fullerenes have been carried out. With the aid of molecular orbital analysis, interaction with cation, molecular electrostatic potential (MESP) analysis and the quantum theory of atoms in molecules (QTAIM), we show that anion encapsulated endohedral fullerene systems behave as larger anions as the electron density of the encapsulated anion is transferred to the surface of the cage.

4.3 Computational Details

All calculations have been done at M06L/6-311++G(d,p)//M06L/6-31G(d,p) level of density functional theory[70, 71] as implemented in the Gaussian 09 suite of programs.[72] In a wide-ranging benchmark study reported from our group, the M06L method has been chosen as the best-performing one among the 382 tested functionals for calculating the geometry and interaction energy of noncovalent dimers close to the CCSD accuracy.[73] Further, to substantiate the accuracy of the results, a benchmark

study has been done using a set of DFT/6-311++G(d,p) methods along with Grimme's dispersion correction.[74, 75] The selected DFT methods are M06L-D3, M062X, M062X-D3, B3LYP, B3LYP-D3, B97D, B97-D3, BP86-D3. The vibrational frequency analysis has been done to confirm the optimized geometries as the energy minima. The interaction energy, E_{int} has been calculated using the supermolecule approach with counterpoise correction to basis set superposition error (BSSE).[76] The electron delocalization in the complex has been analyzed using MESP,[77-79] and the topological study of electron density has been done by locating (3, -1) bond critical points (bcp) between interacting atoms in Bader's QTAIM analysis using AIMAll package.[80]

4.4 Results and Discussion

4.4.1 Structure and Energetics of $X^-@C_{60}$ systems

The optimized geometries of various anion encapsulated endohedral fullerenes ($X^-@C_{60}$, X = F, Cl, Br, OH, NH_2, NO_2, CN, and ClO) are represented in Figure 4.1. $F^-@C_{60}$, shows an off-centered orientation of F^- with interaction distance (d_{int}) to the nearest carbon 2.78 Å. For $Cl^-@C_{60}$ and $Br^-@C_{60}$, the anion is at the centre of the cage with d_{int} 3.53 Å. A very similar observation has been reported by Cui and co-workers in a recent study on endohedral fullerenes with d_{int} 2.68 Å for F^- and 3.54 Å for both Cl^- and Br^-.[69] For other endohedral fullerenes such as $OH^-@C_{60}$, $NH_2^-@C_{60}$, $NO_2^-@C_{60}$, $CN^-@C_{60}$ and $ClO^-@C_{60}$, two or more atoms present in the anions are oriented toward particular carbon centers on the C_{60} cage. The shortest d_{int} of each atom with the carbon center is depicted in Figure 4.1. The interaction energy (E_{int}) of these endohedral systems are in the range 37.8 – 65.2 kcal/mol following the increasing order of NO_2^- < ClO^- < CN^- < Br^- < F^- < Cl^- <OH^- < NH_2^- (Table 4.1). These values suggest that encapsulation of anions in fullerene leads to formation of highly stable endohedral complexes. The benchmark study on E_{int} of $Cl^-@C_{60}$ using various methods ascertains the reliability of E_{int} calculated using M06L method. The E_{int} calculated at M06L-D3, M062X, M062X-D3, B97D, and BP86-D3 agreed well with the M06L results. B3LYP-D3 and B97-D3 methods showed a deviation of 12.3 and 13.4 kcal/mol, respectively from the M06L results.

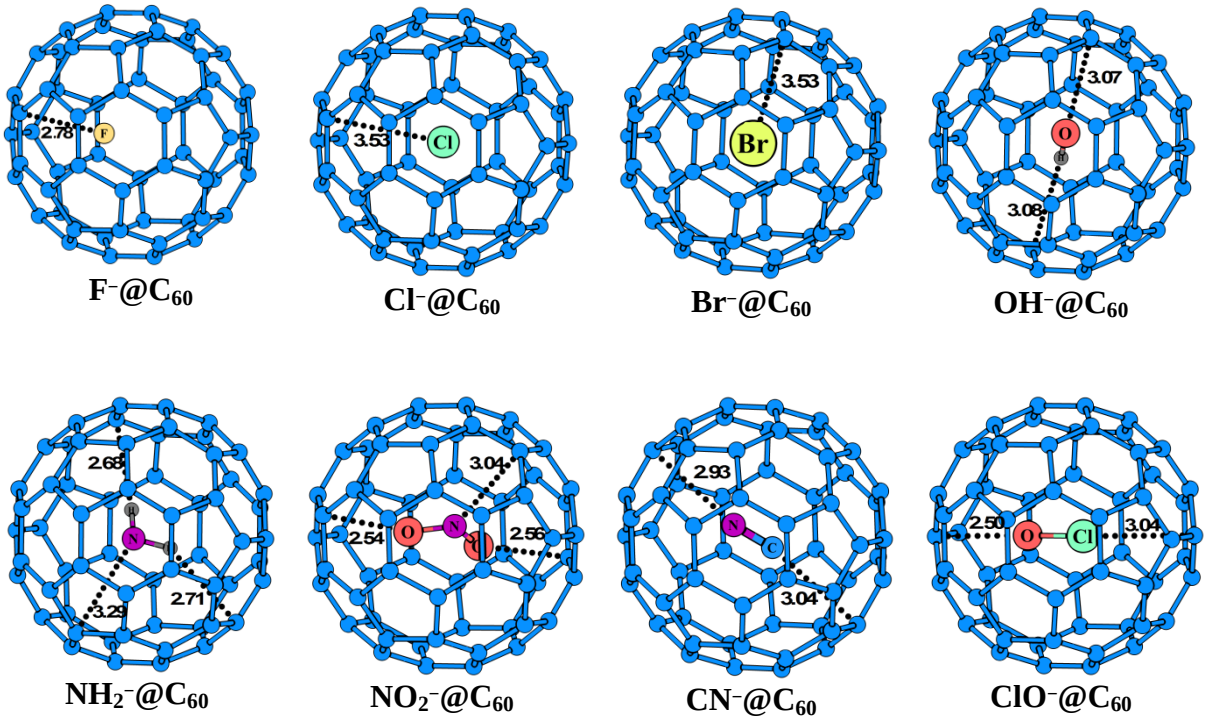

Figure 4.1 Optimized geometries of $X^-@C_{60}$ endohedral fullerene systems at M06L/6-31G(d,p) level. Bond distances are in Å.

Table 4.1 BSSE corrected E_{int} (kcal/mol) of $X^-@C_{60}$ at the M06L/6311++G(d,p)//M06L/6-31G(d,p) level

System	E_{int}
$F^-@C_{60}$	57.3
$Cl^-@C_{60}$	62.9
$Br^-@C_{60}$	53.0
$OH^-@C_{60}$	64.0
$NH_2^-@C_{60}$	65.2
$NO_2^-@C_{60}$	37.8
$CN^-@C_{60}$	52.5
$ClO^-@C_{60}$	43.0

However, the E_{int} at B3LYP method is found to be 28.2 kcal/mol, deviating very much from E_{int} at all other methods. A similar observation was noted in a work by Salehzadeh and coworkers in which the E_{int} using B3LYP method showed a very

high deviation form results at PBE and MP2 methods.[68] This shows that B3LYP is not a reliable method for the present study.

Table 4.2 BSSE corrected E_{int} (kcal/mol) of $Cl^-@C_{60}$ using different methods

Method	E_{int}
M06L	62.9
M06L-D3	62.3
M062X	61.4
M062X-D3	61.9
B3LYP	28.2
B3LYP-D3	50.6
B97D	59.5
B97-D3	49.5
BP86-D3	57.4

*Optimization using 6-31G(d,p) and energy calculation using 6-311++G(d,p) basis sets in all the cases.

4.4.2 Molecular Orbital Analysis

The molecular orbital analysis shows that the energies of fullerene type molecular orbitals of anion encapsulated endohedral fullerenes are comparable with that of C_{60}^- radical anion. Energy level diagram of $Cl^-@C_{60}$ is given in Figure. 2 as a representative example while selected energy levels of all $X^-@C_{60}$ systems are given in Table 4.3. The fullerene orbitals in C_{60}^- and $X^-@C_{60}$ are raised in energy compared to bare C_{60}. The energies of LUMO, HOMO-1, and HOMO-2 of anion encapsulated $X^-@C_{60}$ are analogous to C_{60}^-. For instance, the energies of LUMO, HOMO-1 and HOMO-2 of C_{60}^- are -4.0264, -2.7437, and -0.9765 eV respectively. The corresponding energy values for $Cl^-@C_{60}$ orbitals are -3.9207, -2.6476, and -0.8674 eV respectively. The HOMO of $X^-@C_{60}$ is localized on anion while LUMO lies on the fullerene cage. Figure 3 depicts the HOMO and LUMO of $Cl^-@C_{60}$. Both HOMO and LUMO are a set of three degenerate orbitals. HOMO-1 and HOMO-2 are a set of five and nine degenerate orbitals, respectively.

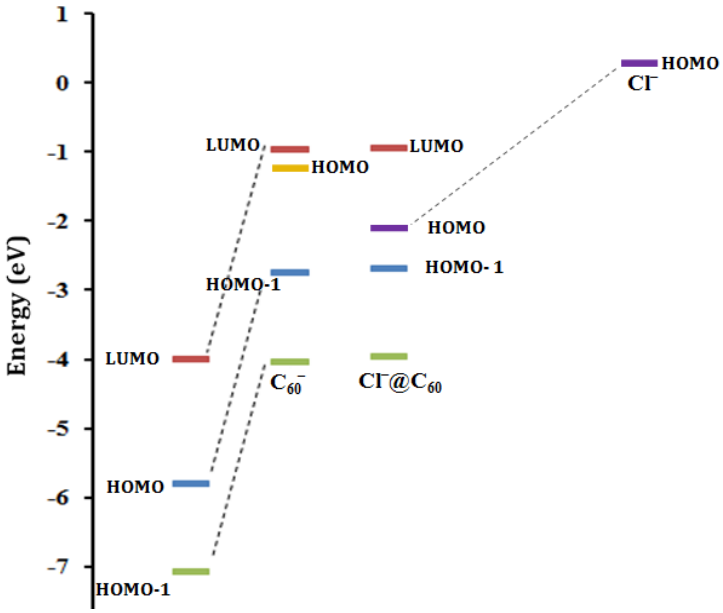

Figure 4.3 Molecular orbital energy levels of C_{60}, C_{60}^-, and $Cl^-@C_{60}$.

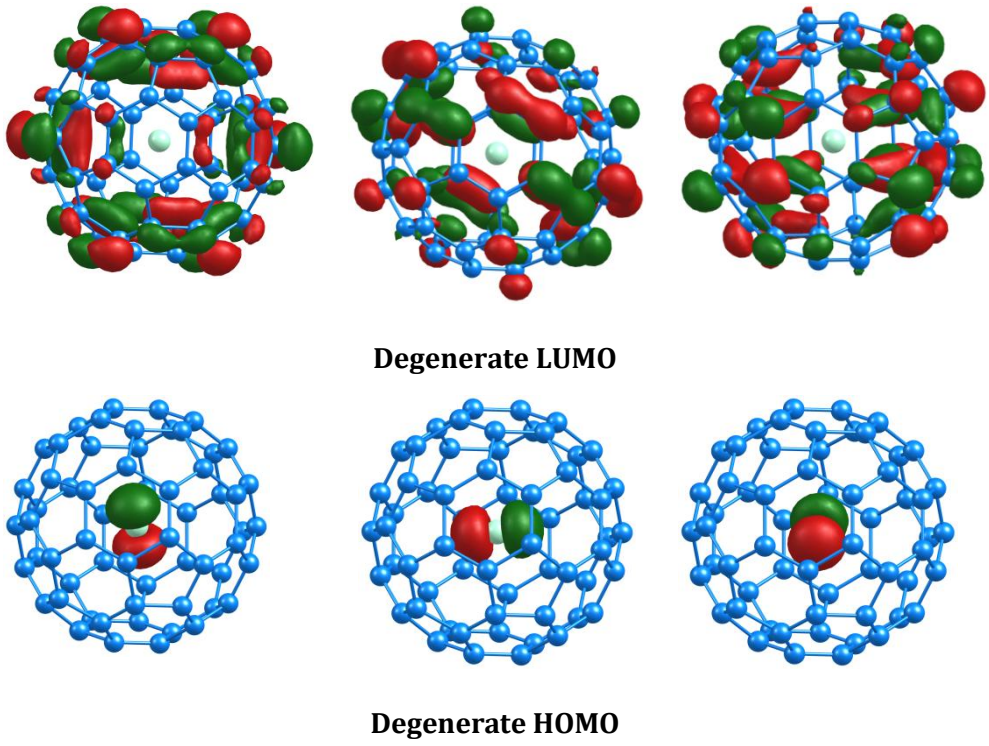

Figure 4.3 HOMO and LUMO of $Cl^-@C_{60}$.

Even though the HOMO lies with the encapsulated anion, it may not be accessible for chemical reactions as the fullerene cage protects the anion. In other words, the reactivity of the electron rich $X^-@C_{60}$ is not decided by HOMO but inner molecular orbitals.

Table 4.3 Molecular orbital energy levels in eV of C_{60}, C_{60}^-, and $X^-@C_{60}$

System	HOMO-2	HOMO-1	HOMO	LUMO
C_{60}	-8.814	-7.079	-5.798	-3.991
C_{60}^-	-4.026	-2.744	-1.138	-0.977
$F^-@C_{60}$	-3.926	-2.646	-1.714	-0.882
$Cl^-@C_{60}$	-3.921	-2.648	-2.432	-0.867
$Br^-@C_{60}$	-3.936	-2.663	-2.081	-0.887
$OH^-@C_{60}$	-3.924	-2.644	-1.101	-0.887
$NH_2^-@C_{60}$	-3.947	-2.666	-1.084	-0.938
$NO_2^-@C_{60}$	-3.955	-2.678	-1.381	-0.941
$CN^-@C_{60}$	-3.922	-2.649	-2.319	-0.892
$ClO^-@C_{60}$	-3.950	-2.107	-1.265	-0.906

4.4.3 MESP Analysis

Figure 4 represents the MESP mapped on the isodensity surface 0.003 au for C_{60}, C_{60}^-, and $Cl^-@C_{60}$. The π-electron density of fullerene is distributed over the surface of the cage. The dark blue pattern observed for C_{60}^- and $Cl^-@C_{60}$ MESP indicates very similar electron dense nature of these systems while the pale green surface seen for C_{60} indicates only a feeble negative MESP. The electron dense nature of carbon cage is revealed in MESP for all $X^-@C_{60}$ species under study. A quantification of the MESP feature is obtained by locating the most negative MESP value (V_{min}) on the fullerene cage. V_{min} of $X^-@C_{60}$ species lies in the range -62.1 – -64.8 kcal/mol, which is very close to the V_{min} -63.5 kcal/mol observed for the radical anion C_{60}^-. The V_{min} of neutral C_{60} is -0.9 kcal/mol

indicating a very low electron density distribution compared to $X^-@C_{60}$ and C_{60}^-. These results suggest that irrespective of the nature of the anion encapsulated in the fullerene, the electron density distribution on the cage is almost the same for $X^-@C_{60}$ species.

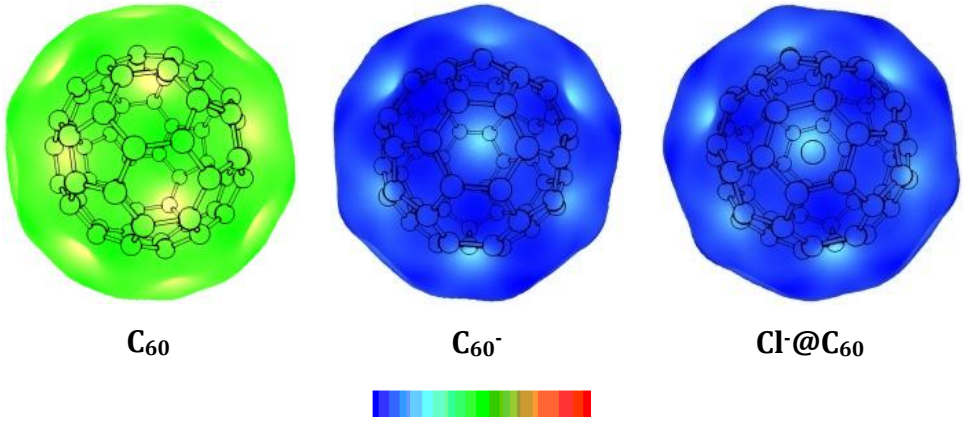

Figure 4.4 MESP of C_{60}, C_{60}^-, and $Cl^-@C_{60}$ plotted at an isosurface value of 0.003 au. The color coding from blue to red indicates MESP values in the range -0.1 – +0.1 au.

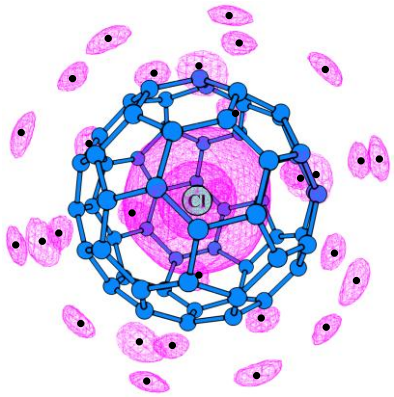

Figure 4.5 MESP of $Cl^-@C_{60}$ at -60.2 kcal/mol at the M06L/6-311++G(d,p) level.

The MESP isosurface of $Cl^-@C_{60}$ at -60.0 kcal/mol is depicted in Figure 4.5 to show the precise locations of the electron rich regions in the system. The negative MESP is observed on the central anion as well as ~1.82 Å above the midpoint region of all the CC bonds at 6-6 ring fusion. The V_{min} points located above the CC bonds (total 30) are represented as black dots in Figure 4.5. They indicate that CC bonds at 6-6 ring fusion with distance 1.394 Å have more localized π-character than the CC bonds at 6-5 ring fusions (1.445 Å). Very similar features are observed for all other $X^-@C_{60}$ systems. Nearly same V_{min} value observed for C_{60}^- and $X^-@C_{60}$ (Table 4.4) suggest that

encapsulation of anion in the fullerene cage can lead to the transfer of excess electron density on the anion to the fullerene cage. Since anion and fullerene cage are connected through only weak noncovalent interactions, the transfer of electron density from anion to the fullerene cage may be considered as a through-space effect. Since the $X^-@C_{60}$ represents a closed shell system, it may exist as a chemically stable anionic entity than the fullerene radical anion.

Table 4.4 V_{min}(cage) in kcal/mol of $X^-@C_{60}$ endohedral fullerene systems at the M06L/6-311++G(d,p) level

System	V_{min} (cage)
C_{60}	-0.88
C_{60}^-	-63.5
$F^-@C_{60}$	-64.8
$Cl^-@C_{60}$	-62.1
$Br^-@C_{60}$	-62.1
$OH^-@C_{60}$	-63.8
$NH_2^-@C_{60}$	-63.4
$NO_2^-@C_{60}$	-63.4
$CN^-@C_{60}$	-62.9
$ClO^-@C_{60}$	-63.9

4.4.4 Interaction with K^+ Cation

The interaction energy of K^+ ($E_{int\text{-}cation}$) with C_{60} and C_{60}^- is 15.3 and 72.9 kcal/mol, respectively. The observed five-fold enhancement in E_{int} for the anion compared to the neutral form can be attributed to the excess electron density in the former. All the $X^-@C_{60}$ systems too show approximately five-fold increase in $E_{int\text{-}cation}$ (70.3 – 73.3 kcal/mol) compared to C_{60} suggesting that the fullerene cage of these systems behave very similar to C_{60}^- (Table 4.5). The observed interaction distance of K^+ with the nearest carbon in C_{60} and C_{60}^- are 3.19, and 2.98 Å, respectively (Figure 4.6). The interaction distance ($d_{int\text{-}cation}$) in $X^-@C_{60}$ systems

are in the range 2.97 – 3.00 Å. The drop in interaction distance for $X^-@C_{60}$ compared to C_{60} suggests the anionic nature of endohedral systems.

Table 4.5 BSSE corrected $E_{int\text{-}cation}$ (kcal/mol) and $d_{int\text{-}cation}$ (Å) of $X^-@C_{60}$ with K^+ at the M06L/6-311++G(d,p)// M06L/6-31G(d,p) level

System	$E_{int\text{-}cation}$	$d_{int\text{-}cation}$
C_{60}	15.3	3.19
C_{60}^-	72.9	2.98
$F^-@C_{60}$	73.0	2.98
$Cl^-@C_{60}$	70.3	3.00
$Br^-@C_{60}$	71.7	2.97
$OH^-@C_{60}$	71.8	3.00
$NH_2^-@C_{60}$	72.7	2.98
$NO_2^-@C_{60}$	71.9	2.98
$CN^-@C_{60}$	72.4	2.99
$ClO^-@C_{60}$	73.3	2.99

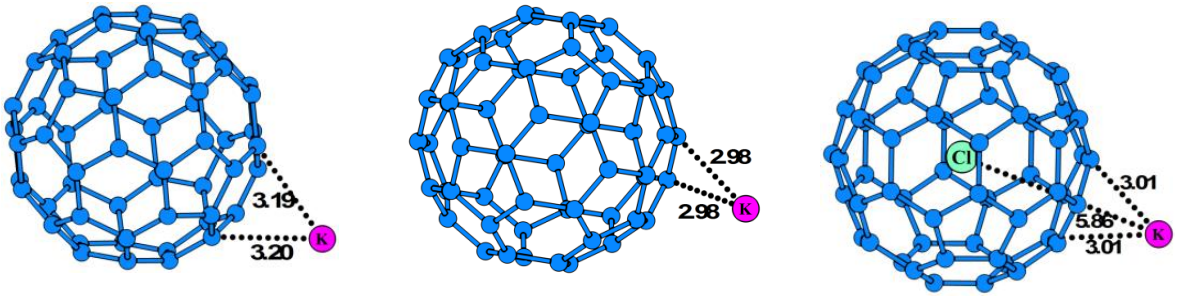

(a) C_{60}...K^+ **(b) C_{60}^-...K^+** **(c) $Cl^-@C_{60}$...K^+**

Figure 4.6 Interaction of C_{60}, C_{60}^-, and $Cl^-@C_{60}$ with K^+ counter cation. Bond distances are in Å.

4.4.5 QTAIM Analysis

The QTAIM molecular plots of $X^-@C_{60}$ systems are shown in Figure 4.7. For all the $X^-@C_{60}$ complexes, bcps are observed between the anion and carbon atoms. In $Cl^-@C_{60}$ and $Br^-@C_{60}$ where the anion is located at the center of the cage, bcps are located between the anion and each of the carbon atoms of C_{60} cage (total 60

bcps). In all other endohedral systems, only a fewer number of bcps are noted; 1, 11, 9, 3, 2 and 8, respectively for $F^-@C_{60}$, $OH^-@C_{60}$, $NH_2^-@C_{60}$, $NO_2^-@C_{60}$, $CN^-@C_{60}$, and $ClO^-@C_{60}$ systems. The electron densities at these bcps (ρ_{bcp}) lie in the range 0.0039 - 0.0225 au. The positive Laplacian values of electron density ($\nabla^2\rho_{bcp}$ in the range 0.0160 - 0.0660 au) indicate the noncovalent nature of the interactions.

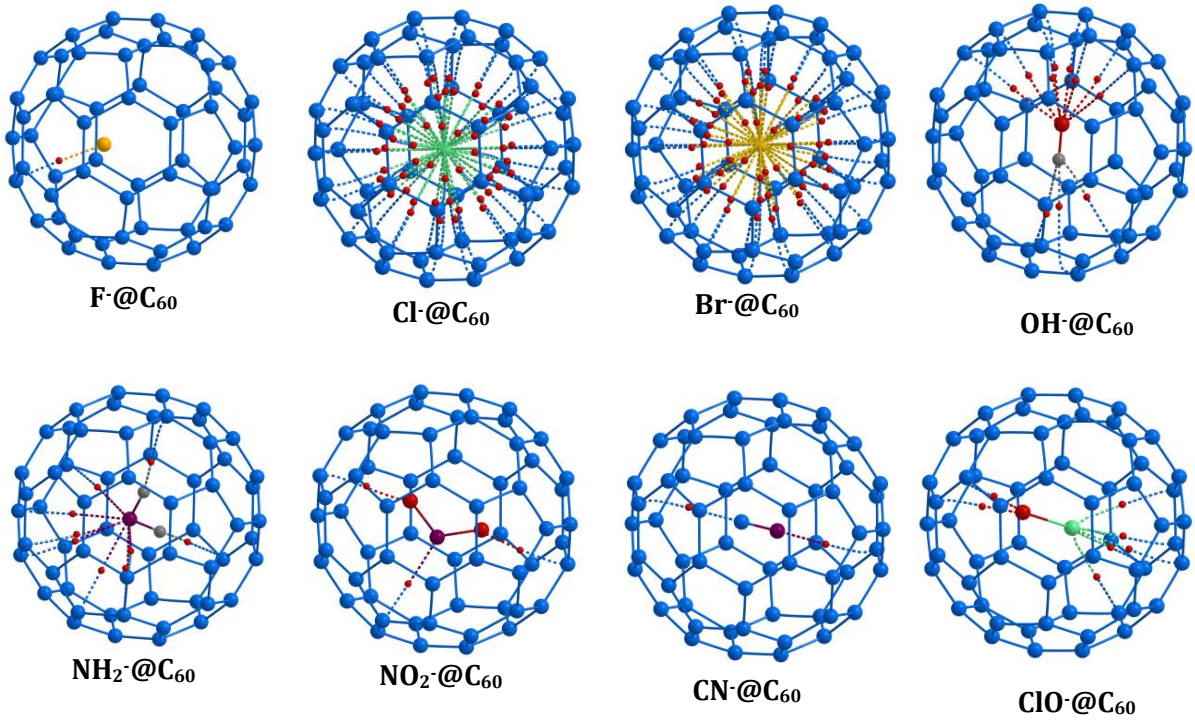

Figure 4.7 QTAIM graphs of $X^-@C_{60}$ systems at the M06L/6-311++G(d,p) level.

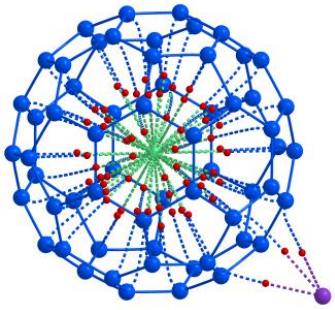

Figure 4.8 QTAIM graphs of $Cl^-@C_{60}...K^+$ at the M06L/6-311++G(d,p) level.

Table 4.6 ρ_{bcp} (au) of $X^-@C_{60}...K^+$ at the M06L/6-311++G(d,p) level

System	ρ_{bcp} (au)
C_{60}	0.0081
C_{60}^-	0.0123
$F^-@C_{60}$	0.0119
$Cl^-@C_{60}$	0.0116
$Br^-@C_{60}$	0.0127
$OH^-@C_{60}$	0.0118
$NH_2^-@C_{60}$	0.0120
$NO_2^-@C_{60}$	0.0114
$CN^-@C_{60}$	0.0121
$ClO^-@C_{60}$	0.0115

Figure 4.8 illustrates the QTAIM molecular plot of the $Cl^-@C_{60}...K^+$ system. The counter cation K^+ shows three bcps with the fullerene cage whereas a bond path between K^+ and anion is not observed. The ρ_{bcp} of $X^-@C_{60}...K^+$ interactions (Table 4.6) is in the range 0.0114 - 0.0127 au which is comparable to the ρ_{bcp} of $C_{60}^-...K^+$ (0.0123 au). These values are significantly higher than the ρ_{bcp} for $C_{60}...K^+$ interaction 0.0081 au. The QTAIM analysis reveals that the anionic nature of $X^-@C_{60}$ systems is similar to that of C_{60}^- radical anion.

4.4.6 Large Endohedral Systems

Figure 4.9 depicts the optimized geometries of $Cl^-@C_{70}$, $Cl^-@C_{84}$, and $Cl^-@C_{90}$ systems showing the d_{int} of Cl^- with the nearest carbon of the cage. In the stable geometries of $Cl^-@C_{70}$ and $Cl^-@C_{84}$, the anion is at off-center position whereas in $Cl^-@C_{90}$, Cl^- is at the center of the cage. The E_{int} of larger endohedral systems such as $Cl^-@C_{70}$, $Cl^-@C_{84}$, and $Cl^-@C_{90}$ is 59.7, 56.1, and 54.0 kcal/mol, respectively. A linear decrease in E_{int} is noted with an increase in cage size (Figure 4.10). For Cl^- anion, C_{60} anion shows the maximum stabilization energy compared to larger cages such as C_{70}, C_{84}, and C_{90}. The larger endohedral systems also possess a high negative V_{min} (cage) comparable to that of C_{60} and C_{60}^- radical anion indicating

the projection of electron density of the encapsulated anion to the cage surface (Table 4.7). Thus, these cages behave as much larger anions.

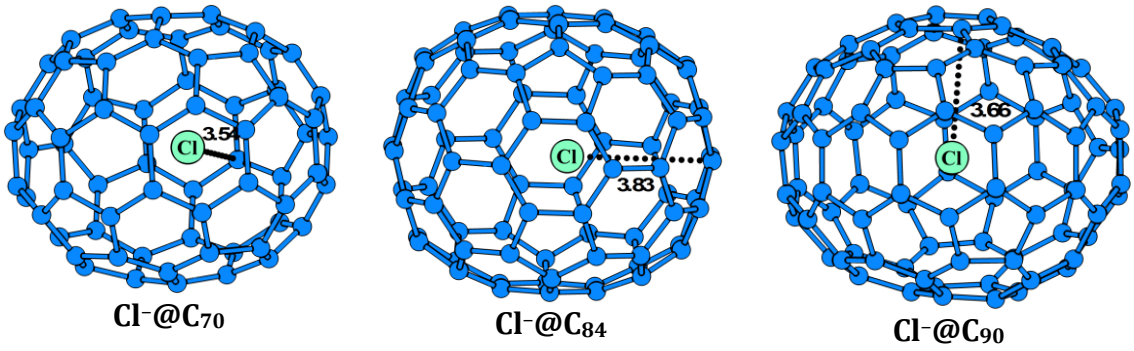

Figure 4.9 Optimized geometries of $Cl^-@C_n$ systems at the M06L/6-31G(d,p) level. Bond distances are in Å.

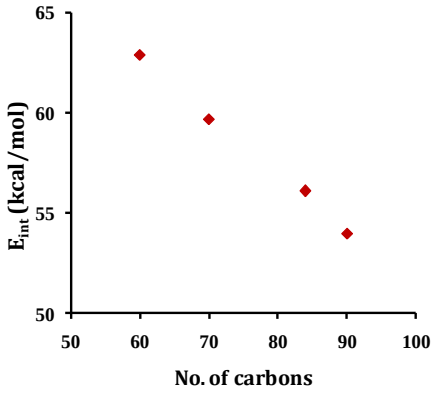

Figure 4.10 Variation of E_{int} with number of carbons in fullerene cage.

Table 4.7 E_{int} and V_{min} (cage) in kcal/mol of $Cl^-@C_n$ systems at the M06L/6-311++G(d,p)//M06L/6-31G(d,p) level

System	E_{int}	V_{min} (cage)
$Cl^-@C_{60}$	62.9	-62.1
$Cl^-@C_{70}$	59.7	-59.2
$Cl^-@C_{84}$	56.1	-55.9
$Cl^-@C_{90}$	54.0	-57.6

4.5 Conclusions

In summary, using DFT methods, we have shown that anion encapsulated endohedral fullerenes behave as large anion with the transfer of electron density

form the anion to the fullerene cage. Anions are stable inside the fullerene cage with significant interaction energies. Not only C_{60}, but larger cages such as C_{70}, C_{84}, and C_{90} have been analyzed for their anion encapsulation property. The molecular orbital analysis substantiates the anionic nature of anion encapsulated endohedral systems. The extent delocalization electron density onto the cage surface of $X^-@C_{60}$ systems has been revealed through MESP analysis. The strength of the interaction of $X^-@C_{60}$ with K^+ counter cation establishes that these systems behave more or less like large anions. The noncovalent nature of the interactions is revealed by QTAIM analysis. The properties of $X^-@C_{60}$ are independent of the encapsulated anion. These larger anions could be proposed as materials for gas storage.

Part B: Endohedral Fullerenes as Three-Dimensional Hydrogen Storage Materials

4.6 Abstract

Anion and cation encapsulated fullerenes, and their ion-pair systems have been proposed as potential hydrogen storage materials. Density functional theory calculations at M06L/6–311++G(d,p)//M06L/6-31G(d,p) level reveal that $Cl^-@C_{60}$, $Na^+@C_{60}$, $Na^+@C_{60}Cl^-@C_{60}$ systems show a notable H_2 binding capacity with 9 – 11 wt% of H_2. The calculated interaction energy (E_{int}) is 45.1, 44.3, and 71.8 kcal/mol for $Cl^-@C_{60}(H_2)_{40}$, $Na^+@C_{60}(H_2)_{40}$, and $Na^+@C_{60}...Cl^-@C_{60}(H_2)_{66}$. The electron delocalization in the H_2 bonded complex is evaluated using molecular electrostatic potential (MESP) analysis. The electron–rich and electron-deficient regions are also visualized by MESP topography. The $C_{60}...H_2$ noncovalent interactions are characterized by locating bond critical points (bcp) in the quantum theory of atoms in molecules (QTAIM) analysis. Also, secondary $H_2...H_2$ interactions that enhance the stability of the complex are noted. Our studies show that such charge separated salt complexes can be utilized for developing novel hydrogen storage systems.

4.7 Introduction

The outstanding physical and chemical properties make endohedral fullerene very much attractive in the fields of chemistry, materials science, pharmaceutical chemistry, and nanotechnology.[17, 81-84] Owing to lightweight, high surface area, porous structure, physisorption properties, *etc.* carbon-based materials have procured much interest as storage systems.[85-92] Pt-C_{60} synthesized by Wang and Tu could adsorb 1.6 wt% of H_2 at high temperatures.[93] The spectroscopic studies showed charge transfer from Pt to the C_{60} cage. In another experimental work reported by Teprovich Jr *et al.* the H_2 adsorption capacities of Na-C_{60} and Li-C_{60} were found to be 1.5 wt% and 1.2 wt%, respectively.[94] The same group reported 5 wt% of H_2 reversible adsorption in Li-doped

fullerene with a Li:C_{60} mole ratio 6:1 at ~270 °C.temperature.[95] Mauron *et al.* synthesized Na intercalated fullerene and its hydrogen absorption and desorption properties.[96] This system could reversibly adsorb 3.5 wt% of H_2 at 200 bar and 200 °C. The obtained samples were investigated by X-ray, *in-situ* neutron powder diffraction, Raman, and FT-IR spectroscopy.

Several theoretical studies on hydrogen storage capacity of fullerenes and their various modifications have been reported. *Ab initio* study reported by Chandrakumar and Ghosh showed that alkali metal doped fullerene systems possess enhanced H_2 binding ability.[97] Na-doped systems with eight metal centers could hold 48 H_2 molecules with ~ 9.5 wt%. In another work reported from the same group transition metal doped porphyrin-like porous fullerene, $C_{24}N_{24}$ was proposed a potential storage material with an uptake of 24 H_2 with ~ 5.1 wt%.[98] First principle studies of hydrogen storage by Sun *et al.* predicted ~ 9 wt% uptake by $Li_{12}C_{60}$ with interaction energy per H_2 ($E_{int/H2}$) 1.72 kcal/mol.[99] Molecular and dissociative adsorption of H_2 on transition metal (Sc, Ti, V, Cr) decorated C_{60} revealed the uptake of 56 H_2 with ~7.5 wt%.[100] Yoon *et al.* reported a first-principle DFT study on the H_2 storage capacity of positively and negatively charged fullerenes C_n (n = 20 – 82).[101] The interaction energy, E_{int} was found to be in the range 4.2 - 7.4 kcal/mol. Compared to neutral fullerenes, 2-5 fold increase in E_{int} was noted for the charged systems (charge, q = -2 to +6) These charged systems showed ~ 8.0 wt% of H_2 when saturated with H_2.

However, to date no theoretical studies have been reported on the study of the interaction of H_2 with anion or cation encapsulated fullerenes. In Part A of this chapter, we have discussed that anion encapsulated fullerenes behave as large anions as the electron density on the anion is transferred to the fullerene cage. Herein, we report the interaction of H_2 with $Cl^-@C_{60}$ and $Na^+@C_{60}$ systems. The H_2 interaction of the endohedral ion pair system $Na^+@C_{60}...Cl^-@C_{60}(H_2)_{66}$ is also studied, and this salt system in which the cation and anion are separated and shielded by fullerene cages is proposed a promising H_2 storage material.

4.8 Computational Details

All calculations have been done at M06L/6-311++G(d,p)//M06L/6-31G(d,p) level as implemented in the Gaussian 09 suite of programs.[72] The optimized geometries are confirmed as energy minima by vibrational frequency analysis. The interaction energy, E_{int} has been calculated using The supermolecule approach with counterpoise correction to basis set superposition error (BSSE) has been used to calculate the interaction energy (E_{int}) of complexes.[76] The electron delocalization in the complex has been analyzed using MESP,[77-79] and the topological study of electron density has been done by locating (3, -1) bond critical points (bcp) between interacting atoms in Bader's QTAIM analysis using AIMAll package.[80]

4.9 Results and Discussion

4.9.1 Interaction of H_2 with $Cl^-@C_{60}$

We have systematically optimized the $Cl^-@C_{60(}H_2)_n$ complexes with n = 1 – 30 with the addition of one H_2 in each step. The $Cl^-@C_{60(}H_2)_{40}$ complex in which the coordination is almost saturated has also been optimized. The geometries of $Cl^-@C_{60}(H_2)$ and $Cl^-@C_{60}(H_2)_{40}$ are represented in Figure 4.11. In $Cl^-@C_{60}(H_2)$ an end-on interaction of H_2 with $Cl^-@C_{60}$ observed. Previous reports on the interaction of H_2 with anions suggest the resultant complex with end-on coordination where the LUMO of H_2 accepts electron density from the HOMO of anion.[102-108] The Cl…H interaction distance is 6.16 Å, and C…H interaction distance (a distance of H_2 to the nearest carbon) is 2.79 Å. The H-H bond length is found to be 0.75 Å. These distances do not vary much in complexes with more number of H_2. In $Cl^-@C_{60}(H_2)_{40}$, H-H bond length is ~0.75 Å, and Cl…H and C…H distances are in the range 6.0 – 6.5 Å and 2.8 – 3.2 Å, respectively. The E_{int} and $E_{int/H2}$ of $Cl^-@C_{60}(H_2)_n$ are given in Table 4.8. For complexes with n = 1- 6, an increase in E_{int} and $E_{int/H2}$ is observed. The E_{int} increase from 0.2 to 6.6 kcal/mol and $E_{int/H2}$ from 0.2 to 6.6 kcal/mol. For complexes with n = 7 - 40 E_{int} increases from 7.0 – 45.1 kcal/mol and $E_{int/H2}$ in the range 0.9 – 1.3 kcal/mol. The $E_{int/H2}$ maintains a constant range even for larger values of n. The calculated weight percent of H_2 in $Cl^-@C_{60}(H_2)_{40}$ is 10.7 wt% proposing this system as hydrogen storage material.

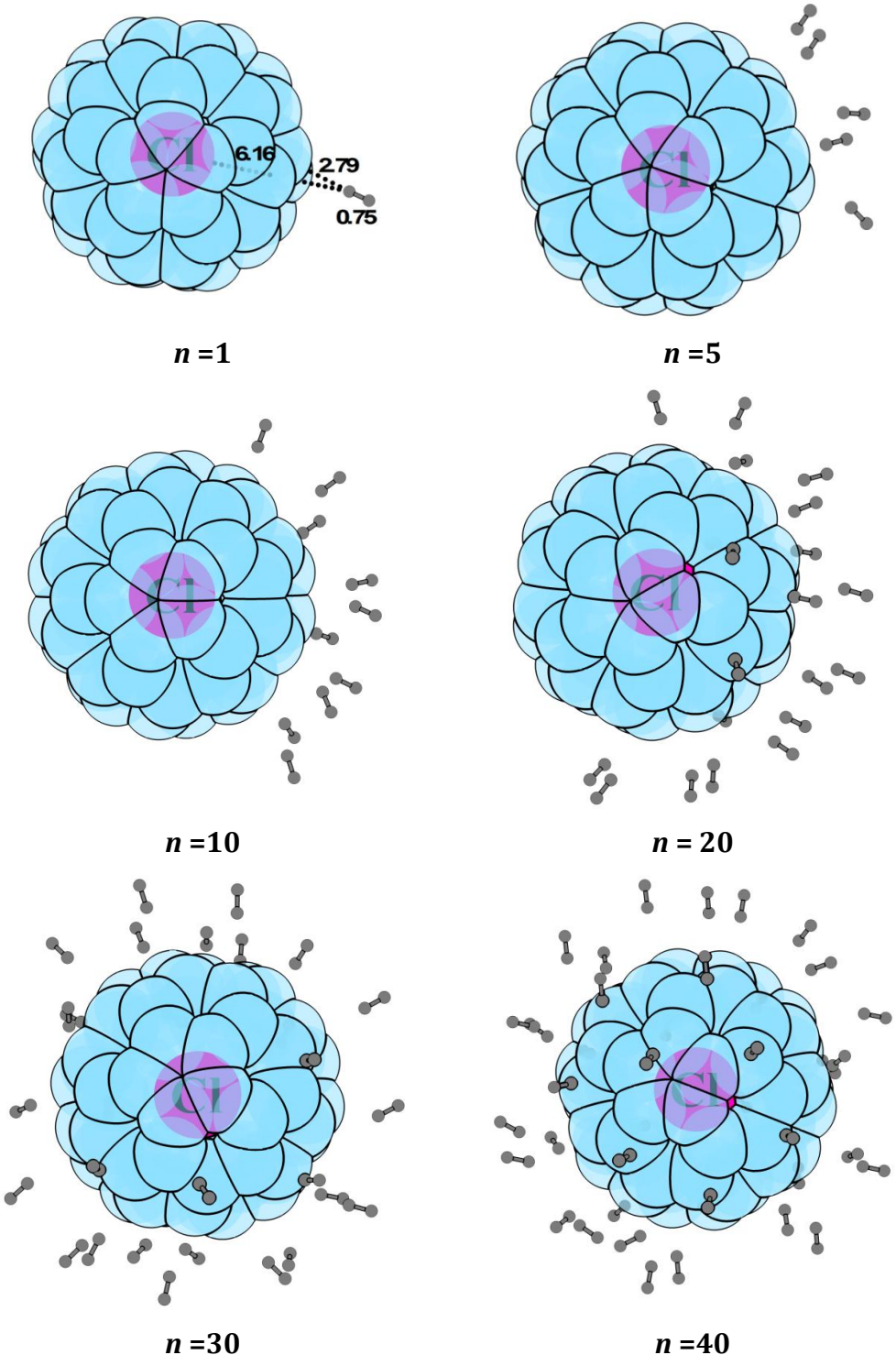

Figure 4.11 Optimized geometries of $Cl^{-}@C_{60}(H_2)_n$ at the M06L/6-31G(d,p) level. Bond distances are in Å.

Table 4.8 BSSE corrected E_{int} and $E_{int/H2}$ in kcal/mol of $Cl^-@C_{60}(H_2)_n$ at the M06L/6-311++G(d,p) level

n	E_{int}	$E_{int/H2}$	*n*	E_{int}	$E_{int/H2}$
1	0.2	0.2	17	17.7	1.0
2	0.8	0.4	18	18.3	1.0
3	1.3	0.4	19	19.2	1.0
4	2.6	0.7	20	22.1	1.1
5	4.2	0.8	21	22.4	1.1
6	6.6	1.1	22	21.9	1.0
7	7.0	1.0	23	23.0	1.0
8	7.5	0.9	24	24.4	1.0
9	9.8	1.1	25	26.1	1.0
10	11.3	1.1	26	27.3	1.1
11	11.3	1.0	27	28.5	1.1
12	12.5	1.0	28	30.2	1.1
13	16.8	1.3	29	30.6	1.1
14	14.5	1.0	30	31.2	1.0
15	15.2	1.0	40	45.1	1.1
16	15.9	1.0	-	-	-

4.9.2 Interaction of H_2 with $Na^+@C_{60}$

The H_2 binding capacity of cation encapsulated fullerene, $Na^+@C_{60}$ has been studied systematically from *n* = 1 to 30 with the addition of one H_2 in each step similar to the study of $Cl^-@C_{60}(H_2)_n$ complexes. The optimized geometries of $Na^+@C_{60}(H_2)$ depicted in Figure 4.12 suggest a side–on the coordination of H_2 oriented toward the center of a six-membered ring of $Na^+@C_{60}$. The formation of T-shaped complexes with side-on coordination of H_2 with cationic systems has been reported previously.[106] The H-H bond length is found to be 0.75 Å. The Na…H interaction distance is 6.10 Å, and C…H interaction distance is 3.49 Å. Not much variation in interaction distances is observed with *n* increasing from 1 to 40.

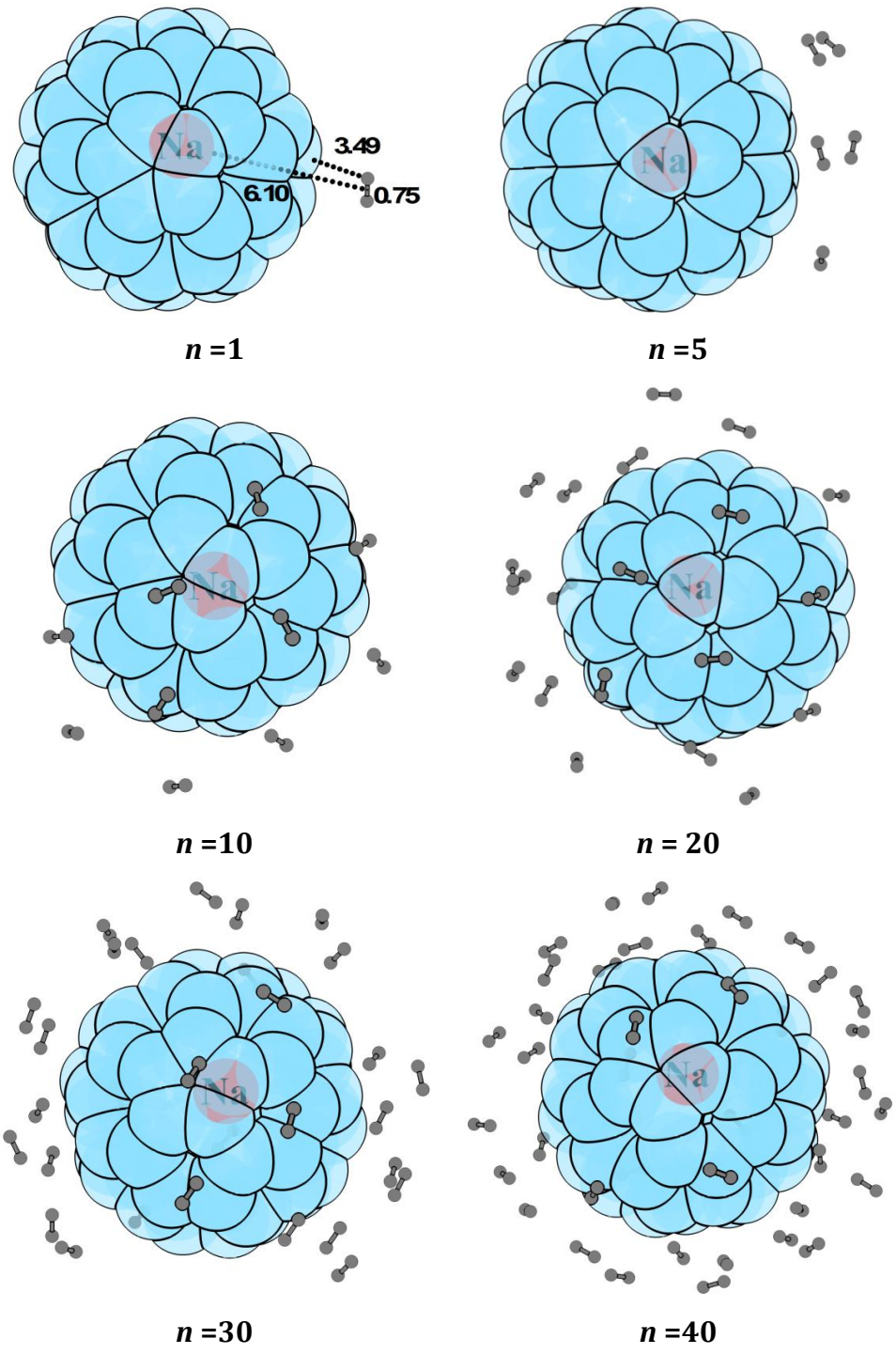

Figure 4.12 Optimized geometries of $Na^+@C_{60}(H_2)_n$ at the M06L/6-31G(d,p) level. Bond distances are in Å.

Table 4.9 BSSE corrected E_{int} and $E_{int/H2}$ in kcal/mol of $Na^+@C_{60}(H_2)_n$ at the M06L/6-311++G(d,p) level

n	E_{int}	$E_{int/H2}$	*n*	E_{int}	$E_{int/H2}$
1	0.8	0.8	17	18.9	1.1
2	1.9	0.9	18	19.9	1.1
3	3.0	1.0	19	21.9	1.2
4	4.8	1.2	20	23.1	1.2
5	6.1	1.2	21	23.7	1.1
6	6.7	1.1	22	24.0	1.1
7	7.9	1.1	23	25.5	1.1
8	10.2	1.3	24	27.1	1.1
9	9.9	1.1	25	28.7	1.1
10	12.1	1.2	26	28.3	1.1
11	13.1	1.2	27	29.6	1.1
12	14.1	1.2	28	31.6	1.1
13	15.3	1.2	29	32.9	1.1
14	16.4	1.2	30	33.8	1.1
15	16.5	1.1	40	44.3	1.1
16	18.2	1.1	-	-	-

In $Na^+@C_{60}(H_2)_{40}$, all H-H bond lengths are ~ 0.75 Å. The H_2 molecules are oriented towards the center of the six-membered and five-membered rings. The E_{int} of $Na^+@C_{60}(H_2)_n$ summarized in Table 4.9 shows a steady increase from 0.8 – 44.3 kcal/mol with *n* varying from 1 to 40. The $E_{int/H2}$ is in the range 0.8 – 1.3 kcal/mol. The high E_{int} values of $Na^+@C_{60}(H_2)_n$ systems suggest that these systems possess H_2 binding capacity comparable to that of $Cl^-@C_{60}(H_2)_n$ systems. The H_2 storage capacity of $Cl^-@C_{60}(H_2)_{40}$ is 10.8 wt%, and thus $Na^+@C_{60}(H_2)_n$ can be recommended as a counter cation for $Cl^-@C_{60}(H_2)_n$ systems.

4.9.3 Interaction of H_2 with $Na^+@C_{60}...Cl^-@C_{60}$

Considering a more realistic approach that an anion is always stabilized by a counter cation, we have studied the H_2 binding affinity of endohedral ion-pair system $Na^+@C_{60}Cl^-@C_{60}$. Figure 4.13 represents the optimized geometry of $Na^+@C_{60}...Cl^-@C_{60}(H_2)_{66}$ in which H_2 molecules interact with the cationic part by side-on coordination and anionic part by end-on coordination. The Na…Cl interaction distance elongates from 8.62 Å in the bare ion- pair system to 8.64 Å in $Na^+@C_{60}...Cl^-@C_{60}(H_2)_{66}$ whereas no change is observed for C…C interaction distance between the two fullerene cages. The C…C bond distance is 1.64 Å in both bare and hydrogenated systems. The H-H bond length is 0.74 -0.75 Å for H_2 molecules bonded to the endohedral ion-pair system. The E_{int} and $E_{int/H2}$ of $Na^+@C_{60}...Cl^-@C_{60}(H_2)_{66}$ are 71.8 and 1.1 kcal/mol, respectively with 9 wt% of H_2. The H_2 binding affinity of anion encapsulated or cation encapsulated fullerenes does not decrease when they combine to form the ion pair. The charge delocalization is achievable in salt systems where the electrostatic interactions between the anion and the cation can be brought down by the presence of shielding systems like fullerenes. Thus $Na^+@C_{60}$ retains a positive charge, and Cl^-C_{60} retains negative charge in the ion-pair complex. The resultant complex $Na^+@C_{60}Cl^-@C_{60}$ is, therefore, a good candidate for H_2 storage.

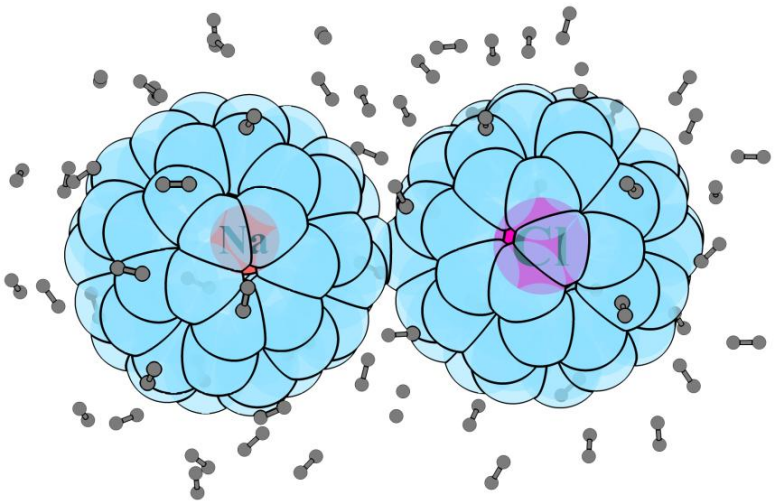

Figure 4.13 Optimized geometries of $Na^+@C_{60}...Cl^-@C_{60}(H_2)_{66}$ at the M06L/6-31G(d,p) level.

4.9.4 MESP Analysis

MESP is used to characterize lone pairs, intermolecular interactions, molecular reactivity *etc.*[77-79, 109, 110] The charge delocalization in endohedral fullerene-H_2 complexes have been studied using MESP topographical analysis. Figure 4.14 represents the MESP topography of $Na^+@C_{60}...Cl^-@C_{60}(H_2)_{66}$ complex textured on to a 0.003 au electron density surface. The V_{min} of $Na^+@C_{60}...Cl^-@C_{60}(H_2)_{66}$ complex is -12.4 kcal/mol. The charge separation in the ion-pair fullerene system is envisaged in the MESP plot. The electron-rich anion encapsulated fullerene part of the complex ($Cl^-@C_{60}$) is represented by blue-green color, and the electron-deficient cation encapsulated fullerene part ($Na^+@C_{60}$) by red color. The delocalized electron density acts as a glue to bind several H_2 molecules in the coordination shell, and the electron density on the fullerene cage decreases with H_2 binding.

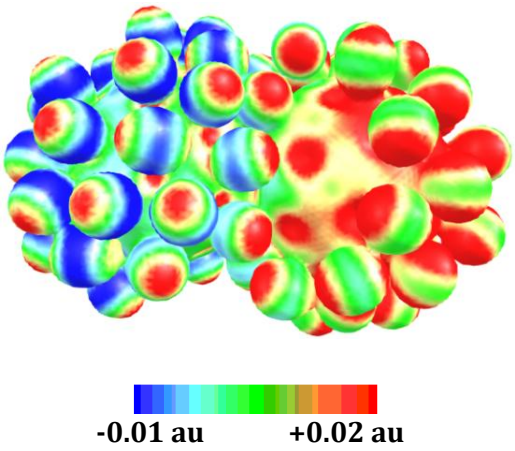

Figure 4.14 MESP of $Na^+@C_{60}...Cl^-@C_{60}(H_2)_{66}$ plotted at 0.003 au isodensity surface. The color coding from blue to red indicates MESP values in the range −0.01 to 0.02 au.

4.9.5 QTAIM Analysis

The QTAIM analysis confirms that all H_2 molecules are connected with the carbons of fullerene cage, by observing bond paths with bcps (Figure 4.15). No direct bond path is observed between H_2 and Cl^- or Na^+. The ρ_{bcp} of C…H interactions are in the range 0.0023 – 0.0077 au. The Laplacian of electron density ($\nabla^2\rho_{bcp}$) is positive for all the interactions indicating the noncovalent nature of bonds. A bcp is noted between the carbons of two fullerene cages. The ρ_{bcp} of this C…C bond is 0.1866 au, and the $\nabla^2\rho_{bcp}$ is negative. This

bond can be assigned as a covalent bond. Several bcps are noted for Cl^-...C_{60} interactions (ρ_{bcp} in the range 0.0065 – 0.0077 au) whereas only one bcp is observed for Na^+...C_{60} interaction (ρ_{bcp} = 0.0079 au). Also, several bcps are located between adjacent H_2 molecules indicating H_2...H_2 dihydrogen interactions. These secondary interactions with ρ_{bcp} in the range 0.0006 – 0.0043 au point towards the formation of an attractive interaction between the adsorbed H_2 molecules. The secondary interactions along with the primary noncovalent interactions lead to the formation of the noncovalently connected endohedral fullerene-H_2 system.

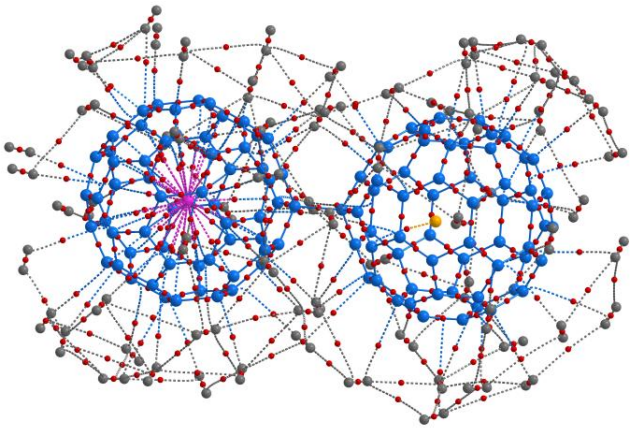

Figure 4.15 QTAIM features of $Na^+@C_{60}$...$Cl^-@C_{60}(H_2)_{66}$ at the M06L/6-311++G(d,p) level.

4.10 Conclusions

The H_2 binding affinity of the anion (Cl^-) and cation (Na^+) encapsulated fullerenes have been explored using DFT methods. The charge on the encapsulated species is transferred to the fullerene cage enhancing the H_2 binding affinity of endohedral fullerene systems as well as their ion-pair combination. The electron density distribution of these endohedral systems has been studied by MESP analysis. The binding nature of H_2 with the electron rich and electron deficient regions is revealed by MESP analysis. The noncovalent interactions of H_2 with fullerene cage have been analyzed by QTAIM analysis. The secondary H_2...H_2 interactions which aid the binding of more H_2 molecules are also located in the ion-pair fullerene system. Thus the endohedral ion pair system $Na^+@C_{60}$...$Cl^-@C_{60}$ could be proposed as a good H_2 storage

system. The present work may show the way to develop such ionic systems in which the cation and anion are separated and shielded by fullerene cage for H_2 storage.

4.11 References

1. D. Bethune, R. Johnson, J. Salem, M. De Vries and C. Yannoni, *Nature*, **1993**, *366*, 123-128.
2. M. N. Chaur, F. Melin, A. L. Ortiz and L. Echegoyen, *Angew. Chem. Int. Ed.* , **2009**, *48*, 7514-7538.
3. S. Guha and K. Nakamoto, *Coord. Chem. Rev.*, **2005**, *249*, 1111-1132.
4. J. R. Heflin, D. Marciu, C. Figura, S. Wang, P. Burbank, S. Stevenson and H. C. Dorn, *Appl. Phys. Lett.*, **1998**, *72*, 2788-2790.
5. A. A. Popov, S. Yang and L. Dunsch, *Chem. Rev.*, **2013**, *113*, 5989-6113.
6. R. Kitaura and H. Shinohara, *Jpn. J. Appl. Phys.*, **2007**, *46*, 881.
7. J. Cioslowski, *Electronic Structure Calculations of Fullerenes and Their Derivatives*, Oxford University Press, New York, NY (United States), **1995**.
8. M. S. Dresselhaus, G. Dresselhaus and P. C. Eklund, *Science of Fullerenes and Carbon Nanotubes: Their Properties and Applications*, Academic press, **1996**.
9. A. Hirsch and M. Brettreich, *Fullerenes: Chemistry and Reactions*, John Wiley & Sons, **2006**.
10. D. M. Guldi, L. Feng, S. G. Radhakrishnan, H. Nikawa, M. Yamada, N. Mizorogi, T. Tsuchiya, T. Akasaka, S. Nagase and M. Ángeles Herranz, *J. Am. Chem. Soc.*, **2010**, *132*, 9078-9086.
11. R. D. Bolskar, *Nanomedicine*, **2008**, *3*, 201-213.
12. H. Kato, Y. Kanazawa, M. Okumura, A. Taninaka, T. Yokawa and H. Shinohara, *J. Am. Chem. Soc.*, **2003**, *125*, 4391-4397.
13. H. Hu, W.-D. Cheng, S.-P. Huang, Z. Xie and H. Zhang, *J. Theor. Comput. Chem.*, **2008**, *7*, 737-749.
14. P. J. Fagan, J. C. Calabrese and B. Malone, *Acc. Chem. Res.*, **1992**, *25*, 134-142.
15. A. L. Balch and M. M. Olmstead, *Chem. Rev.*, **1998**, *98*, 2123-2166.
16. K. Lee, H. Song and J. T. Park, *Acc. Chem. Res.*, **2003**, *36*, 78-86.

17. N. Martín, *Chem. Commun.*, **2006**, 2093-2104.
18. A. Rodríguez-Fortea, A. L. Balch and J. M. Poblet, *Chem. Soc. Rev.*, **2011**, *40*, 3551-3563.
19. J. R. Heath, S. C. O'brien, Q. Zhang, Y. Liu, R. F. Curl, H. W. Kroto, F. K. Tittel and R. E. Smalley, *J. Am. Chem. Soc.*, **1985**, *107*, 7779-7780.
20. S. Aoyagi, E. Nishibori, H. Sawa, K. Sugimoto, M. Takata, Y. Miyata, R. Kitaura, H. Shinohara, H. Okada and T. Sakai, *Nat. Chem.*, **2010**, *2*, 678-683.
21. R. Tellgmann, N. Krawez, S.-H. Lin, I. Hertel and E. Campbell, *Nature*, **1996**, *382*, 407.
22. E. Campbell, R. Tellgmann, N. Krawez and I. Hertel, *J. Phys. Chem. Solids*, **1997**, *58*, 1763-1769.
23. A. Kaplan, A. Bekkerman, B. Tsipinyuk and E. Kolodney, *J. Chem. Phys.*, **2002**, *117*, 3484-3491.
24. T. John, S. Dennis and H. Shinohara, *Chem. Phys. Lett.*, **1997**, *278*, 107-110.
25. Y. Kubozono, H. Maeda, Y. Takabayashi, K. Hiraoka, T. Nakai, S. Kashino, S. Emura, S. Ukita and T. Sogabe, *J. Am. Chem. Soc.*, **1996**, *118*, 6998-6999.
26. Y. Kubozono, T. Ohta, T. Hayashibara, H. Maeda, H. Ishida, S. Kashino, K. Oshima, H. Yamazaki, S. Ukita and T. Sogabe, *Chem. Lett.*, **1995**, *24*, 457-458.
27. E. Nishibori, M. Takata, M. Sakata, M. Inakuma and H. Shinohara, *Chem. Phys. Lett.*, **1998**, *298*, 79-84.
28. Y. Rubin, *Chem. Eur. J.*, **1997**, *3*, 1009-1016.
29. Y. Basir and S. L. Anderson, *Chem. Phys. Lett.*, **1995**, *243*, 45-48.
30. E. G. Gillan, C. Yeretzian, K. S. Min, M. M. Alvarez, R. L. Whetten and R. B. Kaner, *J. Phys. Chem.*, **1992**, *96*, 6869-6871.
31. L. Moro, R. Ruoff, C. Becker, D. Lorents and R. Malhotra, *J. Phys. Chem.*, **1993**, *97*, 6801-6805.
32. S. W. McElvany, *J. Phys. Chem.*, **1992**, *96*, 4935-4937.
33. K. Kurotobi and Y. Murata, *Science*, **2011**, *333*, 613-616.
34. K. Komatsu, M. Murata and Y. Murata, *Science*, **2005**, *307*, 238-240.
35. T. Peres, B. Cao, W. Cui, A. Khong, R. J. Cross, M. Saunders and C. Lifshitz, *Int. J. Mass Spectrom.*, **2001**, *210*, 241-247.

36. A. Krachmalnicoff, R. Bounds, S. Mamone, S. Alom, M. Concistrè, B. Meier, K. Kouřil, M. E. Light, M. R. Johnson and S. Rols, *Nat. Chem.*, **2016**, *8*, 953-957.
37. S. Stevenson, G. Rice, T. Glass, K. Harich, F. Cromer, M. Jordan, J. Craft, E. Hadju, R. Bible and M. Olmstead, *Nature*, **1999**, *401*, 55-57.
38. L. Dunsch and S. Yang, *Phys. Chem. Chem. Phys.*, **2007**, *9*, 3067-3081.
39. S. Yang, A. A. Popov and L. Dunsch, *Angew. Chem. Int. Ed.*, **2007**, *46*, 1256-1259.
40. C. R. Wang, T. Kai, T. Tomiyama, T. Yoshida, Y. Kobayashi, E. Nishibori, M. Takata, M. Sakata and H. Shinohara, *Angew. Chem. Int. Ed.* , **2001**, *40*, 397-399.
41. Y. Iiduka, T. Wakahara, K. Nakajima, T. Nakahodo, T. Tsuchiya, Y. Maeda, T. Akasaka, K. Yoza, M. T. Liu and N. Mizorogi, *Angew. Chem. Int. Ed.*, **2007**, *46*, 5562-5564.
42. S. Osuna, M. Swart and M. Sola, *Phys. Chem. Chem. Phys.*, **2011**, *13*, 3585-3603.
43. Y. Wang, D. Tománek and R. S. Ruoff, *Chem. Phys. Lett.*, **1993**, *208*, 79-85.
44. J. M. Yan and C.-B. Zhu, *J. Mol. Struc.-THEOCHEM*, **1995**, *358*, 167-172.
45. D.-R. Zhang, J.-A. Wu and J.-M. Yan, *J. Mol. Struc.-THEOCHEM*, **1993**, *282*, 187-191.
46. J. Cioslowski, *J. Am. Chem. Soc.*, **1991**, *113*, 4139-4141.
47. J. Cioslowski and K. Raghavachari, *J. Chem. Phys.*, **1993**, *98*, 8734-8741.
48. X. Wu and X. Lu, *J. Am. Chem. Soc.*, **2007**, *129*, 2171-2177.
49. A. A. Popov and L. Dunsch, *Chem. Eur. J.*, **2009**, *15*, 9707-9729.
50. K. Kobayashi, S. Nagase, M. Yoshida and E. Ōsawa, *J. Am. Chem. Soc.*, **1997**, *119*, 12693-12694.
51. E. D. Jemmis, G. Subramanian, G. N. Sastry, G. Mehta, R. N. Shirsat and S. R. Gadre, *Perkin Trans. 2*, **1996**, 2343-2346.
52. R. E. Estrada-Salas and A. A. Valladares, *J. Mol. Struc.-THEOCHEM*, **2008**, *869*, 1-5.
53. E. Brocl/awik and A. Eilmes, *J. Chem. Phys.*, **1998**, *108*, 3498-3503.
54. D. Whitehouse and A. Buckingham, *Chem. Phys. Lett.*, **1993**, *207*, 332-338.
55. P. A. Denis, *J. Phys. Org. Chem.*, **2012**, *25*, 322-326.
56. B. Dunlap, J. Ballester and P. Schmidt, *J. Phys. Chem.*, **1992**, *96*, 9781-9787.
57. M.-S. Son and Y. K. Sung, *Chem. Phys. Lett.*, **1995**, *245*, 113-118.
58. Z. Slanina, F. Uhlík, L. Adamowicz and S. Nagase, *Mol. Simul.* , **2005**, *31*, 801-806.
59. Ş. Erkoç and L. Türker, *J. Mol. Struc.-THEOCHEM*, **2003**, *640*, 57-61.

60. Y. H. Hu and E. Ruckenstein, *J. Am. Chem. Soc.*, **2005**, *127*, 11277-11282.
61. A. A. Popov and L. Dunsch, *J. Am. Chem. Soc.*, **2007**, *129*, 11835-11849.
62. R. Valencia, A. Rodríguez-Fortea, A. Clotet, C. de Graaf, M. N. Chaur, L. Echegoyen and J. M. Poblet, *Chem. Eur. J.*, **2009**, *15*, 10997-11009.
63. O. Shameema, C. Ramachandran and N. Sathyamurthy, *J. Phys. Chem. A*, **2006**, *110*, 2-4.
64. J. Cioslowski and A. Nanayakkara, *J. Chem. Phys.*, **1992**, *96*, 8354-8362.
65. J. Cioslowski and E. D. Fleischmann, *J. Chem. Phys.*, **1991**, *94*, 3730-3734.
66. F. De Proft, C. Van Alsenoy and P. Geerlings, *J. Phys. Chem.*, **1996**, *100*, 7440-7448.
67. P. Ravinder and V. Subramanian, *J. Phys. Chem. A*, **2011**, *115*, 11723-11733.
68. S. Salehzadeh, F. Yaghoobi and M. Bayat, *Comp. Theor. Chem.*, **2014**, *1034*, 73-79.
69. C.-X. Cui, Z.-P. Zhang, L. Zhu, L.-B. Qu, Y.-P. Zhang and Y. Lan, *Phys. Chem. Chem. Phys.*, **2017**, *19*, 30393 - 30401.
70. Y. Zhao and D. G. Truhlar, *Acc. Chem. Res.*, **2008**, *41*, 157-167.
71. Y. Zhao and D. G. Truhlar, *J. Chem. Phys.*, **2006**, *125*, 194101.
72. M. J. Frisch, G. W. Trucks, *et al.* Gaussian 09, Revision D.01; Gaussian, Inc., Wallingford CT, **2013**.
73. K. Remya and C. H. Suresh, *J. Comput. Chem.*, **2013**, *34*, 1341-1353.
74. S. Grimme, *J. Comput. Chem.*, **2006**, *27*, 1787-1799.
75. S. Grimme, J. Antony, S. Ehrlich and H. Krieg, *J. Chem. Phys.*, **2010**, *132*, 154104.
76. S. F. Boys and F. d. Bernardi, *Mol. Phys.*, **1970**, *19*, 553-566.
77. S. R. Gadre and R. N. Shirsat, *Electrostatics of Atoms and Molecules*, Universities Press, Hyderabad, **2000**.
78. P. Politzer and D. G. Truhlar, *Chemical Applications of Atomic and Molecular Electrostatic Potentials: Reactivity, Structure, Scattering: Energetics of Organic, Inorganic, and Biological Systems*, Springer, New York, **1981**.
79. J. S. Murray and K. Sen, *Molecular Electrostatic Potentials:Concepts and Applications*, Elsevier Science, Amsterdam, The Netherlands, **1996**.
80. T. A. Keith, *AIMAll, version 14.04.17*, T. K. Gristmill Software, Overland Park, KS, USA, **2014**.
81. M. Prato, *J. Mater. Chem.* , **1997**, *7*, 1097-1109.

82. H. W. Kroto, M. A. Petrukhina and L. T. Scott, *Fragments of Fullerenes and Carbon Nanotubes: Designed Synthesis, Unusual Reactions, and Coordination Chemistry*, John Wiley & Sons, **2011**.
83. G. Mehta and H. S. P. Rao, *Tetrahedron*, **1998**, *54*, 13325-13370.
84. T. Kawase and H. Kurata, *Chem. Rev.*, **2006**, *106*, 5250-5273.
85. S. Armaković, S. J. Armaković, S. Pelemiš and D. Mirjanić, *Phys. Chem. Chem.Phys.*, **2016**, *18*, 2859-2870.
86. T. Hussain, B. Pathak, M. Ramzan, T. A. Maark and R. Ahuja, *Appl. Phys. Lett.*, **2012**, *100*, 183902.
87. A. Reyhani, S. Z. Mortazavi, S. Mirershadi, A. Z. Moshfegh, P. Parvin and A. N. Golikand, *J. Phys. Chem. C*, **2011**, *115*, 6994-7001.
88. M. Yoon, S. Yang, C. Hicke, E. Wang, D. Geohegan and Z. Zhang, *Phys. Rev. Lett.*, **2008**, *100*, 206806.
89. A. Dillon and M. Heben, *Appl. Phys. A*, **2001**, *72*, 133-142.
90. L. Scanlon, P. Balbuena, Y. Zhang, G. Sandi, C. Back, W. Feld, J. Mack, M. Rottmayer and J. Riepenhoff, *J. Phys. Chem. B*, **2006**, *110*, 7688-7694.
91. Y. Zhang, L. Scanlon, M. Rottmayer and P. Balbuena, *J. Phys. Chem. B*, **2006**, *110*, 22532-22541.
92. C. Cazorla, *Coord. Chem. Rev.*, **2015**, *300*, 142-163.
93. X. Wang and J. Tu, *Appl. Phys. Lett.*, **2006**, *89*, 064101.
94. J. A. Teprovich Jr, D. A. Knight, M. S. Wellons and R. Zidan, *J. Alloys Compd.* , **2011**, *509*, S562-S566.
95. J. A. Teprovich Jr, M. S. Wellons, R. Lascola, S.-J. Hwang, P. A. Ward, R. N. Compton and R. Zidan, *Nano Lett.*, **2012**, *12*, 582-589.
96. P. Mauron, A. Remhof, A. Bliersbach, A. Borgschulte, A. Züttel, D. Sheptyakov, M. Gaboardi, M. Choucair, D. Pontiroli and M. Aramini, *Int. J. Hydrog. Energy*, **2012**, *37*, 14307-14314.
97. K. Chandrakumar and S. K. Ghosh, *Nano Lett.*, **2008**, *8*, 13-19.
98. K. Srinivasu and S. K. Ghosh, *J. Phys. Chem. C*, **2012**, *116*, 25184-25189.
99. Q. Sun, P. Jena, Q. Wang and M. Marquez, *J. Am. Chem. Soc.*, **2006**, *128*, 9741-9745.
100. T. Yildirim, J. Íñiguez and S. Ciraci, *Phys. Rev. B*, **2005**, *72*, 153403.

101. M. Yoon, S. Yang, E. Wang and Z. Zhang, *Nano Lett.* , **2007**, *7*, 2578-2583.
102. T. D. Della and C. H. Suresh, *Phys. Chem. Chem. Phys.*, **2016**, *18*, 14588-14602.
103. T. D. Della and C. H. Suresh, *ACS Omega*, **2017**, *2*, 4505-4513.
104. T. D. Della and C. H. Suresh, *Phys. Chem. Chem. Phys.*, **2017**, *19*, 5830-5838.
105. T. D. Della and C. H. Suresh, *Phys. Chem. Chem. Phys.*, **2018**, *20*, 6227-6235.
106. R. C. Lochan and M. Head-Gordon, *Phys. Chem. Chem. Phys.*, **2006**, *8*, 1357-1370.
107. B. Nyulasi and A. Kovács, *Chem. Phys. Lett.*, **2006**, *426*, 26-29.
108. F. Pichierri, *Chem. Phys. Lett.*, **2012**, *519*, 83-88.
109. P. K. Sajith and C. H. Suresh, *Inorg. Chem.*, **2012**, *51*, 967-977.
110. N. Mohan, C. H. Suresh, A. Kumar and S. R. Gadre, *Phys. Chem. Chem. Phys.*, **2013**, *15*, 18401-18409.

List of Publications

(i) Articles in journals

1. The remarkable ability of anions to bind dihydrogen. **T. D. Della** and C. H. Suresh, *Phys. Chem. Chem. Phys.* **2016***, 18,* 14588-14602*.*

2. Massive dihydrogen uptake by anionic carbon chains. **T. D. Della** and C. H. Suresh, *Phys. Chem. Chem. Phys.* **2017**, *19*, 5830-5838.

3. Dihydrogen binding affinity of polyatomic anions: a DFT study. **T. D. Della** and C. H. Suresh, *ACS Omega* **2017**, *2*, 4505-4513.

4. Sumanene: an efficient π-bowl for dihydrogen storage. **T. D. Della** and C. H. Suresh, *Phys. Chem. Chem. Phys.* **2018**, *20*, 6227-6235.

5. A noncovalent binding strategy to capture noble gases, hydrogen, and nitrogen. C. H. Suresh, N. Mohan and **T. D. Della**, *J. Comput. Chem.,* **2018**, *39*, 901-908.

(ii) Published contributions to academic conferences

1. Presented a poster entitled "Dihydrogen binding affinity of bare anions: A DFT study towards hydrogen storage" in the 15th Indian Theoretical Chemistry Symposium (TCS), held at University of Hyderabad, Hyderabad, during December 14 - 17, 2016.

2. Presented a paper entitled "Dihydrogen binding affinity of anions of different dimensions: A DFT approach towards hydrogen storage" in the HEAM Scientist 2018, A national conference on Hydrogen Energy and Advanced Materials, held at University of Kerala, Karyavattom, during March 5 – 6, 2018.